APPLICATION OF fMRI FOR ACTION REPRESENTATION:

DECODING, ALIGNING AND MODULATING

SALIM MOHAMMED HUSSEIN AL-WASITY

SUBMITTED IN FULFILMENT OF THE REQUIREMENTS FOR THE DEGREE OF

Doctor of Philosophy

DEPARTMENT OF ELECTRICAL AND ELECTRONICS ENGINEERING

COLLEGE OF SCIENCE AND ENGINEERING

UNIVERSITY OF GLASGOW

January, 2018

Abstract

Functional magnetic resonance imaging (fMRI) is an important tool for understanding neural mechanisms underlying human brain function. Understanding how the human brain responds to stimuli and how different cortical regions represent the information, and if these representational spaces are shared across brains and critical for our understanding of how the brain works. Recently, multivariate pattern analysis (MVPA) has a growing importance to predict mental states from fMRI data and to detect the coarse and fine scale neural responses. However, a major limitation of MVPA is the difficulty of aligning features across brains due to high variability in subjects' responses and hence MVPA has been generally used as a subject specific analysis. Hyperalignment, solved this problem of feature alignment across brains by mapping neural responses into a common model to facilitate between subject classifications. Another technique of growing importance in understanding brain function is real-time fMRI Neurofeedback, which can be used to enable individuals to alter their brain activity. It facilitates people's ability to learn control of their cognitive processes like motor control and pain by learning to modulate their brain activation in targeted regions.

The aim of this PhD research is to decode and to align the motor representations of multi-joint arm actions based on different modalities of motor simulation, for instance Motor Imagery (MI) and Action Observation (AO) using functional Magnetic Resonance Imaging (fMRI) and to explore the feasibility of using a real-time fMRI neurofeedback to alter these action representations.

The first experimental study of this thesis was performed on able-bodied participants to align the neural representation of multi-joint arm actions (lift, knock and throw) during MI tasks in the motor cortex using hyperalignment. Results showed that hyperalignment affords a statistically higher between-subject classification (BSC) performance compared to anatomical

alignment. Also, hyperalignment is sensitive to the order in which subjects entered the hyperalignment algorithm to create the common model space. These results demonstrate the effectiveness of hyperalignment to align neural responses in motor cortex across subjects to enable BSC of motor imagery.

The second study extended the use of hyperalignment to align fronto-parietal motor regions by addressing the problems of localization and cortical parcellation using cortex based alignment. Also, representational similarity analysis (RSA) was applied to investigate the shared neural code between AO+MI and MI of different actions. Results of MVPA revealed that these actions as well as their modalities can be decoded using the subject's native or the hyperaligned neural responses. Furthermore, the RSA showed that AO+MI and MI representations formed separate clusters but that the representational organization of action types within these clusters was identical. These findings suggest that the neural representations of AO+MI and MI are neither the same nor totally distinct but exhibit a similar structural geometry with respect to different types of action. Results also showed that MI dominates in the AO+MI condition.

The third study was performed on phantom limb pain (PLP) patients to explore the feasibility of using real-time fMRI neurofeedback to down-regulate the activity of premotor (PM) and anterior cingulate (ACC) cortices and whether the successful modulation will reduce the pain intensity. Results demonstrated that PLP patients were able to gain control and decrease the ACC and PM activation. Those patients reported decrease in the ongoing level of pain after training, but it was not statistically significant.

The fourth study was conducted on healthy participants to study the effectiveness of fMRI neurofeedback on improving motor function by targeting Supplementary Motor Cortex (SMA). Results showed that participants learnt to up-regulate their SMA activation using MI

of complex body actions as a mental strategy. In addition, behavioural changes, i.e. shortening of motor reaction time was found in those participants. These results suggest that fMRI neurofeedback can assist participants to develop greater control over motor regions involved in motor-skill learning and it can be translated into an improvement in motor function.

In summary, this PhD thesis extends and validates the usefulness of hyperalignment to align the fronto-parietal motor regions and explores its ability to generalise across different levels of motor representation. Furthermore, it sheds light on the dominant role of MI in the AO+MI condition by examining the neural representational similarity of AO+MI and MI tasks. In addition, the fMRI neurofeedback studies in this thesis provide proof-of-principle of using this technology to reduce pain in clinical applications and to enhance motor functions in a healthy population, with the potential for translation into the clinical environment.

Contents

List of Figures

List of Tables

Acknowledgements

Throughout my PhD I received a tremendous amount of support from multiple people and organisations. I would like to take this opportunity to thank them for helping me achieve what I thought was unachievable.

First and foremost, I thank Allah, the almighty, for helping me and giving me the knowledge and strength to successfully complete this PhD project.

I would like to thank my supervisors Aleksandra Vuckovic and Frank Pollick for their support and guidance during my PhD. Alexandra thank you for always being available to offer good advice. Frank, I would like to particularly thank you for you constant help throughout my PhD and offering feedback whenever it was needed, and for enabling me to present my research in many different and interesting conferences around the world.

I would like to thank the lab members of Alexandra's and Frank's labs, which always shown support and gave their advice during and outside lab meetings. I would like to specifically thank Kristian Stefanov and Dana Kanel For their assistance and helping me complete two of my experiment. I'd also like to thank Xinyi Zhao for her help with analysis in one of my studies. Finally, I would like to thank Abdullah Habib for his support and his willingness to help.

I would also like to thank Professor Lars Muckli and his lab for their continuous support and guidance regarding fMRI, fMRI analysis and helping me develop that skills that I needed. Thanks a lot guys this would have been a lot more difficult without you.

I would also like to thank our collaborators, Prof. Yasuharu Koike and his lab in Tokyo institute of technology, for his hospitability, hosting me during my time in Japan and for introducing me to different fMRI analysis techniques. Dr. Stefan Vogt, for his scientific feedback and proofreading of my experimental chapters. Prof. Rainer Goebel and Armin Heinecke for

welcoming me into their research group and helping me preforming and learn advance fMRI analysis using brain voyager. I would also like to thank SNIAPSE and Dr. Kristin Flegal for providing me with funding for training programs. Finally, I would like to show my sincere gratitude and appreciation to my sponsor, the Higher Committee for Education Development in Iraq, for their administrative and financial support.

I'd like to thank my godfather for his limitless support throughout my entire life. I would like to express my deepest gratitude to my mother, two sisters, aunty and mother-in-law for all their moral support and prayers. I would not have gotten this far without their love and encouragement. Most importantly, no words can express my gratitude and thanks to my wife for caring for my family while I was busy with my study, and for her patience and endless support. I appreciate all her sacrifices, you are my rock. I would also like to acknowledge my two lovely princesses, Noorhan and Shams, who are the pride and joy of my life. Thank you for being the most supportive family in the world and helping me accomplish my PhD dream.

Finally, I would like to thank my friends Karrar Fadihil, Muhanad Hussein, Saif Saad, Saif Saed, Manaf Al-Taleb, Mohammed Jarjees, Caesar Al-Ameri, Sarah Comincioli, Margaret Armentano, Bethel Osuagwa, Jose Alberto Martin, Aso Muhamed, Ary Al-Jaff, Yahia Madkhali, Greta Todorova and Mohi Chowdhury for being patient with me and always being there to offer their help and support over the years.

Dedication

This work is dedicated to my beloved family

My parents: Mom and Dad

My two young sisters

My wife

And for my two lovely daughters

Author's Declaration

I, Salim Mohammed Hussein Al-Wasity, hereby declare that except where explicitly reference is made to the contribution of others, this thesis is the result of the work of the named and has not been submitted for any other degree at the University of Glasgow or any other institution.

January 2018

Abbreviations

2D	Two Dimensional Space
3D	Three Dimensional Space
ACC	Anterior Cingulate Cortex
ADHD	Attention Deficit Hyperactivity Disorder
AIC	Anterior Insula Cortex
ALE	Activation Likelihood Estimation
ANN	Artificial Neural Networks
ANOVA	Analysis of Variance
AO	Action Observation
AO+MI	Simultaneous Action Observation And Motor Imagery
B_0	external magnetic field
BA	Brodmann Area
blPFC	Bilateral Dorsolateral Prefrontal Cortex
BOLD	Blood Oxygenation Level Dependent
BPI	Brachial Plexus Injury
BSC	Between-Subject Classification
CBA	Cortex Based Alignment
CBF	Cerebral Blood Flow
CBV	Cerebral Blood Volume
CCNi	Centre For Cognitive Neuroimaging
$CMRO_2$	Cerebral Metabolic Rate of Oxygen
CNP	Central Neuropathic Pain
CS_{final}	Final Common Spaces
CS_{ini}	Intermediate Common Spaces
dPM	Dorsal Premotor Cortex
E	Extraction Fraction
EEG	Electroencephalography
EPI	Echo-Planar Imaging
EVI	External Visual Imagery
FFX	Fixed Effect Analysis
fMRI	Functional Magnetic Resonance Imaging

FWHM	Full Width At A Half Maximum
GLM	General Linear Model
GM	Gray Matter
GNB	Gaussian Naïve Bayes
HDR	Hemodynamic Response
Hz	Hertz
IBI	Inter-Block Interval
ICA	Independent Components Analysis
IFG	Inferior Frontal Gyrus
IFG	Inferior Frontal Gyri
IIC	Intensity Inhomogeneities Correction
IPL	Inferior Parietal Lobule
IR	Impulse Response
ISI	Inter-Stimulus Interval
IVI	Internal Visual Imagery
J	angular momentum
KI	Kinesthetic Imagery
LCD	Liquid Crystal Display
LDA	Linear Discriminant Analysis
LH	Left Hemisphere
LI	Laterality Index
M_0	Net Magnetization
M1	Primary Motor Cortex
MDS	Multi-Dimensional Scaling
ME	Motor Execution
MfG	Middle Frontal Gyrus
MI	Motor Imagery
mm	Millimetre
mm^3	Cubic Millimetre
MNI	Neurological Institute Template
MNS	Mirror Neuron System
MRI	Magnetic Resonance Imaging
ms	Millisecond

MVPA	Multivariate Pattern Analysis
NF	Neurofeedback
NPSI	Neuropathic Pain Symptom Inventory
OFC	Orbitofrontal Cortex
PcG	Precentral Gyrus
PGIC	Patient Global Impression Of Change
PLP	Phantom Limb Pain
PM	Premotor Region
PPC	Posterior Parietal Cortex
PPI	Psychophysiological Interaction
pre-SMA	Pre-Supplementary Motor Area
rACC	Rostral Anterior Cingulate Cortex
RDM	Representational Dissimilarity Matrix
RFX	Random Effect Analysis
RH	Right Hemisphere
ROI	Region Of Interest
RS	Subject's Aligned (Rotated) Space
RSA	Representational Similarity Analysis
rTMS	Repetitive Transcranial Magnetic Stimulation
S	Subject's Representational Space
s	Second
sACC	Subgenual Anterior Cingulate Cortex
SEM	Standard Error of The Mean
SI	Primary Somatosensory Cortex
SMA	Supplementary Motor Area
SNR	Signal-To-Noise Ratio
SPL	Superior Parietal Lobule
SVM	Support Vector Machines
T_1	Longitudinal Relaxation
T_2	Transverse Relaxation
TBV	Turbo-Brainvoyager
TCP/IP	Transmission Control Protocol/Internet Protocol
TE	Echo Time

TM	Transformation Parameters
TMS	Transcranial Magnetic Stimulation
TR	Repetition Time
μ	magnetic moment
v_0	Larmor frquency
VI	Visual Imagery
vlPFC	Bilateral Ventrolateral Prefrontal Cortex
VMIQ-2	Vividness Of Movement Imagery Questionnaires-2nd Version
vmPFC	Ventromedial Prefrontal Cortex
vPM	Ventral Premotor Cortex
VT	Temporal Cortex
WM	White Matter
WSC	Within Subject Classification
x,y,z	3D Talairach Coordinates
γ	Gyromagnetic ratio
α	Flip angle

Publications:

Conference and Proceeding

Shim, L. S., Al-Wasity, S., McKay, L., Ahlstrom, U., Lui, P., Pemble, C., Crabbe, F., and Pollick, F. 2014. "The Effect of Stimulus Quality in Comparing Intact to Scrambled Point-Light Displays". In *OHBM*. Hamburg, Germany.

Al-Wasity, S., Vuckovic, A., Vogt, S., Koike, Y., and Pollick, F. 2016. "Using Multi-Voxel Pattern Analysis to Decode Motor Imagery of Complex Actions". In *OHBM*. Geneva, Switzerland.

Al-Wasity, S., Vuckovic, A., Vogt, S., Koike, Y., and Pollick, F. 2016. "Hyperalignment Improves between Subject Classification of fMRI Brain Activity during Motor Imagery". In *SfN*. San Diego, United States.

Al-Wasity, S., Vuckovic, A., and .Pollick, F. 2017. "Up-regulation of Supplementary Motor Area activation with fMRI neurofeedback improves motor reaction time". In *SfN*. Washington DC, United States.

Al-Wasity, S., Kanel, D., Stefanov, K., and Pollick, F. 2017. "Empathy and the use of real-time fMRI to learn voluntary regulation of the anterior insula". In *rtFIN*. Nara, Japan.

Pollick, F, Al-Wasity, S., and Vuckovic, A. 2017. "Enhancing Motor Reaction Time using Real-Time Functional MRI Neurofeedback of Supplementary Motor Area". In *rtFIN*. Nara, Japan.

Chapter 1 : General Introduction

1.1 Summary

In this first chapter of the thesis, the basic concepts and terms used throughout the thesis are defined. The chapter introduces the neuroanatomy of the brain and motor network. It highlights the concept of motor cognition. This chapter also introduces the nature of MR signals and the properties of the haemodynamic neural response. It concludes with the themes and aims of the thesis.

1.2 Neuroanatomy of the brain

The human brain has fascinated and perplexed modern and ancient scientists throughout the centuries. During the last decades, researchers have developed novel techniques to better understand our brain functions and structures. Since this thesis focuses on the brain's cortical motor network, the following section presents some general considerations about this netwrok.

1.2.1 Brain structure

The brain has a complex anatomy and a tiered structure, with around 100 billion nerve cells. The normal adult human brain weights about 1.4 Kg, which corresponds to only 2% of body weight, yet the energy consuming processes account for approximately 25% of total body glucose utilisation (Squire, 2013).

The brain can be divided into the cerebrum, the brain stem and the cerebellum as shown in figure 1.1. The schematic diagram of the subdivision of the brain is illustrated in figure 1.2.

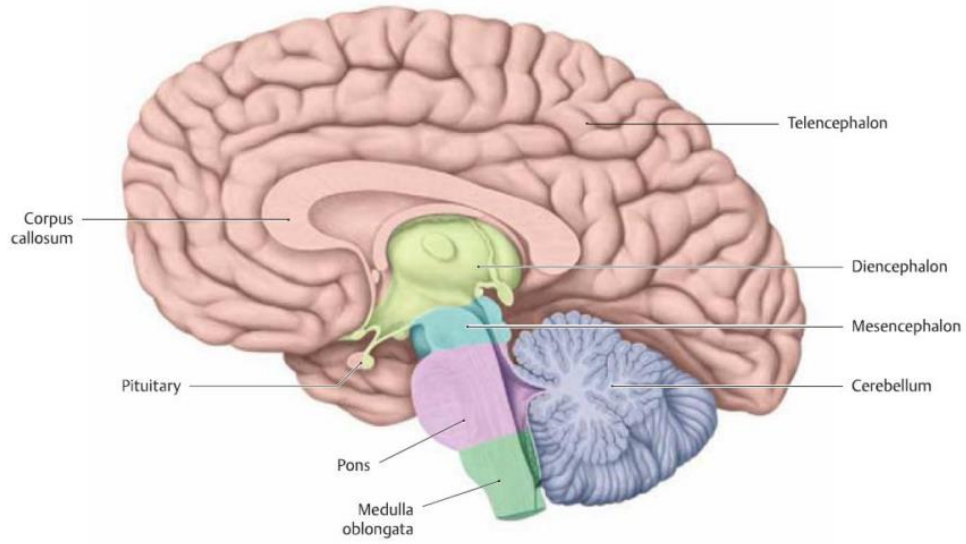

Figure 1.1. Main divisions of brain anatomical structure (Schünke *et al.*, 2010).

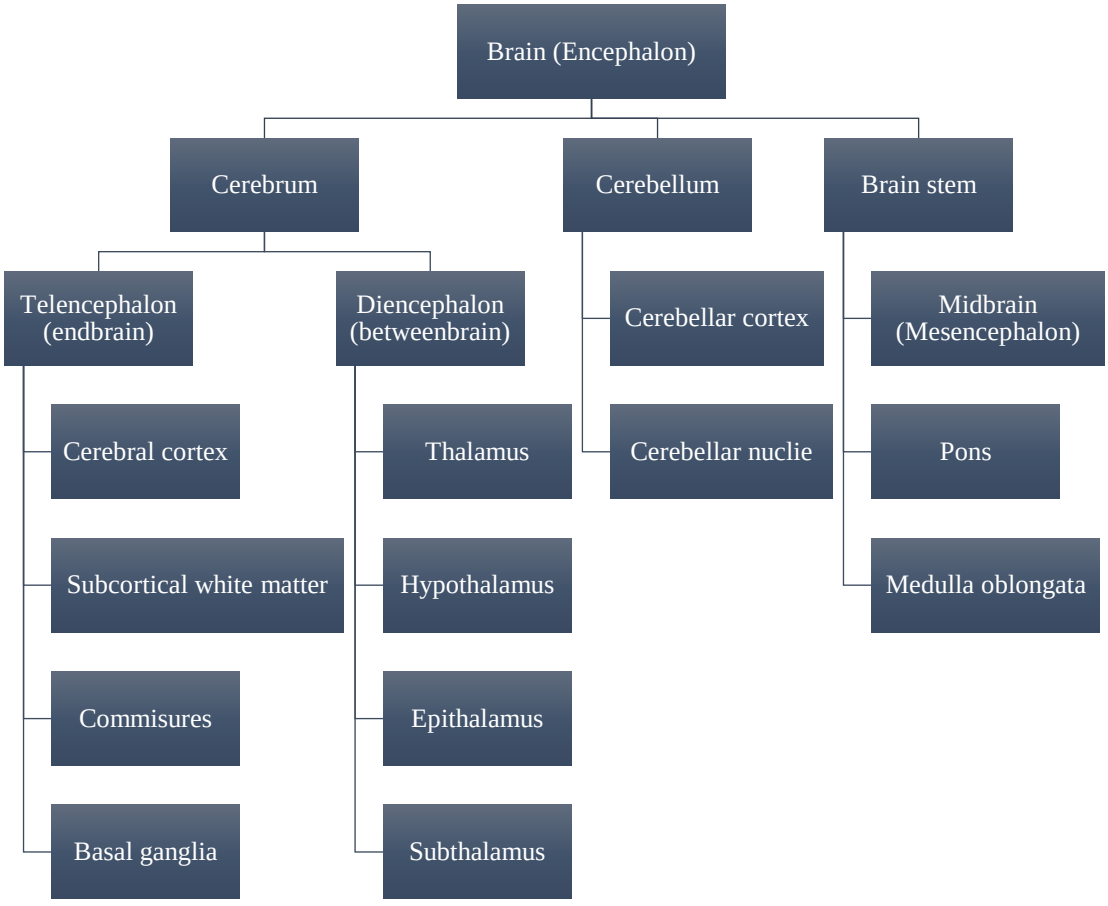

Figure 1.2. Subdivision of the brain structure (adapted from Squire, 2013).

The most complex functions occur in the cerebrum. For instance, the hypothalamus has many vital roles, such as the control of conscious behaviour, emotions and instincts, and the

automatic control of body processes. It screens and pre-processes all the flux of sensory information before sending it to the cerebral cortex. The cerebral cortex is responsible for conscious, sensation and cognitive activity, including language, reasoning, learning and memory (Carter *et al.*, 2009). The cerebral cortex consists of two hemispheres linked together by the corpus callosum, which contains more than 200 million nerve fibres. The cerebellum complements brain functioning, for example, in terms of controlling body movement coordination (like balance and posture). Subconscious or autonomic regulation mechanisms are controlled by the brain stem. The pons is involved in learning and remembering motor skills. Finally, the medulla oblongata is the centre for respiratory, cardiac and vasomotor monitoring and regulation (Carter *et al.*, 2009; Snell, 2010).

1.2.2 Cerebral Hemispheres

The cerebrum constitutes more than three-quarters of the brain's total volume, and is divided into two cerebral hemispheres (telencephalon), which include the cerebral cortex, the commissures, the subcortical white matter and the basal ganglia (a complex of deep grey matter masses). The cerebrum comprises two types of tissue, known as white and grey matter, as shown in figure 1.3. The grey matter (GM) consists of neuronal cell bodies and glial cells, axons, dendrites and synapses. In contrast, the white matter (WM) contains axons and their associated glial cells. Many axons are myelinated, allowing for rapid nerve impulse conduction and giving WM its pale appearance (Snell, 2010; Squire, 2013). The GM is distributed over the surface of the cerebral cortex, the basal ganglia, which includes the caudate nucleus and putamen (collectively called the corpus striatum), and the globus pallidus as well as the claustrum and amygdala.

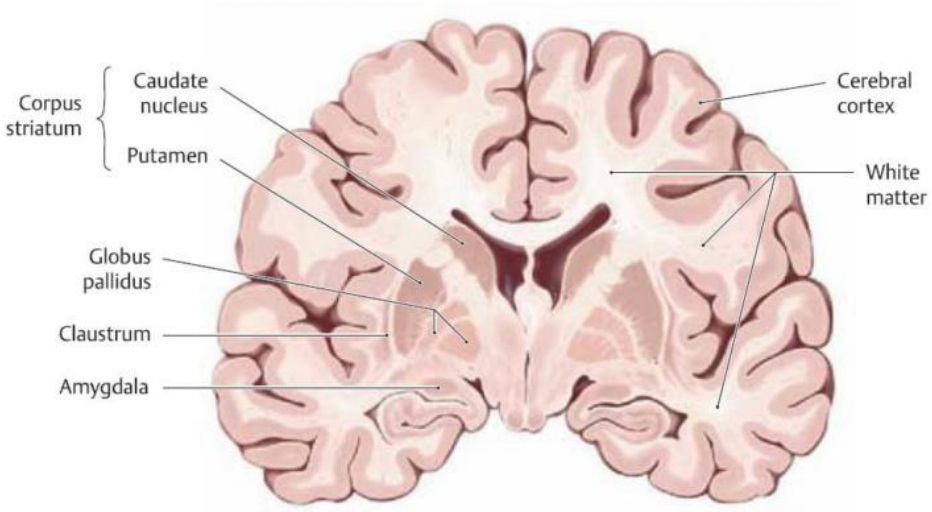

Figure 1.3. Coronal section showing the GM and WM in the brain (Schünke *et al.*, 2010).

The surfaces of the cerebral hemispheres contain many gyri, sulci and fissures, meaning that more than 50% of the cortex's area (approximately 0.8 m^2) is hidden within the grooves (sulci and fissures). These grooves separate the cortical regions into the frontal, parietal, occipital, temporal, insula and limbic lobes, as shown in figure 1.4 (Carter *et al.*, 2009). For instance, the longitudinal fissure separates the cerebral hemispheres, the central sulcus (fissure of Rolando) divides the frontal and the parietal lobe, the parietooccipital sulcus separates the parietal from the occipital lobes, and the insula lies deep within the lateral sulcus.

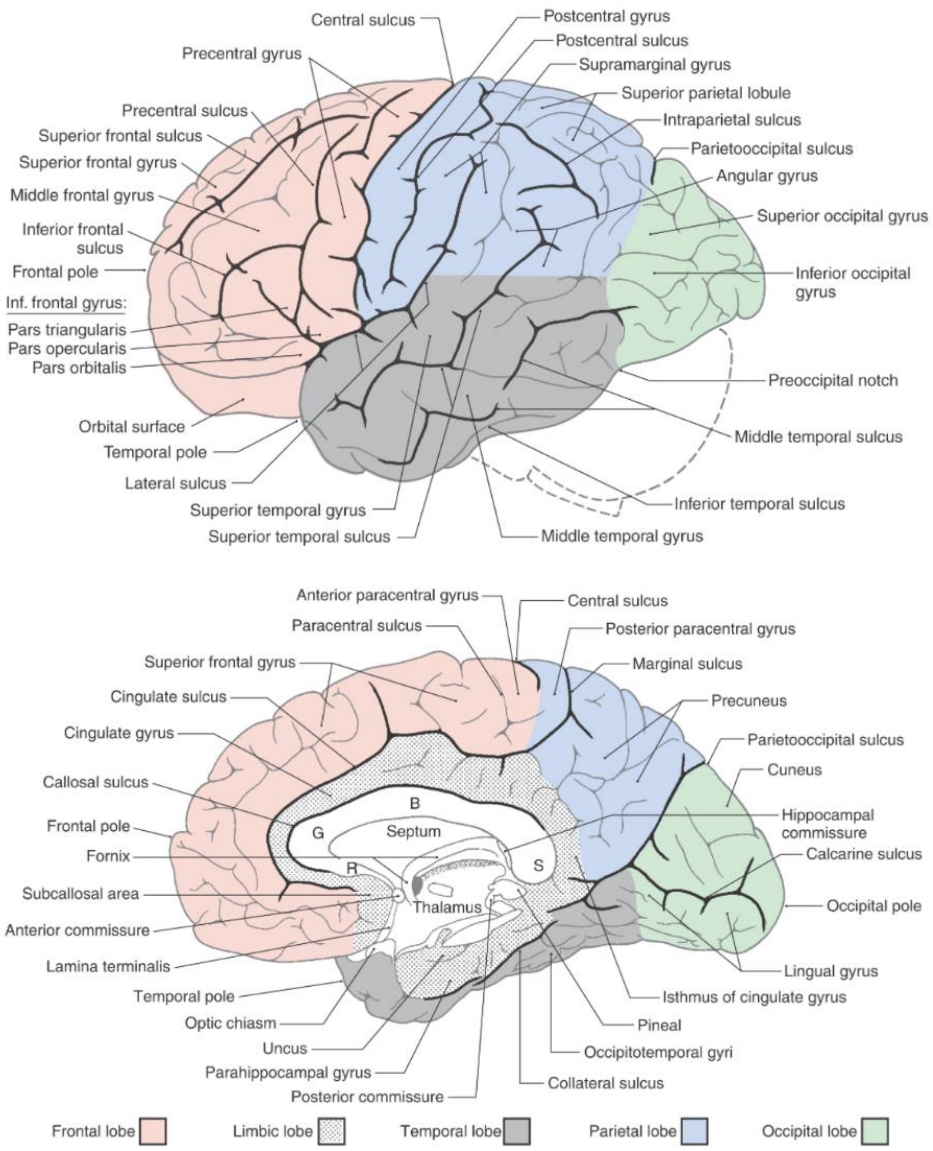

Figure 1.4. Left lateral (top) and medial (bottom) views of the cerebral hemisphere, showing the landmarks used to divide the cortex into its main lobes (Haines and Ard, 2013).

1.2.3 Cerebral cortex

The cerebral cortex is the outer layer of the cerebrum, constituting about 40% of the brain by weight and containing an average of 16 billion neurons (Herculano-Houzel, 2009). There are three types of cortices (Strominger *et al.*, 2012):

- Allocortex: consists of three layered cortices, mostly found in the limbic system.
- Neocortex: frequently found in most of the cerebral hemisphere; contains six layers.

- Mesocortex: a form of Neocortex that connects the Allocortex and Neocortex. It contains three to six layers and includes regions such as the cingulate gyrus and insula (limbic lobe).

1.2.4 Functional areas

Korbinian Brodmann, in 1909, divided the cortex into functional regions based on the distribution of the neurons in different layers of neocortex (cytoarchitectonics). These are known as Brodmann's areas (BA) (Brodmann, 2006). More than 40 areas are distinguished on the lateral and medial surfaces of the brain, as shown in figure 1.5.

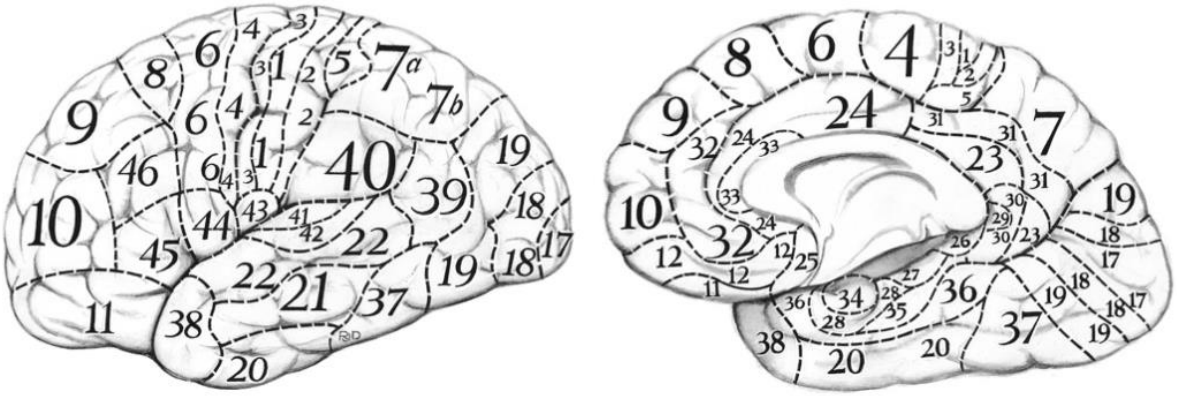

Figure 1.5. Lateral (left and medial (right) surfaces of the human cerebral cortex with numbers indicating the areas of Brodmann (Strominger *et al.*, 2012).

1.2.5 Blood vessels of the head

The brain and the body are critically dependent on an uninterrupted supply of oxygenated blood. Nearly 20% of the blood in the body circulates in the brain, which represents 2% of the body weight. Brain vessels, as shown in figure 1.6, provide the means for this uninterrupted blood supply. The vessels' sizes, positions and numbers vary between individuals. The blood transports oxygen, nutrients, and other necessary substances to keep the brain tissues working properly. The arteries carry oxygenated blood, with all its nutrients, and the veins carry the deoxygenated blood (Snell, 2010).

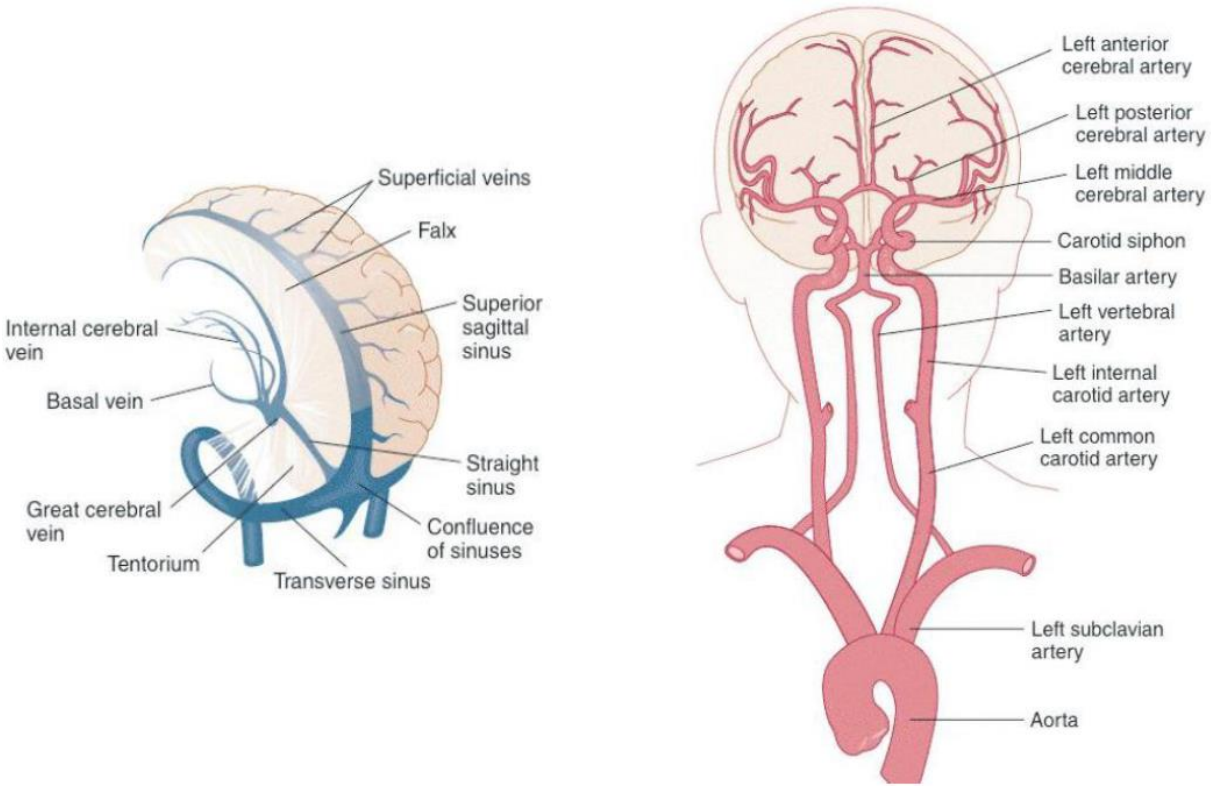

Figure 1.6. Main vessels of the brain, showing a three dimensional view of veins and sinuses (left) and the major cerebral arteries (right) (Brodal, 2010).

1.3 The organisation of the fronto-parietal motor network

Since this thesis focuses on the brain motor network, the following section presents a brief introduction to the anatomical structure of the motor system within the frontal and parietal lobes.

1.3.1 Frontal lobe

The cortical motor network contains the sensorimotor cortex and the premotor regions (PM), as shown in figure 1.7. The sensorimotor cortex is divided into the primary motor cortex (M1) or BA 4, situated anteriorly to the central sulcus in the frontal lobe, and the primary somatosensory cortex (SI), situated posteriorly to the central sulcus in the parietal lobe (Mayka et al., 2006).

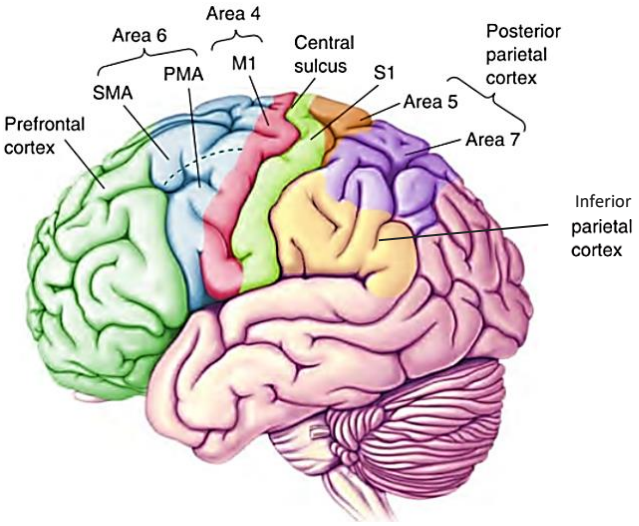

Figure 1.7. These areas of the neocortex are involved in the control of voluntary movement. BA 4 and BA 6 constitute the motor cortex (adapted from Grillner, 2007).

The M1 is organised in a somatotopical fashion (homunculus) as shown in figure 1.8, where the leg control area is localised medially, while the hand, face and tongue control areas are laterally situated. The fingers, hands, and face are represented by disproportionately large areas, corresponding to their involvement in tasks that require high precision and fine motor control (Bear *et al.*, 2007). The M1 serves in the execution of voluntary movements through its direct corticospinal projections to the spinal motor neurons, which control limb, hand, foot and digit movements, and to the cranial nerve motor neurons which control facial movements (Kolb and Whishaw, 2003; Graziano, 2006). It also projects to other motor structures such as the basal gangalia and the red nucleus (Kolb and Whishaw, 2003).

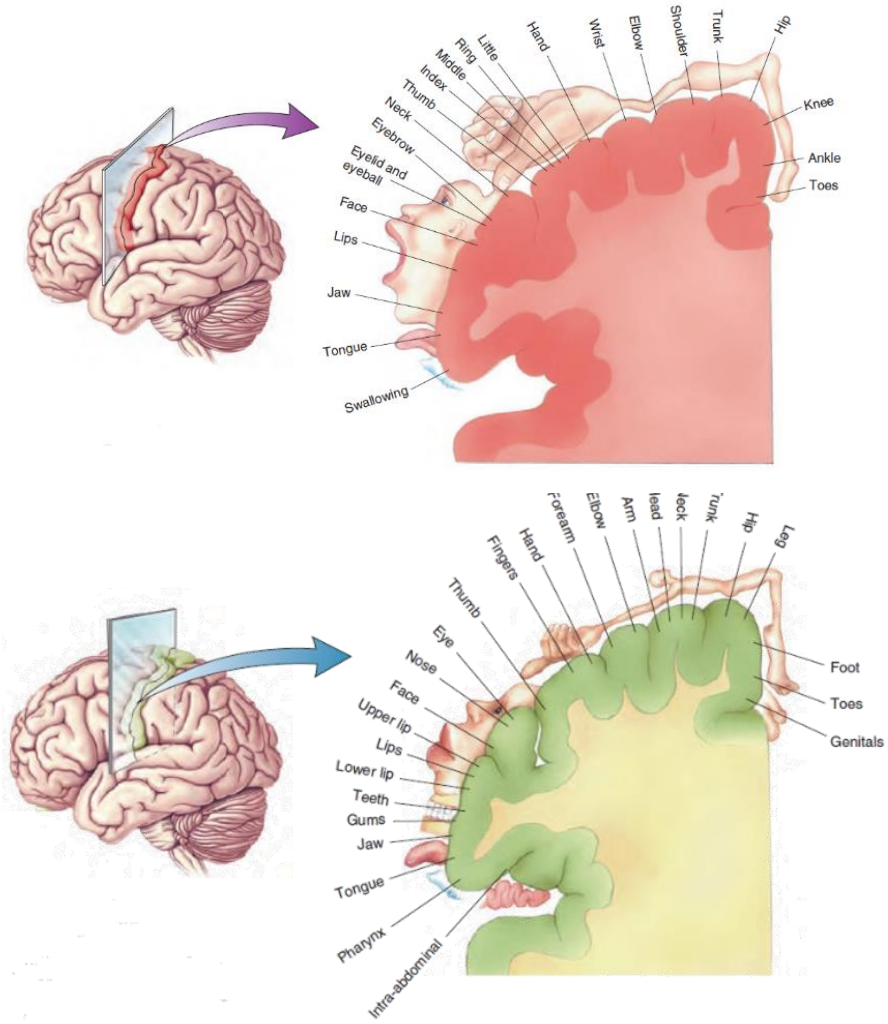

Figure 1.8. A somatotopic map of the human sensorimotor cortex. This map is a cross section through the precentral gyrus (shown at top) representing M1 (BA 4), and the postcentral gyrus (shown at bottom) representing SI (BA 1, BA 2, BA 3). The neurons in each area are most responsive to the body parts illustrated above them (Bear *et al.*, 2007)**.**

The PM (BA 6) can be divided into two parts: the lateral premotor cortex and the mesial premotor cortex as shown in figure 1.7. The mesial premotor cortex can further be divided into the pre-supplementary motor area (pre-SMA) rostrally and the supplementary motor area proper (SMA proper) caudally. The lateral premotor cortex can be subdivided along the dorsal and ventral plane into the dorsal premotor cortex (dPM) and ventral premotor cortex (vPM) (Mayka et al., 2006). The areas of premotor cortex show a much coarser somatotopy, with multiple motor maps and greater functional complexity. It is suggested that the dPM

participates in the planning and preparation of movement, and that the supplementary motor area encodes sequences of movements (Graziano, 2006). Moreover, the dPM contributes to the action selection network, and the left dPM in particular plays a dominant role in action selection (O 'shea et al., 2007). Furthermore, the premotor cortex serves an integrative role of converging input from the subcortical motor (basal ganglia and cerebellum) and parietal cortex afferents, and it also influences movement directly through corticospinal projections and indirectly through projections to the primary motor cortex (Dum and Strick, 1991; Kolb and Whishaw, 2003). Thus PM regions are connected to areas concerned with the execution of limb movements. In addition, the PM cortex receives projections from the dorsolateral prefrontal cortex, which suggests that this prefrontal region has some role in the control of limb and eye movements (Kolb and Whishaw, 2003).

1.3.2 Parietal lobe

The parietal lobe can be divided into two functional regions: the anterior region, which is known as SI or BA 1, BA 2 and BA 3, and the posterior region, which is referred to as the posterior parietal cortex (PPC).

Similarly to M1 homunculus, SI homunculus (figure 1.8) illustrates the somatotopy of the primary somatosensory cortex where the representation of the hand separates that of the face and the head, while the genitals are mapped onto the most hidden part of S1, somewhere below the toes. The relative size of the cortex devoted to the mouth, tongue and fingers is correlated with the density of sensory input received from these body regions compared to the trunk, arms and legs. Size on the map is also related to the importance of the sensory input from that part of the body (figure 1.8). BA 3 can be subdivided into BA 3a and BA 3b as shown in figure 1.9. BA 3b is the primary somatosensory cortex, because it receives dense inputs from the thalamus, and its neurons are very responsive to somatosensory stimuli. BA 3a also receives a dense input from the thalamus, but this region is concerned with the sense of body position

rather than touch. BA 1 and BA 2 receive dense inputs from area 3b. The projection from 3b to area 1 sends mainly textural information, while the projection to area 2 emphasises size and shape (Bear *et al.*, 2007).

Functional imaging studies have shown that the somatosensory and primary motor cortices are frequently co-activated, indicating a close functional integration between these regions (Rowe and Siebner, 2012).

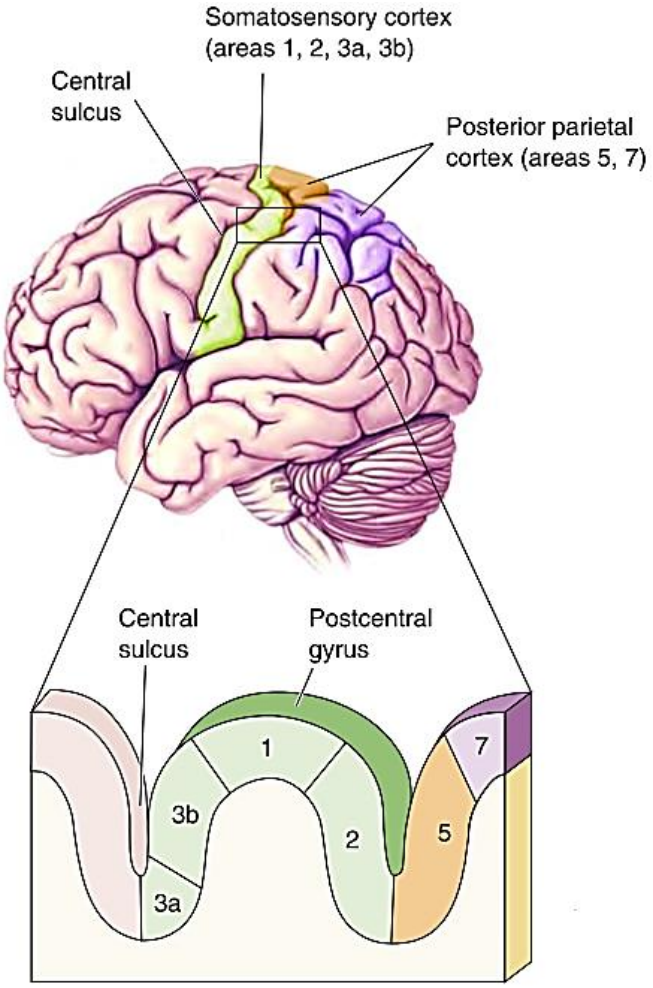

Figure 1.9. Somatosensory region of the cortex located in the parietal lobe, showing the subdivisions of the postcentral gyrus (SI) (Bear *et al.*, 2007).

The PPC includes the superior parietal lobule (SPL) (BA 5 and BA 7), the parietal operculum (BA 43), the submarginal gyrus (BA 40) and the angular gyrus (BA 39). Together the submarginal gyrus and the angular gyrus are known as the inferior parietal lobule (IPL)

(Kolb and Whishaw, 2003). The PPC is connected to the prefrontal cortex (BA 46), and they both project to the same regions of the paralimbic cortex, the temporal cortex, the hippocampus and various cortical regions. BA 5 receives most of its connections from SI. Its cortical outputs are to M1, to SMA, to PM and to BA 7. This region plays some role in guiding movements by providing information about limb position. While BA 7 has a heavy somatosensory input from SI through BA 5, it also receives inputs from M1 and PM, along with a small visual input. Its output connections are similar to those of BA 5, which provide some similar information to the motor system (Kolb and Whishaw, 2003). In general, the PPC plays an important role in the perception and interpretation of spatial relationships, accurate body image, and the learning of tasks involving coordination of the body in space. These functions involve a complex integration of somatosensory information with that from other sensory systems, particularly the visual system (Bear *et al.*, 2007).

1.4 Motor control

The central motor system is arranged as a hierarchy of three control levels, with the forebrain at the top and the spinal cord at the bottom. The function of each level depends heavily on the sensory information received. The highest level, represented by the associated regions of the neocortex and basal ganglia of the forebrain, is concerned with strategy: the goal of the movement and the movement strategy that best achieves that goal. At that level, sensory information generates a mental image of the body and its relationship to the environment. The middle level, represented by the motor cortex and cerebellum, is concerned with tactics such as the sequences of muscle contractions required in space and time to smoothly and accurately achieve the strategic goal. The tactical decisions are based on the memory of sensory information from past movements. The lowest level, represented by the brain stem and spinal cord, is concerned with execution: activation of the motor neuron and interneuron pools that

generate the goal-directed movement and maintain posture, muscle length, and tension by relying on sensory feedback (Kolb and Whishaw, 2003).

1.5 Common Coding theory

The relationship between action and perception has been of interest to scientists for many years. Actions can be represented in terms of the perceptual effects they have on the environment (Hommel, 2009). It is believed that there are certain aspects of perception and action that share a common representational domain, such that action codes are tightly bound to the perceptual codes that represent the effects of those actions. In this way, actions may be planned in terms of their effects and, in the reverse direction, perception of effects can lead to the occurrence of a related action (Prinz, 1997).

The idea that the neural representations of actions and effects are closely related has implications beyond the planning and control of actions in the domain of motor cognition. For example, in action imagination, it has been suggested that bound neural codes can be activated at sub-motor threshold levels such that by imagining the perceptual effects (visual feedback) of an action, the motor components of that action can be effectively rehearsed (Wong *et al.*, 2013; Yoxon *et al.*, 2015). Moreover, it has been demonstrated that the perception of another's actions can activate the cognitive representation of that action (van der Wel *et al.*, 2013). This mechanism allows one to interpret the actions of another, and use this information to make decisions about the action possibility, coordinate one's actions with another or, in a social context, infer intentions or desires (Blakemore and Decety, 2001). However, in all of these processes, motor output is activated at levels that are below the threshold for actual actions to emerge. Effectively, in all of these cases, perceptions or thoughts of perceptions activate simulations of the desired action. That is, the activation of a perceptual representation in turn leads to the activation of the internal components of an action, without acting on the

environment. This approach heavily implicates the neural simulation of action in the success of the motor cognitive processes described.

1.6 Neural Simulation of Actions

Evidence for neural motor simulation in action imagination and perception has been broadly drawn from both neurophysiological and behavioural studies that have reported that the motor system is active in action imagination and perception. Jeannerod, (1995, 2001) suggested that the neural simulation of action could be the singular mechanism underlying various processes associated with motor cognition. In his neural simulation theory, he states the neural simulation of action occurs whenever there is activation of the cortical areas associated with movement in the absence of any voluntary action (Jeannerod, 2001). These simulations are involved in many tasks, ranging from the more conscious simulation in action imagination, to tasks that involve primarily subconscious simulation, such as the observation of a given action, followed by a prediction or judgement about the feasibility of the action. Interestingly, despite the obvious differences in the consciousness of simulation between these two tasks, both have been shown to elicit activation of cortical motor areas. Therefore Jeannerod, (2001) suggested neural simulation of action to be a unifying mechanism for such motor cognitive processes. Furthermore, the neural simulation of action may be an important mechanism for the common representation of action and perception, as proposed in the common coding theory.

1.7 Magnetic Resonance Imaging

Magnetic resonance imaging (MRI) is a relatively new discipline in the field of applied sciences. A main thrust has come from the high-quality imaging of soft tissues in the human body and metabolic processes without radiation, as is necessary for X-ray imaging. MRI is a

powerful imaging tool because of its flexibility, safety and sensitivity to a broad range of tissue properties as well as noninvasive.

All MRI replies on a core set of physical concepts that were discovered by Rabi, Bloch, Purcell and other pioneers during the first half of the twentieth century (Huettel et al., 2008). MRI uses the magnetic properties of tissue to produce an image. It stems from the application of nuclear magnetic resonance (NMR) to radiological imaging. The word (magnetic) refers to the use of an assortment of magnetic fields and (resonance) refers to the need to match the radio frequency of an oscillating magnetic field to the precessional frequency of the spin of some nucleus in a tissue molecule.

1.7.1 A Brief Overview of Nuclear Magnetic Resonance

The source of the resonance in an NMR experiment is that the protons and neutrons that constitute a nucleus possess an internsic angular momentum called spin. All protons, neutrons and electrons have the same angular momentum and it cannot be changed. However, the direction of angular momentum (axis of spin) can be changed. When protons (and neutrons) combine to form a nucleus, they combine in pairs with oppositely oriented spins. Therefore, nuclei with an even number of protons and even number of neutron such as ^{12}C have no net spin because theydistributing the same amount of charge in opposite directions, while nuclei with odd number of protons and odd number of neutrons such as ^{13}C do have a net spin. Hydrogen nucleus has a single proton and thus it has a net spin. It is far more abundant in the body than any other nucleus that makes it the primary focus for MRI (Buxton, 2009).

Consider a single proton of hydrogen atom. In regular conditions, thermal energy lets the proton to spin about its axis (figure 1.10A). This spin motion has two effects: first, its spin creates superficial electrical current, which generates a magnetic source and a torque when it is placed within a magnetic field. The strength of this magnetic source or maximum torque per unit of magnetic field is the magnetic moment (μ). Second, because the proton has an odd

atomic mass number, its spins results in an angular momentum (J). Due to the right-hand rule, both μ and J are vectors pointing in the same direction. As the nucleus spins, the changing magnetic field produces a magnetic moment and the moving mass results in angular momentum (figure 1.10B) (Huettel et al., 2009).

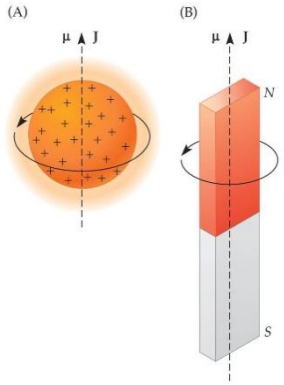

Figure 1.10, Similarities between spinning proton (A) and spinning magnet (B): both have angular momentums (J) and magnetic moments (μ) (Huettel et al., 2009).

In absence of an external magnetic field (B_0), the spin axes of the protons are oriented randomly and tend to cancel each other out as shown in figure 1.11A. Thus the net magnetization (M_0), which is the sum of all magnetic moments from spins of different nuclei orientations, is null. To increase the M_0 of the protons, a strong magnetic field is applied to align the axes of spin of the protons as illustrated in figure 1.11B. However, these protons gain a gyroscopic motion called precession as shown in figure 1.11C. Protons precess around an axis parallel (low-energy) or anti-parallel (high-energy) to the magnetic field with an angle between protons' axes of spin and the direction of the external magnetic field (Huettel et al., 2009). The precession frequency (known as Larmor frequency) is determine by the type of nucleus and it is proportional to the strength of the B_0. The fundamental equation of Larmor frequency v_0 is (Buxton, 2009):

$$v_0 = \gamma B_0 \tag{1.1}$$

Where γ is gyromagnetic ratio (a constant for a given type of nucleus). B_0 is the magnetic field strength.

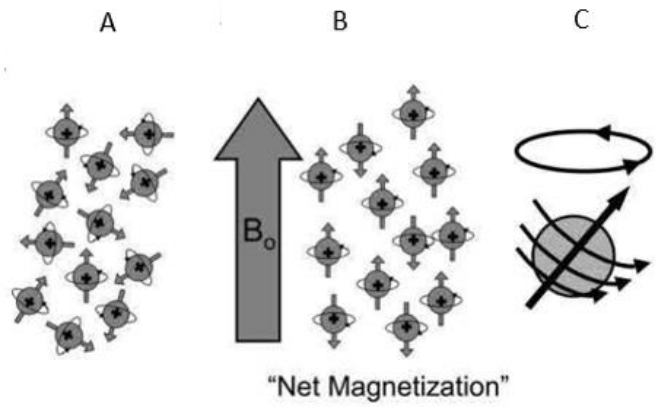

Figure 1.11. (A) In the absence of an external magnetic field, protons are aligned randomly. (B) When an external magnet (B_0) is applied, protons are either aligned along (parallel to) or against (anti-parallel) to magnetic field. A net magnetization will be produced parallel to the main magnetic field. (C) Precession of a proton within a magnetic field (Pooley, 2005).

1.7.2 Excitation

The M_0 of all the nuclei in a volume provides the source for the MR signal. It is analogous to a vector with two components: a transverse component that is perpendicular to the B_0, and it is equal to zero because protons do not spin in phase. The second component is a longitudinal component that is aligned along the longitudinal field direction with a magnitude proportional to the difference between the number of precessions in the parallel and anti-parallel states. Nevertheless, this generates a weak magnetization and cannot directly measured under the equilibrium conditions because it is many orders of magnitude weaker than B_0 (Huettel *et al.*, 2008, Carter and Shieh, 2015).

To measure M_0, a radiofrequency (RF) pulse oscillating at Larmor frequency is applied to produce a magnetic field B_1 perpendicular to B_0. The field B_1 is several orders of magnitude smaller than B_0. Nevertheless, this causes disturbances among the low-energy nuclei (parallel aligned with B_0) because some of them will absorb the electromagnetic energy and jump to a high-energy state (anti-parallel), effectively converting the longitudinal magnetization into transverse magnetization. This process known as excitation (Buxton, 2009). Within each

precessional rotation, M_0 tips farther away from B_0, tracing out a widening spiral as shown in figure 1.12.

These RF pulses are regularly characterized by the flip angle (α) they make. The flip angle can be controlled by the strength and duration of the RF pulse. This pulse is generated by a transmitter coil.

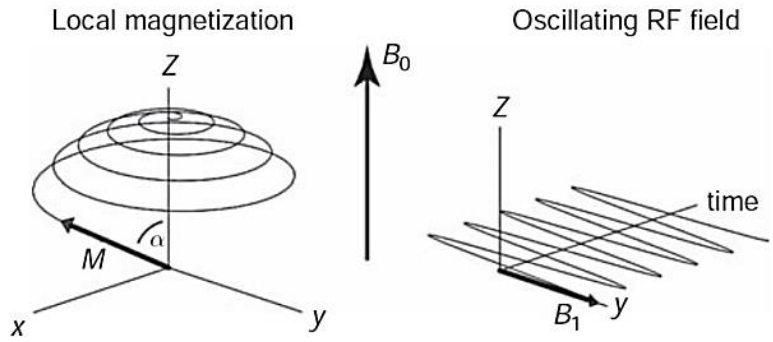

Figure 1.12. The excitation of the M_0 by applying a radiofrequency (RF) pulse. The RF pulse is a small oscillating field B_1 perpendicular to B_0 that cause M_0 to tipped away from the longitudinal axis by a flip angle (α) (Buxton, 2009).

1.7.3 Relaxation

When the RF pulses are turned off, the excitation of the nuclei stops. Some of these high-energy nuclei will return to low state by emitting an electromagnetic oscillation equals to the energy difference between these two states, so that the equilibrium can be restored. Eventually, the longitudinal magnetization increases to its original value, while the transversal magnetization decreases to zero by losing its coherence (Carter and Shieh, 2015). The emitted energy provides the MR signal data and it can be detected using a radiofrequency coil tuned to Larmor frequency. This signal detected through receiver coils does not remain stable forever (Huettel et al., 2008). These changes known as relaxation, and it divided into longitudinal relaxation and transverse relaxation.

1.7.3.1 Longitudinal Relaxation

Following the excitation, the longitudinal magnetization is zero. The magnetization then begins to recover back in the longitudinal axis. This is called longitudinal relaxation or T_1 relaxation. It is relatively slow; typically form a few hundred milliseconds to a few seconds. The recovery rate is characterized by the tissue-specific time constant T_1, which corresponds to the time taken for the magnetization to recover to 63% of its equilibrium value as shown in figure 1.13 (Pooley, 2005; Huettel et al., 2008).

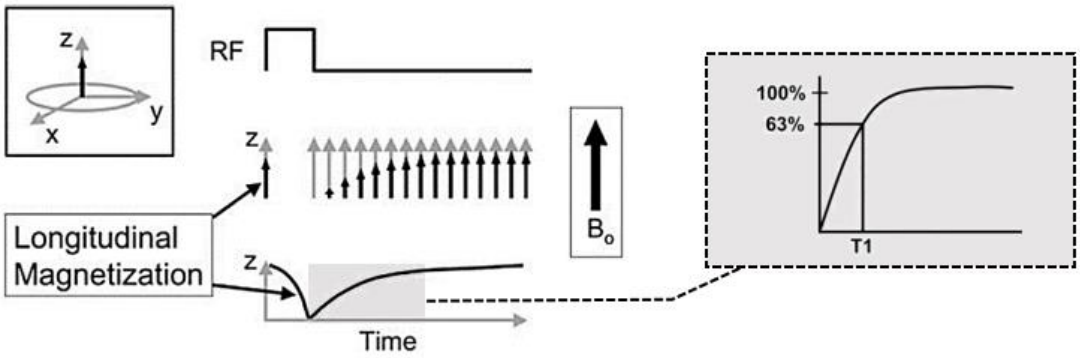

Figure 1.13. Longitudinal (T_1) relaxation. The excitation causes longitudinal magnetization to become zero. Once the RF pulse ceases, the longitudinal magnetization will return in a direction parallel to the main magnetic field by releasing energy to the surrounding environment. The gray box illustrates the definition of T_1, which is the time that it takes the longitudinal magnetization to grow back to 63% of its final value (Pooley, 2005).

1.7.3.2 Transverse Relaxation

During the excitation, the net magnetization, which reflects the vector sum of individual spins, being greatest because the protons begin to precess at the same phase and frequency. However, over time, the spin-spin interaction causes changing in the precession frequency that leads spins to lose coherence and therefore an exponential decay in the MR signal that is known as T_2 decay. Furthermore, magnetic field inhomogeneities will cause different spins to precess at slightly different Larmor frequency according to equation 1.1, leading to addition decay in T_2. The combined effects of spin-spin interaction and magnetic field inhomogeneities called

T_2^* and result in spins dephase relatively quickly (typically within a few tens of millisecond) and diminishing net magnetization in transverse axis as illustrated in figure 1.14. The transverse relaxation (T_2) corresponds to the time taken for the transverse magnetization to drop to 37% of its initial size (Pooley, 2005; Huettel *et al.*, 2008).

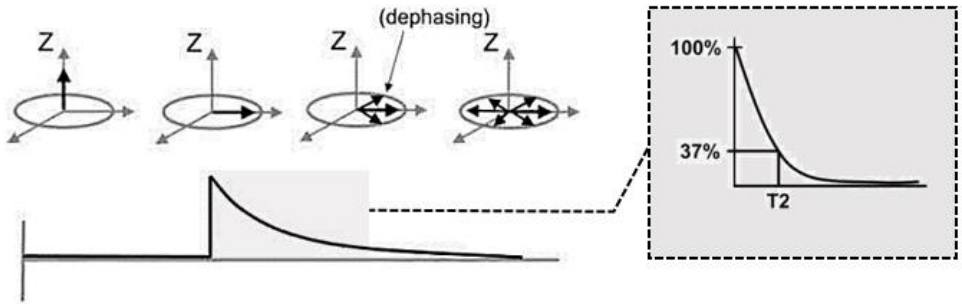

Figure 1.14. Transverse (T_2) relaxation. Immediately after the excitation, transverse magnetization is maximized; it then begins to dephase and the resultant MR signal decreases. The gray box illustrate Definition of T_2 which is defined as the time that it takes the transverse magnetization to decrease to 37% of its starting value (Pooley, 2005).

1.7.4 Image Acquisition

MR images can be generated by dividing the acquired MR signal into components with different frequencies and phases in a method known as spatial encoding. This encoding relies on manipulating the local resonant frequency through the control of local magnetic field by applying magnetic field gradients to resolve spatial information in three dimensions (x, y and z). Therefore, in an MR scanner, there are three gradient coils in addition to the RF coils and the coils of the magnet (B_0) itself. Each gradient coil produces a magnetic field that varies linearly along a particular axis (Buxton, 2009).

Spatial localization is made in three steps: slice selection, phase encoding and frequency encoding, each step is related with one gradient: slice selection gradient (Gz), phase encoding gradient (Gy) and frequency encoding gradient (Gx).

In the first step (slice selection), a gradient (Gz) is turned on along the slice selection axis (z-axis, perpendicular to the desired slice), consequently the precession frequency of the protons varies linearly along the z direction. An RF pulse is simultaneously applied with a bandwidth that matches the range of precession frequencies in the desired slice plane. This causes a shift in the net magnetization of the protons in this plane. As no protons located outside the slice plane are excited, they will not emit a signal. Immediately after the excitation, the affected spins begin to undergo T_1 and T_2 relaxation processes (Huettel *et al.*, 2008).

Once a slice is selected, all excited spins contribute to the MR signal. Thus, the next step is to apply additional gradients that cause spins at different spatial locations to precess at different frequencies so that their individual contribution can be measured and identified. During the interval between the RF pulse and the data acquisition, a phase encoding or a gradient field (Gy) is applied in the vertical direction (y-axis) of the slice selected in the first step. While it is applied, it modifies the spin resonance frequencies, inducing dephasing, which persists after the gradient is interrupted. After this step, all the protons precess in the same frequency but each local precessing magnetization is marked with a phase offset proportional to its y-position.

During a frequency-encoding step, a gradient field (Gx) is applied in the horizontal direction (x-axis) of the slice selected in the first step. This gradient modifies the spin resonance frequencies along the horizontal direction. It thus creates proton columns, which all have an identical Larmor frequency. This gradient is applied during the data acquisition period as shown in figure 1.15 (Buxton, 2009).

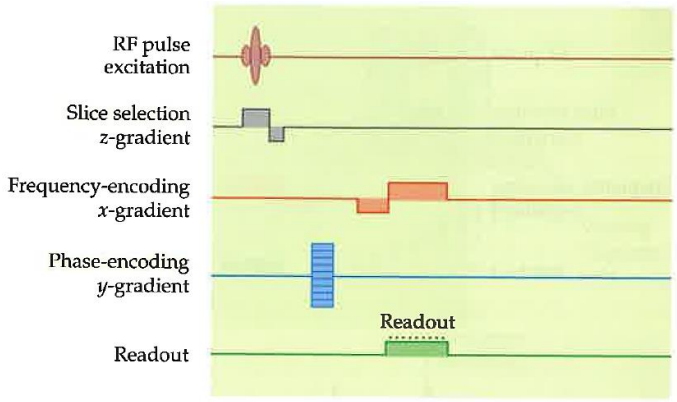

Figure 1.15. A schematic diagram of imaging pulse sequence. During the FR pulse, a Gz is applied (slice selection), and during the read-out of the MR signal, a Gx is applied (frequency encoding) and between these two encodings a Gy is applied (phase encoding) (Huettel *et al.*, 2008).

1.7.5 Image Reconstruction

The acquired data of a given slice, which are a mix of RF signals with different amplitudes, frequencies and phases, are stored in the k-space (spatial frequencies) and they require a 2D inverse Fourier Transform to create a spatially informative image of the slice. The central portion of k-space describes the low-spatial-frequency components, which in image space is a low-resolution image. On other hand, the outer edges describe the high frequencies, which determine image brightness as illustrated in Figure 1.16 (Buxton, 2009).

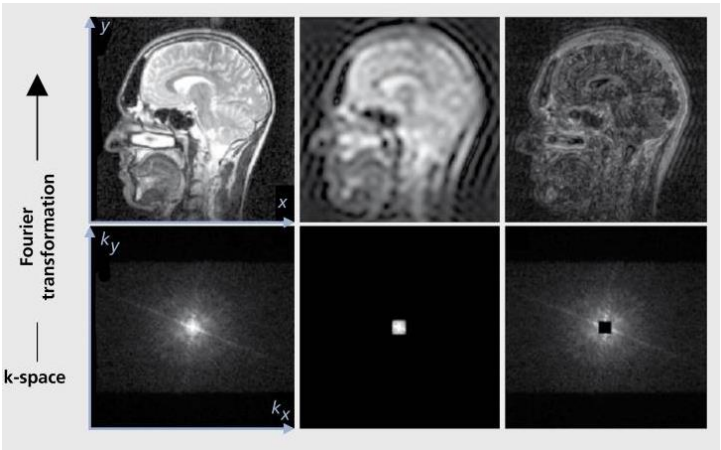

Figure 1.16. The contribution of different parts of k-space to image space (Schad, 2004).

1.7.6 MR pulse Sequences

The arrangement of radiofrequency pulses and magnetic gradients used to collect the MR signal is known as a pulse sequence. The basic format of a pulse sequence diagram consists of a series of horizontal lines, each representing how a different component of the scanner changes over time as shown in figure 1.15. These components are essential for any imaging sequence and they consist of an RF excitation pulse, gradients for spatial encoding and signal acquisition. When performing an image acquisition (Huettel et al., 2009).

1.7.6.1 Conventional Imaging sequences

There are two primary types of imaging sequences, which are:

- Spin-echo imaging

Spin-echo (SE) sequences use a second 180^{o} RF pulse called refocusing pulse to compensate for spins dephasing caused by magnetic field inhomogeneity. The refocusing pulse is applied at one-half of the TE time. The SE pulse sequence can produce PD- weighting, T_1-weighting, and T_2-weighting (Pooley, 2005; Huettel *et al.*, 2008)

- Gradient-echo imaging

Gradient-echo (GE) sequences use a single RF pulse of less than 90^{o} without 180^{o}. The smaller flip angle and lack of 180^{o} RF pulse allow the TR to be much shorter which leads to fast imaging times. Even though there is no 180^{o} RF pulse to produce a spin echo, gradient pulses can be used to dephase and rephase the signal in the transverse magnetization. In this case, T_1 and T_2^* image contrast can be generated weighting (Pooley, 2005; Huettel *et al.*, 2008).

1.7.6.2 Fast imaging sequences

To understand the function of the brain, fast pulse sequences have been developed to acquire large number of images within a short time period, at approximately the same rate as

the physiological change of interest. These sequences use variants of gradient-echo approaches and they are sensitive to T_2^* contrast.

The most common fast imaging sequence for fMRI is Echo-Planar Imaging (EPI). It generates a rapid series of gradient echoes to fill the k-space in a back and forth pattern as shown in figure 1.17. EPI requires strong gradients and rapid switching capabilities, since different sets of gradients must be cycled to enable the 90° turn in k-space pattern. The initial negative gradients pulses (G_x and G_y) move the sampling in k-space to bottom left. After that a repeated gradient echo produces a back and forth trajectory through k-space (Huettel *et al.*, 2008; Buxton, 2009).

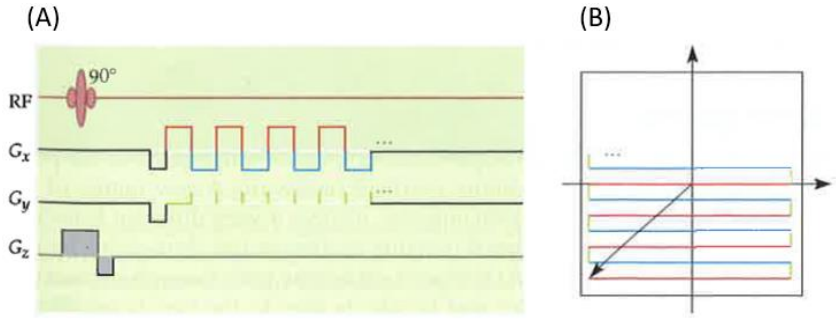

Figure 1.17. An EPI sequence (A) and its k-space trajectory (B). The black arrow in the k-space represents the initial negative G_x and G_y gradients used to move to the bottom left of k-space.

1.7.7 Contrast and Weights

Static contrasts have been widely used in MRI because of their ability to explain basic tissue characteristics. It can be defined as the intensity difference between two types of tissues. These contrasts can be derived using the fundamental concepts of T_1 and T_2 recovery. Following the excitation, the longitudinal and transverse magnetizations can be described as:

Longitudinal magnetization (Huettel *et al.*, 2008)

$$M_z(t) = M_0\left(1 - e^{-\frac{t}{T_1}}\right) \qquad 1.2$$

Transverse magnetization

$$M_{xy}(t) = M_0 e^{-\frac{t}{T_2}} \quad 1.3$$

Where T_1 and T_2 are time constants shown in table 1.1 for a magnetic field strength of 1.5T.

When performing an image acquisition, there are two factors need to be considered. The first factor is the repetition time (TR) which is the time interval between two consecutive excitation pulses, usually expressed in seconds. Often, consecutive excitations occur at time intervals not long enough to make full recovery of the longitudinal magnetization. Thus, under such short TR, the transverse magnetization can be described as:

$$M_{xy}(t) = M_0 \left(1 - e^{-\frac{TR}{T_1}}\right) e^{-\frac{t}{T_2}} \quad 1.4$$

The second factor is the echo time (TE) which is the time interval between excitation and data acquisition, usually expressed in milliseconds. Thus, by replacing the term (*t*) in equation 1.4 with TE to give the MR signal for an image with a given TE:

$$M_{xy}(t) = M_0 \left(1 - e^{-\frac{TR}{T_1}}\right) e^{-\frac{TE}{T_2}} \quad 1.5$$

The above equation provides the foundation for manipulating the MR signal from a particular tissue by controlling TR and TE. However, in MRI, the contrast between multiple tissue types is important and it can be expressed as the difference between the MR signals associated with each as described in equation 1.6

$$C_{AB} = M_{0A} \left(1 - e^{-\frac{TR}{T_{1A}}}\right) e^{-\frac{TE}{T_{2A}}} - M_{0B} \left(1 - e^{-\frac{TR}{T_{1B}}}\right) e^{-\frac{TE}{T_{2B}}} \quad 1.6$$

Where C_{AB} is the contrast between two types of tissue (A and B), M_{0A} and M_{0B} are the net magnetization for tissue A and B, T_{1A} and T_{1B} are the T_1 values for A and B, and T_{2A} and T_{2B} are the T_2 values for A and B.

Table 1-1. Rough values for the time constant T_1 and T_2 at field strength of 1.5T (Huettel *et al.*, 2008).

Time constant	Gray matter	White matter	Cerebrospinal fluid
T_1	900ms	600ms	>2000ms
T_2	100ms	80ms	2000ms

1.7.7.1 Proton Density Imaging

Proton-density (PD) imaging or PD-weighting provides contrast based on the sheer number of protons presented within a voxel, which differ in different tissue types. To maximize the PD-weighting, a pulse sequence with a TR value greater than T_1 and a TE value less than T_2 is used as shown in figure 1.18 (Huettel *et al.*, 2008). When the TR is much greater than T_1, the term (e^{-TR/T_1}) from equation 1.6 becomes 0 and when the TE is much less than T_2, the term (e^{-TE/T_2}) from equation 1.6 approaches 1. The resulting equation for PD-contrast is:

$$C_{AB} = M_{0A} - M_{0B} \qquad 1.7$$

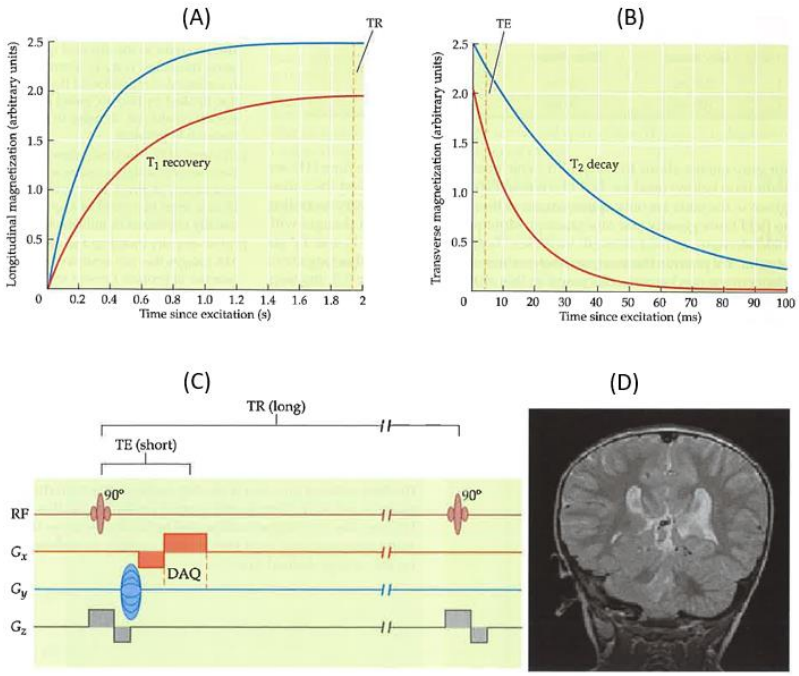

Figure 1.18. Selection of long TR value (A) and short TE value (B) for PD imaging, shown as vertical dashed lines on two different tissue types (red and blue). (C) A pulse sequence used for PD imaging. (D) The resulting brain image using a very long TR and a very short TE (Huettel *et al.*, 2008).

1.7.7.2 T_1-weighting

The T_1-werighted image provides structural contrast for anatomical images of the brain based on the T_1 values of the tissues. T_1-weighted images can be obtained by using an intermediate TR value that maximizes the difference in T_1-contrast between different tissue types and a very short TE value to minimize T_2 contrast (TE much less than T_2) as shown in figure 1.19. Therefore, equation 1.6 can be rewritten as (Huettel *et al.*, 2008):

$$C_{AB} = M_{0A}\left(1 - e^{-\frac{TR}{T_{1A}}}\right) - M_{0B}\left(1 - e^{-\frac{TR}{T_{1B}}}\right) \qquad 1.8$$

In the above equation C_{AB} depends on TR but not TE and also, the proton density of the tissue always contribute to the contrast.

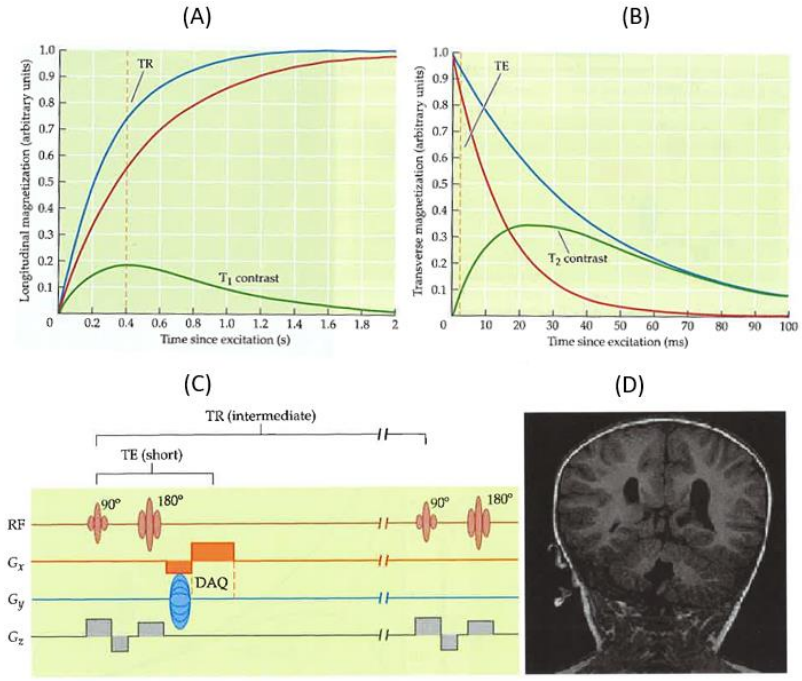

Figure 1.19. Selection of an intermediate TR value (A) and a short TE value (TE) for T_1-weighting shown as vertical dashed lines on two different tissue types (red and blue), the green lines show the relative contrast associated with different TR and TE. (C) A spin-echo pulse sequence used for T_1-weighted images. (D) The resulting brain image using an intermediate TR and a very short TE (Huettel *et al.*, 2008).

1.7.7.3 T_2-weighting

The T_2-weighted images have maximal signal in fluid-filled regions such as CSF and ventricles, which is important for many clinical application such as tumours. In T_2-weighted images, the amount of signal loss depends on the time between excitation and data acquisition. T_2-weighted images can be generated using a very long TR to minimize the T_1-contrast (TR is much greater than T_1) and an intermediate TE value to maximize the T_2 contrast between different tissue types as shown in figure 1.20. Thus, the resultant formula is completely depends on the TE value as described below (Huettel *et al.*, 2008):

$$C_{AB} = M_{0A}e^{-\frac{TE}{T_{2A}}} - M_{0B}e^{-\frac{TE}{T_{2B}}} \qquad 1.9$$

These images can only be obtained using a spin-echo pulse sequence. This sequence allows for true spin-spin relaxation by introduces 180° pulse at halfway time between excitation and TE to reverse the loss of phase coherence caused by field inhomogeneity.

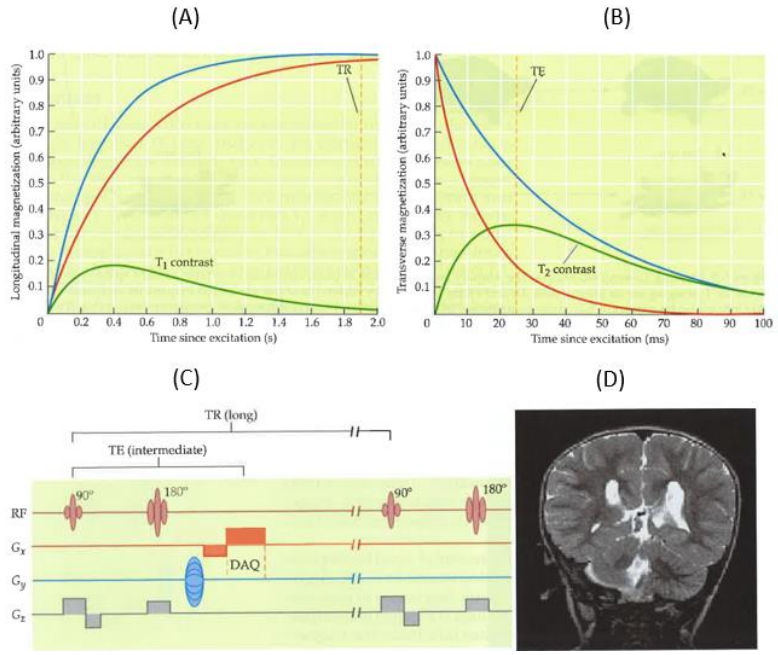

Figure 1.20. Selection of a very long TR value (A) and an intermediate TE value (TE) for T_2-weighting shown as vertical dashed lines on two different tissue types (red and blue), the green lines show the relative contrast associated with different TR and TE. (C) Only spin-echo pulse sequence (with 180° refocusing pulse) is used for T_2-weighted images. (D) The resulting brain image using a very long TR and an intermediate TE (Huettel *et al.*, 2008).

1.7.7.4 T_2^*-weighting

The T_2^*-weighted images are sensitive to the amount of deoxygenated haemoglobin which changes according to the metabolic demands of active neurons and hence, it is the contrast basis for fMRI. Like T_2- weighted images, T_2^*-contrast is provided by pulse sequences with long TR and medium TE values. An additional requirement is that these pulse sequence use magnetic field gradients to generate the signal echo, instead of refocusing pulses, which eliminate field inhomogeneity effects (Huettel et al., 2009).

1.8 Functional Magnetic Resonance

Functional Magnetic Resonance Imaging (fMRI) is one of the remarkable developments of MRI. It is an indirect approach to imaging brain activity, conducted at high spatial resolution. fMRI relies on detecting changes in the metabolic state of the brain by using MR signals. Since the early 1990's, this technique has grown explosively to become an indispensable tool in neuroscience research (Ogawa *et al.*, 1990).

1.8.1 Physiological basis of neural activation and MR signal

fMRI does not detect neural activity, but it measures the physiological changes that are associated with neuronal activity. The neuronal activity induces an increase in oxygen consumption, and subsequently the cerebral blood flow (CBF), the blood volume (CBV) and the cerebral metabolic rate of oxygen (CMRO2) increase. Accordingly, the local oxygen extraction fraction (E) reduces, leading to an increase in O_2 content of the capillaries and veins. Therefore, neuronal activity is expressed in terms of a relative increase in oxyhaemoglobin compared to deoxyhaemoglobin (Huettel et al., 2008), as explained in figure 1.21.

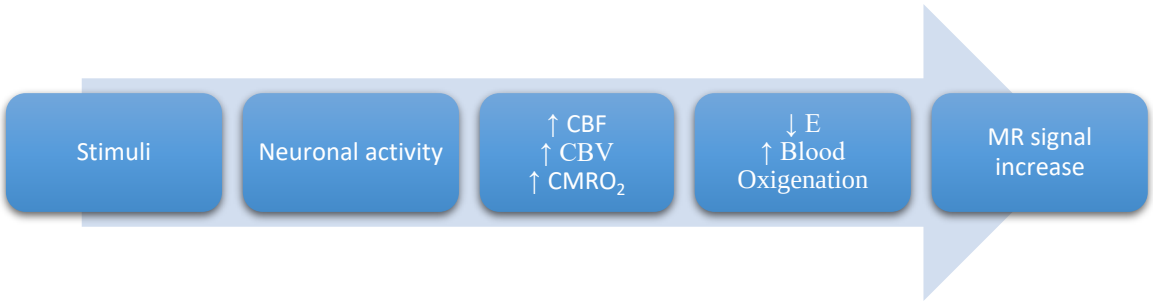

Figure 1.21. The physiological basis of the MR signal (adapted from Buxton, 2009).

In 1982, Thulborn and colleagues demonstrated T_2^* relaxation changes in blood samples due to the magnetic susceptibility variations caused by the presence of paramagnetic deoxyhaemoglobin (Edelman, 2006). Therefore, the relative increase in oxyhaemoglobin concentration can be detected by MRI as a weak transient rise in the T_2^* weighted signal. This signal change is known as a blood oxygenation level dependent (BOLD) signal.

1.8.2 The BOLD haemodynamic response

A changes in BOLD signal caused by neural activity is known as a haemodynamic response (HDR). The shape of HDR varies with the stimulus properties and the underlying neuronal activity. Increasing the neuronal activity would therefore increase the HDR amplitude, whereas increasing the duration of neuronal activity would increase the HDR width. The underlying physiology of the BOLD response (shown in figure 1.22) can be summarised in three stages (Huettel *et al.*, 2008):

- **Initial dip**: of 1 to 2 seconds duration that has been attributed to the transient increase in the amount of deoxygenated haemoglobin and transient decrease in blood volume produced by the very rapid capillary dilatation in the voxel.
- **Peak:** After a short latency, the metabolic demands due to the increased neuronal activity over baseline levels result in an increased inflow of oxygenated blood. In another words, more oxygen is supplied to the area than is extracted, resulting in a decrease in the concertation of deoxygenated haemoglobin. Therefore, the BOLD

signal increases above the baseline about 2 seconds after the onset of the neuronal activity, rising to a maximum value at about 5 seconds.

- **Undershoot:** After the neuronal activity has discontinued, the BOLD signal decreases in amplitude to below the baseline level, and remains below baseline for an extended interval.

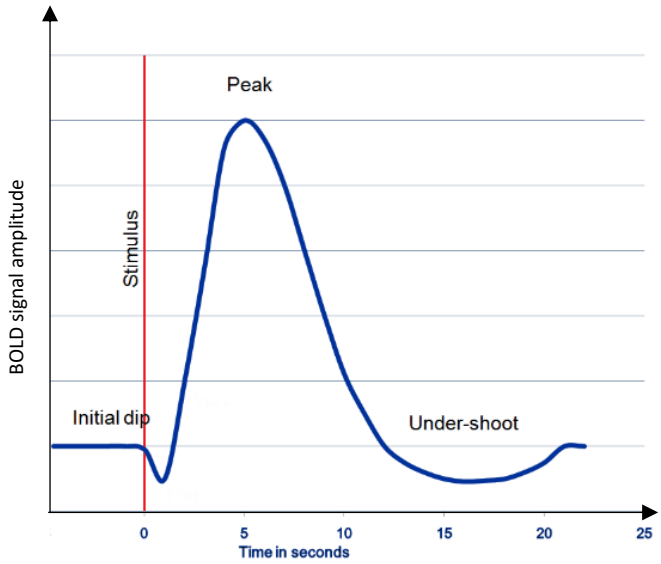

Figure 1.22. Schematic representation of BOLD haemodynamic response.

1.8.3 Decoding Neural Responses

Information is encoded in our brain as pattern of neural responses (Tong and Pratte, 2012). This information can be gleaned from interactions with the outside world, or can be generated by internal processes such as thinking. One of the great challenges for cognitive neuroscience is to develop algorithms for decoding neural activity, and decipher this information. Computational algorithms for encoding information into neural activity and extracting information from measured activity afford us an understanding of how percepts, memories, thought, and knowledge are represented in patterns of brain activity.

Conventional neuroimaging analysis methods have focused on characterising the relationship between cognitive tasks and brain regions, thus they are known as univariate

approaches. These methods look for clusters of neighbouring voxels that show a statistically significant response to the experimental conditions, and group analysis is typically performed after anatomical alignment of individual brains and sufficient spatial smoothing to overcome between-subject anatomical variability. Although the univariate approach reduces noise, it also reduces signal by neglecting the information carried by voxels with weaker (i.e. non-significant) responses to a particular condition. In addition, the spatial smoothing blurs out fine-grained spatial patterns that might discriminate between experimental conditions (Friston et al., 1995b; Kriegeskorte et al., 2006).

The past 15 years have seen significant advances in the development of methods for decoding human neural activity, such as multivariate pattern analysis (MVPA), representational similarity analysis (RSA), hyperalignment, and stimulus-model-based encoding and decoding. The introduction of MVPA has revolutionised fMRI research by changing the research question from what a region's function is, to what information is represented in a region and how that information is encoded and organised (Haxby et al., 2014). MVPA uses machine learning methods to distinguish patterns of neural activity that are distributed across neurons or cortical regions and are associated with different stimuli or cognitive states (Haxby *et al.*, 2014), as shown in figure 1.23.

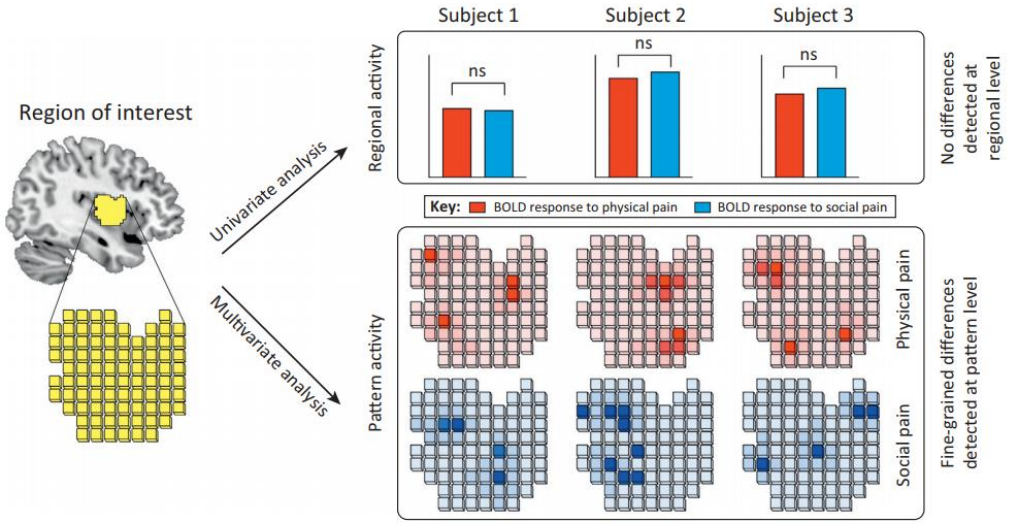

Figure 1.23. Univariate vs multivariate analysis of fMRI data (Iannetti *et al.*, 2013).

1.9 Themes and Aims

The aim of this thesis is to decode and align the motor representation of multi-joint arm actions based on different modalities of motor simulation, for instance Motor Imagery (MI) and Action Observation (AO) using functional Magnetic Resonance Imaging (fMRI), and to explore the feasibility of using real-time fMRI neurofeedback to alter these action representations.

In order to achieve this goal, I attempt to answer two related but distinct questions:

- Can a multivariate pattern analysis be used to decode different representational spaces associated with different actions and modalities, and to construct a common representational space of the frontal and parietal motor regions using hyperalignment? This question is addressed in experimental chapters 4 and 5.
- Can a real-time fMRI neurofeedback system be implemented for the purpose of manipulating cognitive processes in real-time, and thus achieve mechanistic and causal changes of the brain functions as well as behavioural functions? This question is addressed in experimental chapters 6 and 7.

In the first experimental chapter, the neural representations of natural multi-joint actions (lift, knock and throw) were examined using fMRI in the left motor region. This was achieved by acquiring the neural responses to brain states during motor imagery (MI) and action observation combined with motor imagery (AO+MI) tasks involving the three natural actions, and during an AO+MI task of 25 blended actions. The blended actions' neural responses were used to derive hyperalignment parameters, and allow us to map subjects' representational spaces of an independent MI task into a common representational space. Further analysis was conducted to assess the order in which participants entered the hyperalignment algorithm on creating a common model representational space. Finally,

hyperalignment was validated based on between-subject classification (BSC) of the neural response patterns.

In the second experimental chapter, the hyperalignment algorithm was extended to align motor and motor-related regions. This was carried out by addressing the problems of localisation and cortical parcellation in extending hyperalignment to the fronto-parietal motor regions, using cortex based alignment prior to the hyperalignment. Further to this, the shared neural code between AO+MI and MI tasks of different hand actions were investigated using RSA.

The third and fourth experimental chapters focus on the use of fMRI neurofeedback to modulate brain activation. In the third experimental chapter, phantom limb pain patients were trained to use fMRI neurofeedback to down regulate the activity of premotor (PM) and anterior cingulate (ACC) cortices, and it was assessed whether the successful modulation reduced pain intensity.

In the fourth experimental chapter, fMRI neurofeedback was used to train healthy participants to up-regulate SMA activation during an MI task of complex body actions, and the behavioural changes (motor reaction time) caused by a successful modulation were explored.

In summary, this thesis extends the use of hyperalignment to the fronto-parietal motor regions, and validates it at different levels of motor representation. Moreover, it sheds light on the effect of AO on MI by examining the neural representations of AO+MI and MI tasks. In addition, the studies in this thesis provide proof-of-principle of using fMRI neurofeedback to reduce pain in clinical settings, and enhance motor functions in healthy populations, with the potential for longer-term translation into clinical environments.

Chapter 2 : Literature Review

Theme 1: Action simulation and common model space

2.1 Introduction

fMRI allows us to examine cortical structures at a high degree of spatial resolution, letting us explore the neurobiology of brain regions and investigate the connectivity of cortical–subcortical networks (Koush et al., 2013). The superior spatial resolution enables MVPA to decode subtle differences between stimulus-evoked activity patterns, to discriminate between spatially overlapping populations, and to study action specificity of neural representations. Using this analysis technique, the patterns evoked across groups of fMRI voxels by the viewing, imagining or performing of specific actions can be distinguished and aligned to a common functional model.

2.2 Motor Simulation

Motor simulation can be defined as the internal representation of a motor programme without any overt actions (Jeannerod, 2001). It has two major modalities: motor imagery (MI), which is defined as imagining the execution of an action without any physical output, and action observation (AO) which means watching others performing actions. MI can be divided into two different modalities: visual imagery (VI) and kinaesthetic imagery (KI) (Guillot *et al.*, 2009). VI involves the self-generation of actions from a first (internal VI) or third (external VI) person perspective. During the first person perspective (IVI), people visualise the action as it would happen in real-life, and see images ‘as if through their own eyes’. During external visual

imagery (EVI), people imagine, like spectators, the action that somebody is performing. In contrast, KI includes the sensations of how it feels to perform an action, including the force and effort perceived during movement. This can only be experienced with an IVI (Vogt *et al.*, 2013). A large body of research has examined the advantages of MI in aiding elite athletic performance (Williams *et al.*, 2015), improving motor ability in healthy and clinical populations (for review see: Schuster *et al.*, 2011), skill acquisition (Lotze and Halsband, 2006) and rehabilitation (Ietswaart *et al.*, 2011). Similarly, AO has gained increasing attention since early 2000s following the discovery of the mirror neuron system (MNS) in monkeys (Gallese *et al.*, 1996; Rizzolatti *et al.*, 1996) and in humans (Fabbri-Destro and Rizzolatti, 2008). Mirror neurons fire both when an action is physically performed and when it is being observed. AO plays an important role in motor learning through imitation (Buccino *et al.*, 2004) and has been used in neurorehabilitation (Buccino, 2014) and in consolidation of motor memories (Zhang *et al.*, 2011).

An activation likelihood estimation (ALE) analysis highlighted that MI and AO recruit motor and motor related regions which overlap extensively with one another, and overlap with the regions involved in motor execution (ME) (Caspers *et al.*, 2010; Hétu *et al.*, 2013; Hardwick *et al.*, 2017). The conjunction analysis across MI, AO and ME has identified a consistent activation in the fronto-parietal motor network, in areas including:

- **Premotor Cortex (PM)**: A bilateral ventral premotor (vPM), dorsal premotor (dPM) and supplementary motor area (SMA) shown to be consistently involved during MI, AO, and ME. The PM plays important roles in the planning, preparation and execution of actions (Hoshi *et al.*, 2007). Imagined and executed actions require almost the same amount of time to be performed, suggesting that MI also includes planning and preparation phases with an inhibitory execution (Guillot and Collet, 2017). vPM is believed to play a major role in fine motor coordination (Davare *et al.*, 2009), while

dPM has a limited contribution towards movement execution (Dum and Strick, 2005), and therefore is proposed to play a role in action selection (Rushworth *et al.*, 1998). SMA is the medial region of the PM, and it is associated with linking conditional roles with actions (i.e. where an action A is performed by a condition B) (Nachev *et al.*, 2008), and internally initiated movements that require sequences of actions (Nachev *et al.*, 2007; Hoffstaedter *et al.*, 2013).

- **Primary Motor Cortex (M1)**: The involvement of M1 in action simulation is controversial. Caspers et al., (2010) found evidence that M1 may only be recruited during action observation when participants view actions with the intention to imitate them. Similarly, Hétu et al., (2013) found no evidence of consistent recruitment of M1 during motor imagery, and Hardwick et al. (2017) found consistent involvement of M1 only during ME. Jeannerod (2001) reported that M1 activation during MI and AO was less than during ME, suggesting that M1 may be active at a different, lower level, which is not sufficient to induce a local maxima (Lotze and Halsband, 2006).
- **Somatosensory Cortex**: The involvement of the somatosensory cortex during MI reflects kinaesthetic aspects of motor imagery, while in AO, its recruitment is proposed to extend the mirror properties beyond the motor system (Keysers and Gazzola, 2009). In ME, sensory input provides critical feedback for the accuracy of the movements, allowing comparison between the actual and expected sensory consequences of movements (Muckli and Petro, 2017).
- **Parietal Cortex**: The parietal cortex is an important multisensory hub involved in processing visuomotor information for the online control of movements, guided by a visual input (Block *et al.*, 2013). In Block et al (2013), the bilateral inferior parietal lobule region (IPL) was consistently activated across all modalities. IPL is involved in various cognitive functions, such as the processing of tactile information (Klann *et al.*,

2015) and storing several motor representations that are organised somatotopically (Cooke *et al.*, 2003; Rozzi *et al.*, 2008). The involvement of IPL reflects the interaction between the parietal and premotor cortices during visumotor control of motor functions, and the internal recruitment of these motor representations (Wise *et al.*, 1997).

Although distinct brain structures are identifiable for AO, MI and ME individually (Lorey *et al.*, 2013; Filimon *et al.*, 2015), the ALE analysis identified that a wide network of regions were active during both MI and ME, including the cerebellum, basal ganglia, and mid-cingulate cortex (Hardwick *et al.*, 2017). The cerebellum contains multiple representations of the body, and Lobule VI contains body representations that are most prominent during movement execution (Schlerf *et al.*, 2010). The basal ganglia are associated with response selection and speed of imagined and executed actions. Both MI and ME recruited regions of mid-cingulate cortex that are proposed to play a role in movement production.

While the majority of previous research has focused on MI or AO as independent approaches, or on the similarities and differences between these two forms of motor simulation, there is now an emerging body of research showing the potential advantages for MI guided by AO (AO+MI) (Vogt *et al.*, 2013; Eaves *et al.*, 2016). AO+MI involves imagining the physiological sensations and kinaesthetic experiences of actions (MI task), and synchronising these with the congruent observed action (AO task). Combining these two modalities into one (AO+MI) could engage more of the frontal-parietal network than is involved in ME, and give greater control over the content and vividness of action simulation (Holmes and Calmels, 2008). Few studies have examined the recruited cortical brain regions during AO+MI, MI and AO (for review see (Eaves *et al.*, 2016)). Macuga & Frey (2012) reported that brain regions recruited in AO are a subset of those involved in AO+MI, which in turn are a subset of those involved in imitation. Nedelko et al. (2012) and Villiger et al., (2013) also reported that AO+MI increased neural activity over the AO in parts of the cerebellum, inferior frontal gyrus, inferior

parietal cortex, SMA, vPM and left insula. Taube et al. (2015) showed that AO+MI had a greater neural activity in the caudal supplementary motor area (SMA), basal ganglia, and cerebellum compared to AO; and in the bilateral cerebellum and precuneous compared to MI. AO+MI has been used as a tool to improve performance in a golf putting task (Smith and Holmes, 2004) and a bicep curl strength test (Wright and Smith, 2017) over 6 weeks of intervention. Clinically, AO+MI has been used in rehabilitation programs, but it has shown a mixed effect. Small scale studies have targeted stroke patients with upper limb motor dysfunction, and these have provided promising results in terms of improvement in motor functions over 4 weeks intervention (Ertelt *et al.*, 2007; Sun *et al.*, 2016). However, Ietswaart et al. (2011) reported that AO+MI intervention did not enhance motor recovery of stroke patients with persistent upper limb motor weakness. An interesting next step could now involve a more in-depth examination into the precise anatomical substrates involved in different AO+MI tasks, using multivariate pattern analysis (MVPA) of fMRI data.

2.3 Multivariate Pattern Analysis

In the last few years, there has been increasing interest in fMRI studies that have used multivariate pattern analysis (MVPA) to look at the pattern of neural responses across multiple voxels that carry information about the experimental conditions (Haxby *et al.*, 2001; Haynes and Rees, 2006; Norman *et al.*, 2006). MVPA uses machine learning techniques to classify patterns of neural responses associated with different stimuli or cognitive states, and it has more sensitivity to detect fine scale information than traditional univariate analyses. Classification performance depends mainly on:

- The number of voxels included in the analysis. The decoding performance decreases dramatically as the number of voxels exceeds the number of time points. Therefore, it is essential to select only the informative voxels involved in processing the experimental conditions. As a result, the MVPA approach contains a feature selection

step prior to the classification, in which only a subset of voxels is included (Cox and Savoy, 2003).

- The Classifier (for review see (Misaki *et al.*, 2010)). The majority of MVPA studies have used linear and non-linear classifiers, such as correlation-based classifiers (Haxby *et al.*, 2001), neural networks without a hidden layer (Polyn. Sean M. *et al.*, 2005), linear discriminant analysis (LDA) (Haynes and Rees, 2005; Mandelkow *et al.*, 2016), support vector machines (SVM) (Song *et al.*, 2011; Pilgramm *et al.*, 2016), and multinomial sparse logistic regression (Shibata *et al.*, 2011).

The first pioneering work on MVPA, by Haxby et al. (2001), showed that categorical information (faces, animals, and objects) was associated with distinct patterns of brain activity within the ventral temporal lobe. Subsequent studies targeting the visual regions have shown that MVPA can also discriminate between other cognitive states. For example Kamitani & Tong (2005) reported that activity patterns in early visual regions could predict which image of several oriented gratings was being viewed by the subject. Moreover, subsequent fMRI studies have reported that animate and inanimate visual objects lead to highly differentiated patterns of activity in the ventral temporal cortex (Kriegeskorte *et al.*, 2008c; Naselaris *et al.*, 2009). Reddy et al. (2010) found that activity patterns in the ventral temporal cortex could predict whether participants were imagining famous faces, famous buildings, tools, or food items. Similar findings were documented in studies of working memory for faces, places, and common objects (Lewis-Peacock and Postle, 2008). MVPA not only decodes the neural patterns associated with cognitive tasks, but also reconstructs the presented visual images from the BOLD response (Miyawaki *et al.*, 2008). Recent fMRI studies have started to use MVPA to investigate the neural underpinnings of phonological and language processing. Formisano et al. (2008) showed that activity patterns in the auditory cortex could discriminate which vowel sound was heard by participants who were listening to audio clips of three different speakers.

Likewise, Raizada et al. (2010) found that neural responses in the auditory cortex in native English speakers showed a better discrimination of the syllables /ra/ or /la/ than those in Japanese speakers, who have a difficulty differentiating between these phonemes. In terms of motor functions, MVPA has been used to decode the neural signatures of ME, MI and AO within brain regions when achieving actions jointly activated by all three modalities (Filimon *et al.*, 2015). Pilgramm et al. (2016) decoded the neural activity in the frontal and parietal regions during imagining of right-hand simple actions (aiming, extension–flexion and squeezing movements), while Zabicki et al. (2016) classified imagined and executed three different right-hand simple actions (aiming, extension–flexion and squeezing movements). Thus, this leaves the question of whether multi-joint arm actions in 3D space could be decoded from the frontal-parietal motor regions unanswered.

Whereas MVPA examines whether the neural patterns for different experimental conditions are distinguishable, Representational Similarity Analysis (RSA), which was proposed by Kriegeskorte and colleagues, analyses how they are related by exploring the geometry of stimuli representations (Kriegeskorte *et al.*, 2008a). RSA demonstrates that the representations of the same stimuli in different brain regions can differ even if the MVPA classification accuracy is equivalent (Kriegeskorte *et al.*, 2008c; Connolly *et al.*, 2012). Furthermore, it converts the response patterns from feature (voxel) space to a set of distances between patterns, overcoming the problem of feature correspondence across subjects' brains, and allowing comparison of the similarity between different representation structures and model predictions. Zabicki *et al.*, (2016) utilised RSA to highlight that the neural representational structure of MI and ME are neither distinct nor exactly the same, suggesting that they instead exhibit a similar structural geometry with respect to different types of action. RSA is a powerful technique that could be applied to characterise representational geometry and to deepen the understanding of different motor modalities.

MVPA is a subject-dependent analysis that builds a new classifier for each participant's brain. Therefore, any shared response similarity across participants can only be explained by shared coarse-grained information that can be retrieved by univariate analyses. This raises the question of whether we also share the same fine-scale representations.

2.4 Common Model Representational Space

One of the limitations of MVPA is the between-subject variance of response patterns caused by misaligned representational spaces across subjects (Haxby *et al.*, 2014). The ability to align the representational spaces that can bring the fine-grained response patterns into correspondence across subjects is essential for group analysis in the MVPA framework. In addition, it can facilitate between-subject classification (BSC) by building a common model of representational space, rather than the typical subject-specific model (Kay et al., 2008; Naselaris et al., 2011; Nishimoto et al., 2011; Filimon et al., 2015; Pilgramm et al., 2016). It has been reported that the classification accuracy drops when predicting another subject's responses (Haxby et al., 2011; Cox & Savoy, 2003) because of the idiosyncratic neural responses across subjects and the imperfections in aligning brains across subjects.

BSC requires a spatial or functional correspondence to align fine-grained topographies across subjects. Anatomical alignment approaches define anatomical features either in volume or surface spaces to fit a template space. Talairach normalisation (Talairach and Tournoux, 1988) performs a piecewise affine transformation to align the 3D volume of the brain to a template using anatomical landmarks. Surface-based alignment is an advanced method of anatomical alignment that matches the curvature of cortical surfaces across subjects (Frost & Goebel, 2012; Fischl et al., 1999). Whilst this technique establishes a spatial correspondence across subjects, it still does not afford BSC accuracies approaching those of Within Subject Classification (WSC), due to the inter-subject functional loci variability (Caspers et al., 2006; Rademacher et al., 1993).

On the other hand, functional alignment maps the neural responses from the 3D Cartesian space into high-dimensional space, allowing alignment of the representational space across brains. Conroy *et al.*, (2009) aligned subjects' cortical surfaces using functional connectivity of surface nodes, removing the dependance for temporal correspondence. Similarly, Sabuncu *et al.*, (2010) performed functional alignment of the cortex across-subjects by using a rubber-sheet-like warping of cortical surfaces that maximised the between-subject correlation of time-locked activity during movie viewing.

In 2011, ten years after the first MVPA paper came out, the features correspondence problem was solved with a new proposed method called hyperalignment (Haxby *et al.*, 2011), which functionally aligns representational spaces in the ventral temporal cortex (VT) across subjects and derives a common model space in VT. Information represented in the brain of all the subjects is similar and time-locked to the stimuli, but their representational spaces are not aligned. Hyperalignment has enabled the transformation of individual representational spaces into a high-dimensional common model space, in which each voxel is a dimension. It requires regions that are functionally equivalent across subjects. Hyperalignment uses Procrustean transformation iteratively (Schönemann, 1966) to rotate each subject's representational space to best match a reference space, and align the coarse and fine scale topographies by finding the optimal orthogonal transformation matrix that minimises the Euclidean distances between two sets of response patterns. These parameters can map the individual voxel space into a high dimensional common space (and vice versa). Haxby et al., (2011) tested the ability of hyperalignment to align fine-scale neural patterns by predicting which 18 second segment out of more than 1000 such segments a subject was watching. The prediction performance was significantly higher for the hyperaligned data (accuracy=70.6%, SEM=2.6%, chance<1%) than for anatomically aligned data (accuracy=32%, SEM=2.5%). Moreover, the researchers validated the hyperalignment by successfully performing BSC of categories in two additional

fMRI experiments, involving faces and objects categories in one experiment, and different animal species in the other, and comparing with BSC based on anatomical alignment. Since hyperalignment is the alignment of voxel spaces, it can be applied to data from any experiment that is in the same voxel grid as the one on which hyperalignment parameters were derived. Guntupalli *et al.*, (2016) extended the previous work by deriving a common model space for the whole cortex that rotates individual brain spaces into the common representational space using a searchlight hyperalignment. The common model space with general validity was derived by measuring neural patterns of cortical activity evoked by viewing and listening to a complex, dynamic movie (Raiders of the Lost Ark). At the present BSC based on hyperalignment has only been reported for fMRI data from the visual and auditory cortices (Haxby *et al.*, 2011; Guntupalli *et al.*, 2016), and so, this raises the question of whether hyperalignment can align the fine-scale representation of the motor regions or not.

Theme 2: Modulating brain activity using fMRI neurofeedback

2.5 Introduction

Neurofeedback can be defined as a closed loop system that allows the subject to voluntarily control the neural activity of a defined brain region(s), guided by visual or auditory feedback of the neural signal presented back to them (Birbaumer *et al.*, 2013). Since the 1960s, studies have reported that subjects can learn to regulate different components of EEG spectrum by operant training, using the feedback information extracted from EEG signal as a reward (Ruiz *et al.*, 2014). These studies have highlighted that the self-regulation learnt by neurofeedback training might lead to specific behavioural changes, and therefore it could be used as a therapeutic tool for neuronal and psychiatric disorders (Birbaumer, 2006; Marzbani *et al.*, 2016). However, EEG-neurofeedback is typically limited by relatively poor spatial resolution and inability to access subcortical regions.

The ongoing development of computer hardware and software has facilitated the rapid analysis of fMRI data in real time. For this reason, fMRI neurofeedback has usually been chosen as the basis for the development of neurofeedback systems, providing whole brain coverage and high spatial resolution despite the haemodynamic response delay. It allows participants to modulate their brain activity based on online feedback signals presented via interactive tools, whilst they are still being scanned. This is unlike traditional fMRI studies which analyse brain activation offline, after they are evoked by a particular cognitive task. fMRI neurofeedback has been used for many diverse applications. Principally, it has allowed us to study the relation between brain activity as an independent variable and behaviour as a dependent variable. It is possible that in the future, the behavioural modifications enabled by the self-regulation of brain regions could represent a novel therapeutic approach for neurological disorders.

2.6 fMRI neurofeedback in healthy participants

The majority of fMRI neurofeedback studies have trained healthy participants to modulate the activation of various brain regions, including the amygdala, insula, inferior frontal gyrus (IFG), anterior cingulate cortex (ACC) and sensorimotor cortex. These areas relate to emotion, cognition, perception and movement. Training a participant to self-regulate specific brain regions has allowed them to alter their brain's functional output, leading to associated cognitive and behavioural changes (for review see Ruiz *et al.*, 2014).

The first ever fMRI neurofeedback experiment was conducted by Posse *et al.*, (2003). It explored the feasibility of using this methodology to regulate amygdala activation during a mood self-regulation paradigm, which was aided by presentation of sad and neutral faces. All the participants achieved self-induced sadness (reported as a self-rating for the intensity of experienced sadness), and their amygdala activation levels were correlated with their self-mood ratings. Similarly, Weiskopf *et al.*, (2003) successfully employed fMRI neurofeedback to up-

regulate the BOLD signal of the ACC. However, the study did not include any behavioural measurement. In an early work, Caria *et al.*, (2007) extended the use of fMRI neurofeedback to regulate anterior insular activity. Participants were successfully trained to up-regulate the BOLD signal acquired from the right anterior insula by recalling autobiographical emotional events. In addition, participants achieved self-regulation of the insula without the presence of feedback information immediately after the neurofeedback training, indicating that the learnt mental strategy can persist during a transfer session after training. Interestingly, two control groups were included in this study, neither of which managed to self-regulate the insula activity. In a subsequent work, Caria *et al.*, (2010) explored the relationship between self-regulation and emotional behaviour. Participants were presented with emotionally negative or neutral pictures and were asked to rate the emotional valence of these pictures. Their results revealed a significant increase of the BOLD signal in the left anterior insula associated with rating aversive pictures more negatively after self-regulation. Hamilton *et al.*, (2011) examined the feasibility of using fMRI neurofeedback to down-regulate the BOLD signal of the subgenual anterior cingulate (sACC) cortex using positive affective strategies. Participants were able to modulate the sACC activity, unlike the control group who were trained with sham feedback. Zotev *et al.*, (2014) documented the first implementation of simultaneous multimodal fMRI and EEG neurofeedback based on a novel design for integrating fMRI and EEG data streams. Participants were trained using an fMRI-EEG neurofeedback system to self-regulate simultaneously the BOLD signal in the left amygdala and frontal EEG power asymmetry in the high-beta band during retrieval of happy autobiographical memories. Paret *et al.*, (2016) reported that the successful down-regulation of Amygdala activity by neurofeedback while viewing aversive pictures was associated with increased functional connectivity of the right amygdala with the ventromedial prefrontal cortex (vmPFC). On the other hand, Marxen *et al.*, (2016) successfully demonstrated the ability of participants to utilise

fMRI neurofeedback to differentially alternate the BOLD signal from the bilateral amygdala corresponding with the prescribed regulation direction. Self-regulation was positively correlated with subjective arousal ratings and negatively correlated with agreeableness and susceptibility to anger.

Similarly to the work carried out on emotional regions, researchers have also attempted to induce behavioural changes in other brain structures. Yoo *et al.*, (2006) used fMRI neurofeedback to increase the BOLD signal of the auditory cortex during sound stimulation. The results showed that participants who received the feedback from the auditory cortex were able to up-regulate their activation compared to a control group. Rota *et al.*, (2009) trained participants to modulate the right IFG to influence speech processing and language-related performance. Linguistic tests were used before and after the neurofeedback training to assess the behavioural impact. Participants achieved voluntary regulation of their IFG along with an improvement in the identification accuracy of emotional prosodic intonations.

Along with the above mentioned brain regions, sensorimotor areas have been one of the most studied regions, and these have clinical implications for motor rehabilitation after central nervous system injury. They might also be useful for the creation of brain–computer interfaces. Yoo *et al.*, (2008) documented the long term effect of fMRI neurofeedback training to regulate M1 activity during a MI task with the right hand. Participants learnt to self-regulate the BOLD signal of the hand motor area compared to the control group, who had difficulty in adopting a mental strategy to maintain the regulation. Chiew *et al.*, (2012) trained participants to maximise the laterality index (LI) of M1 (the difference in activity between the contralateral and ipsilateral regions) during a kinaesthetic MI task. Increasing the laterality of motor related activity is associated with better motor outcomes, and therefore using neurofeedback to increase laterality may provide a potential therapy outcome for stroke patients (Ward, 2004; Neyedli *et al.*, 2017) . This study reported mixed findings from neurofeedback; only half of the

participants were able to increase the LI value. On the other hand, Berman *et al.*, (2012) reported that participants learnt to modulate their brain activity within the M1 region during a finger tapping task, however, they were unable to achieve self-regulation during an MI task of finger tapping. Johnson *et al.*, (2012) addressed the inherent delay of the haemodynamic response by comparing two approaches of continuous and intermittent presentation of feedback information extracted from the left PM region during a MI task. The results of this study suggested that intermittent presentation of feedback information is more effective in self-regulating the PM activity than continuous presentation. Similarly, Hui *et al.*, (2014) investigated the changes in motor network connectivity involved in MI and ME influenced by fMRI neurofeedback of the right PM area. The results revealed connectivity changes in the MI network between the PM and posterior parietal regions, and in the ME network between the right cerebellum and M1/primary sensory cortex during the up-regulation of right PM activity. In a subsequent work, Sousa *et al.*, (2015) highlighted the efficacy of a single session of fMRI neurofeedback to up-regulate the left PM region activity during an MI task compared to a control group. In addition, the neurofeedback group showed increased activation in motor regions extending beyond the target region (left PM), including the SMA, basal ganglia and cerebellum. Moreover, Scharnowski *et al.*, (2015) used fMRI neurofeedback to simultaneously modulate the differential BOLD signals of SMA and parahippocampal regions. The results indicated that the learnt self-regulation of these functionally distinct brain regions caused functionally specific behavioural effects (i.e. shortening of motor reaction times and specific interference with memory encoding). Sepulveda *et al.*, (2016) examined the differential effect of feedback, explicit instructions and monetary reward while training participants to up-regulate the SMA signal. Participants were divided into 4 groups and were trained over two days on one of four protocols: feedback only, feedback+explicit instruction (MI task), feedback+monetary reward and feedback+explicit instructions (MI task)+monetary reward.

The findings showed that the highest BOLD signal in SMA during the neurofeedback training was achieved using feedback+ monetary reward protocol, and also, the feedback protocol increased the BOLD signal significantly between day1 and day2.

2.7 Clinical applications of fMRI neurofeedback

The reported behavioural modifications caused by fMRI neurofeedback in healthy participants has motivated the use of this methodology in clinical populations. DeCharms *et al.*, (2005) executed the first clinical neurofeedback study, which demonstrated the use of self-regulation of rostral ACC to modulate the pain perception of chronic pain patients, who subsequently reported a decrease in their level of pain intensity after the neurofeedback training. Following this, Haller *et al.*, (2010) conducted a pilot study with chronic tinnitus patients who were trained to decrease their auditory cortex activation. Five of six patients learnt to down-regulate the activation of their auditory cortex, and two of them reported a decrease in their tinnitus. Subramanian *et al.*, (2011) trained patients suffering from Parkinson's disease to self-regulate their SMA activity over two scanning sessions. Patients who were successfully trained showed an improvement in finger tapping speed and clinical ratings of motor symptomatology. Sitaram *et al.*, (2012) successfully trained healthy participants and stroke patients to up-regulate their vPM activation using fMRI neurofeedback. To assess the effects of self-regulation, paired pulses of transcranial magnetic stimulation (TMS) were used to induce intracortical inhibition and facilitation. The results showed a reduction in intracortical inhibition associated with the increase in vPM signal after neurofeedback training, indicating a beneficial effect of self-regulation training on motor cortical output. Ruiz *et al.*, (2013) showed that patients with chronic schizophrenia can learn to self-regulate the BOLD signal in the anterior insula by use of fMRI neurofeedback in a face emotion recognition paradigm.

In summary, fMRI neurofeedback studies have targeted different brain regions including the amygdala, anterior insula, IFG, several subdivisions of the ACC, and several

sensorimotor regions. The results of most of these studies have shown that if self-regulation learning occurs, this effect is specific for the target ROI and is not due to general arousal or artifactual confounds. Furthermore, recent studies have used larger groups (average=18) of participants, and have included one or more control groups who are trained with sham feedback, in order to prove that neurofeedback training is the specific factor that leads to self-regulation and behavioural modification. These behavioural changes, in a healthy population, have included modulation of affective states, modifications in the evaluation of emotional visual stimuli, and changes in auditory attention, linguistic processing and motor performance. In patients, behavioural modulations have included the reduction of tinnitus, modulation of accuracy in recognising emotional faces, and modulation of motor performance. In addition, with few exceptions (DeCharms *et al.*, 2005; Haller *et al.*, 2010; Hamilton *et al.*, 2011), most of these studies have focused in the up-regulation of brain signals, and therefore the question of whether subjects can voluntarily learn to *decrease* the activation of a particular brain area remains unsolved. This is an important factor for brain disorders in which an abnormal over-activation underlies the psychopathology.

2.8 Learning mechanisms underlying neurofeedback training

The underlying mechanisms of fMRI neurofeedback training that result in learned self-regulation of brain activation are not yet clearly understood, but they are most likely to be multifactorial, including both bottom-up and top-down processes (Auer *et al.*, 2016; Paret *et al.*, 2016; Nicholson *et al.*, 2017). Controlling the feedback signal evoked from contingent brain activation may engage multiple types of learning and brain regions (Power and Petersen, 2013; Strehl *et al.*, 2014).

Behavioural changes and/or brain structural or functional alteration are the main outcomes of learning gained by experience. In terms of behaviour, learning can result in improved perceptions (Fahle, 2002), memory recall and recognition (Yonelinas, 2002),

anticipation/prediction and motor action (Cano-De-La-Cuerda *et al.*, 2015; Kwasnicka *et al.*, 2016). Within neural structures, learning may result in enhanced (Schwartz *et al.*, 2002) or attenuated sensory network activation (Grill-Spector *et al.*, 2006), activation in learning and memory networks (Poldrack *et al.*, 2001), changes to the multivariate representational space of brain regions (Folstein *et al.*, 2013), changes to functional connectivity (Büchel *et al.*, 1999), increased grey matter volume (Draganski *et al.*, 2004), and changes in white matter (Zatorre *et al.*, 2012). These changes in behaviour and brain structure/function are potential targets for fMRI neurofeedback induced by different learning mechanisms.

One of the proposed mechanisms is association learning, which can be defined as the process by which an association between two stimuli or between a behaviour and a stimulus is learned (Sulzer *et al.*, 2013). This learning approach consists of two paradigms: operant (trial and error) and classical conditioning. Operant learning theory is often used to explain neurofeedback learning (Birbaumer *et al.*, 2013). In this learning form, the probability of a physiological response is associated with the presence of a reinforcing stimulus (feedback signal), with a reward for desirable behaviour and/or a punishment for undesirable behaviour. The reward can be provided by either feedback information (visual or auditory signal) (Sepulveda *et al.*, 2016; Neyedli *et al.*, 2017), a social affiliation (Zamorano *et al.*, 2015) or monetory gain (Bray *et al.*, 2007a). In contrast, classical conditioning can be used to associate an interoceptive cue with increased brain activity during neurofeedback training, i.e. the participant learns by being aware of a specific association between self-generated thought processes and control of the feedback signal, and learns to subsequently use that learnt strategy for promoting self-regulation outside the scanner (Scharnowski and Weiskopf, 2015).

One limitation of the associative learning model is that it does not take into account the use of explicit instruction during the neurofeedback training. Therefore, Lacroix, (1986) proposed a dual process theory that involves feedforward and feedback learning processes to

understand neurofeedback learning using explicit strategies. Feedforward processes are active, where the naïve participants retrieve an effective mental strategy using the provided explicit instructions. Repeated matching of the feedback signal with successful mental imagery strategies is mediated through interoceptive awareness. Through the neurofeedback training, the internal model improves in efficiency, is stored in implicit memory (Strehl *et al.*, 2014) and may become automatic (Kober *et al.*, 2013). Alternatively, the feedback processes are active when the participants do not receive explicit instructions and they have to search for a new mental strategy to control the feedback signal based on trial and error (Sitaram *et al.*, 2017). Therefore, the dual process paradigm suggests that giving explicit instruction about the mental strategy that controls the selected brain region's activation can help participants to reduce the time needed to construct a new strategy (Sepulveda *et al.*, 2016).

An important question is whether there are brain regions which guide or control neurofeedback learning. These putative brain regions would be commonly activated across multiple neurofeedback learning paradigms regardless of the targeted region, and would interact with the specific brain region being modulated.

2.9 Regions involved in self-regulation regardless of the targeted areas

In the last 15 years, fMRI neurofeedback studies have placed growing importance on self-regulation of neural activity in various brain regions. Because these studies have focused on the regulated brain regions, little is known about the target-independent regions or regions associated with neurofeedback training.

Emmert *et al.*, (2016) conducted a post-hoc analysis of data involving nine different target regions based on twelve fMRI neurofeedback studies from different research groups including 175 subjects and 899 neurofeedback runs. Data analysis involved a first level general linear model (GLM) to model individual neurofeedback blocks. In second level analysis, a fixed effect analysis (FFX-GLM) was used to combine all the runs per subject. At the third

level, a random effect analysis (RFX-GLM) was performed to combine all subjects of all studies, resulting in an overall mixed effects model. The GLM analysis identified a common brain network which was consistently activated during the self-regulation process, regardless of the targeted regions. This network includes:

- **Anterior insula cortex (AIC)**: is involved in interoceptive cognition and self-awareness processes required during neurofeedback (Critchley *et al.*, 2004).
- **Basal ganglia**: are implicated in interoceptive processes (Schneider *et al.*, 2008) and in motivational processes (Arsalidou *et al.*, 2013). In addition, the basal ganglia are important for learning, while the dorsomedial striatum is known to be engaged in declarative learning, and the dorsoventral striatum is an essential region mediating procedural learning (Balleine and O 'doherty, 2010).
- **Temporo-parietal area**: the involvement of this area could be related to integration of the visual feedback and feedback-related processes involving the recall of memories (Zimmer, 2008), as well as self-processing and multisensory integration of body-related information (Arzy *et al.*, 2006)
- **Anterior cingulate cortex (ACC)**: the activation of the ACC might reflect motivational aspects of the neurofeedback, such as the rewarding effect of positive feedback and avoidance of negative feedback (Magno *et al.*, 2006; Posner *et al.*, 2007).
- **Bilateral dorsolateral and ventrolateral prefrontal cortex (dlPFC and vlPFC respectively)**: the activation of the dlPFC and vlPFC are related to the mental imagery used during the neurofeedback (Lotze and Halsband, 2006). The right AIC and vlPFC are involved in cognitive control tasks such as motor inhibition, reorienting and action updating using the fronto-basal-ganglia network (Posner *et al.*, 2007; Aron *et al.*, 2014).

- **Visual association area including the temporo-occipital junction**: Activation within these regions might reflect visual feedback processing and visual imagery (Zimmer, 2008).

Moreover, the GLM analysis revealed some brain regions that were deactivated during neurofeedback, including the posterior cingulate cortex (PCC), precuneus and transverse temporal region. The deactivation of the transverse temporal region might reflect a shift of focus away from scanner noise during the task due to visual feedback (Laurienti *et al.*, 2002).

Examining these regions within the context of known brain networks may help to shed light on the underlying mechanisms involved in neurofeedback. The dlPFC and the posterior parietal cortex form part of a network that is activated during demanding cognitive tasks, involving moment-to-moment monitoring of task performance, and manipulations of working memory and decision making (Koechlin and Summerfield, 2007; Sridharan *et al.*, 2008). Moreover, the AIC and ACC, together with the ventral striatum, are the main components of the saliency network which deals with competitive, context-specific stimulus selection (Menon, 2015). Menon and Uddin, (2010) suggested that this network coordinates task-related information processing by recruiting various other, more specialised networks. For neurofeedback, these might include reward-learning areas, recruiting the striatum (Samejima *et al.*, 2005; Daniel and Pollmann, 2014), the frontal cortex (O'Doherty *et al.*, 2003) and areas responsible for interoception (Lerner *et al.*, 2009) such as parts of the AIC. The PCC and precuneus are parts of the default mode network that are deactivated during cognitively demanding tasks (Raichle and Snyder, 2007; Raichle, 2015).

Amongst the majority of fMRI neurofeedback studies, M1 and PM have been the most targeted regions, however, further research needs to explore the feasibility of fMRI neurofeedback to regulate SMA activity (Scharnowski et al., 2015; Sepulveda et al., 2016), due

to the important function role of the SMA in motor learning, planning and execution, during MI of complex actions (Grefkes et al., 2008; Nachev et al., 2008).

Chapter 3 : General Methodology

3.1 Experimental design

fMRI experiments are conducted to test scientific hypotheses. To test a given hypothesis, an experiment needs to be designed to manipulate a dependent variable (BOLD signal) using independent variables (stimuli) (Huettel *et al.*, 2008). These experiments must be performed in a controlled environment, taking into account the temporal characteristics of the BOLD signal and any possible confound effects. Typically, there are two types of fMRI studies: block and event-related design. Block design experiments are used to average neural responses across many trials grouped together in one block, in order to increase the SNR. In contrast, event-related design experiments allow us to investigate the transient changes in brain activity in reaction to a given stimulus (Petersen and Dubis, 2012).

The fundamental concept in designing an fMRI experiment is to convolve the BOLD response with the stimuli functions, in order to obtain the predicted fMRI response. The BOLD signal shown in figure 3.1 is an impulse response (IR), and this comprises a peak occurring at 4-6s followed by an undershoot from 10-30s. The shape of this response differs between people and different brain regions within the same individual. In other words, IR acts as a low pass filter that passes the low frequencies and attenuates the high frequencies (Henson, 2006).

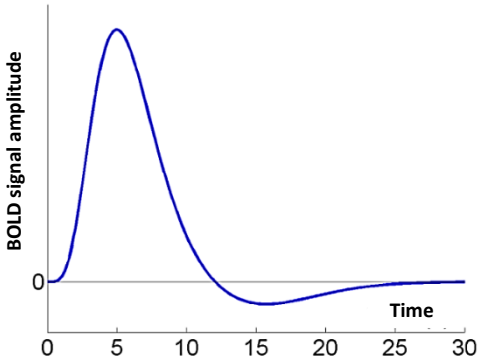

Figure 3.1. An impulse response represented by the BOLD signal. It consists of a peak at 4-6s followed by an undershoot from 10-30s (Henson, 2006).

The event related design shows one stimulus at a time, and compares the fMRI response with a baseline or with other responses. For stimuli which are presented every 16s and 4s, the convolution results with the IR are shown in figure 3.2. However, neither of the above designs are efficient in this case, due to the majority of the stimulus energy having been removed during high pass filtering.

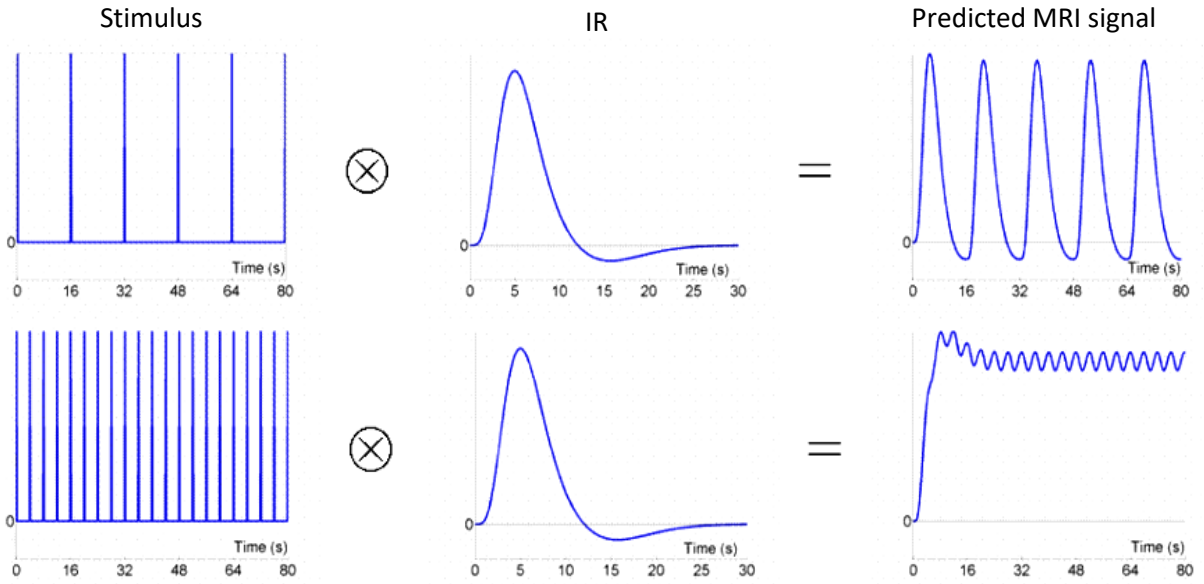

Figure 3.2. Convolving IR with a stimuli presented every 16s (top row) or every 4s (bottom row) (Henson, 2006).

In a blocked design, the stimuli of one condition are presented continuously for a period of time then followed by either a null block or different block of conditions. For a block of 5

stimuli shown every 4s alternating with 20s of null block, the predicted fMRI response is shown in figure 3.3.

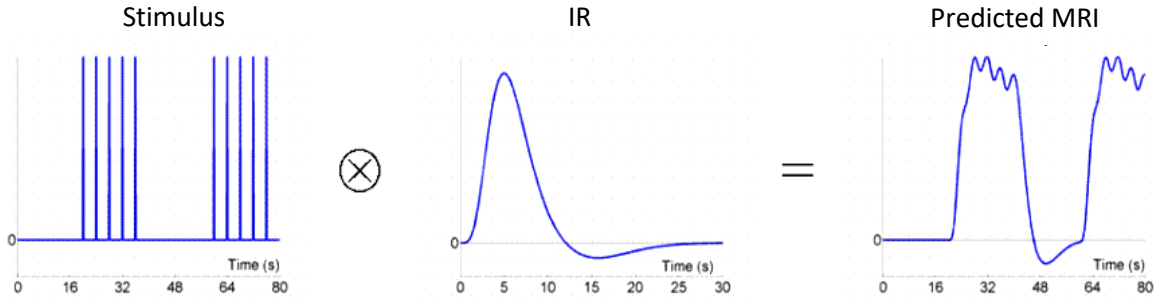

Figure 3.3. Convolving the IR with a block of 5 stimuli presented every 4s, alternating with 20s of null block (Henson, 2006).

Applying the Fourier transformation to the responses shown in figure 3.3, the IR acts as a low pass filter in the frequency domain and passes the majority of the signal, including the fundamental frequency and attenuates the high frequency harmonics as shown in figure 3.4. The fundamental frequency corresponds to a sinusoidal frequency that best models the basic on-off alternation of the block design, whilst the harmonics capture the sharper edges of the square-wave function relative to this fundamental sinusoid. Therefore, the optimal block design would be to modulate the neural activity in a sinusoidal scheme with a frequency that matches the peak amplitude of the IR spectrum. A block design is only efficient when the block length is short; 15-50 seconds for task blocks and 15-50 seconds for null blocks (Henson, 2006).

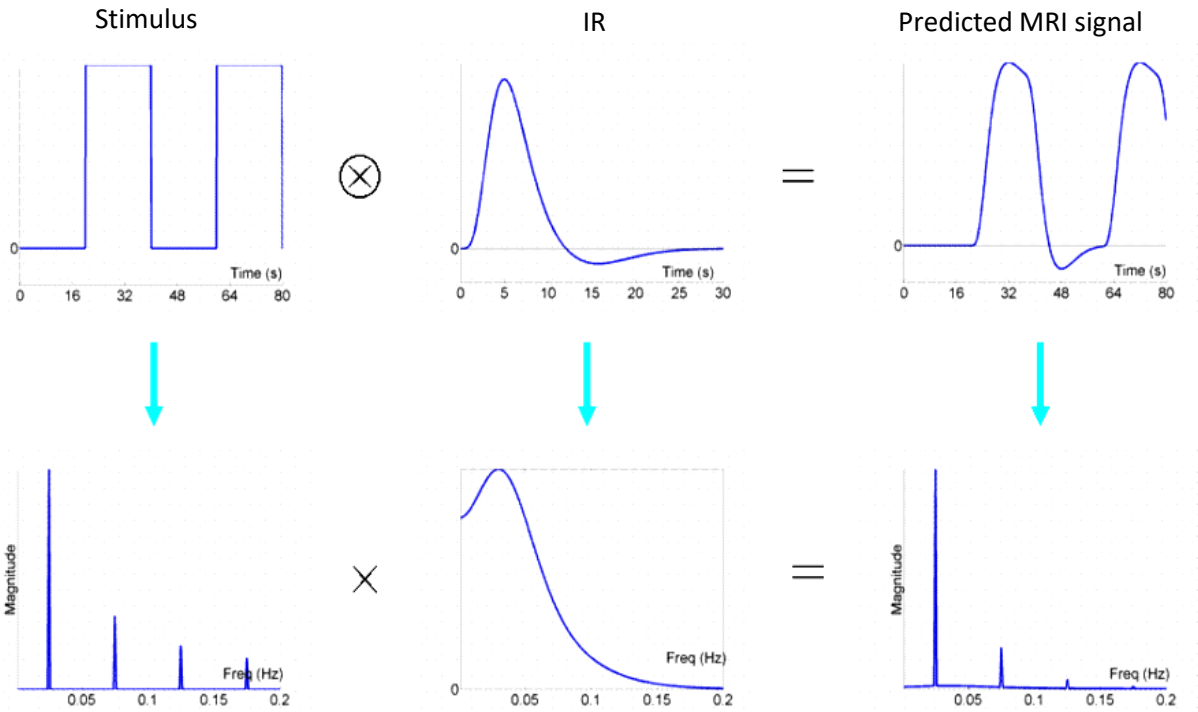

Figure 3.4. The convolution of IR with a block of stimuli along with the predicted fMRI signal in time domain (top row) and in the frequency response (bottom row). IR acts as a low pass filter passing the low frequencies but supressing the high frequencies of the stimuli energy (Henson, 2006).

3.2 fMRI data Preprocessing

This section covers the standard steps that are performed for most fMRI data (functional and anatomical scans). The preprocessing of the functional scans involves slice acquisition time correction, head motion correction, high-pass filter, linear drift removal and spatial smoothing. The processing of anatomical scans involves intensity correction and Brain extraction. All the data in this thesis were preprocessed using the BrainVoyager QX 2.8 software package.

3.2.1 Functional Data preprocessing

Typically, fMRI data consist of a 3D-matrix (volume) of volumetric pixels (voxels) that is repeatedly sampled over time. Each voxel contains a BOLD signal, which changes over time and represents an indirect measurement of the neural activity. An fMRI experiment might have

an image volume of 70×70×32 voxels, which is sampled every 2 seconds for a total of 5 minutes. Prior to the statistical analysis, a series of computational operations known as a preprocessing are performed on the raw data to reduce artefact and noise-related components of fMRI data, and make it ready for further analysis.

3.2.1.1 Slice time correction

fMRI data are collected in the form of slices selected by radiofrequency excitation pulses, followed by simultaneous data collection throughout the slice. The slices of each volume are selected to have equal spacing in time across one TR. This could be done by collecting the data either in ascending or descending slice order (for instance 1-2-3-4-5-…-31-32). Most fMRI scans nowadays are using interleaved slice acquisition, where all the odd-numbered slices are collected first, and then all the even-numbered ones are collected, to avoid cross slice excitation. The disadvantage of this technique is that the BOLD signals of contiguous parts of the brain are acquired at non-adjacent time points. Therefore, slice acquisition time correction solves this discrepancy by temporally interpolating the voxels' time courses so that it is assumed they are being collected simultaneously. The most common forms of interpolation are linear, cubic spline or Sinc (Huettel *et al.*, 2008).

3.2.1.2 Motion correction

The most damaging and frustrating problem in fMRI data acquisition is head motion. For example, small sub-voxel motion may corrupt the data, and result in that subject needing to be excluded from the experiment. The purpose of motion correction is to realign the functional images to a reference image, such that every voxel will have the same coordinates throughout the experiment. This will improve the quality of the images and increase signal-to-noise ratio (SNR). Rigid-body transformation parameters with three rotation parameters (x, y and z) and three translation parameters (roll, pitch and yaw) are calculated to realign all the functional images to the first image (reference image). These parameters are estimated

iteratively, using an optimisation algorithm to minimise the sum of the square of the differences between the reference image and each subsequent image (Friston *et al.*, 1995; Huettel *et al.*, 2008). The tri-linear sinc Interpolation approach is used to detect motion using linear interpolation, and to correct it using sinc interpolation (Huettel *et al.*, 2008).

3.2.1.3 High pass filter and low frequency drift

fMRI data can be contaminated by low frequency fluctuations caused by different sources varying over time. The most common sources of noise are temperature variation within the subject, or scanner hardware and low frequency physiological artifacts like respiration and heart rate. These artifacts will significantly reduce the power of statistical analysis and invalidate event-related averaging, which assumes stationary time courses, therefore removing low frequencies. Correcting drifts is one of the most important preprocessing steps, and these can be removed by using a high-pass filter, performed by using GLM with Fourier basis. The GLM is used to estimate the presence of low frequencies in a voxel's time course. The projected time course from a GLM based on the predictors (in this case sines and cosines for low frequencies) will then be subtracted from the original data, resulting in a filtered time course (Huettel *et al.*, 2008; Ashby, 2011).

3.2.2 Anatomical Data preprocessing

Intensity inhomogeneities in anatomical images (T1) can substantially reduce the accuracy of segmentation and functional co-registration (figure 3.5A). A well-known method of Intensity inhomogeneities correction (IIC) is based on surface fitting approach, in which low-order polynomials are used to model low frequency intensity variation (known as a bias field, see figure 3.5B) in a subset of selected voxels belonging to the white matter. This field is then removed from the data, producing a homogeneous intensity image (figure 3.5C) (Vovk *et al.*, 2007).

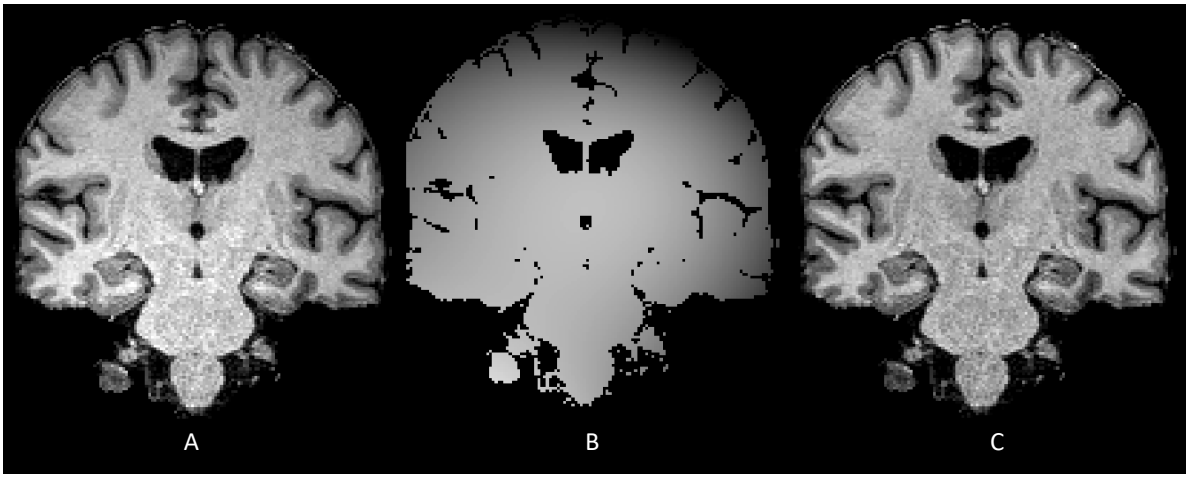

Figure 3.5. Intensity inhomogeneity difference before and after the IIC. (A) T1 image before IIC, (B) low frequency intensity variations, (C) T1 image after IIC.

3.2.3 Co-registration

The differences between the functional and anatomical images are noticeable. Typically, the functional data have low resolution with unidentified and blurry structure (figure 3.6A). In contrast, the anatomical images seem remarkably detailed, with clear outlines of the sulci and gyri, and distinct boundaries between the grey and white matter, as seen in figure 3.6B (Huettel *et al.*, 2008).

Co-registration is necessary to improve the spatial localisation of the functional images. The low resolution functional images are aligned to the high resolution structural images using a rigid body transformation (3 rotation and 3 translations).

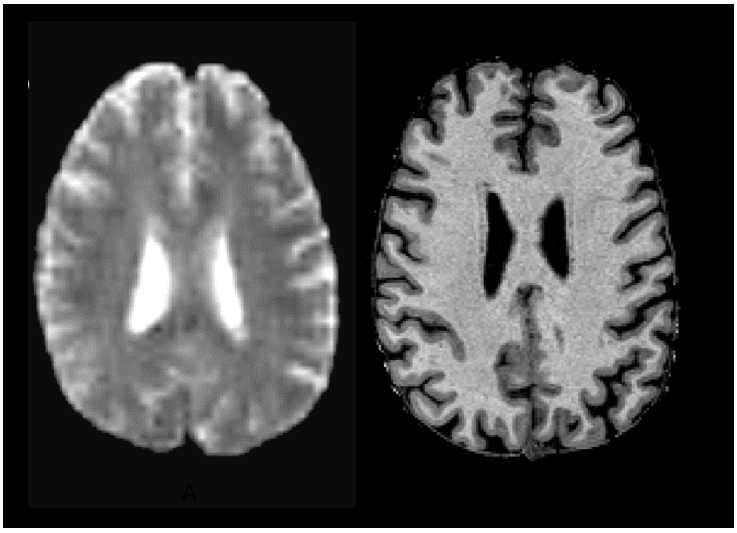

Figure 3.6. Comparison of functional image (A) and anatomical image (B). Structural landmarks that are visible in one structural image may not be distinguishable in functional images of the same slice.

3.2.4 Spatial Normalisation

Human brains differ in size and shape. These variations extend to every identifiable brain region, meaning that even major landmarks like the calcarine sulcus can have different positions and orientations. Consequently, normalisation is used to stretch, squeeze and warp subjects' anatomical images into a standard anatomical space or template like Montreal Neurological Institute template (MNI) (Evans *et al.*, 1993) and Talairach space (Talairach and Tournoux, 1988). Normalisation allows for group level statistical analyses to be performed and for these to be compared across subjects and studies at specific anatomical coordinates.

3.3 fMRI data Analysis

fMRI employs a BOLD signal to map the neural activity associated with different cognitive functions, for instance motor control, sensory processing and emotional functions (Kwongt *et al.*, 1992). The BOLD signal is generated because of the haemodynamic and metabolic modulations associated with neural oscillations (Logothetis *et al.*, 2001). In order to map the brain region(s) involved in a given cognitive function, the BOLD signal at each voxel

is analysed (Jezzard *et al.*, 2003a). There are two categories of fMRI data analysis: Hypothesis-driven analysis (or mass-univariate analysis) and data-driven analysis (or Multi-Voxel Pattern Analysis, MVPA). The mass-univariate analysis is a model based approach that uses the General Linear Model (GLM) to make statistical inferences about task-related brain regions. It requires prior information of the protocol and the hypothesis of the experiment to model the expected response. On the other hand, MVPA is a model free approach that identifies the unique spatial patterns of neural activity associated with different aspects of brain functions.

3.3.1 General Linear Model

General Linear Model (GLM) is one of the most common statistical approaches in fMRI univariate analysis. It assumes that the BOLD signal of a given voxel can be modelled as a weighted sum of one or more independent variables along with unexplained variance or noise (Huettel *et al.*, 2008). GLM analysis does not benefit from the spatial structure of the fMRI data, and it is performed on an individual voxel basis. All the voxels are treated independently and are arranged along one dimension per time point for ease of calculation.

The GLM equation is expressed in matrix formulation as:

$$\boldsymbol{Y} = \boldsymbol{X\beta} + \boldsymbol{\epsilon} \tag{3.1}$$

Where $\boldsymbol{Y} = [\boldsymbol{y_1}, \dots, \boldsymbol{y_n}]^{\boldsymbol{T}}$ is a column vector containing BOLD signal of ($\boldsymbol{n}$) time-points at a given voxel. $\boldsymbol{X}$ is $\boldsymbol{n \times d}$ design matrix which specifies the linear model to be evaluated. $\boldsymbol{\beta} = [\boldsymbol{\beta_1}, \dots, \boldsymbol{\beta_d}]^{\boldsymbol{T}}$ is a column vector of ($\boldsymbol{d}$) model parameters. Finally, $\boldsymbol{\epsilon} = [\boldsymbol{\epsilon_1}, \dots, \boldsymbol{\epsilon_n}]^{\boldsymbol{T}}$ is the residual error vector. The model parameters ($\boldsymbol{\beta}$) can be estimated by minimising the least square error $\boldsymbol{\epsilon^2}$ between the actual and fitted values, which can be written as (Mahmoudi *et al.*, 2012):

$$\boldsymbol{\epsilon^2} = (\boldsymbol{Y} - \boldsymbol{X\beta})^{\boldsymbol{T}}(\boldsymbol{Y} - \boldsymbol{X\beta}) \tag{3.2}$$

By setting the least square error to zero, we get the estimated model parameters ($\widehat{\boldsymbol{\beta}}$) as shown below:

$$\widehat{\boldsymbol{\beta}} = (\boldsymbol{X}^{\boldsymbol{T}}\boldsymbol{X})^{-1}\boldsymbol{X}^{\boldsymbol{T}}\boldsymbol{Y} \quad (3.3)$$

Obtaining a useful statistic by taking into account the level of uncertainty is an important step of this analysis. The solutions to the GLM equation (3.1) are the estimated model parameters (also known as beta-weights). Under the null hypothesis, dividing these parameters (or explained variance) by the residual error (unexplained variance) should follow a statistical distribution called the F-distribution, and their significance can be evaluated as a function of the available degrees of freedom (which depends on the number of time points and the number of regressors) (Huettel et al. 2008; Jezzard et al. 2003).

All fMRI studies include multiple sessions, subjects and often more than one group. To make a generalisation to the population from which those subjects were drawn, two approaches are used for intersubject analysis, which are known as fixed and random effects analyses. The fixed effect analysis (FFX) assumes that the experimental effect on the BOLD signal is fixed across all subjects. The data from all subjects are treated as coming from a single subject by concatenating all runs of all subjects. Therefore, the statistical inference of FFX analysis is restricted to the sample of subjects used in the study. In order to make an inference about the population from which the subjects were sampled, a random effects analysis (RFX) is used to assess the variability of the effects across subjects. In this analysis, subjects are considered to be a representative sample of a population (Huettel *et al.*, 2008).

3.3.2 Multi-voxel Pattern analysis

Over the last few years MVPA has had a growing importance in the prediction of mental states from fMRI data. Traditional univariate analysis blurs the neural responses by spatially averaging the statistically significant activation across voxels. Therefore it detects the coarse scale information, thus increasing SNR but excluding voxels with non-significant activation that might potentially contain fine-grained information. In contrast, MVPA can detect the coarse and fine scale information (patterns) distributed across multiple voxels, including those

with weaker activation (Haxby et al., 2011). MVPA employs machine learning techniques including classification to find the relationship between the spatial brain activity and experimental conditions. It involves four steps (Norman *et al.*, 2006):

- fMRI data have a large number of features (voxels) compared to the number of trials (data-points). Therefore to avoid the curse of dimensionality, a subset of voxels is selected based on anatomical landmarks or functional signatures to reduce the feature dimensionality (Mahmoudi *et al.*, 2012) as shown in figure 3.7(a).
- Brain responses evoked from a given task are represented as points in a high dimensional space, then fMRI data are partitioned into two datasets as shown in figure 3.7(b).
- One dataset is used to train a classifier to find a separating boundary between different conditions, as shown in figure 3.7(c).
- An independent dataset (not used in training) is used to evaluate the capability of the trained classifier to discriminate between different conditions: figure 3.7(d).

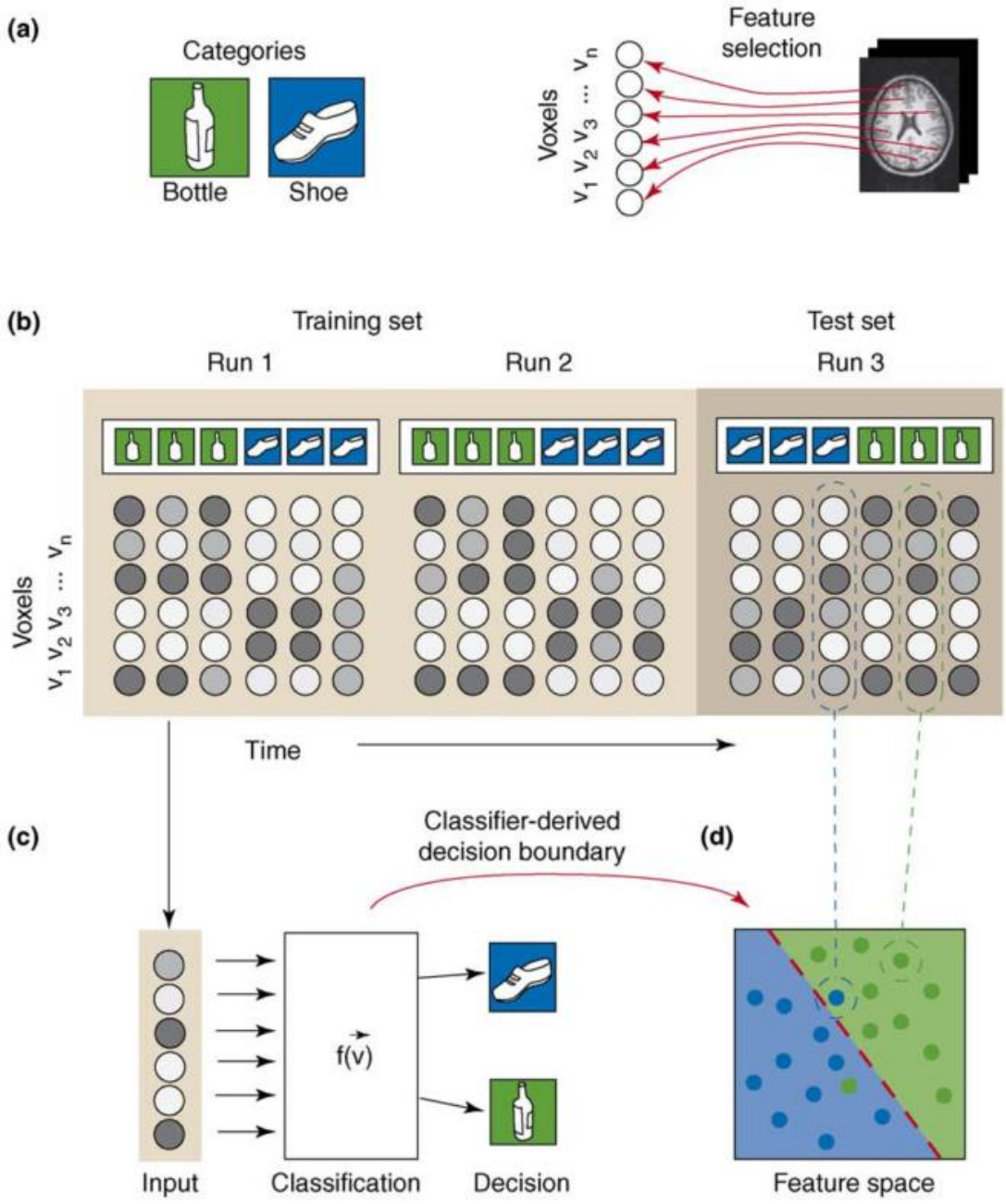

Figure 3.7. Illustration of fMRI data analysis using MVPA. (a) participants observe two stimuli (bottles and shoes). A feature selection approach is used to determine which voxels are included in the classification. (b) fMRI data are split into two datasets, a training set and a testing set. Each pattern is labelled according to the corresponding stimulus (bottle or shoe). (c) The training set is used to train a classifier that maps between patterns and stimulus and estimates the decision boundary in the high dimensional space (red dashed line). (d) The trained classifier is evaluated using an independent dataset (testing set)

3.3.3 Basic concept of representational space

Neural responses or activity patterns are distributed in space and time, and they can be analysed by mapping them from a subject's native space into a neural representational space. This space is a high-dimensional space in which dimensions are fMRI voxels and neural responses are points or vectors in that space. Thus if neural responses measured with fMRI have 500 voxels, then the representational space has 500 dimensions. Numerically, the neural responses in a representational space form a matrix in which each column is a voxel vector and each row is a response vector. The voxel vector represents the differential responses of that voxel to different conditions or stimuli. The profile of differential responses is called a tuning function (Haxby *et al.*, 2014; Guntupalli *et al.*, 2016). Figure 3.8 illustrates the concepts of high-dimensional space in two-dimensional space by mapping the neural responses of two voxels.

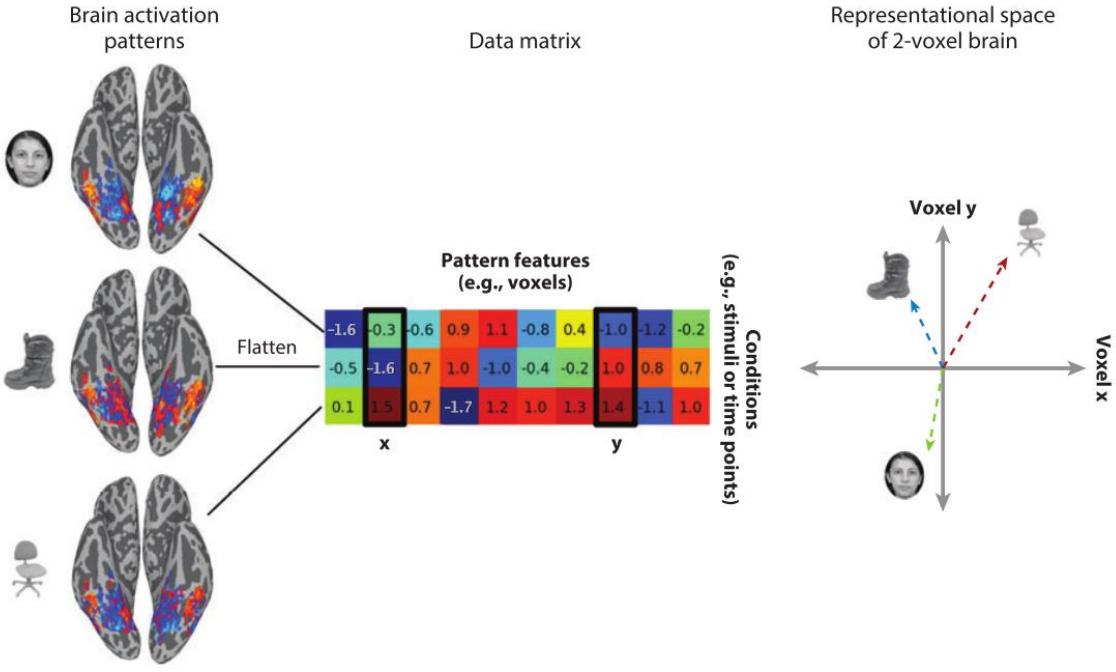

Figure 3.8. Illustration of two-dimensional representational space mapped from the native volumetric space. Neural responses (time-points) of two voxels (pattern features) are projected into high-dimensional space (Haxby *et al.*, 2014).

3.3.4 Classification

Classification, or decoding, is a mathematical process performed on multiple voxels to predict a stimulus category. In the context of fMRI, features may represent a group of voxels, examples may represent trials in the experimental run, and classes may represent the type of stimulus. Classifiers estimate the decision function that takes the values of various features (independent variables) as examples and predicts the class (dependent variable) of those examples. To obtain the decision function, fMRI data must be partitioned into a training set and a testing set. The classifier is trained using the training dataset. The training phase maps the features to the class label by assigning a weight to each feature. If more than two classes are present in the experimental design, the analysis can be transformed into a combination of multiple two-class problems (i.e., each class versus all the others), then a voting scheme is used to predict the winning class (Haxby et al., 2011; Misaki et al., 2010; Reddy et al., 2009). The classifier is then evaluted using the testing set to determine its performance in discriminating new responses.

Prior to training classifiers, fMRI data need to be transformed into examples. There are different ways of producing these examples, such as using either the raw data at a single TR, averaging raw data at multiple TRs of one task block, or using GLM estimated parameters (β-weights or *t*-values) for a given experimental condition (Pereira *et al.*, 2008)

Classifiers can use different algorithms to find the optimal decision boundary, such as Support Vector Machine, Linear Discriminant Analysis (LDA), Gaussian Naïve Bayes (GNB) and Artificial Neural Networks (ANN). Misaki et al., (2010) compared the classification performance of six different classifiers (pattern-correlation classifier, *k*-nearest neighbours, LDA, GNB, and linear and nonlinear SVM), and found that linear SVM classifiers performed the best in dealing with large high-dimensional datasets and their flexibility in decoding diverse sources of brain data.

In the simplest linear form of SVMs for two classes, the goal is to estimate a decision boundary (a hyperplane) that separates with maximum margin a set of positive examples from a set of negative examples (figure 3.9). Each example is an input vector x_i ($i = 1, ...,N$), having M features (i.e., x_i in R^M), and is associated with one of two classes $y_i = -1$ or $+1$. For example, in fMRI research, the data vectors x_i contain BOLD values at discrete time points (or averages of time points) during the experiment, and features could be a set of voxels extracted in each time point; $y = -1$ indicates condition A, and $y = +1$ indicates condition B.

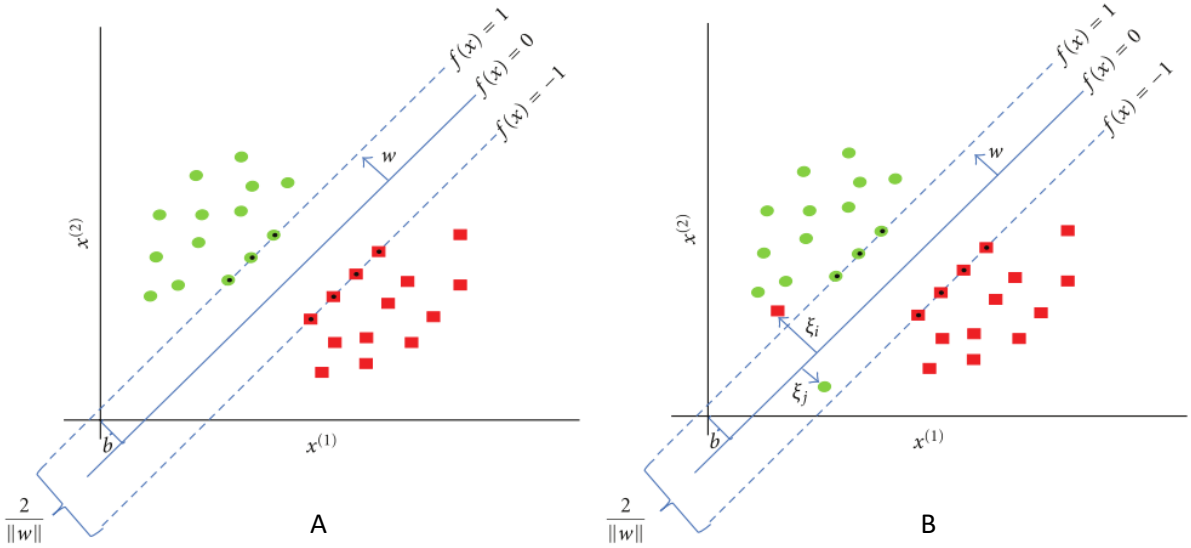

Figure 3.9. 2D space demonstration of the decision boundary of the linear SVM. (A) The hard margin on linearly separable examples where no training errors are permitted. (B) The soft margin where two training errors are introduced to make data nonlinearly separable. Dotted examples are called the support vectors.

If we assume that data are linearly separable, meaning that we can draw a line on a graph of the feature $x^{(1)}$ versus the feature $x^{(2)}$ separating the two classes when $M = 2$ and a hyperplane on graphs of $x^{(1)}$, $x^{(2)}$, ... , $x^{(M)}$ when $M > 2$, the SVM produces the discriminant function $\boldsymbol{f}$ with the largest possible margin:

$$\boldsymbol{f}(\boldsymbol{x}) = \boldsymbol{w}.\boldsymbol{x} + \boldsymbol{b} \tag{3.4}$$

$\boldsymbol{w}$ is the normal weight vector of the separating hyperplane, $\boldsymbol{b}$ is referred to as the bias, which translates the hyperplane away from the origin of the feature space, and (**.**) is the inner product:

$$\boldsymbol{w}.\boldsymbol{x} = \sum_{\boldsymbol{j=1}}^{\boldsymbol{M}} \boldsymbol{w}^{(j)}\boldsymbol{x}^{(j)} \tag{3.5}$$

SVM attempts to find the optimal hyperplane $\boldsymbol{w}\,.\,\boldsymbol{x} + \boldsymbol{b} = 0$ which maximises the margin magnitude $\mathbf{2}/\|\boldsymbol{w}\|$, that is, it finds $\boldsymbol{w}$ and $\boldsymbol{b}$ by solving the following primal optimisation problem (subject to $\boldsymbol{y_i}\,(\boldsymbol{x_i}\,.\,\boldsymbol{w} + \boldsymbol{b}) \geq 1$, $\forall i \in \{1, \ldots, N\}$):

$$\min_{\boldsymbol{w},\boldsymbol{b}} \frac{\mathbf{1}}{\mathbf{2}}\|\boldsymbol{w}\|^{\mathbf{2}} \tag{3.6}$$

For linearly separable data (figure 3.9, A), the SVM produces a discriminant function with the largest possible margin, and since the decision line separates the two classes without error, it is referred to as the hard margin SVM. It can be shown that finding the maximal margin corresponds to solving an optimisation problem, which involves minimising the term $\frac{\mathbf{1}}{\mathbf{2}}\|\boldsymbol{w}\|^{\mathbf{2}}$ under the constraint that all exemplars are classified correctly. The term $\|\boldsymbol{w}\|$ refers to the norm or length of a vector, which is obtained as follows:

$$\|\boldsymbol{w}\| = \sqrt[2]{\boldsymbol{w}.\boldsymbol{w}} \tag{3.7}$$

However, in practice, data are often not linearly separable. The generalised SVM, which is able to handle non-separable data by allowing errors, is referred to as the soft margin SVM (figure 3.9, B). It involves minimising the term (subject to $\boldsymbol{y_i}\,(\boldsymbol{x_i}\,.\,\boldsymbol{w} + \boldsymbol{b}) - 1 + \boldsymbol{\xi_i} \geq 0$, $\forall i \in \{1, \ldots, N\}$, $\boldsymbol{\xi_i} \geq 0$):

$$\min_{\boldsymbol{w},\boldsymbol{b},\boldsymbol{\xi}} \frac{\mathbf{1}}{\mathbf{2}}\|\boldsymbol{w}\|^{\mathbf{2}} + \boldsymbol{C}\sum_{\boldsymbol{i=1}}^{\boldsymbol{N}} \boldsymbol{\xi_i} \tag{3.8}$$

The new term on the right side sums the (potential) errors produced for exemplars for a given weight vector. The $\boldsymbol{\xi_i}$ values are called slack variables; a slack variable is 0 in the case

of no error. If a pattern falls within the margin or even on the right side or on the other side of the decision boundary (miss-classification), the slack variable for this pattern is positive. The cost or penalty constant $\boldsymbol{C} > 0$ is very important, since it sets the relative importance of maximising the margin and, thus, generalisation performance (small C value) and minimising the number of classification errors (large C value). The latter case forces slack variable $\boldsymbol{\xi_i}$ to be smaller, approximating the behaviour of the hard margin (Mahmoudi *et al.*, 2012).

3.3.5 Feature selection and Searchlight

Feature selection determines which voxels will be included in the classification analysis. Therefore, the dimensionality of the fMRI data need to be reduced, and selection of only the informative voxels increases the classifier performance. There are many approaches to selecting informative features (voxels), like focusing on a functionally localised region (Haxby *et al.*, 2001), fitting a GLM model and selecting voxels with highest statistics rank (Polyn. Sean M. *et al.*, 2005), and blind signal separation methods such as Principal Components Analysis (PCA) and Independent Components Analysis (ICA) (McKeown *et al.*, 2003; Rowe and Hoffmann, 2006).

Among the above mentioned approaches, Kriegeskorte et al., (2006) introduced a new method called Searchlight as an alternative technique by which to select the most informative voxels, and to exclude the noisy voxels that might affect the classifier generalisation performance. In this approach, an MVPA is applied to classify the stimuli within a local neighbourhood around each voxel in the brain, and store the classification accuracy in the centre voxel. The neighbourhood voxels are usually defined roughly as a sphere, as shown in figure 3.10, i.e. voxels within a certain (Euclidean) distance from the visited centre voxel. This approach produces a whole brain multivariate information map which reflects the informative voxels in distinguishing stimuli.

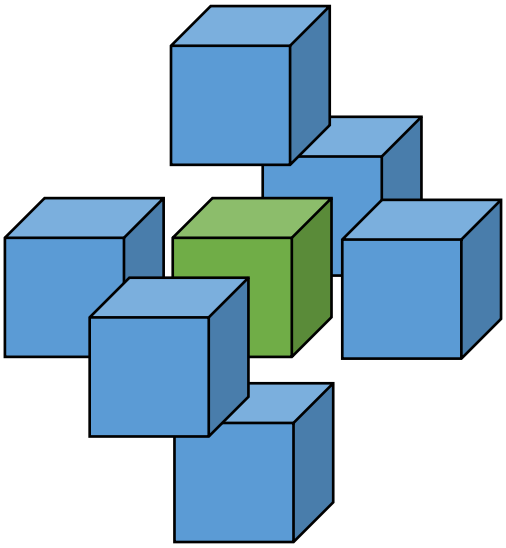

Figure 3.10. Sphere (Searchlight) of one voxel distance from the centre voxel (green). The total number of voxels in this Searchlight is 7.

3.3.6 Representational Similarity Analysis (RSA)

RSA is a novel data analysis method proposed by Kriegeskorte et al. (2008) to explore the structure in terms of distances between neural response vectors within a representational space, as shown in figure 3.11. It aims to connect different branches of neuroscience by providing a framework for comparing activity patterns in the brain that represent some cognitive processes. These activity patterns can come from various sources, like different subjects, species or modalities, such as electroencephalography (EEG) or fMRI. The central notion in RSA is a representational dissimilarity matrix (RDM). This matrix encodes the similarity structure between different activity patterns, which in turn represent different experimental conditions. Therefore comparing RDMs instead of activity patterns directly allows us to compare the representations of cognitive states not only between different subjects or species, but also between different modalities, and even between computational models as illustrated in figure 3.12.

RSA consists of six steps, and can be applied to different sources of data such as single-cell or electrode array recording, fMRI, EEG or any other modality of brain activity measurement (Kriegeskorte *et al.*, 2008a; Nili *et al.*, 2014). The steps are as follows:

- **Estimating the activity patterns**: The analysis starts by estimating the activity patterns for each experimental condition.
- **Measuring activity-pattern dissimilarity**: In this step, the dissimilarity is calculated between the activity patterns associated with each pair of conditions, and together these values form a RDM. In this thesis, the correlation distance was used as a dissimilarity measure which is equal to 1-linear correlation between pattern as shown below:

$$\textbf{Correlation distance} = 1 - \frac{\sum_{i=1}^{n}(u_i - \bar{u})\,(v_i - \bar{v})}{\sqrt{\sum_{i=1}^{n}(u_i - \bar{u})^2}\sum_{i=1}^{n}(v_i - \bar{v})^2} \qquad (3.9)$$

  $\mathbf{u_i}$ and $\mathbf{v_i}$ are the voxel intensity values of two response vectors elicited by two different experimental conditions. $\bar{\mathbf{u}}$ and $\bar{\mathbf{v}}$ are the means of vectors **U** and **V** respectively. The RDM is a square matrix with the row and column length equalling the number of experimental conditions. The matrix is symmetrical around a diagonal of zeroes (the dissimilarity between each condition and itself is 0).
- **Predicting representational similarity with a range of models**: RSA can compare model predictions to actual brain representations, which could give new insights into the inner workings of different brain regions. These models need to simulate some aspect of the information processing that is occurring in the brain during the experiment. Thus, the term model has a different meaning here than in GLM analysis, where it often refers to a statistical model that does not simulate brain information processing, such as the design matrix.
- **Comparing dissimilarity matrices**: After calculating RDMs that encode the representation of different experimental conditions in either different regions or

models, they can be visually or quantitatively compared. For such comparisons the similarity of the RDMs could be measured by using 1-correlation as a measure of dissimilarity between RDMs.

- **Testing relatedness of two dissimilarity matrices**: A statistical inference on the RDM correlation is performed to decide whether two RDMs are related, and whether there are differences in the degree of relatedness between RDMs.
- **Visualising the similarity structure of representational dissimilarity matrices by multi-dimensional scaling (MDS)**: MDS is a general purpose dimensionality reduction algorithm for arranging high-dimensional space into a much lower dimensional space (usually 2D or 3D), while at the same time trying to preserve the proportional distances between points (i.e. similar entities will be placed together, dissimilar entities apart).

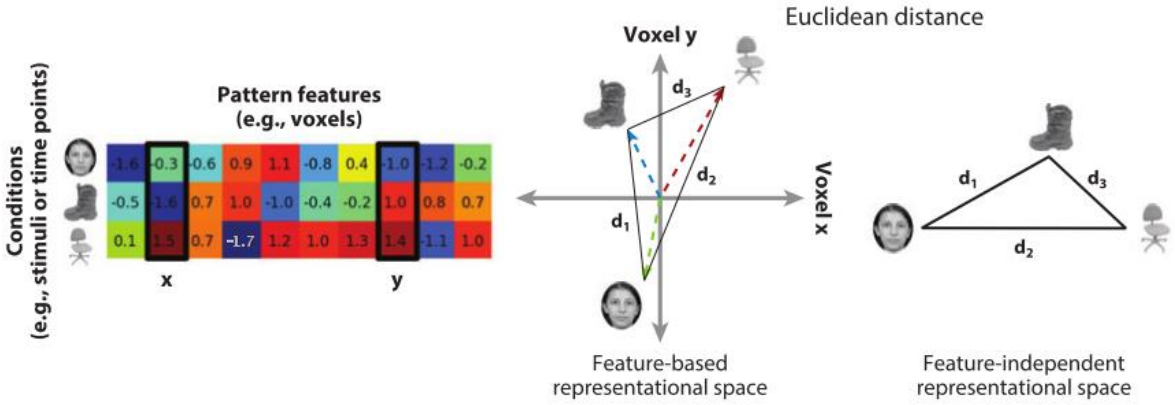

Figure 3.11. RSA examines the distances between response vectors in the high-dimensional representational space. In this example a Euclidean distance is used to measure the distance between vectors (Haxby *et al.*, 2014).

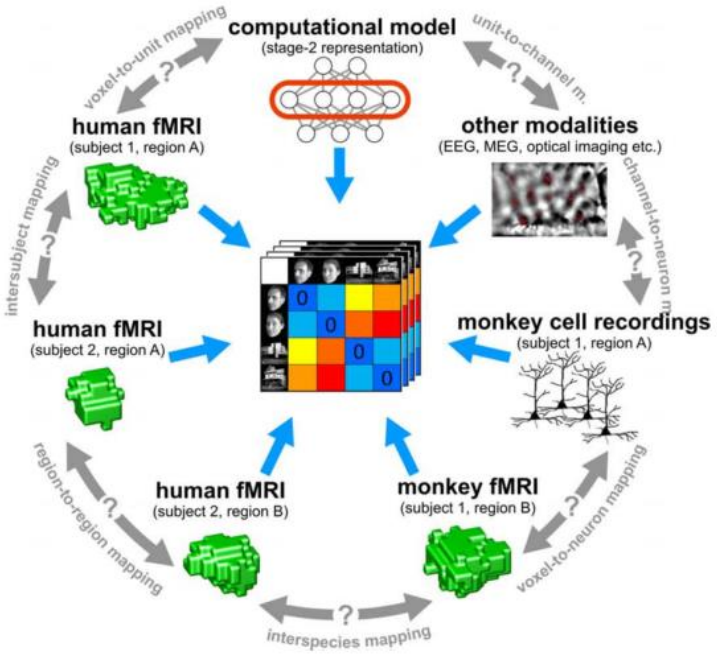

Figure 3.12. Illustration of how RDMs facilitate the comparison of cognitive states between different subjects, species, modalities and regions in the brain (Kriegeskorte *et al.*, 2008a).

3.3.7 Hyperalignment

Although the neural response vectors of different subjects watching an identical sequence of stimuli are similar and time-locked to the stimuli, their high dimensional representational spaces are poorly aligned. Hyperalignment builds a common model space by aligning representation spaces of individuals' brains. This common model space affords between-subject classification (BSC) accuracies that are equivalent to within-subject classification (WSC). Hyperalignment uses Procrustes transformation (Schönemann, 1966) iteratively to rotate a subject's representational space and bring it into optimal alignment with a reference space. It finds the orthogonal transformation matrix for each subject that rotates that subject's representational space into the common space as shown in figure 3.13. Iterative alignments of individual representational spaces update the reference space, producing a common representational space.

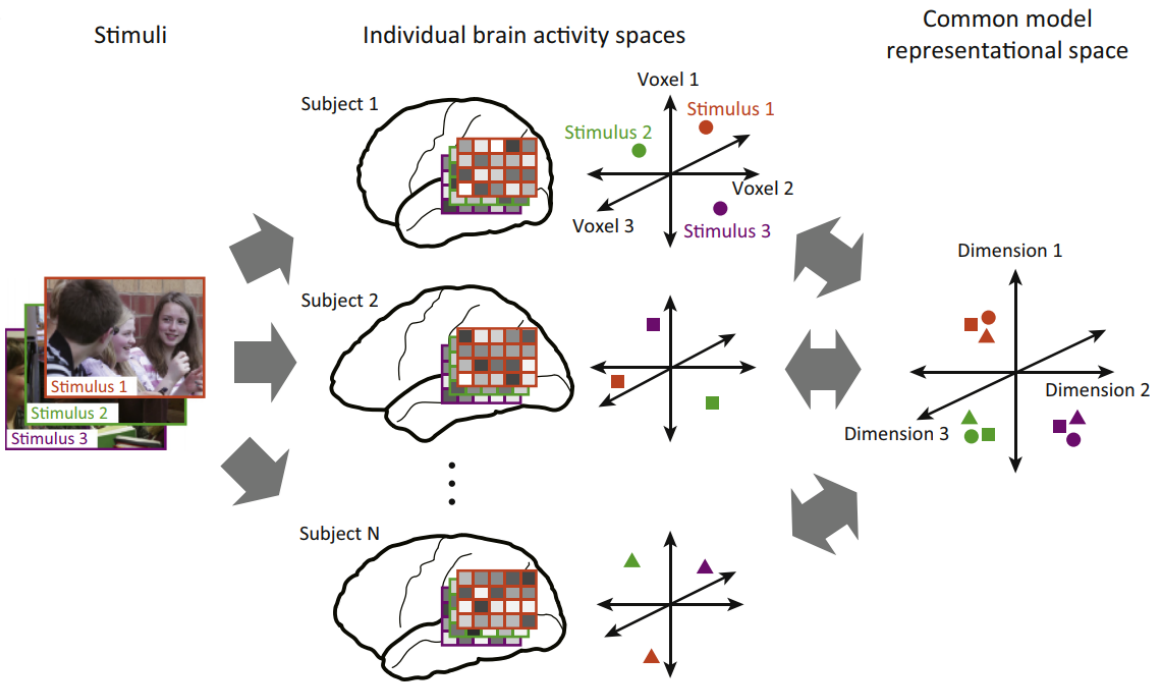

Figure 3.13. Schematic diagram of Hyperalignment. High-dimensional representational spaces of different subjects watching an identical sequence of stimuli are not aligned. Hyperalignment rotates individuals' representational spaces into a common model space, using Procrustes transformation (Nishimoto and Nishida, 2016).

Hyperalignment consists of three stages: during the first stage, an arbitrary subject is chosen to be a reference subject. The 2nd subject's response vectors are aligned to the reference subject's vectors using Procrustean transformation, and then the 3rd subject is aligned to the mean response vectors of the first 2 subjects, and so on. In the second stage, each subject's response vector is aligned to the mean response vectors of the first stage (intermediate common space), and new response vectors are computed by averaging all the subjects' aligned (rotated) vectors, which would be the final common model space. During the last stage, hyperalignment transformation parameters are calculated for each subject to map their voxel space into the final common model space, as shown in figure 3.14.

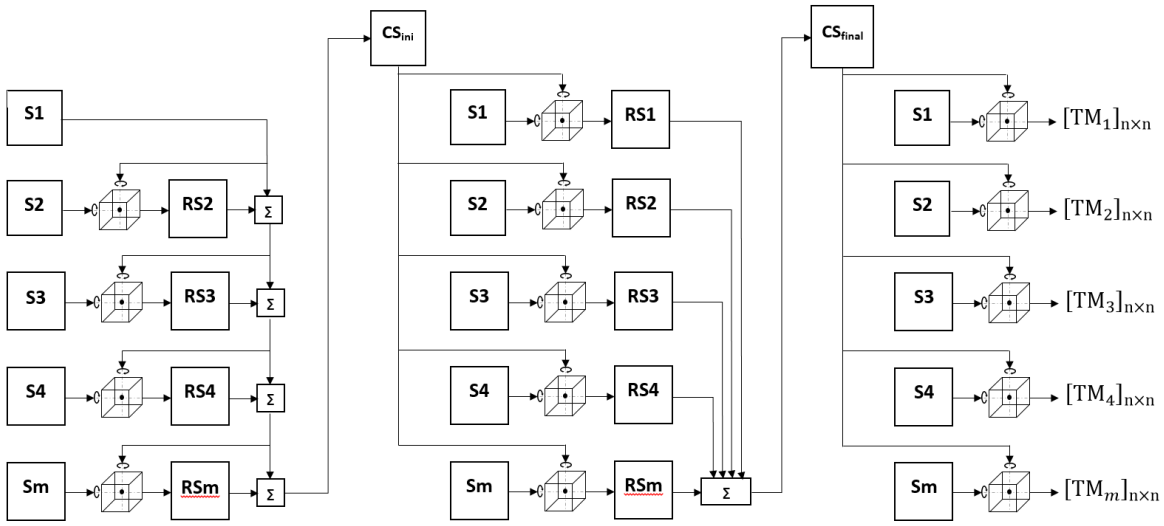

Figure 3.14. A block diagram of the hyperalignment method used to derive a common representational space and transformation parameters (TM) using Procrustean transformation. S is the subject's representational space, RS is the subject's aligned (rotated) space using procrustean transformation, CS_{ini} is the intermediate common space, CS_{final} is the final common space and $\sum$ is the average of the representational spaces.

3.4 fMRI Neurofeedback

fMRI neurofeedback is a closed loop system that measures the BOLD signal, pre-processes it in real-time, and based on this, provides feedback information to the subject to enable the control of brain activities, as illustrated in figure 3.15.

3.4.1 fMRI neurofeedback system description

In general, most fMRI neurofeedback systems consist of the subject, signal acquisition, signal pre-processing, signal analysis and feedback.

3.4.1.1 Signal acquisition

fMRI neurofeedback experiments were conducted using a 3 Tesla Siemens Tim Trio MRI scanner at CCNi with a 32-channel head coil. Whole brain images were acquired using an Echo-Planar Imaging (EPI) sequence. Images were reconstructed in real-time and were

transmitted volume by volume to the analysis computer, which hosted Turbo-BrainVoyager (TBV) (Brain Innovation, Maastricht, The Netherlands) via a TCP/IP protocol.

3.4.1.2 Signal pre-processing

TBV was used to pre-process the acquired volumes in real-time. This includes linear de-trending, slice timing correction, 3D motion correction and spatial smoothing using a Gaussian kernel with full width at a half maximum (FWHM) of 8mm, then added to a cumulative GLM.

3.4.1.3 Signal analysis

The average time course of selected regions of interest (ROIs) were exported to a custom script running on MATLAB (Mathworks Inc., Natick, MA, USA) to calculate the feedback signal.

- **Single-ROI fMRI neurofeedback paradigm:** the feedback signal is calculated based on the following equation:

$$\boldsymbol{bar\ height}\ (\boldsymbol{t}) = \left(\frac{\boldsymbol{ROI_{target}(t) - ROI_{t_{base}}}}{\boldsymbol{ROI_{t_{base}}}}\right) - \left(\frac{\boldsymbol{ROI_{reference}(t) - ROI_{r_{base}}}}{\boldsymbol{ROI_{r_{base}}}}\right) \quad (3.10)$$

  Where, $ROI_{target}(t)$ and $ROI_{reference}(t)$ are the average BOLD signals of target and reference ROIs during the neurofeedback block at time t. ROI_{t_base} and ROI_{r_base} are the average BOLD signals of the last three volumes in the fixation block of target and reference ROIs, respectively. The reference ROI, used to correct for global scanning effects, encompassed a rectangular region covering all the voxels within an axial slice distant from the target region.

- **Connectivity neurofeedback paradigm**: The magnitude of the feedback signal is estimated using a Pearson correlation as described below:

$$\boldsymbol{bar\ height}\ (\boldsymbol{t}) = \frac{\sum_{i=1}^{n}(\boldsymbol{x_i} - \bar{\boldsymbol{x}})\ (\boldsymbol{y_i} - \bar{\boldsymbol{y}})}{\sqrt{\sum_{i=1}^{n}(\boldsymbol{x_i} - \bar{\boldsymbol{x}})^2}\sqrt{\sum_{i=1}^{n}(\boldsymbol{y_i} - \bar{\boldsymbol{y}})^2}} \quad (3.11)$$

Where *x*, *y* are time courses of ROI_1 and ROI_2 respectively computed from a sliding window, $\bar{x}$ and $\bar{y}$ are the average BOLD signal within the sliding window of ROI_1 and ROI_2 respectively, and *n* is the duration of a window (in volumes) (Liew *et al.*, 2016).

3.4.1.4 Feedback signal

The feedback signal was presented as a fluctuating thermometer bar relative to the percentage change of the BOLD signal calculated using equation 3.10. An LCD projector was used to display the thermometer onto a rear projection screen that could be viewed through a mirror mounted on the head coil. The delay associated with continuous feedback depends on the image acquisition and processing time. Due to the recent advancements in computer technology, the time involved in processing one volume does not typically exceed 100ms. However, the BOLD signal, which is an indirect measure of the brain activity, has an inherent delay of about 4-6 seconds after the stimulus onset. The feedback signal was updated continuously (continuous feedback) every TR, though intermitted feedback has also been demonstrated (Johnson *et al.*, 2012) by presenting the feedback signal at the end of each task block. The latter approach enables averaging of the feedback signal, and means that subjects do not need to consider the BOLD delay.

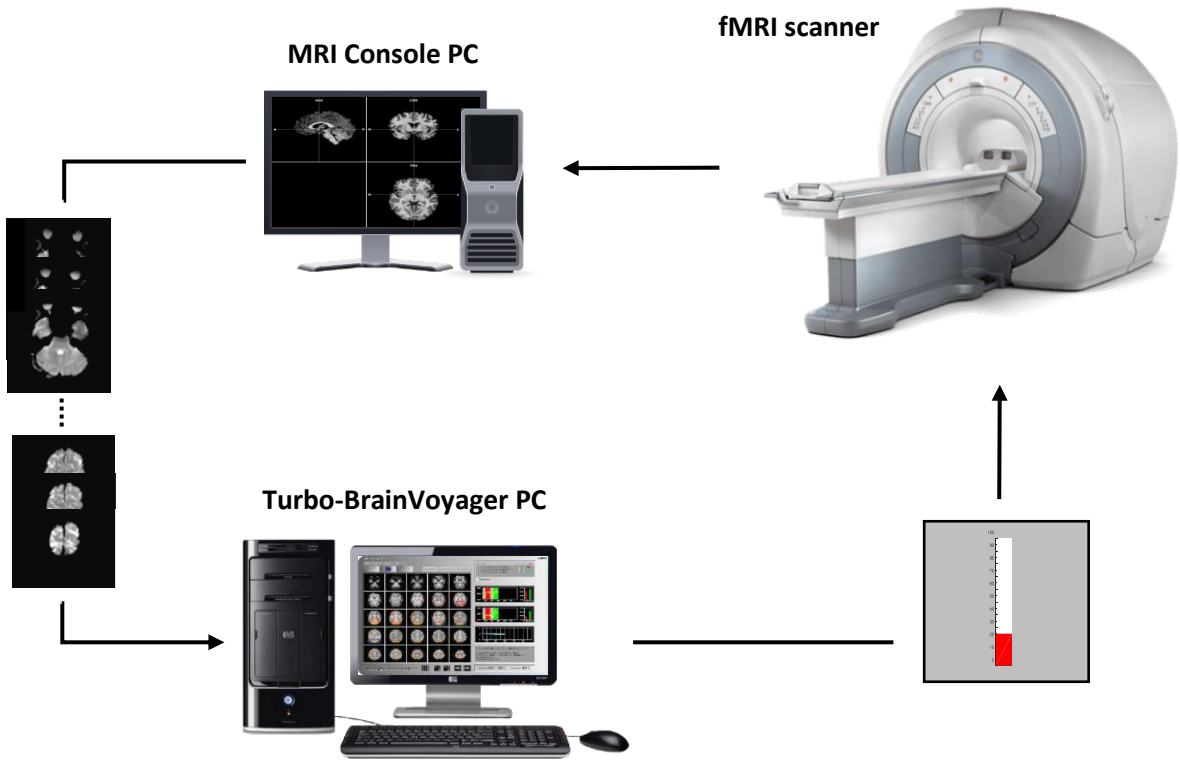

Figure 3.15. A schematic diagram of a real-time fMRI neurofeedback system. The three main components - signal acquisition, pre-processing and analysis - are conducted by two different computers connected through a fast TCP/IP connection.

3.4.2 fMRI neurofeedback design considerations

The design of the neurofeedback experiment depends on its objectives, which may range from demonstrating that self-regulation affects behavioural functions in healthy participants (Shibata *et al.*, 2011; Sitaram *et al.*, 2012; Scharnowski *et al.*, 2015) to clinical improvements in patients (DeCharms *et al.*, 2005; Haller *et al.*, 2010; Ruiz *et al.*, 2013). However, the majority of the fMRI neurofeedback studies utilise the same experimental procedure, which includes:

3.4.2.1 Definition of the target region

The definition of the regions of interest depends on the behavioural changes that are being explored. For example, experiments that aim to modulate motor reaction time target activity in the motor cortex, such as the primary motor cortex (M1) (Chiew *et al.*, 2012) and

supplementary motor cortex (Scharnowski *et al.*, 2015). Clinically, a few such studies have been conducted, such as modulating pain perception by regulating the rostral anterior cingulate cortex (rACC) (DeCharms *et al.*, 2005). The feedback signal may be the average BOLD signal of a given ROI (Blefari *et al.*, 2015), the differential activity in two ROIs (Neyedli *et al.*, 2017), connectivity between two brain networks (Megumi *et al.*, 2015) or the output of a MVPA classifier (Shibata *et al.*, 2011). ROIs can be either functionally delineated using a functional localiser (Berman *et al.*, 2012; Auer *et al.*, 2015b), or anatomically defined using brain atlas or macroscopic anatomical landmark (Marins *et al.*, 2015).

3.4.2.2 Instructions

One unresolved factor of the neurofeedback learning procedure is the instructions. There are two types of strategies for self-regulation: implicit and explicit mental strategies. Explicit strategies inform the subject to use a specific approach for modulating the brain activity, while implicit strategies provide no information and allow the subject to search for an effective mental approach. Explicit instructions help subjects to learn the task faster, reducing the expensive scanning time. However, recent studies have investigated the use of the implicit approach to learn self-regulation in one single session (Shibata *et al.*, 2011; Sepulveda *et al.*, 2016). Another study has demonstrated the use of the implicit approach with monetary reward being the optimal strategy for self-regulation, compared to implicit, explicit and explicit with monetary reward (Sepulveda *et al.*, 2016).

3.4.2.3 Task design

Most fMRI neurofeedback studies utilise block design for the modulation task. This type of experimental design is efficient in increasing SNR and overcoming the inherited delay of BOLD responses. The block design comprises a task block (15-50 seconds) during which subjects are instructed to modulate the BOLD signal, followed by a rest block of similar duration, during which they relax and/or count numbers (Hanakawa, 2011). Usually, a single

run contains fewer than 10 blocks to avoid fatigue and loss of focus, and is repeated 2-10 times within one experimental session. The number of neurofeedback sessions varies from one single session (Caria *et al.*, 2007; Blefari *et al.*, 2015) to 12 sessions (Auer *et al.*, 2015b). Interestingly, Scharnowski et al. (2012) employed a different number of sessions per subject, based on the individuals' ability to achieve success of regulation.

3.4.2.4 Transfer runs after neurofeedback training

The goal of neurofeedback experiments is to investigate the behavioural changes occurring during the neurofeedback training that remain after the training has ended, when they are no longer viewing the feedback information (for instance, thermometer) or are outside the MRI. In clinical applications, maintaining acquired skills after neurofeedback training and applying them to real-life situations is the ultimate goal. Transfer runs are conducted at the end of an experimental session (Yoo *et al.*, 2008; Sitaram *et al.*, 2012; Auer *et al.*, 2015b).

3.4.2.5 Experimental control conditions

Control groups have been used to prove that feedback information is necessary for self-modulation of brain activity, compared to the effect of repetitive training using simple instructions. Control groups receive sham feedback derived from another participant in the experimental group (Zhao *et al.*, 2013; Hui *et al.*, 2014), randomly generated signals (Johnson *et al.*, 2012) or information from another ROI functionally unrelated to the target region (DeCharms *et al.*, 2005; Scharnowski *et al.*, 2012).

3.4.2.6 Behavioural changes due to neurofeedback training

The main objective of neurofeedback training is to test the behavioural effects arising from learning to regulate the brain activity. These effects are dependent on the function of the targeted ROIs.

Chapter 4: Hyperalignment of motor cortical areas for action observation with motor imagery

4.1 Abstract

Multivariate Pattern Analysis (MVPA) has grown in importance due to its capacity to use both coarse and fine scale patterns of brain activity. However, a major limitation of multivariate analysis is the difficulty of aligning features across brains, which makes MVPA a subject specific analysis. Recent work by Haxby et al., (2011) introduced a method called Hyperalignment that explored neural activity in ventral temporal cortex during object recognition and demonstrated the ability to align individual patterns of brain activity into a common high dimensional space to facilitate Between-Subject Classification (BSC). Here we examined BSC based on Hyperalignment of motor cortex during a task of motor imagery of three natural actions (lift, knock and throw). To achieve this we collected brain activity during the combined tasks of action observation and motor imagery to a parametric action space containing 25 stick-figure blends of the three natural actions. From these responses we derived Hyperalignment transformation parameters that were used to map subjects' representational spaces of the motor imagery task in the motor cortex into a common model representational space. Results showed that BSC of the neural response patterns based on Hyperalignment exceeded both BSC based on anatomical alignment as well as a standard Within Subject Classification (WSC) approach. We also found that results were sensitive to the order in which participants entered the Hyperalignment algorithm. These results demonstrate the

effectiveness of Hyperalignment to align neural responses across subjects in motor cortex to enable BSC of motor imagery.

4.2 Introduction

Multivariate Pattern Analysis (MVPA) has evolved as an effective tool in the analysis of fMRI data and its usefulness has been shown in its ability to decode the neural responses associated with a variety of different brain states, including for instance, low-level visual features in the early visual cortex (Kay et al., 2008), auditory stimuli in the auditory cortex (Formisano et al., 2008), and motor actions in sensorimotor cortex (Zabicki et al., 2016; Pilgramm et al., 2016; Wurm & Lingnau, 2015; Oosterhof et al., 2013; Oosterhof et al., 2012). A major limitation of MVPA (for review, see Haxby et al., 2014) is that it requires a subject-dependent analysis which uses a new classifier model for each individual brain because the structure of neural activation varies across subjects. Accordingly, it has been shown that the classifier performance drops when predicting another subject's responses (Haxby et al., 2011; Cox & Savoy, 2003). One possible explanation for this drop in performance of classifiers for Between-Subject Classification (BSC) might be idiosyncratic neural responses across subjects, and another possibility is that it arises from imperfections in aligning brains across subjects. BSC requires a spatial correspondence to align fine-scale topographies across subjects' brains. Current approaches align anatomically defined features either in volume or surface spaces to fit a template space. Talairach normalization (Talairach & Tournoux, 1988) performs a piecewise affine transformation to align the 3D volume of the brain to a template using anatomical landmarks. Surface-based alignment is an advanced method of anatomical alignment that aligns the curvature of cortical surfaces across subjects (Frost & Goebel, 2012; Fischl et al., 1999). Whilst these techniques establish a spatial correspondence across subjects, they still do not afford BSC accuracies approaching those of Within Subject Classification

(WSC), due to inter-subject functional loci variability (Caspers et al., 2006; Rademacher et al., 1993).

To address these issues with BSC, Haxby and colleagues (Haxby et al., 2011; Haxby et al., 2014; Guntupalli et al., 2016) recently developed an algorithm called Hyperalignment to align subjects' representational spaces of Ventral Temporal (VT) cortex into a high-dimensional common space. Hyperalignment parameters that map the individual voxel space into a high dimensional common space (and vice versa), were obtained based on brain responses while subjects watched a movie ('Raiders of the Lost Ark') at full length (Haxby et al., 2011). Hyperalignment uses Procrustean transformation iteratively (Schönemann, 1966) to align the coarse and fine scale topographies by finding the optimal orthogonal transformation matrix that minimize the Euclidean distances between two set of response patterns. Haxby et al. (2011) applied the resulting subject-independent classifiers to data from two category perception experiments and found that the classification accuracy of the BSC obtained via Hyperalignment of VT cortex was equivalent to that of conventional WSC, thus confirming the validity of the common model space across a range of stimuli.

We pursued two main objectives with the present study. (1) Since, at present, classification performance using BSC via Hyperalignment has only been documented for fMRI data from VT cortex, we wanted to assess whether Hyperalignment can be successfully be applied to motor cortical areas, namely primary motor (M1) and premotor cortices (PM). (2) Our second, more applied motivation was to generate a subject-independent classifier that could in the future be used in real-time fMRI decoded neurofeedback applications involving motor imagery, in order to reduce scanning and analysis time compared to employing subject-dependent MVPA. In addition, in clinical work, subject-independent classifiers could then build on normal brain activity instead of a patient's potentially abnormal one (Rana et al., 2013).

Our fMRI experiment consisted of two sessions, where the first served to obtain the common model space, and the second session was used to contrast WSC and BSC accuracies. Rather than asking participants to physically perform motor actions, we employed two well-researched forms of motor simulation (Jeannerod, 2001; Filimon et al., 2015), namely action observation (AO) and motor imagery (MI). The neural substrates of motor execution, AO, and MI are at least partly overlapping, and both AO and MI have been shown to facilitate motor learning (e.g., Higuchi et al., 2012). AO and MI have also been successfully applied in motor rehabilitation (see Vogt et al., 2013). In addition, WSC of individual actions has already been demonstrated for both observed and imagined actions (Zabicki et al., 2016; Pilgramm et al., 2016; Wurm & Lingnau, 2015; Oosterhof et al., 2013; Oosterhof et al., 2012).

In the first session, participants engaged in a combination of action observation and motor imagery ('AO+MI') of n=25 action stimuli, as to provide a base for deriving a common model space. Whilst AO and MI have traditionally been studied in isolation and by different research groups, there is now growing evidence that both forms of motor simulation can be used concurrently, and that AO+MI generates both enhanced behavioural effects and more robust neural activation patterns than AO or MI alone (for review, see Vogt et al., 2013, and Eaves et al., 2016). All stimuli used in Session 1 were stick figure displays that were blended, with varying weights, between three natural multijoint actions that anchored the space of blended movements (lifting, knocking, and throwing; Vangeneugden et al., 2009). This set of blended movements are biomechanically possible actions that sample the space between the anchor points and thus provide a set of movements specially adapted for study of the anchor points.

In the second fMRI session, participants engaged in pure MI of the three natural (lifting, knocking, and throwing) actions that formed the basis of the above blend space. We used this independent dataset in order to contrast the classification accuracy of the subject-independent

classifiers derived from the Hyperalignment with the accuracy of classifiers based on conventional anatomically aligned data. We have previously shown that these actions can indeed be decoded from the individual's motor cortex using WSC (Al-Wasity et al., 2016). Specifically, in the present study we applied Hyperalignment procedures to motor cortical areas to pursue the following aims:

1. To assess the effect of permutating the order in which participants were entered in the Hyperalignment procedure to generate a common model, in order to obtain the most discriminative subject-independent classifiers.
2. Based on the above, to validate the classification accuracy of BSC derived from Hyperalignment with (a) that derived from anatomically aligned data, and (b) with the accuracy of WSC where a new classifier is tailored for each subject.
3. To contrast the classification accuracy of two different ways of obtaining classifiers via Hyperalignment, (a) those obtained from a separate fMRI session (Session 1), and (b) those obtained within-session (Session 2) via a split-half procedure.
4. Finally, to assess the cost in classification accuracy when the to-be-classified participant's data were excluded from the dataset used for the Hyperalignment (as to inform future applications of decoded neurofeedback where this scenario would be the norm).

4.3 Methods

4.3.1 Participants

Ten right-handed individuals (age 32.5 ±7.6, 8 male) with normal or corrected to normal vision participated in the experiment. All subjects provided their informed consent for the experiment. The study was approved by the Ethics Committee of the College of Science and Engineering, University of Glasgow.

4.3.2 Stimuli

Stimuli consisted of a set of 28 movies that depicted the human body as a stick figure, with point-lights at the major joints, performing arm actions (Vangeneugden et al., 2009). All movies had a duration of 2000ms with a total of 120 frames shown at 60Hz and with a resolution of 256×256 pixels. Three of the 28 movies were the 3 actions of lifting, knocking and throwing, subsequently referred to as the 'natural actions'. The remaining 25 movies were 2-way and 3-way blends of these 3 actions (Figure 4.1), subsequently referred to as the 'blended actions'. The blended actions were made using the algorithm of Kovar and Gleicher (2003), which preserves the constraints of biomechanical movement. They were created in a step size of 16.6% change of the weighting of the original actions producing 15, 2-way blended actions (Figure 4.1, outer triangle) and 10, 3-way blended actions (Figure 4.1, inner triangle and centre).

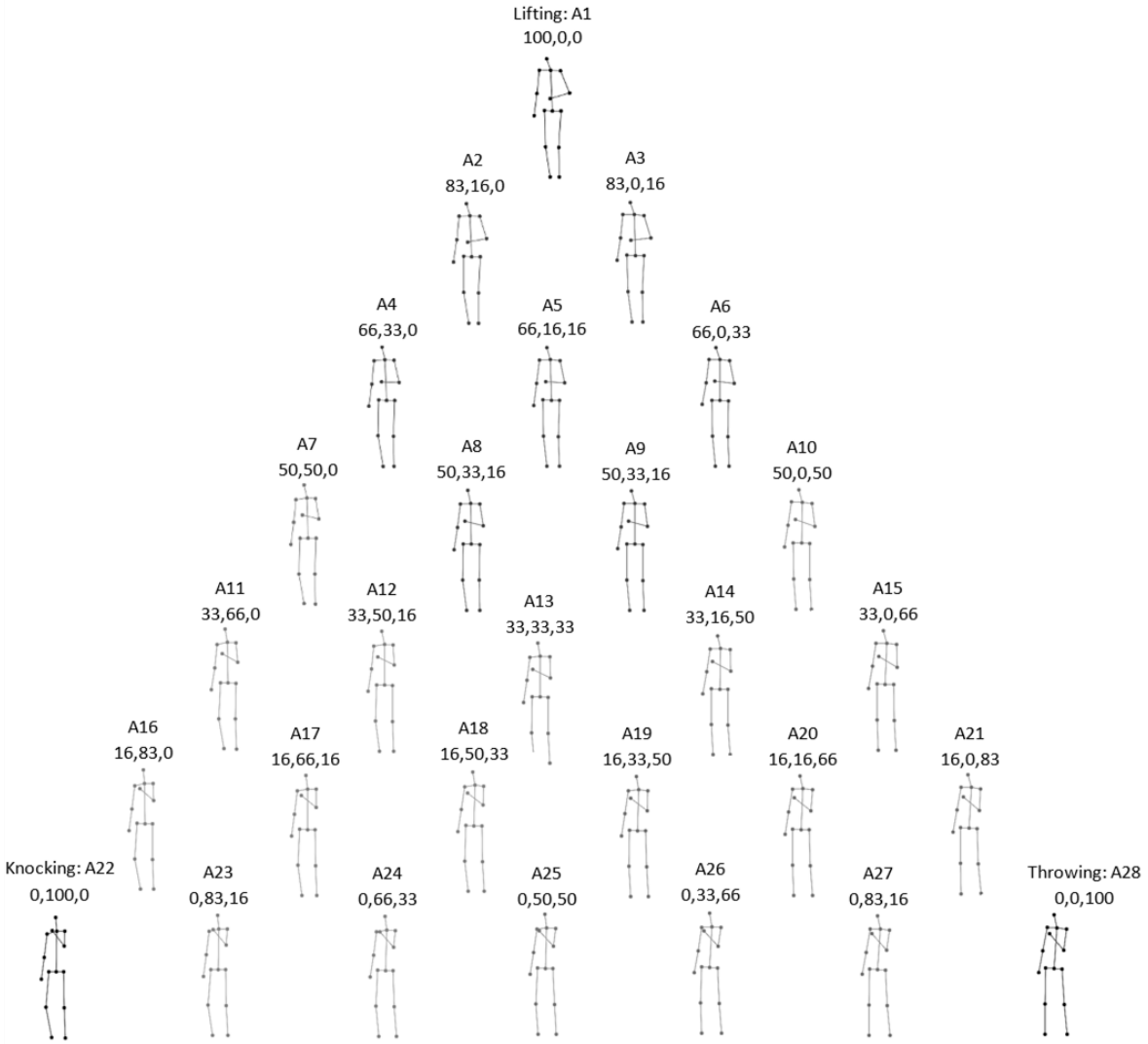

Figure 4.1. The stick-figures displaying the 60th frame of each action along with the blending weights (the percentage change of lifting, knocking and throwing respectively).

4.3.3 Apparatus and Procedure

Each participant attended two different scanning sessions. The stimuli were displayed via a LCD projector onto a rear projection screen that was viewed through a mirror mounted on the head coil. Videos subtended approximately 2.6 horizontal and 8.8 vertical degrees of visual angle. Stimulus presentation was controlled using Presentation software (Neurobehavioral Systems, Inc.).

4.3.3.1 Session 1: Blended action stimuli

In Session 1, subjects were presented with the 25 movies of the blended actions and engaged in concurrent action observation and motor imagery (AO+MI) involving their right arms. The movies were presented in 10 separate runs of 320s each using a block design. Each run started with 20s fixation and contained 6 blocks of stimuli with 12s of inter-block interval (IBI). Within a block, 14 pseudorandomly chosen actions were presented with a variable inter-stimulus interval (ISI) that ranged from 500ms to 1000ms pseudorandomly as shown in figure 4.2 (A). As a catch trial to enforce attention, subjects performed a fixation colour change task by pressing a response button with their left hand when the fixation colour changed from black to red. All subjects observed the same sequence of the runs, blocks and trials.

4.3.3.2 Session 2: Natural action stimuli

In Session 2, only the three natural action displays (lifting, throwing and knocking) were used. This session comprised a pure MI task, and an action observation with motor imagery task (AO+MI), where the AO component in the latter task served to remind partipants on the details of each action (note that the data from this AO+MI condition will not be described in the present chapter). In both tasks, subjects were instructed to imagine moving their right arm. During the pure MI condition, participants were prompted by a pacing tone that was presented over MRI-compatible headphones and controlled via Presentation software (Neurobehavioral Systems, Inc.). The auditory pacing signal consisted of beeps (100ms duration at 500Hz) repeated every 2s. Subjects were instructed to synchronize their MI with that signal. The videos were shown in a block design of 8 runs, 456s each. Each run started with 20s fixation at the beginning and consisted of 9 chunks, with each natural action presented 3 times randomly. A chunk consisted of a block of AO+MI, a short IBI of 4s, and a block of pure MI followed by a long IBI of 12s. Each block lasted for 16s and either had 8 videos of the same action for the case of AO+MI or a black screen for the case of MI (figure 4.2,B).

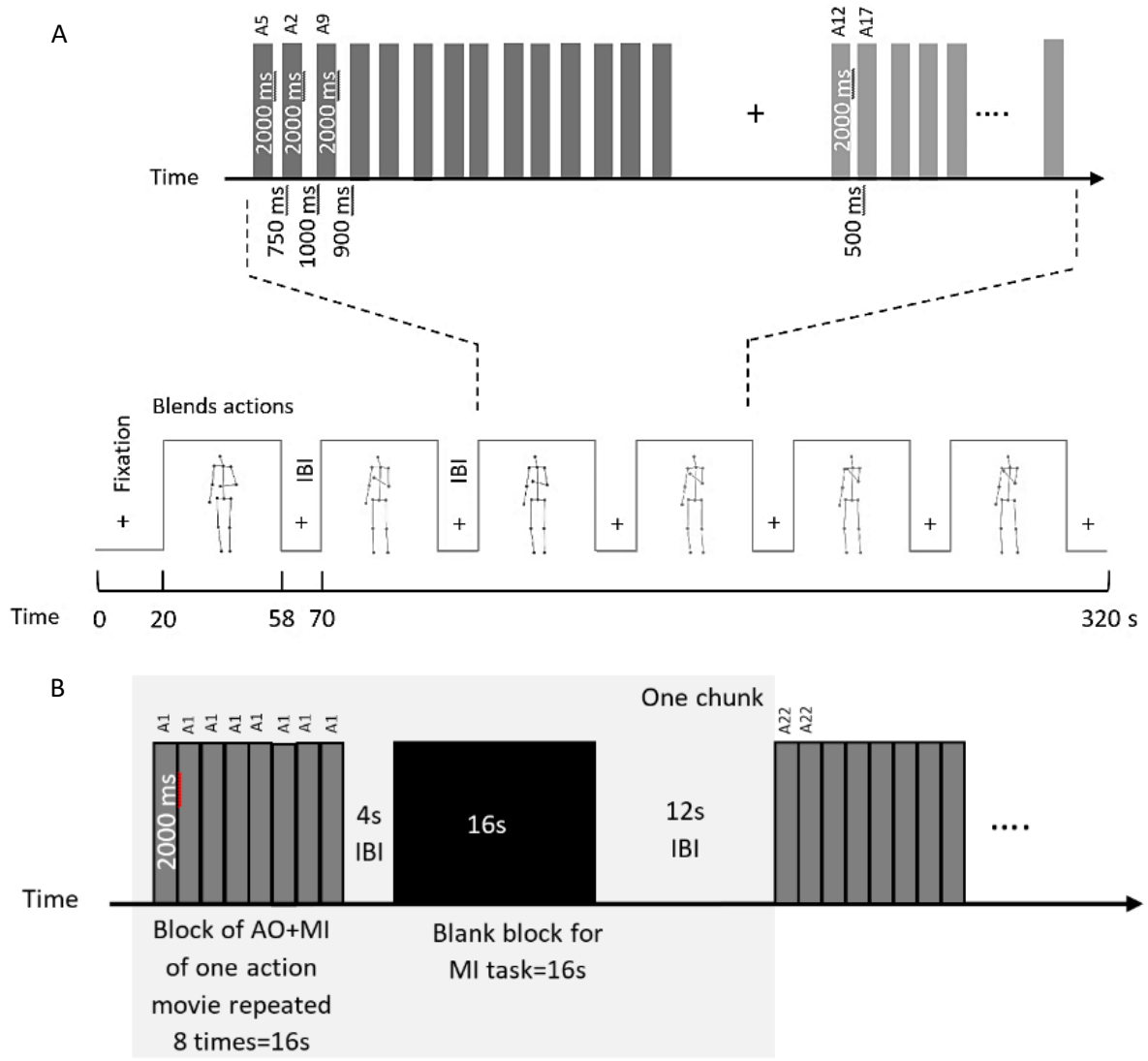

Figure 4.2. (A) Experimental design of blended actions session. Each run consisted of 6 blocks of 38s with IBI of 12s. After 20s fixation, subjects started to simultaneously perform action observation and motor imagery (AO+MI). In each block, 14 video trials of 2000ms each were presented with a variable ISI from 500-1000ms. (B) Experimental block design of natural actions session. Each run contained 9 chunks (gray shaded area), and there were 3 chunks for each action. A chunk comprised an AO+MI block with 8 repetition of the same action video of 16s, a short IBI of 4s, a pure MI block of 16s and a long IBI of 12s. After 20s fixation, participants observed and imagined (AO+MI) doing an action simultaneously for 8 times then imagined (MI) it 8 times assisted by a pacing tone.

4.3.4 Imaging protocol

Subjects were scanned in a 3 Tesla Siemens Tim Trio MRI scanner at the University of Glasgow Centre for Cognitive Neuroimaging (CCNi) with a 32-channel head coil. T1 weighted structural scans were acquired at the middle of each session (TR=2000ms, TE=2.52ms, 192 sagittal slices, 1 mm^3 isotropic voxels and image resolution 256×256). T2*-weighted functional scans were collected with an Echo-Planar Imaging (EPI) sequence (TR=2000ms, TE=30ms, whole brain coverage with 32 axial slices, with 0.3 mm gap, 3 mm^3 isotropic voxel).

4.3.5 fMRI data preprocessing

Data were preprocessed using BrainVoyager QX 2.8.4 (Brain Innovation, Maastricht, The Netherlands). Preprocessing involved slice scan-time correction with cubic-spline interpolation, 3D motion correction with Trilinear/Sinc interpolation, linear trend removal and high-pass filtering with a cutoff set to 2 cycles. All the functional volumes of each session were aligned to a reference volume, which was the first functional volume after the anatomical scan. The functional data of each subject of both sessions were spatially aligned to a common anatomical space to establish a voxel correspondence across sessions and then normalized to Talairach space (Talairach and Tournoux, 1988).

4.3.6 fMRI data analysis

All further fMRI data were analysed using MATLAB (version 9.0.0.341360, Mathworks), NeuroElf v1.0 (www.neuroelf.net) and PyMVPA 2-2.6.0 (Hanke et al., 2009; www.pymvpa.org).

4.3.6.1 Voxel selection

A gray matter mask, derived using a Talairach brain atlas in BrainVoyager, was used to extract data from Brodmann areas 4 and 6 of the left hemisphere. The resultant mask had

1758 mm^3 isotropic voxels. The time-series of activation for each voxel was normalized using z-score and shifted by 2 TRs (4 s) to account for the hemodynamic delay.

4.3.6.2 Building a common model representational space using Hyperalignment

Brain activation patterns can be considered as vectors in a high-dimensional space in which each dimension is a feature (fMRI voxel). Although the space of individual subjects are not aligned, they are time locked to the stimuli (Haxby et al., 2011). Hyperalignment uses Procrustean transformation iteratively to map subjects' representational spaces into a common model space by deriving transformation parameters for each subject. This process consists of three stages: during the first stage, an arbitrary subject is chosen to be a reference subject. The 2nd subject's response vectors are aligned to the reference subject's vectors using Procrustean transformation and then the 3rd subject is aligned to the mean response vectors of the first 2 subjects and so on. In the second stage, each subject's response vector are aligned to the mean response vectors of the first stage (intermediate common space) and new response vectors are computed by averaging all the subjects' aligned (rotated) vectors which would be the final common model space. During the last stage, Hyperalignment transformation parameters are calculated for each subject to map their voxel space into the final common model space as shown in Figure 4.3. This common model space and transformation parameters were derived using the response vectors of all subjects during the AO+MI task of the blended actions stimuli session.

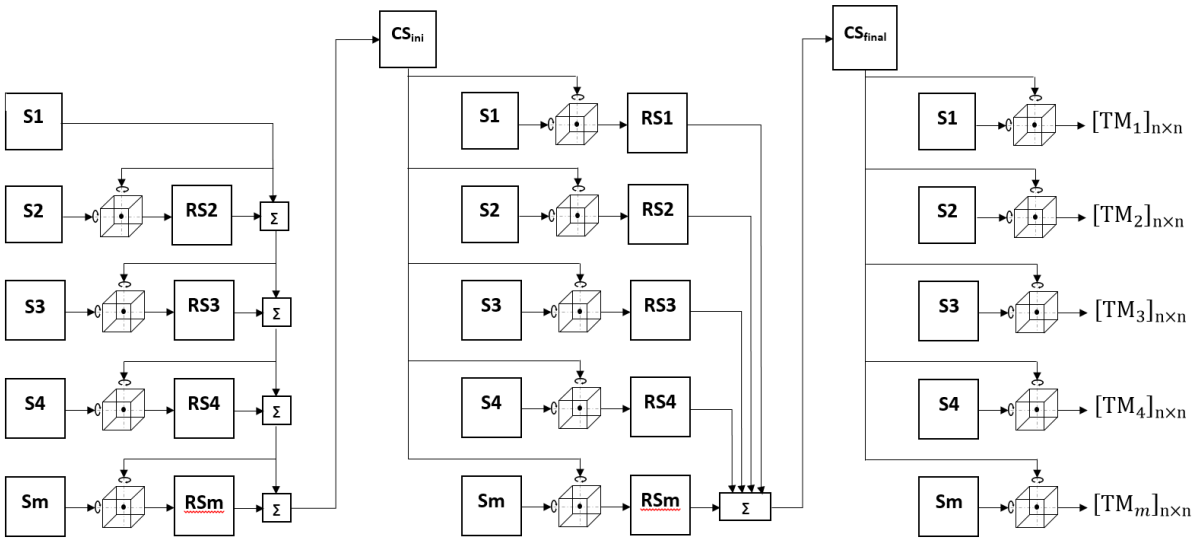

Figure 4.3. A block diagram of the Hyperalignment method used to derive a common representational space and transformation parameters (TM) using Procrustean transformation. S is the subject's representational space, RS is the subject's aligned (rotated) space using procrustean transformation, CS_{ini} is the intermediate common spaces, CS_{final} is the final common space and $\sum$ is the average of representational spaces.

4.3.6.3 Mapping the subject's representational space into the common model space

Subjects' representational spaces of the MI task obtained during the natural actions session can be aligned altogether by multiplying each subject's transformation parameters with the voxels' responses as illustrated in equation 4.1.

$$\boldsymbol{M}_{(k\times n)} = \boldsymbol{V}_{(k\times n)}\boldsymbol{T}_{(n\times n)} \quad (4.1)$$

Where $\boldsymbol{M}(k\times n)$ is the mapped matrix in the common model space (k time points, n voxels), $\boldsymbol{V}(k\times n)$ is the voxels' responses in Talairach space and $\boldsymbol{T}(n\times n)$ is the Hyperalignment transformation parameters.

4.3.6.4 Multi-Voxel Pattern Analysis

For information decoding, a multiclass linear Support Vector Machine (SVM) (Hausfeld *et al.*, 2014) implemented in PyMVPA (LIBSVM, C=-1.0) was used for the classification (lifting vs. knocking vs. throwing) of the brain activity during the MI task with

natural actions. The multiclass problem was translated into a series of binary classifications paired with a majority voting scheme to determine the predicted class (Haxby et al., 2011; Misaki et al., 2010; Reddy et al., 2009). For within subject classification (WSC), a leave-one-run-out approach was used, which resulted in 8 fold cross-validation. A leave-one-subject-and-one-run-out scheme was used for between subject classification (BSC), which generated 80 folds cross-validation across runs and subjects (Haxby et al., 2011). For each modality, data within similar stimulus blocks of each run were averaged to substitute the response patterns for that stimulus, such that 3 samples correspond to the three action stimuli per run. A SVM searchlight approach (Kriegeskorte et al., 2006) with a sphere radius of 3 voxels was used to define the network of regions that had information to decode the three stimuli, and the accuracies of all searchlight were mapped onto a cortical surface for visualization. WSC was performed by training the SVM classifier on the data from seven runs (7 runs × 3 stimuli samples = 21 pattern vectors) and tested on the left-out eighth run (3 pattern vectors) of each subject independently. For BSC, the SVM classifier was trained on the data from 1 run in 9 subjects (1 run × 9 subjects × 3 stimuli samples = 27 pattern vectors) and tested on the left out run of the left out subject (1 run × 1 subjects × 3 stimuli samples =3 pattern vectors). BSC was performed on the data that were aligned anatomically using Talairach space and on the data that were mapped in the common space using Hyperalignment.

4.3.6.5 Common model space generalization

The common model space was derived by averaging all the subjects' rotated representational spaces during the second stages of Hyperalignment (see Figure 4.3). To test the generalization of this model for a new representational space that had not played any role in deriving it, a leave one subject out of Hyperalignment procedure was performed to create a common model space and then to map the left out subject to that space and derive the transformation parameters. BSC based on Hyperalignment was conducted by training the SVM

classifier on the Hyperaligned data of 9 subjects and tested using the newly mapped subject data.

4.3.6.6 Common model space sensitivity

To compute the common model representational space a reference subject is chosen arbitrarily (when the number of voxels are equal across subjects) during the first stage of Hyperalignment and the rest of the subjects contribute by different weights (see Figure 3), To test the sensitivity of the common model space to the choice of reference subject and subject order, the subject order was shuffled 2000 times prior to calculating Hyperalignment and for each time a new common model space and transformation parameters were computed to map subjects' activation patterns of MI task and then to predict the MI class (lift, throw or knock).

4.4 Results

The results of the two fMRI recording sessions are reported. In Session 1, 10 subjects performed an AO+MI task to presentation of 25 videos displaying a parametric set of action blends of lifting, knocking and throwing. These data were used to compute Hyperalignment transformation parameters that allowed us to transform the data of individual subjects into a common model space. In Session 2, the same subjects performed pure MI to presentation of 3 videos displaying the actions lifting, knocking and throwing. From these data, SVM classifiers were used to decode the MI conditions of each individual subject using that subject's anatomically aligned data and hyperaligned data. In the following, we first explore the sensitivity of the common model space to the subject order used to estimate Hyperalignment parameters. Following this, we use the subject order that produced the highest performance of the common model space and map all the subjects' MI data to it. Then we compare between WSC, BSC based on anatomical alignment and BSC based on Hyperalignment using the blended actions for each modality separately. Additionally, we compare between BSC based

on Hyperalignment derived using the 25 blended actions and the 3 natural actions. Finally, we examine the impact of a common model generalization on BSC.

4.4.1 Sensitivity of the common model space to subject order

To assess the influence of the subject order on the common model space, 2000 permutations of subject order were performed to derive new common model spaces and Hyperalignment transformation parameters using the neural responses of the 25 blended actions. From this, the data of the MI task were mapped into the common model spaces and the distribution of BSC was estimated. Figure 4.4 presents the sorted distribution of classification accuracies based on Hyperalignment using a box-whisker plot with a median classification accuracy of 52.9% and a maximum of 67% (A), along with logarithmic scaled two-tailed t-test results between BSC based on Hyperalignment and Anatomical alignment (B).

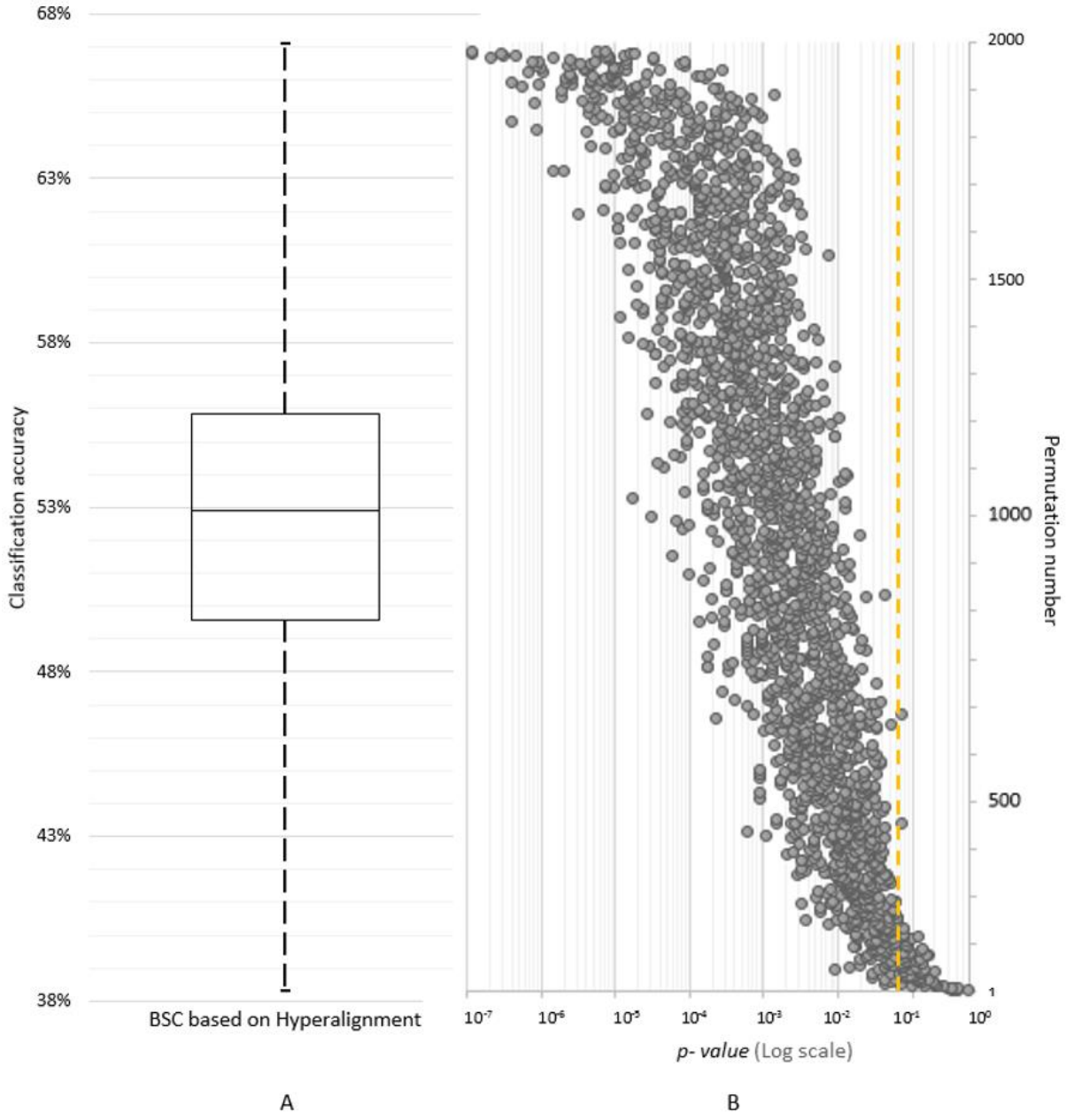

Figure 4.4. (A) a box-whisker plot of BSC based on Hyperalignment of 2000 permutations of subject order showing the classificsation accuracies of different orders of subjects, (B) logarithmic scale of two-tailed t-test betweens BSC based on Hyperalignment and BSC based on Anatomical alignment, dashed line is p=0.05.

4.4.2 Between-Subject Classification after Hyperalignment based on brain response to the 25 blended actions

The common representational space and the Hyperalignment transformation parameters were derived using the neural responses of the 25 blended actions obtained while participants performed AO+MI. In this study, 130 voxels were selected using a Searchlight approach and were used as a ROI for all the subsequent analyses. BSC using Hyperalignment was performed using subjects' response patterns on the MI task (lift, knock, and throw) respectively that were mapped into the common space using the associated Hyperalignment parameters. As a comparison, BSC using anatomical alignment was also performed on the subjects' data that were aligned based on anatomy using Talairach space (Talairach and Tournoux, 1988). BSC accuracies using both Hyperalignment and anatomical alignment were relatively stable over a wide range of voxels sets. As an additional step, BSC values were compared to WSC in which an individual classifier was constructed for each subject.

Figure 4.5 shows the Searchlight maps of BSC based on Hyperalignment and BSC based on anatomical alignment. Due to Hyperalignment, the representational space of Searchlight spheres are well aligned with an overall accuracy above 33.3% (chance level) using a common model space with a peak of (47.5%) in Supplementary Motor Area as well as M1 and dorsal PM (dPM) regions in contrast to anatomical alignment with a peak of (38.75%) in M1.

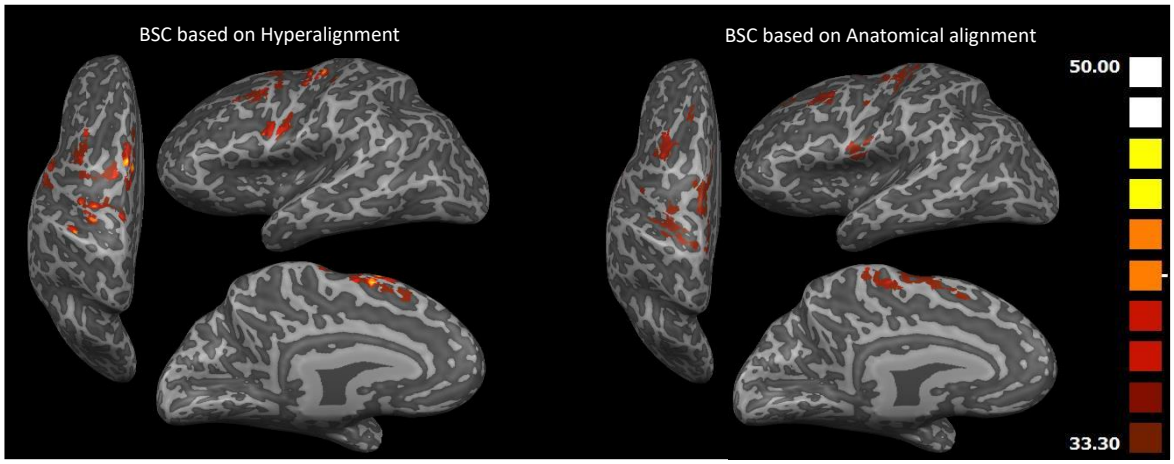

Figure 4.5. Searchlight maps of BSC based on Hyperalignment (left) and BSC based on anatomical alignment (right) using MI task (lifting, throwing and knocking). Hyperalignment transformation parameters were derived using the responses of blends action movies.

BSC accuracy of anatomically aligned data were (36.26%, SEM=2.5%, chance=33%). However, after the Hyperalignment, BSC predicted the three actions with an accuracy of 67.08% (SEM=4.1%), and it was significantly better than the anatomical alignment (two-tailed t-test, $p < 0.0001$). On the other hand, the average WSC accuracy was less than the BSC of Hyperaligned data (48.3%, SEM=3.29%) as shown in figure 4.6. The confusion matrix of BSC based on Hyperalignment shows that the classifier identifies the individual actions as shown in figure 4.7, on the contrary, BSC based anatomical alignment does not show any discrimination among actions.

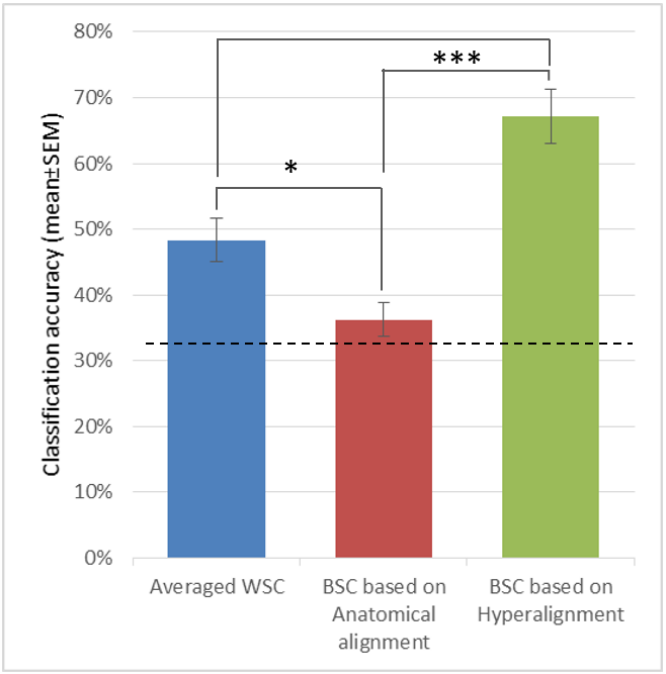

Figure 4.6. The classification accuracies (mean ±SEM) for averaged WSC, BSC based on Anatomical alignment and BSC based on Hyperalignment, dashed line indicates chance level (33%). * $P \leq 0.05$, ** $P \leq 0.01$, *** $P \leq 0.001$.

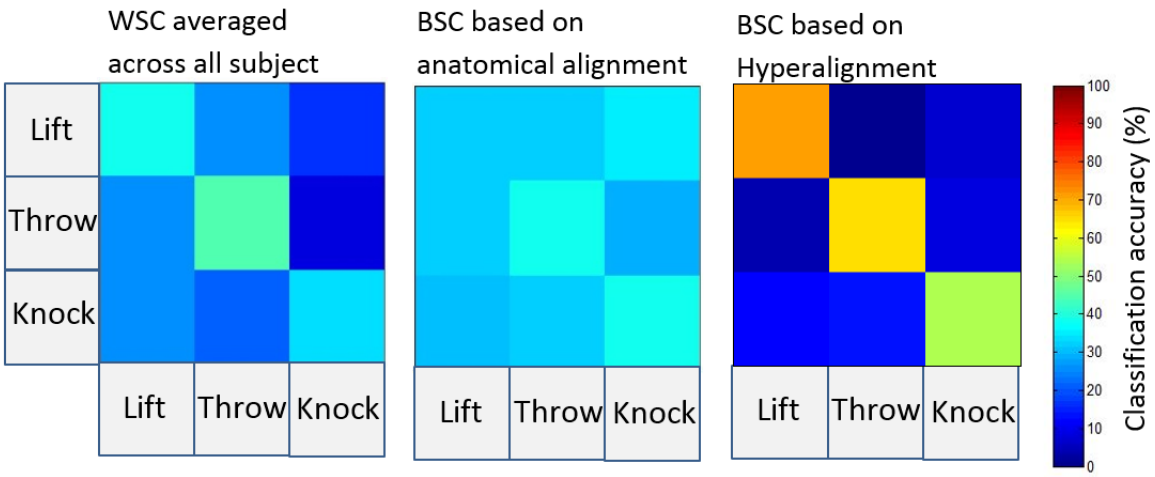

Figure 4.7. Confusion matrices for action classification using WSC, BSC based anatomical alignment and BSC based on Hyperalignment.

4.4.3 Between-Subject Classification after Hyperalignment based on brain response to the natural actions

The common representational space and the Hyperalignment transformation parameters can be derived from other sources of fMRI data (Haxby et al., 2011). Thus, in addition to the common representational space and Hyperalignment transformation parameters based on neural responses of the AO+MI task on the blended actions we ran another analysis to investigate whether the Hyperalignment parameters derived using only the neural responses of the MI task on the three natural actions would afford a high BSC accuracy. The common space was derived using all runs but one of the subjects. Then the left out run of each subject was mapped into the common space using the Hyperalignment parameters obtained earlier. To avoid double dipping (Kriegeskorte et al., 2009), a classifier was trained on the left out runs of all the subjects except one and was tested on the data of the left out run in the left out subject and hence, the test data play no role either in training the classifier or in Hyperalignment. BSC accuracy after Hyperalignment based on the data of the same session was almost comparable to Hyperalignment based on the blended action movies (69.17%, SEM=2.42% versus 67.08%, SEM=4.1%) respectively.

4.4.4 Common space model generalization

We conducted further analysis to study the decoding effect of aligning new subjects to the common model space who have not contributed to derive it. Figure 4.8 shows the BSC based on Hyperalignment of a common model derived using either all the subjects' data or by mapping a new subject to a pre-prepared common model. The comparison demonstrates that both BSCs based on Hyperalignment are statistically better than BSC based on anatomical alignment (two-tailed *t*-test $P \leq 0.0002$). Thus, although engaging all the subjects' representational spaces fine tunes the common model space, aligning a new subject's

representational space to a pre-defined common model still shows benefit over BSC based on anatomical alignment. This property could prove beneficial during a paradigm using online fMRI classification.

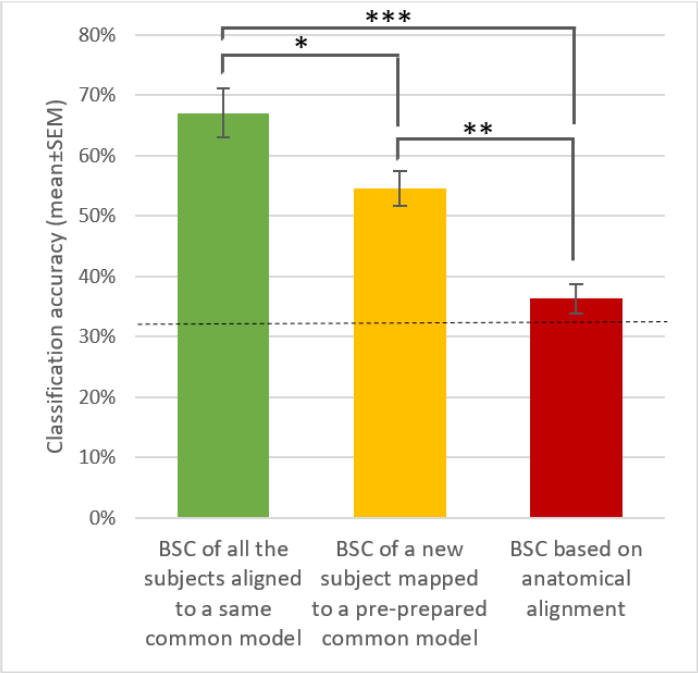

Figure 4.8. BSC based on Hyperalignment of a common model space derived using all the subjects' data or derived using all the subject except one. Dashed line is chance level=33%. * $P \leq 0.05$, ** $P \leq 0.01$, *** $P \leq 0.001$.

4.5 Discussion

In this paper, we performed Hyperalignment to map the functional voxel spaces of the activity in individual subjects' motor cortex into a common model space. Hyperalignment uses Procrustean transformation to rotate subject's representational axes into a common coordinate system in which the neural responses for the same stimuli or tasks are in optimal alignment across individuals. This model is a high-dimensional representational space that captures the fine-scale topographies and their variability across brains. Hyperalignment computes the transformation parameters for each subject that can be applied to map a different set of response vectors using the same subjects' voxels, into a common model space. Previously, Haxby and

colleagues have explored the feasibility of using Hyperalignment to align fMRI data in visual and auditory cortices (Haxby *et al.*, 2011; Guntupalli *et al.*, 2016), however it is unknown whether the technique works to align other brain regions. Here, we used Hyperalignment to compute a common model representational space of the motor cortex from data obtained while participants performed an AO+MI task, and we validated that model by decoding the brain activity during MI of different arm actions.

The first aim of our research was to explore whether the order in which participants were entered into the Hyperalignment procedure mattered for the generation of a discriminative subject-independent classifier. Previous reports of Hyperalignment results did not provide any analysis of subject order (Haxby, et al., 2011), however the Hyperalignment algorithm is potentially sensitive to subject order. The inter-subject response variability to the task and different weights of subject's contribution toward computing the intermediate common model (see Fig. 4.4) influence the Hyperalignment algorithm in its ability to rotate and align response vectors of the same stimulus across subjects. The results of our permutation test that shuffled the subjects order and computed a new common model in each iteration showed that subject order had a profound effect. Why subject order had a substantial effect for our study exploring motor cortex is an area deserving further research. To be effective the common model representational space must be capable of capturing the fine-grained representation structures encoded in subjects' responses and the motor cortex might provide more inter-subject response variability for the representation of actions than obtained in the representation of objects in temporal cortex (Haxby, et al., 2011). Another possible source of variability is in the tasks used as Haxby and colleagues (2011) used a natural dynamic audiovisual stimulus (e.g. watching a movie), while we used a set of blended movements that densely sampled a particular movement space and had participants perform a visuomotor task (AO+MI). While both are inherently multisensory (audiovisual versus visuomotor) it could be that Haxby et al.'s

audiovisual task produces less response variability in temporal cortex than our AO+MI task produces in SMA and dorsal premotor areas. In addition, the representation of different arm actions among a space of actions might be more sensitive to perturbation than the representation of different visual objects.

Based on the above, the second (and main) aim of this study was to compare the classification accuracy of BSC derived from Hyperalignment with BSC using anatomical alignment, and with the more standard WSC approach, using a separate dataset that involved a pure MI task. Importantly, the results demonstrated that mapping from individuals' voxel spaces into a high dimensional common space affords a BSC that significantly exceeds the BSC based on anatomical alignment. In addition, the standard individualised WSC-based classification accuracy exceeded that of BSC with anatomical alignment, but also the former was significantly lower than BSC based on Hyperalignment (see Fig. 6). The average WSC of the MI task in left motor cortex was comparable to that reported in the studies by Zabicki et al. (2016) and Pilgramm et al. (2016). Interestingly, our paradigm involved imagining moving the whole right arm (complex actions) while the above two studies used simple actions that only engaged the fingers of the right hand. Our findings illustrate that Hyperalignment offers higher classification accuracies by building a common model of the motor cortex to increase the power of MVPA to detect the fine scale information across participants.

In the above validations, Hyperalignment parameters had been obtained from the AO+MI task in Session 1, and these were shown to be successful for the classification of the fMRI signal during the MI task in Session 2. However, Hyperalignment parameters can be computed from any fMRI data (Haxby *et al.*, 2011), thus it is not clear what limits there are for creating valid classifiers. Accordingly, our third aim was to contrast two different classifications based on Hyperalignment, one based on the above model, and the other using the fMRI signal from the MI task of all runs except one of the subjects. Indeed, our results

showed that both models afforded comparable levels of classification accuracy. These results further demonstrate the flexibility of Hyperalignment to align subjects' representational spaces using different data sources.

Finally (aim 4), we were interested in whether Hyperalignment would be successful in the situation when data from a subject not used in the original Hyperalignment creation process was encountered. To explore this we examined the cost in classification accuracy when a to-be-classified participant's data were excluded from the dataset used for the Hyperalignment and showed that although there was a decrease in performance, it was still better than BSC based on anatomical alignment. Such a situation would arise if Hyperalignment based on one set of participants would be used to perform classification on data from a new subject and could be expected in applications like real-time decoded neurofeedback. A new subject would require a mapping of their neural responses into a previously computed common model and an estimate of their transformation parameters based on neural responses to the original data set could be used to obtain the transformation parameters. The computed parameters would be used to transform each new subject's data into the common model space and subsequently, feedback would be given by a pre-trained classifier that identifies the brain states of the new subject Hyperaligned data.

In conclusion, we introduce here a common high dimensional model of the motor cortex that capture the fine grained structure of brain responses during MI task of natural actions. This model is derived by using a Hyperalignment algorithm that rotates subjects' representational spaces into one common space, affording high BSC accuracies compared to BSC based on anatomical landmarks. Hyperalignment can be used to align data from similar experiments into one common model that establishes a functional correspondence of fine-scale topographies across brains, enabling the use of these datasets to examine neural representations and

individual differences. More importantly for MVPA analysis, this common model would reduce the time and cost of scanning by avoiding collecting extra data to train classifiers.

4.6 Rationale for the experimental chapters 4 and 5

The aims of the experimental chapter 4 were to examine the feasibility of using the left hemisphere motor cortex (M1 and PM) as a ROI to decode the representational spaces of multi-joint arm actions (lift, knock and throw) during MI task and also, to map subjects' representational spaces of that ROI into a common model space using hyperalignment. This common space facilitated building a subject independent classifier that is capable to predict the correct class (actions) from a new subject's data. Classification accuracies based on hyperaligned data were higher than those based on anatomically aligned data or within-subject classification. Furthermore, chapter 4 identified that the subject order entering hyperalignment algorithm is important to creating a robust common model representational space. This adds to recent literature the use of hyperalignment to align motor representational spaces across subjects after optimizing the subject order. In the next experimental chapter (chapter 5), these finding of hyperalignment were extended by mapping the fronto-parietal motor regions (12 symmetrical ROIs in both hemispheres). These ROIs were delineated using cortex based alignment for a better anatomical localization prior to applying hyperalignment. In addition, the shared neural code evoked from AO+MI and MI tasks was evaluated using cross-modal classification and the similarity of different actions (lift, knock and throw) and modalities (AO+MI and MI) representations was examined using RSA.

Chapter 5 : Testing Neural Similarity of Multi-Joint Arm Actions during Motor Imagery and Motor Imagery with Action Observation using Multivariate Pattern Analysis

5.1 Abstract

Motor simulation theory proposes that motor imagery (MI) and action observation (AO) partially activate the same motor network, which is involved in motor execution (ME). Previous fMRI studies have used univariate analysis to demonstrate that combining AO and MI (AO+MI) elicits stronger neural activation in the ME network than MI or AO in isolation. However, it is unclear to what extent AO+MI and MI use the same neural code. In the present studies, we used multivariate pattern analysis (MVPA), hyperalignment and representational similarity analysis (RSA) to align and to characterise the neural representations associated with AO+MI and MI within the fronto-parietal motor network. During functional magnetic resonance imaging scanning, 10 participants concurrently observed and imagined (AO+MI) or imagined (MI) 3 different types of multi-joint right arm actions. The results of MVPA showed that the action types, along with their modality (AO+MI or MI) could be decoded at a level that was significantly above chance either from the participant's representational space or from the common representational space derived using hyperalignment. This was also true for cross-modality decoding. However, the classification performance of action types based on AO+MI or MI tasks was not statistically significant. Moreover, representational dissimilarity matrices of frontal-parietal motor regions showed that AO+MI and MI representations formed separate

clusters, but that the representational organisation of action types within these clusters was identical. For most ROIs, this pattern of results best fits with a model that assumes a low-to-moderate degree of similarity between the neural patterns associated with different actions during AO+MI and MI tasks. Therefore, the neural representations of AO+MI and MI are neither the same nor totally distinct, but exhibit a similar structural geometry with respect to different types of action. Additionally, we can cautiously conclude that MI dominates in AO+MI conditions.

5.2 Introduction

Over the last two decades, there has been an increased interest in the motor simulation theory proposed by Jeannerod (2001). This theory proposed that the acts of observing and imagining motor actions both activate the neural network involved in motor execution. It also suggested that every action involves a covert state that includes the goal of the action and its sensory consequences. Motor imagery (MI) and action observation (AO) are two forms of covert actions (Vogt *et al.*, 2013; Filimon *et al.*, 2015), which are simulated by individuals in the absence of motor output (Hanakawa *et al.*, 2008; Blefari *et al.*, 2015). MI is defined as a cognitive process in which a subject imagines performing an action in the absence of motor output (Hétu *et al.*, 2013). It is a complex, internal, conscious rehearsal of visual and/or kinaesthetic aspects of movements (Hanakawa *et al.*, 2008; Munzert *et al.*, 2009; Vogt *et al.*, 2013). It has been suggested that MI facilitates motor skill acquisition and motor learning (Schuster *et al.*, 2011), and enhances motor performance (Gentili *et al.*, 2010) in a similar way to physical practice, resulting in cortical plastic changes following repetitive mental training (Miller *et al.*, 2010). Clinically, MI has been used in motor rehabilitation after stroke (Malouin and Richards, 2013). Similarly, AO has gained increasing interest following the discovery of mirror neuron systems (MNS) in non-human primates (Gallese *et al.*, 1996; Rizzolatti and Sinigaglia, 2010) and in the human brain (Fabbri-Destro and Rizzolatti, 2008; Oztop *et al.*,

2013). Mirror neurons discharge during both the execution of goal-directed movements and the observation of other individuals who are performing similar movements. AO elicits an internal motor representation of the observed action (Rizzolatti and Sinigaglia, 2010). It forms the basis of learning through imitation (Buccino *et al.*, 2004), and has been recommended as a neurorehabilitation tool (Buccino, 2014). Whilst AO and MI have traditionally been studied in isolation and by different research groups, there is now growing evidence that both forms of motor simulation can be used concurrently, and that AO+MI generates both enhanced behavioural effects and more robust neural activation patterns than AO or MI alone (for review, see Vogt et al., 2013, and Eaves et al., 2016).

In terms of the neural substrates underlying MI and AO, they recruit motor and motor-related regions including the supplementary motor area (SMA), the premotor cortex (PMC), and posterior parietal regions such as the inferior and the superior parietal lobe (IPL and SPL respectively), which overlap both with one another and with regions involved in motor execution (ME) (Caspers *et al.*, 2010; Hétu *et al.*, 2013). This neural overlap with ME networks facilitates motor learning and rehabilitation using MI and AO. Based on this, the majority of evidence generally advocates for MI and AO being two independent techniques that are useful for improving motor abilities. While the majority of previous research has focused on MI or AO in isolation, there is now a growing body of brain imaging studies demonstrating that observing an action while imagining the same action (AO+MI) evokes significantly stronger activation in the motor execution network compared with observing or imagining the action independently (Macuga and Frey, 2012; Nedelko *et al.*, 2012; Eaves *et al.*, 2016). Taube et al., (2015) reported that AO+MI had a unique neural signature and it evoked greater neural activity in the SMA, basal ganglia, and cerebellum compared to AO, and in the bilateral cerebellum and precuneus compared to MI. Other fMRI studies have reported that AO+MI increased the neural activity over the AO in parts of the cerebellum, inferior frontal gyrus, IPL and SMA

(Nedelko *et al.*, 2012), ventral premotor cortex (PMv) and left insula (Villiger *et al.*, 2013). However, all of these studies used univariate data analysis to map the overall brain activity changes associated with a given stimulus or cognitive task (Jezzard *et al.*, 2003a). This form of traditional fMRI data analysis does not consider the distributed changes of activation patterns within a region of interest (ROI) which may occur in the absence of overall amplitude modulation.

In contrast to the univariate approach, a multivariate pattern analysis (MVPA) allows us to investigate the representational content of the neural population code (Haynes and Rees, 2006; Mur *et al.*, 2009; Kriegeskorte, 2011; Mahmoudi *et al.*, 2012; Haxby *et al.*, 2014). This approach detects the distributed activity patterns across multiple voxels, including those with weaker activation (Haxby *et al.*, 2011), and links them to a given stimulus or experimental condition. Previous studies have documented the feasibility of MVPA for decoding imagined and/or executed hand actions from frontal and parietal regions (Pilgramm *et al.*, 2016; Zabicki *et al.*, 2016). Furthermore, Filimon et al., (2015) decoded action modalities (AO, MI and ME) from neural activity patterns in motor and motor related regions. Pilgram et al., (2016) provided evidence that patterns of activity within the primary motor, premotor and parietal (IPL and SPL) regions differentiate between three different types of imagined hand actions: a force production task, an aiming task, and an extension–flexion task, while Zabicki et al., (2016) demonstrated that these actions, as well as their modalities (MI or ME), can be decoded using the elicited neural activity pattern within the fronto-parietal motor network.

The MVPA is a subject dependent analysis which tailors a new classifier model for each subject; this is necessary because the structure of neural activation varies across different brains (Haxby *et al.*, 2014). It has been documented that classification performance drops when predicting another subject's responses (Haxby *et al.*, 2011). Haxby and colleagues (Haxby et al., 2011; Haxby et al., 2014; Guntupalli et al., 2016) addressed this limitation by developing

an algorithm called hyperalignment to functionally align subjects' representational spaces and to create a common high dimensional representational space of the VT cortex. Our previous work (chapter 4) showed that hyperalignment can be used to align subjects' representational spaces in the motor cortex into a common representational model. Our results demonstrated that hyperalignment can align the neural responses across subjects' motor cortices and can significantly improve between-subject classifications better than anatomical alignment.

The current study addressed the following objectives: (1) Since, at present, classification performance of action types has been only documented for MI and ME, we wanted to assess whether different types of multi-joint arm actions can be decoded from the neural activity pattern during pure MI and AO+MI conditions to allow a more integrative view. (2) Our second aim was to create a subject-independent classifier to reduce scanning and analysis time compared to employing subject-dependent MVPA by parcellating the motor and motor-related area using CBA and then aligning these regions using hyperalignment. (3) The third aim was to examine whether MI and AO+MI share similar neural codes by attempting cross-modality classification. All the aims mentioned above explored the effect of AO on MI. (4) Our last aim was to study the similarity between the representations of different hand actions during MI and AO+MI by using RSA.

Our fMRI experiment consisted of two sessions; the first was used to obtain the common model space, and the second was used to evaluate the classification accuracies. Our participants had either to imagine (MI) or observe and imagine (AO+MI) different multi-joint right arm actions: knocking, throwing and lifting, as well as blended actions (Vangeneugden *et al.*, 2009).

In the first session, participants engaged in an AO+MI task of n=25 blended action stimuli, in order to provide a base for deriving a common model space. All stimuli used in Session 1 were stick figure displays that were blended, with varying weights, between three

natural multi-joint actions that anchored the space of blended movements (lifting, knocking, and throwing; Vangeneugden et al., 2009). This set of blended movements are biomechanically possible actions that sample the space between the anchor points and thus provide a set of movements specially adapted for study of the anchor points.

In the second fMRI session, participants engaged either in AO+MI or pure MI of the three natural (lifting, knocking, and throwing) actions that formed the basis of the above blend space. We then decoded the action types (knocking vs throwing vs lifting) and the modality (AO+MI vs MI) based on the neural activity pattern they evoked in the motor, premotor and parietal cortices. Separate classifiers were trained and tested for each ROI of each subject in order to obtain an index of pattern discriminability. In the next step, we applied a hyperalignment approach (Haxby *et al.*, 2011) to align ROIs across participants prior to the decoding and to generate subject-independent classifiers. Then, we classified across the 2 modalities (MI and AO+MI) for each given action to test whether MI and the AO+MI of specific arm movements shared a similar neural code. Finally, we used Representation Similarity Analysis (RSA) (Kriegeskorte *et al.*, 2008a) to characterise the representational geometry of different action types and modalities in every motor area, and compared them with several computational models: the action type model, the modality model, and 3 different mixed models (Khaligh-Razavi and Kriegeskorte, 2014).

5.3 Methods

5.3.1 Participants

Ten right-handed individuals (mean age±SD= 32.5 ±7.6, 8 male) with normal or corrected to normal vision participated in the experiment. All subjects provided their informed consent for the experiment. The study was approved by the Ethics Committee of the College of Science and Engineering, University of Glasgow.

5.3.2 Stimuli

The stimuli consisted of a set of 28 movies that depicted the human body as a stick figure, with point-lights at the major joints, performing arm actions (Vangeneugden et al., 2009). All movies had a duration of 2000ms, with a total of 120 frames shown at 60Hz and a resolution of 256×256 pixels. Three of the 28 movies were the 3 actions of lifting, knocking and throwing, subsequently referred to as the 'natural actions'. The remaining 25 movies were 2-way and 3-way blends of these 3 actions (figure 5.1), subsequently referred to as the 'blended actions'. The blended actions were made using an algorithm from Kovar and Gleicher (2003), which preserves the constraints of biomechanical movement. They were created in a step size of 16.6% change of the weighting of the original actions, producing 15 2-way blended actions (figure 5.1, outer triangle) and 10 3-way blended actions (figure 5.1, inner triangle and centre).

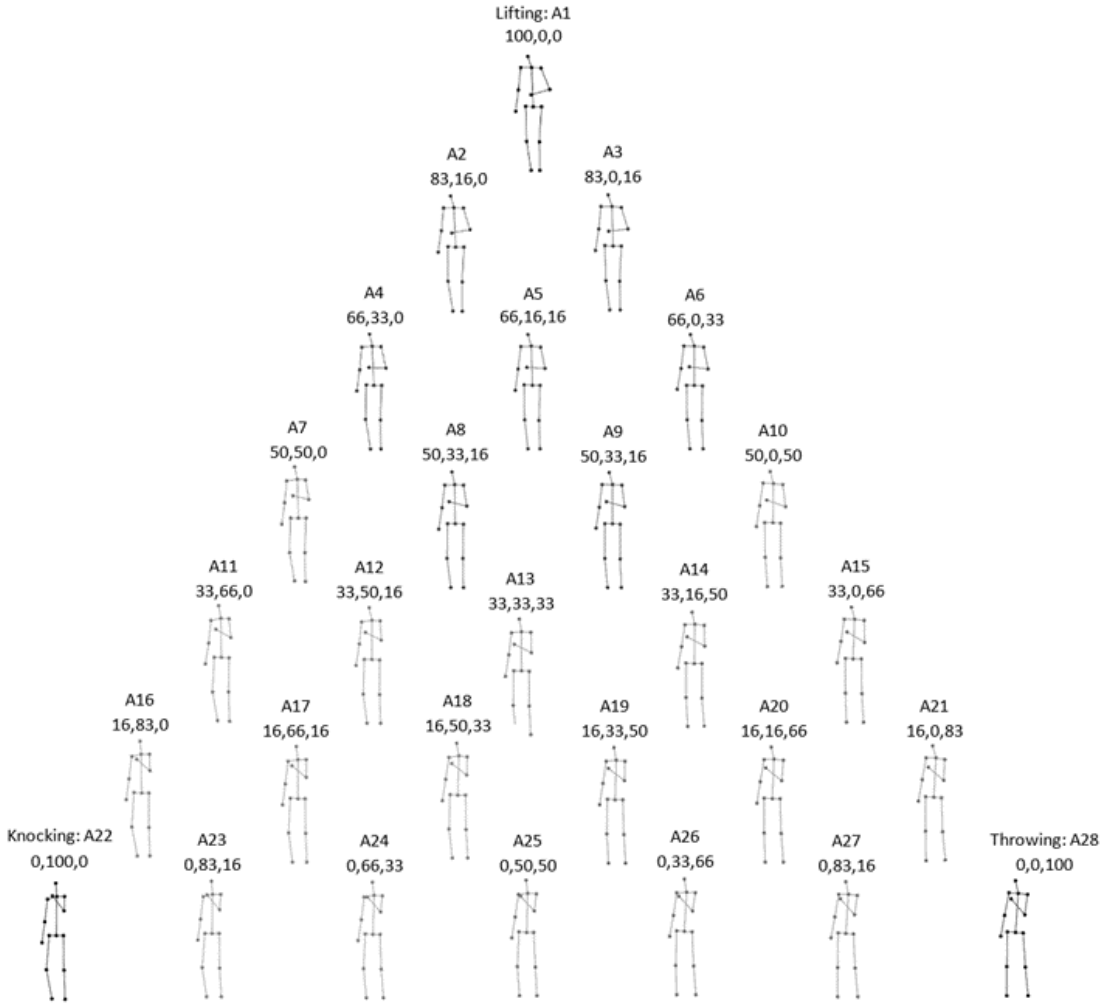

Figure 5.1. The stick-figures displaying the 60th frame of each action along with the blending weights (the percentage change of lifting, knocking and throwing respectively).

5.3.3 Apparatus and Procedure

Each participant attended two different scanning sessions. The stimuli were displayed via a LCD projector onto a rear projection screen that was viewed through a mirror mounted on the head coil. Videos subtended approximately 2.6 horizontal and 8.8 vertical degrees of visual angle. Stimulus presentation was controlled using Presentation software (Neurobehavioral Systems, Inc.).

5.3.3.1 Session 1: Blended action stimuli

In Session 1, subjects were presented with the 25 movies of the blended actions, and were engaged in AO+MI tasks involving their right arms. The movies were presented in 10 separate runs of 320s each using a block design. Each run started with 20s fixation and contained 6 blocks of stimuli with 12s of inter-block interval (IBI). Within a block, 14 pseudorandomly chosen actions were presented with variable interstimulus intervals (ISI) that ranged from 500ms to 1000ms pseudorandomly as shown in figure 5.2 (A). As a catch trial to enforce attention, subjects performed a fixation colour change task by pressing a response button with their left hand when the fixation colour changed from black to red. All subjects observed the same sequence of the runs, blocks and trials.

5.3.3.2 Session 2: Natural action stimuli

In Session 2, only the three natural action displays (lifting, throwing and knocking) were used. This session comprised a pure MI task and an AO+MI task. In both tasks, participants were instructed to imagine moving their right arm. During the pure MI condition, they were prompted by a pacing tone that was presented over MRI-compatible headphones and controlled via Presentation software (Neurobehavioral Systems, Inc.). The auditory pacing signal consisted of beeps (100ms duration at 500Hz) repeated every 2s. Subjects were instructed to synchronise their MI with that signal. The videos were shown in a block design of 8 runs, 456s each. Each run started with 20s fixation at the beginning and consisted of 9 chunks, with each natural action presented 3 times randomly. A chunk consisted of a block of AO+MI, a short IBI of 4s, and a block of pure MI followed by a long IBI of 12s. Each block lasted for 16s and either had 8 videos of the same action (for the case of AO+MI), or a black screen (for the case of MI), as shown in figure 5.2(B). A catch trial was included where subjects performed a fixation colour change task.

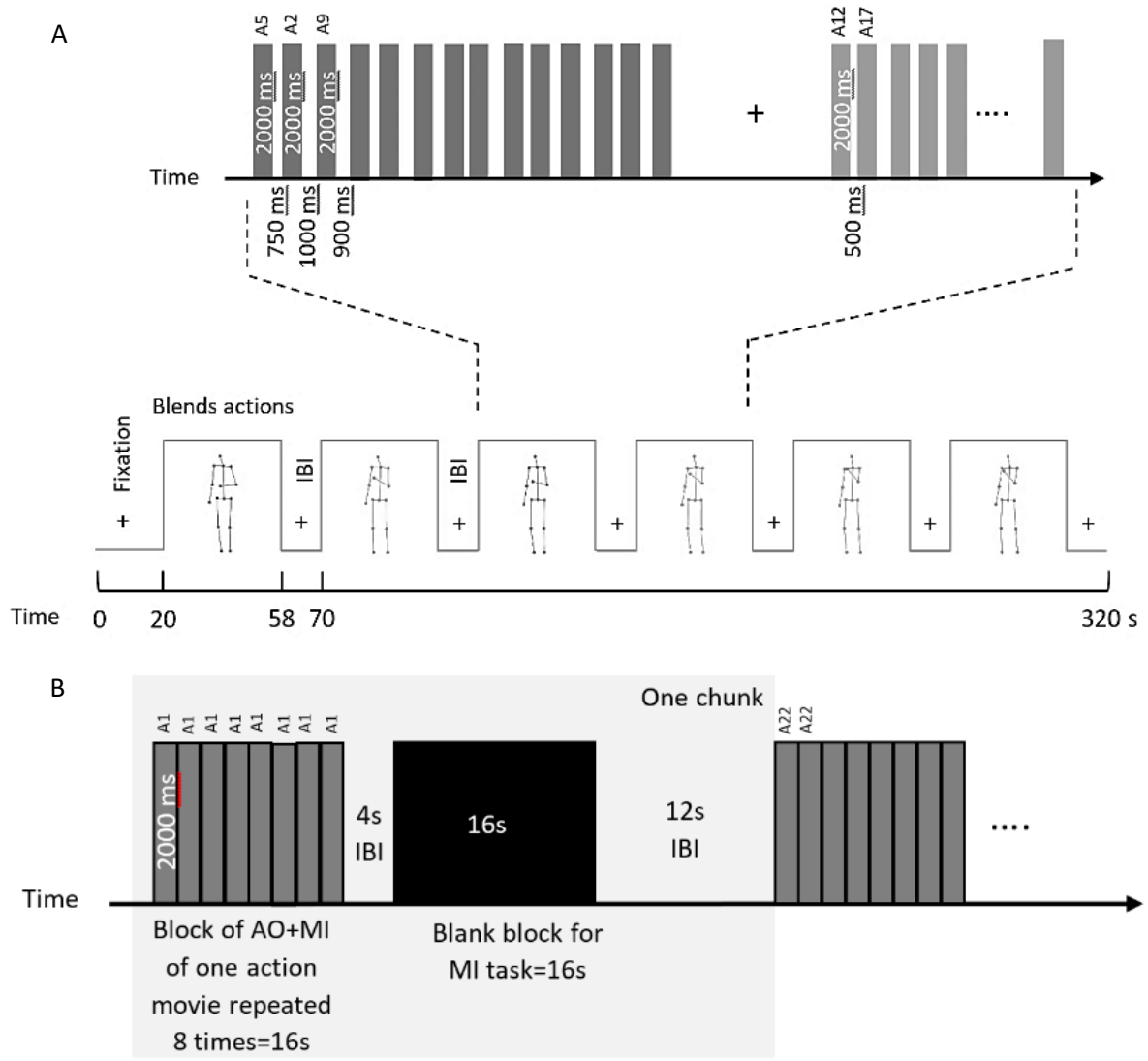

Figure 5.2. (A) Experimental design of blended actions session. Each run consisted of 6 blocks of 38s with IBI of 12s. After 20s fixation, subjects started to perform the AO+MI task. In each block, 14 video trials of 2000ms each were presented with a variable ISI from 500-1000ms. (B) Experimental block design of natural actions session. Each run contained 9 chunks (gray shaded area), and there were 3 chunks for each action. A chunk comprised an AO+MI block with 8 repetitions of the same action video of 16s, a short IBI of 4s, a pure MI block of 16s and a long IBI of 12s. After 20s fixation, participants observed and imagined (AO+MI) doing an action simultaneously 8 times, then imagined (MI) it 8 times assisted by a pacing tone.

5.3.4 Imaging protocol

Subjects were scanned in a 3 Tesla Siemens Tim Trio MRI scanner at the University of Glasgow Centre for Cognitive Neuroimaging (CCNi) with a 32-channel head coil. T1 weighted structural scans were acquired at the middle of each session (TR=2000ms, TE=2.52ms, 192 sagittal slices, 1 mm3 isotropic voxels and image resolution 256×256). T2*-weighted functional scans were collected with an Echo-Planar Imaging (EPI) sequence (TR=2000ms, TE=30ms, whole brain coverage with 32 axial slices, with 0.3 mm gap, 3 mm^3 isotropic voxel).

5.3.5 fMRI data processing

The raw data were preprocessed using BrainVoyager QX 2.8.4 (Brain Innovation, Maastricht, The Netherlands). The preprocessing of anatomical scans involved Intensity inhomogeneities correction and brain extraction. The preprocessing of functional data involved slice scan-time correction with cubic-spline interpolation, 3D motion correction with Trilinear/Sinc interpolation, linear trend removal and high-pass filtering with a cut-off set to 2 cycles. All the functional volumes of each session were aligned to a reference volume, which was the first functional volume after the anatomical scan. The functional data of each subject of both sessions were spatially aligned to a common anatomical space in order to establish a voxel correspondence across sessions, and this was then normalised to Talairach space (Talairach and Tournoux, 1988).

5.3.6 fMRI data analysis

All further fMRI data were analysed using MATLAB (version 9.0.0.341360, Mathworks), NeuroElf v1.0 (www.neuroelf.net) and PyMVPA 2-2.6.0 (Hanke et al., 2009; www.pymvpa.org).

5.3.6.1 Cortex based alignment

Cortex based alignment (CBA) aligns individuals' brains using curvature information of the cortex (Fischl *et al.*, 1999; Frost and Goebel, 2012). CBA reduces the anatomical

variability by matching the gyri and sulci across brains. For each subject, the anatomical scan was used to reconstruct the cortical surface of each hemisphere. These folded surfaces were inflated into spherical representations, which provides a parameterisation surface for the subsequent cortical alignment. The curvature information (gyri and sulci) of the folded cortices were maintained as a curvature map on the spherical representation. Then the curvature information was smoothed with respect to the surface, in order to provide spatially extended gradient information that drives intercortex alignment by minimising the mean squared differences between the curvature of a source and a target sphere, using an iterative coarse to fine matching procedure. Finally, alignment of an individual folded brain to BrainVoyager standard atlas was computed with respect to this intermediate spherical representation.

5.3.6.2 Regions of Interest

Regions of Interest (ROIs) were defined based on previous findings reported in motor simulation literatures (Hétu *et al.*, 2013) and delineated anatomically on an individual basis using a CBA approach. We parcelled six grey matter masks pre-hemisphere as shown in figure 5.3 using BrainVoyager Talairach atlas as follows:

- Primary motor cortex (M1) defined as the precentral gyrus or Brodmann area (BA) 4.
- SMA defined as the region that anterior of the paracentral sulcus and superior of the cingulate sulcus.
- Dorsal and ventral premotor areas (dPM and vPM) defined as the superior and inferior part of BA6.
- SPL defined as a region bounded by the upper part of postcentral sulcus, intraparietal sulcus and parietooccipital fissure.
- IPL defined as the supra-marginal gyrus rostrally and the angular gyrus caudally.

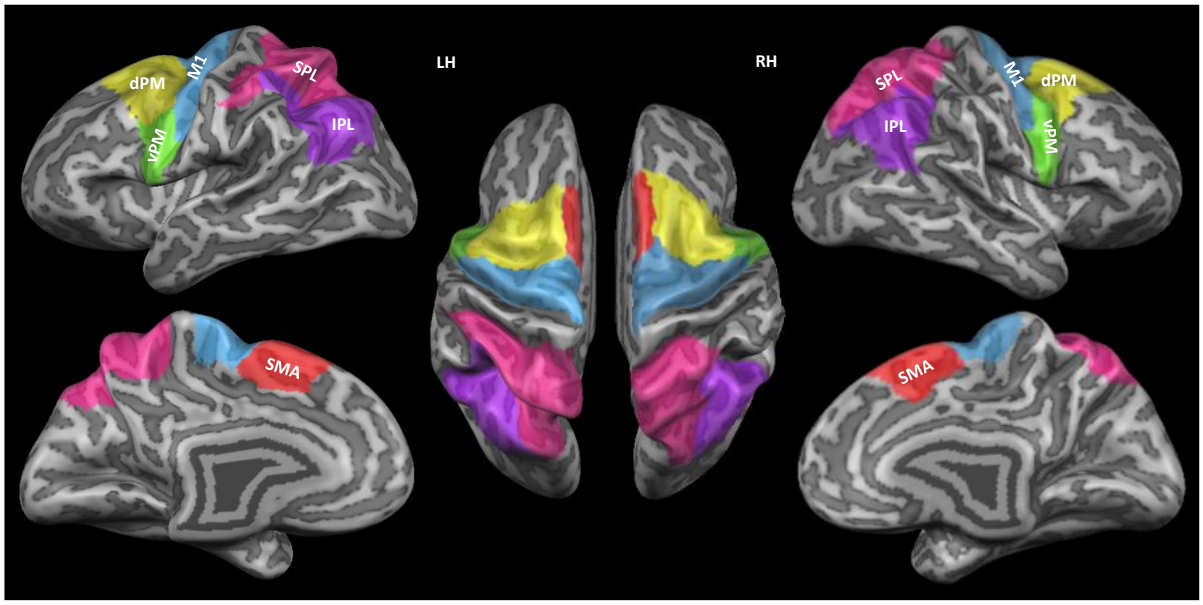

Figure 5.3 The anatomical parcellation of ROIs using CBA is shown on the inflated brain of one participant. LH and RH are the left and right hemisphere.

For each ROI, data within similar stimulus blocks of each run were averaged to substitute the response patterns for that stimulus, such that 6 samples correspond to the three action stimuli and two modalities per run. The time-series of each voxel was normalised using z-score and shifted by 2 TRs (4 s) to account for the haemodynamic delay.

5.3.6.3 Aligning the subject's representational space into a common space using hyperalignment

Brain activation patterns can be considered as vectors in a high-dimensional space in which each dimension is a feature (fMRI voxel). Although the space of individual subjects are not aligned, they are time locked to the stimuli (Haxby et al., 2011). Hyperalignment uses Procrustean transformation iteratively to map subjects' representational spaces into a common model space by deriving transformation parameters for each subject. The common model space and transformation parameters were derived using the response vectors of all subjects during the AO+MI task of the blended actions stimuli session. Then subjects' representational spaces from the AO+MI and MI tasks obtained during the natural actions session were aligned by

multiplying each subject's transformation parameters with the voxels' responses, as illustrated in equation 5.1.

$$\boldsymbol{M}_{(\boldsymbol{k}\times\boldsymbol{n})} = \boldsymbol{V}_{(\boldsymbol{k}\times\boldsymbol{n})}\boldsymbol{T}_{(\boldsymbol{n}\times\boldsymbol{n})} \quad (5.1)$$

$\boldsymbol{M}(k\times n)$ is the mapped matrix in the common model space (k time points, n voxels), $\boldsymbol{V}(k\times n)$ is the voxels' responses in Talairach space, and $\boldsymbol{T}(n\times n)$ is the hyperalignment transformation parameters. Finally, the subject order was shuffled 2000 times prior to hyperalignment, and for each time a new common model space and new transformation parameters were computed to map subjects' activation patterns in AO+MI and MI tasks.

5.3.6.4 Searchlight analysis

In this study we performed a searchlight analysis for each ROI separately, to search for a neural activity pattern that carried information about the content of the experimental conditions (Kriegeskorte *et al.*, 2006). The searchlight approach has been successfully employed to decode multivariate neural activity patterns of different action types and modalities (Pilgramm *et al.*, 2016; Zabicki *et al.*, 2016). For this analysis, a searchlight sphere of 3 voxels was centred on each cortical grey matter voxel for each participant's brain, and the classification accuracies of 8 fold cross-validation (leave one run out) were then averaged to give a mean accuracy score for that sphere, which was then assigned back onto the central voxel. This process was repeated for every voxel in the brain, resulting in an accuracy map for each participant. Finally, we subtracted chance level (33.3) from these maps and combined them using one-sample t-tests to compare the group accuracy to chance. The resultant map was then thresholded at $p<0.05$ using a cluster level threshold estimator, and mapped onto a cortical surface for visualisation. This analysis highlighted voxels where the local patterns of activation reliably discriminated across action types and modalities.

Furthermore, we performed an additional searchlight analysis using the hyperaligned data to serve as a control analysis, to examine whether the common model space of each ROI

carried information to discriminate between our experimental conditions for each modality (AO+MI or MI) separately. To run a searchlight analysis across participants, similar ROIs need to have the same number of voxels. Therefore, we selected the top 90% of voxels of the smallest ROI, based on the previous individual searchlight analysis, and masked all the participants' corresponding ROIs. The searchlight of each ROI consisted of a sphere with a radius of 3 voxels centred on each grey matter voxel for the common regions across participants. The classification accuracies of 10 fold cross-validation (leave one subject out) were then averaged and projected back onto the central voxel, yielding an accuracy map for all participants. Finally this map was overlaid on a cortical surface for visualisation. In both scenarios, significant clusters were identified anatomically based on the nearest grey matter using a Talairach Daemon (Lancaster *et al.*, 2000).

5.3.6.5 Multivariate Pattern Analysis

The MVPA was used to test whether MI and AO+MI of different arm actions (lift, knock, throw) elicit discriminable neural patterns in a given ROI which are sufficient to classify the experimental conditions. For this purpose, a multiclass support vector machine (SVM) (Hausfeld et al. 2014) implemented in PyMVPA (LIBSVM, C=-1.0) was used for decoding (lifting vs. knocking vs. throwing) of the brain activity during the MI and AO+MI tasks. The multiclass problem was translated into a series of binary classifications paired with a majority voting scheme to determine the predicted class (Haxby et al., 2011; Misaki et al., 2010; Reddy et al., 2009). For Within Subject Classification (WSC), we performed MVPA by training the SVM classifier on the raw data of seven runs, and tested on the left-out eighth run (leave one run out cross validation scheme). The procedure was repeated until each run served as a test run, and then we calculated the mean classification accuracy across folds. In addition, we re-labelled all 6 conditions (3 actions by 2 modalities) according to their modality, and used a similar procedure to decode the neural pattern according to modality (AO+MI vs MI).

For Between-Subject Classification (BSC) using the hyperaligned data, we trained the SVM classifier on the raw data from 1 run in 9 subjects and evaluated the left out run of the left out subject, using a leave-one-subject-and-one-run-out cross validation scheme. In both scenarios, we repeated the MVPA analysis for MI and AO+MI conditions of each ROI separately, and tested the statistical significance using a one-sample *t*-test against chance (33.3%). All P values were corrected for multiple ROIs using the Holm–Bonferroni method (Holm, 1979). A paired-sample t-test between modalities was conducted to test for a significant difference. In order to test for significant differences between the classification accuracies for AO+MI and MI, we performed a 2×6×2 (Hemisphere×ROI×modality) repeated-measures ANOVA.

5.3.6.6 Cross Modality Classification

To evaluate the degree of shared neural patterns of different arm actions across MI and AO+MI, we performed a cross-modality classification. In this analysis, we attempted the same procedure for WSC described above, but the SVM classifier was trained with MI data and decoded the action types of AO+MI data and vice versa. Significant classification accuracies were determined by *t*-test as described above.

5.3.6.7 Representational Similarity Analysis

We analysed the representational geometry of neural responses to our 6 experimental conditions (3 actions for 2 modalities) by calculating the representational dissimilarity matrix (RDM) (Kriegeskorte *et al.*, 2008a). For this analysis, we used an RSA toolbox developed by Nili et al., (2014). We obtained the t-maps for each action of each modality using BrainVoyager.

For each ROI, we computed the pairwise correlation between all the activity patterns associated with conditions using correlation distance (1- Pearson linear correlation), yielding a 6×6 RDM. RDMs were calculated separately for each run and averaged for each subject, which

produced 10 RDMs (one per subject) for each of the 12 ROIs. These RDMs were used to estimate the noise ceiling and the similarity between each subject's RDM and model RDMs. Then we employed multidimensional scaling (MDS) to arrange the high-dimensional RDM space onto 2 dimensional space, such that the distance between them reflected the similarities between the response patterns.

We then compared the 12 ROIs RDMs against 5 model predictions to arbitrate between theoretical stances regarding AO+MI and MI. These models were (figure 5.4):

- Pure modality model: This model assumes a categorical distinction between the 2 modalities (AO+MI and MI). In this model RDM, the dissimilarities for all within-modalities were 0 and for a cross-modality were 1.
- Pure actions type model: This model assumes a categorical distinction between the 3 actions (lifting, knock and throwing), regardless of the modality. The dissimilarities between identical action types were 0 and between different actions were 1.
- Mixed models: 3 models were used to predict the dependency of a given neural pattern on modality as well as action type. In all models, the dissimilarities between different actions within the same modality were 0.5 and between modalities were 1. The dissimilarities of an identical action between modalities varied in accumulated steps of 0.25, and they were 0.25, 0.5 and 0.75, named as M25, M50, and M75 respectively. These model predictions examined different degrees of similarity between neural patterns evoked by the AO+MI and MI of a given action. For instance, the M75 model assumes a low degree of similarity between neural patterns associated with a given action type during AO+MI and MI.

We compared ROIs and model RDMs using Kendall's rank correlation coefficient τA, which is the proportion of pairs of values that are consistently ordered in both variables. Kendall's τA is recommended when comparing models that predict tied ranks (model RDMs)

with models that make more detailed predictions (ROIs RDMs) (Nili *et al.*, 2014). To assess the significance by which these models explain variance in a given ROI RDM, a one-sided Wilcoxon signed-rank analysis was used across subjects. To account for multiple testing, we controlled the false-discovery rate at 0.05.

The amount of variance explained by a model RDM is limited by the variability across subjects. Thus, an estimation of the noise ceiling is needed to indicate how much variance of ROIs RDMs was expected to be explainable by a model RDM (given the noise level). The noise ceiling consists of upper and lower edges corresponding to upper and lower bound estimates on the group-average correlation with the RDM predicted by the unknown true model. The average of all subject RDMs can be used as an estimate of the true model RDM. The average correlation of this average RDM provides the upper bound. We estimated the lower bound by employing a leave-one-subject-out approach. We computed and averaged each single-subject RDMs correlation with the average of the other subjects' RDMs. A model RDM is assumed to capture the true dissimilarity structure of a given ROI RDM when its correlation reaches the lower bound of the ceiling.

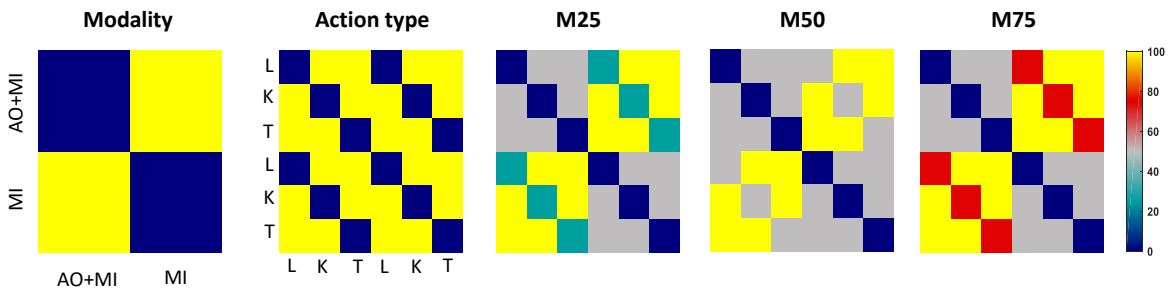

Figure 5.4. RDM of different model predictions that assume different similarities of action pattern based on action type and modality. The first RDM shows a modality based model that assumes equal neural patterns for each action within a similar modality. The second RDM is an action type based model that assumes similar neural responses for a given action across modalities. The remaining 3 mixed models assume variable dependency between modality and action type, and the dissimilarity of action types were varied as: 0.25(M25), 0.5(M50) and 0.75(M75) respectively. All the mixed models assume a dissimilarity of 0.5 between different action types within one modality, and a dissimilarity of 1 between different action types between two modalities. AO+MI: Action observation and motor imagery, MI: motor imagery, L: Lift, K: Knock and T: Throw.

5.4 Results

The results of the two fMRI sessions are reported. In Session 1, 10 subjects performed an AO+MI task to presentation of 25 videos which displayed a parametric set of action blends of lifting, knocking and throwing. These data were used to compute hyperalignment transformation parameters that allowed us to transform the data of individual subjects into a common model space. In Session 2, the same subjects performed AO+MI and MI to presentation of 3 videos which displayed the actions lifting, knocking and throwing. From these data, SVM classifiers were used to decode the action types during the AO+MI and MI conditions, by using individual subject data and hyperaligned data. In order to do this, we first explored the subject order that produced the highest performance of the common model space, and mapped all the subjects' AO+MI and MI data onto it. Second, we used searchlight to explore the voxels that carried information about the content of the actions using the individual

data and the hyperaligned data. Then, we compared WSC and BSC based on hyperalignment for each modality separately. Finally, we examined the similarity of the neural codes between AO+MI and MI of different arm actions, using RSA.

5.4.1 Aligning subjects' representational spaces using hyperalignment

To obtain the optimal common model space, 2000 permutations of subject order were performed for each ROI, in order to derive new common model spaces and hyperalignment transformation parameters using the neural responses of the 25 blended actions. From this, the data from the AO+MI and MI tasks of each ROI were mapped onto the common model spaces using the associated hyperalignment parameters, and they were then prepared for the subsequent analyses.

5.4.2 Searchlight analysis

We applied a searchlight approach to examine whether and where neural patterns carried information about the action types and modalities. The searchlight analysis based on individuals' data revealed that actions during AO+MI condition could be decoded accurately from activity patterns within the left vPM as well as the bilateral M1 and SPL, however, no significant clusters were found in the dPM, SMA or IPL. In addition, the searchlight analysis showed significant clusters in the left M1 and SPL for MI condition, but no significant clusters survived in the right hemisphere, as shown in figure 5.5 and table 5.1.

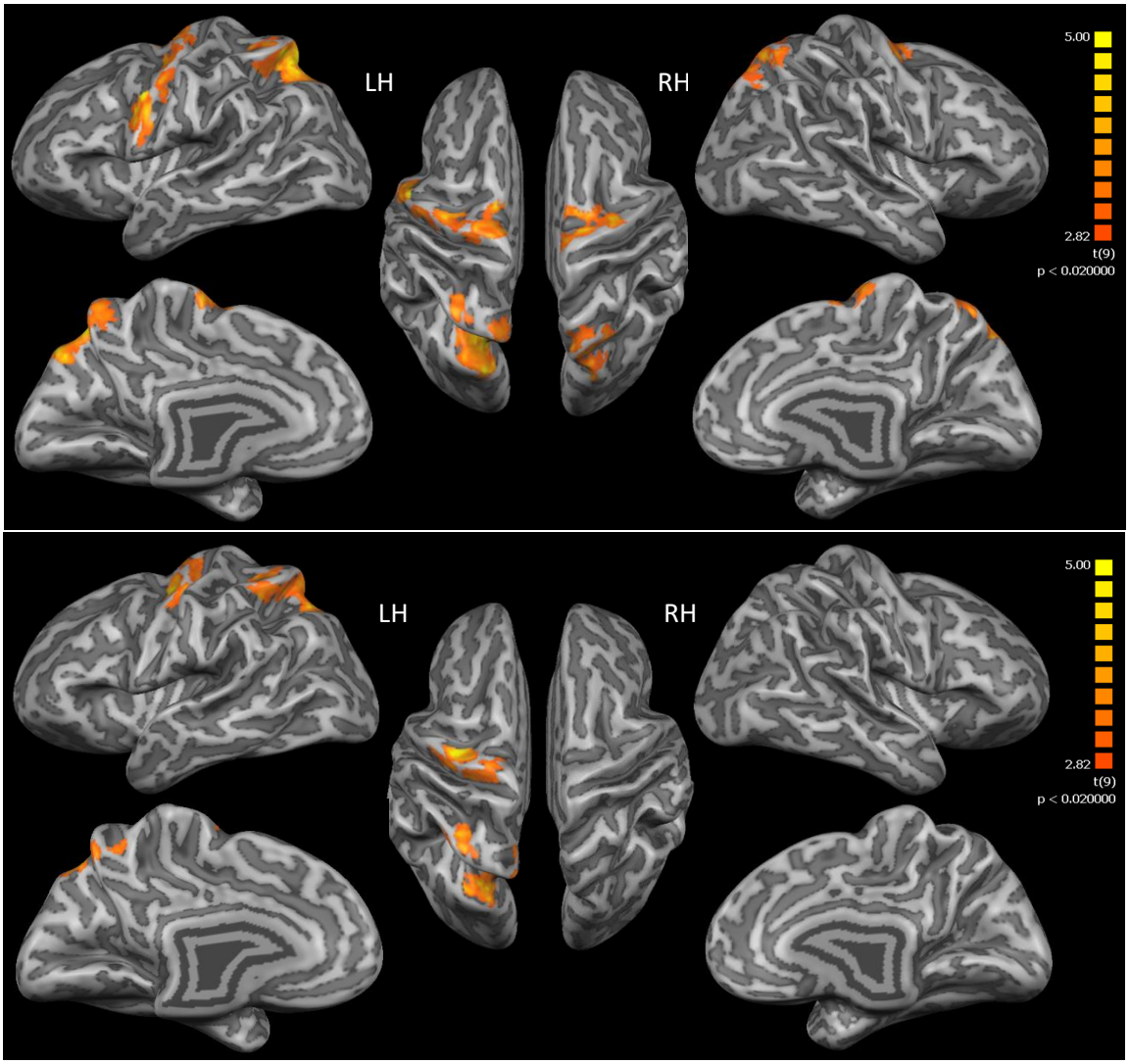

Figure 5.5. Results of the searchlight analysis using individuals' data, showing brain regions where action types could be decoded from the neural pattern evoked during the AO+MI condition (A) and MI condition (B). The colour scale indicates searchlight decoding performance at group level (all t>2.82; thresholded using a cluster level threshold estimator at p<0.05).

Table 5-1. Cluster coordinates with above chance (33.3%) decoding of action types in AO+MI and MI conditions. $P<0.05$, whole brain Bonferroni correction on cluster level.

Modality	**ROI**	**Left/ Right**	**Talairach Coordinates**			***t*-value**	**Cluster size (voxels)**
			x	***y***	***z***		
AO+MI	vPM	L	-48	2	31	9.04	3397
	M1	L	-12	-7	48	6.08	8416
		R	15	-10	61	6.28	6441
	SPL	L	-18	-58	49	6.88	16061
		R	15	-61	55	5.55	7161
MI	M1	L	-30	-10	49	6.71	6540
	SPL	L	-24	-46	52	7.24	10455

In addition to the previous analysis, we applied a searchlight approach to the hyperaligned data to explore which regions of the brain exhibited common fine-grained neural patterns, after mapping individuals' representational spaces onto a common model space. This analysis confirmed that action types could be distinguished from the activity patterns evoked under MI and AO+MI conditions in bilateral SMA, dPM, vPM, M1, IPL and SPL as shown in figure 5.6 and table 5.2.

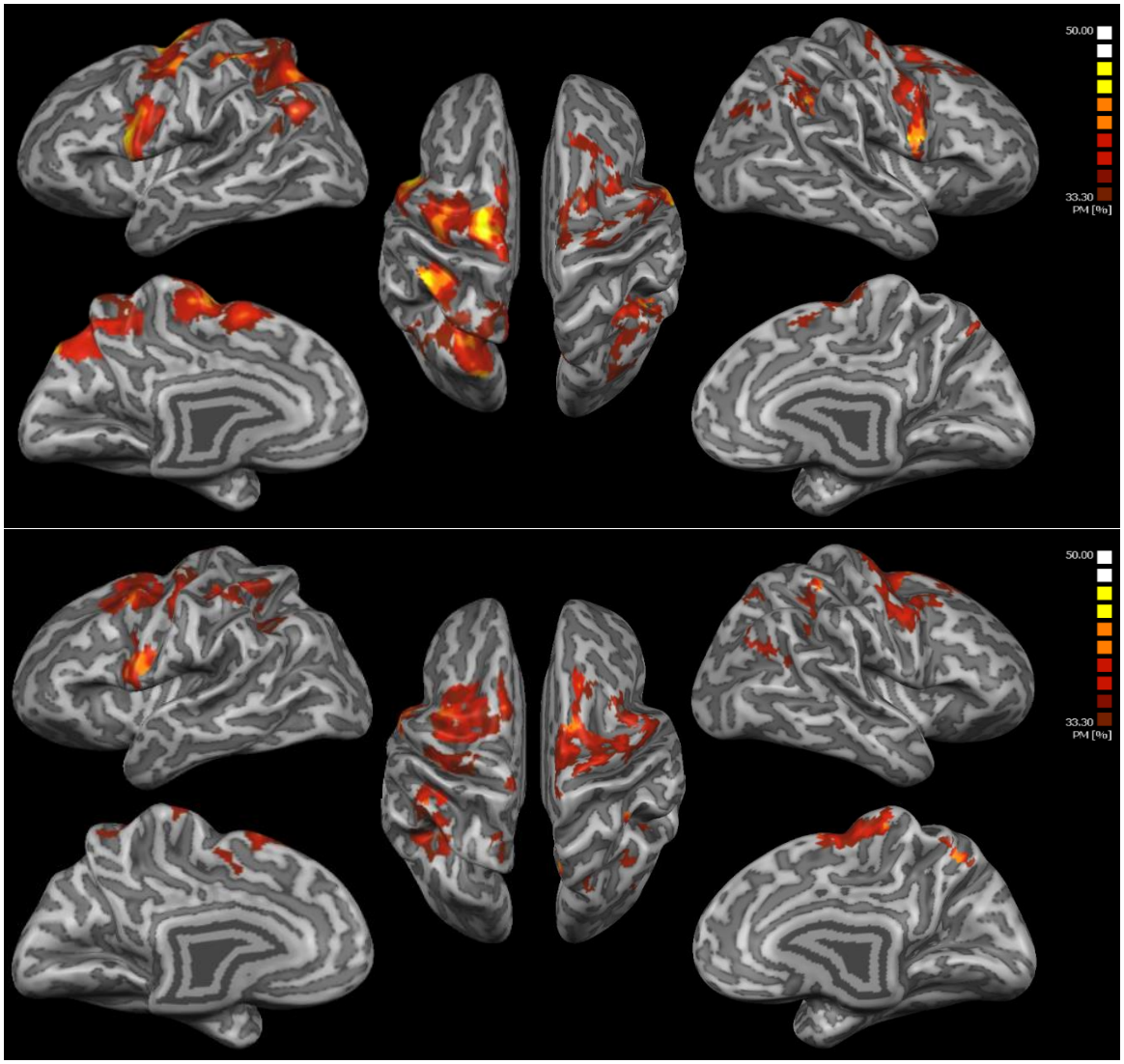

Figure 5.6. Results of searchlight analysis using the hyperaligned data, revealing brain regions with common fine-grained structure from which action types could be decoded during the AO+MI condition (A) and MI condition (B). The colour scale indicates searchlight decoding accuracy.

Table 5-2. Clusters coordinates with above chance (33.3%) decoding of action types in AO+MI and MI conditions using the hyperaligned data.

Modality	ROI	Left/ Right	Talairach Coordinates			Accuracy	Cluster size (voxels)
			x	y	z		
AO+MI	SMA	L	0	5	53	43.3	2269
		R	3	8	52	37.9	483
	dPM	L	-33	3	40	43.3	4269
		R	29	20	46	40.4	1598
			27	8	52	40.8	1859
	vPM	L	-50	11	7	48.7	4654
		R	61	8	19	47.5	3990
	M1	L	-18	-9	64	49.5	9429
		R	21	-1	60	42.5	3767
			33	-15	55	39.9	649
	IPL	L	-36	-46	45	38.3	1033
			-48	-61	31	45.4	2663
		R	42	-44	34	46.2	4510
			33	-73	28	38.7	1013
	SPL	L	-52	-28	55	52.9	15896
		R	3	-64	47	39.1	341
MI	SMA	L	-9	9	58	42.9	1690
		R	9	24	61	38.7	426
	dPM	L	-30	3	64	48.3	10596
		R	15	14	54	42.9	3240
	vPM	L	-52	2	22	45.8	2793
		R	48	12	46	42.5	877
	M1	L	0	-22	67	40.4	488
			-39	-16	46	43.7	3910
		R	12	2	65	45.4	8010
	IPL	L	-32	-49	43	41.6	3342
		R	48	-62	22	40.4	840
			40	-55	43	38.3	770
	SPL	L	-12	-48	55	40.4	827
			-48	-35	58	42.9	2772
			-54	-32	40	42.9	496
		R	39	-37	52	44.1	739
			9	-55	45	43.7	1529

5.4.3 MVPA results

In order to examine whether the neural pattern within a given ROI carried information about the action types during either the AO+MI or MI conditions, we compared the decoding accuracy of WSC, in which a new classifier was tailored for each subject, for each ROI separately against chance level (33.3%) for both modalities. For AO+MI (see figure 5.7), the

type of action could be decoded at a level significantly above chance in the bilateral SMA, dPM, vPM, M1, IPL and SPL. In addition, the imagined action could be classified at a level of accuracy that was significantly above chance in the bilateral dPM, vPM, M1, IPL, and SPL as well as in the left SMA. No significant classification was found in the right SMA. Action modality (AO+MI vs MI) could be decoded at a level of accuracy that was significantly above chance from every ROI as shown in figure 5.8. All *p* values were derived from one-sample *t*-tests and were corrected for multiple testing using the Holm–Bonferroni approach. The repeated measures ANOVA revealed a significant main effect of ROI ($F(5,45)=6.792$, $p<0.00008$), but no main effect of hemisphere ($F(1,9)=2.73$, $p<0.13$), modality($F(1,9)=2.6$, $p<0.14$), hemisphere×modality interaction ($F(1,9)=0.007$, $p<0.937$), ROI×modality interaction ($F(5,45)=0.229$, $p<0.948$), hemisphere×ROI interaction ($F(5,45)=0.861$, $p<0.514$) or hemisphere×ROI×modality interaction ($F(5,45)=0.572$, $p<0.721$).

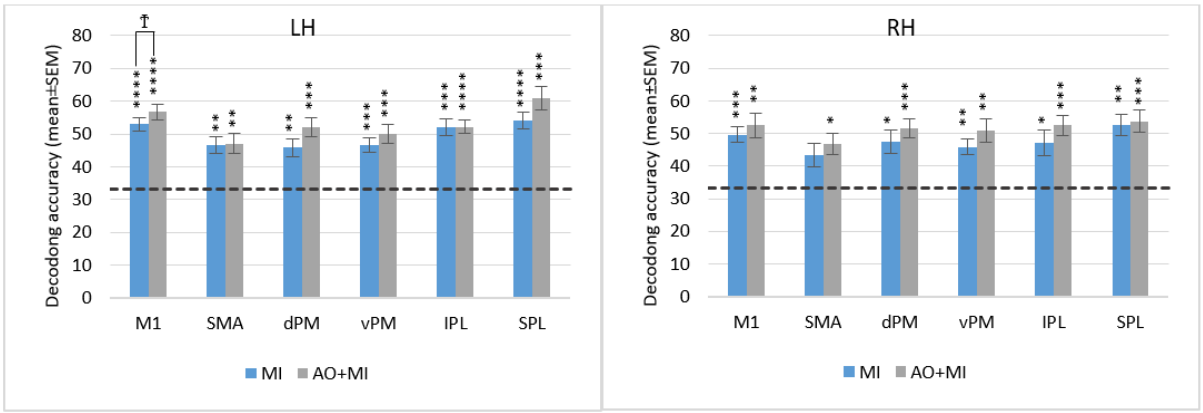

Figure 5.7. Decoding accuracy of action types (lift vs knock vs throw) using individuals' data during MI and AO+MI. Bars indicate the mean accuracy (% correct) with which the type of action could be decoded in a given ROI. Left and right figures represent the left and right hemispheres respectively. The dashed line represents chance level. M1: primary motor cortex, SMA, supplementary motor area, dPM: dorsal premotor area, vPM: ventral premotor area, IPL: inferior parietal lobule, SPL: spurious parietal lobule. SEM: standard error mean. LH, RH: left and right hemispheres. ϯ: $p<0.05$, *: $p<0.01$, **: $p<0.001$, ***: $p<0.0001$, ****: $p<0.00001$.

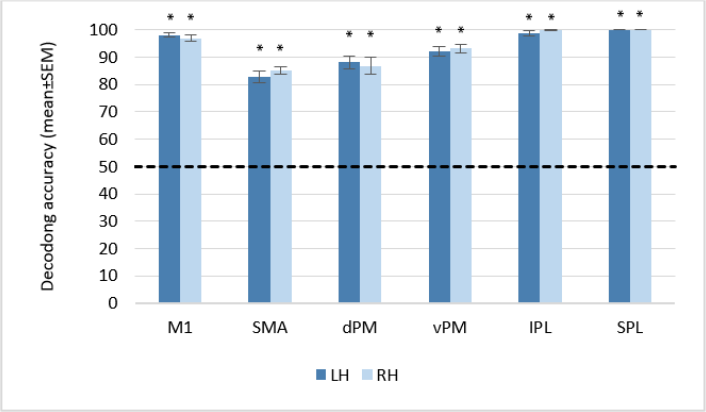

Figure 5.8. Mean decoding accuracy of modality type (AO+MI vs MI). Bars indicate the mean accuracy (% correct) with which the type of modality could be decoded in a given ROI. Error bars are standard error mean. The dashed line represents chance level (50%). *: p<0.0001. M1: primary motor cortex, SMA, supplementary motor area, dPM: dorsal premotor area, vPM: ventral premotor area, IPL: inferior parietal lobule, SPL: spurious parietal lobule. SEM: standard error mean. LH, RH: left and right hemispheres.

The BSC analysis using the hyperaligned data revealed that the type of action could be classified at a level of accuracy that was significantly above chance from all the ROIs, regardless of the modality. figure 5.9 shows the classification accuracies of both modalities after mapping the participants' representation spaces from each ROI onto a common representational model. The repeated measure ANOVA showed no significant main or interaction effects of hemisphere ($F(1,7)=0.289$, $p<0.6$), ROI ($F(5,35)=1.74$, $p<0.151$), modality ($F(1,7)=0.343$, $p<0.577$), hemisphere×ROI interaction ($F(5,35)=0.21$, $p<0.956$), hemisphere×modality interaction ($F(1,7)=0.026$, $p<0.877$), ROI×modality interaction ($F(5,35)=0.676$, $p<0.645$), or hemisphere×ROI×modality interaction ($F(5,35)=0.28$, $p<0.921$).

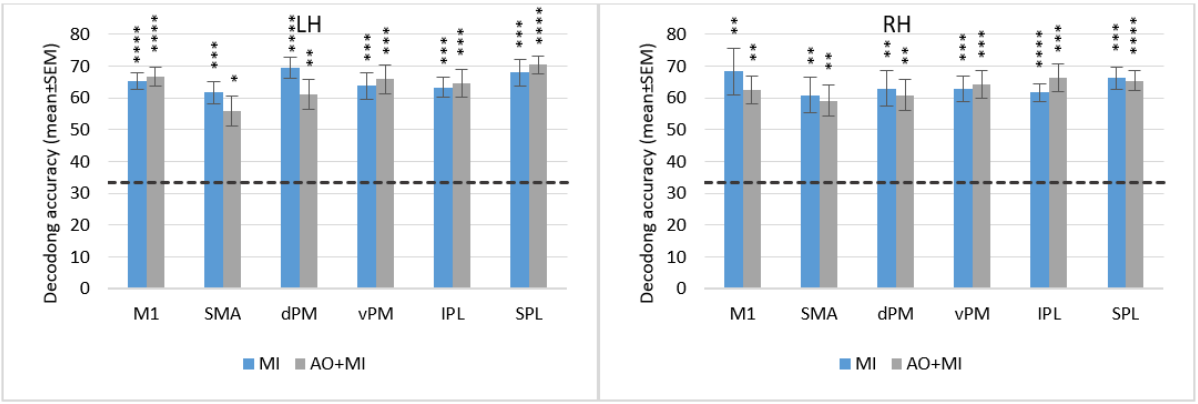

Figure 5.9. Decoding accuracy of action types (lift vs knock vs throw) using hyperaligned data during both modalities (MI and AO+MI). Bars indicate the mean accuracy (% correct) with which the type of actions could be decoded in a given ROI using BSC. Left and right figures represent left and right hemispheres respectively. The dashed line represents the chance level. M1: primary motor cortex, SMA, supplementary motor area, dPM: dorsal premotor area, vPM: ventral premotor area, IPL: inferior parietal lobule, SPL: spurious parietal lobule. SEM: standard error mean. LH, RH: left and right hemispheres. *: p<0.01, **: p<0.001, ***: p<0.0001, ****: p<0.00001.

5.4.4 Cross modality classification

Classifications of MI patterns with a classifier trained on AO+MI data and vice versa showed significant accuracies in some of our ROIs. The actions during the AO+MI condition could be (significantly) accurately decoded with a classifier trained on MI patterns in right IPL and bilateral M1, dPM and SPL. Significantly accurate classification of MI actions using a classifier trained on AO+MI data was found in the left vPM, right dPM as well as bilateral M1, IPL and SPL. All p values were estimated using one-sample t-tests, corrected for multiple ROIs using the Holm–Bonferroni method as shown in figure 5.10. The repeated measures ANOVA showed no significant main or interaction effects of hemisphere (F(1,9)=0.197, p<0.66), ROI (F(5,45)=0.63, p<0.67), classifier (F(1,9)=1.37, p<0.27), hemisphere×ROI interaction (F(5,45)=0.19, p<0.96), hemisphere×classifier interaction (F(1,9)=0.37, p<0.55), ROI×classifier interaction (F(5,45)=0.6, p<0.69) or hemisphere×ROI×classifier interaction (F(5,45)=0.778, p<0.57).

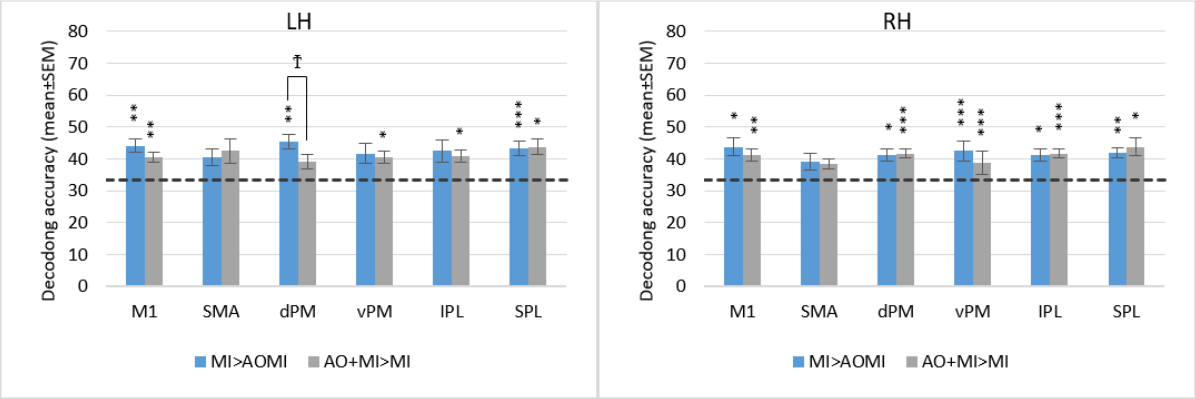

Figure 5.10. Cross-modality classification of action types (lift vs knock vs throw). Bars indicate the mean accuracy (% correct) with which the type of actions could be decoded in a given ROI using a classifier trained on MI and tested on AO+MI (MI>AO+MI) and vice versa (AO+MI>MI). The left and right figures represent left and right hemispheres respectively. The dashed line represents chance level. M1: primary motor cortex, SMA, supplementary motor area, dPM: dorsal premotor area, vPM: ventral premotor area, IPL: inferior parietal lobule, SPL: spurious parietal lobule. SEM: standard error mean. LH, RH: left and right hemispheres. †: $p<0.05$, *: $p<0.01$, **: $p<0.001$, ***: $p<0.0001$.

5.4.5 Representational Similarity Analysis

In order to compute the RDMs of each ROI, we compared the neural responses associated with each pair of conditions using correlation distance (1- Pearson linear correlation). RDM is a symmetric matrix which contains widths and heights corresponding to the number of conditions (6×6) and a diagonal of zeros. The brain RDMs were calculated for each run separately and averaged for each subject as shown in figure 5.11.

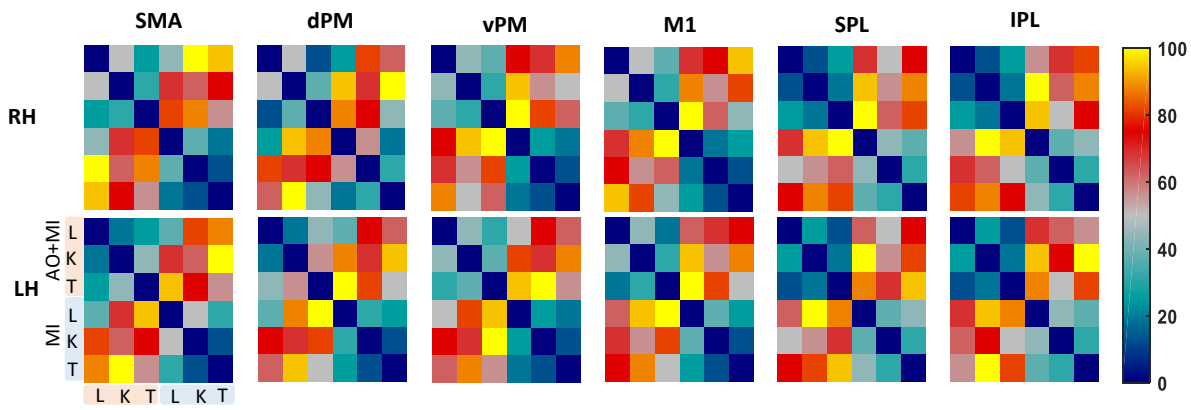

Figure 5.11. Mean RDMs (averaged across subjects) of neural responses associated with 6 experimental conditions (L: lift, K: knock and T: throw, in two modalities: AO+MI and MI) for every ROI.

Next, we computed the correlation between brain and model RDMs, as shown in figure 5.12. This figure illustrates how well the 5 model predictions explain the response pattern dissimilarities seen in the brain RDMs of several ROIs. The MDS plot (figure 5.13) provides an intuitive overview of the relationship between the brain and model RDMs. The action type model did not correlate significantly with any ROI RDMs (Kendall τA, mean=-0.031), however the modality and the 3 mixed model correlated significantly with each ROI RDM (mean Kendall τA correlation for modality, M25, M50 and M75 were 0.3, 0.188, 0.269 and 0.35 respectively). The majority of brain RDMs were best explained by 4 RDMs models. The M75 model provided the best fit for data in all brain RDMs, while the action type model best explained the data in right dPM and left SMA. These two models assume that the correlation between AO+MI and MI for a given action type is relatively low compared to correlations due to shared modality. Therefore, for the majority of ROIs, the pattern similarity was primarily driven by the modality rather than the action type.

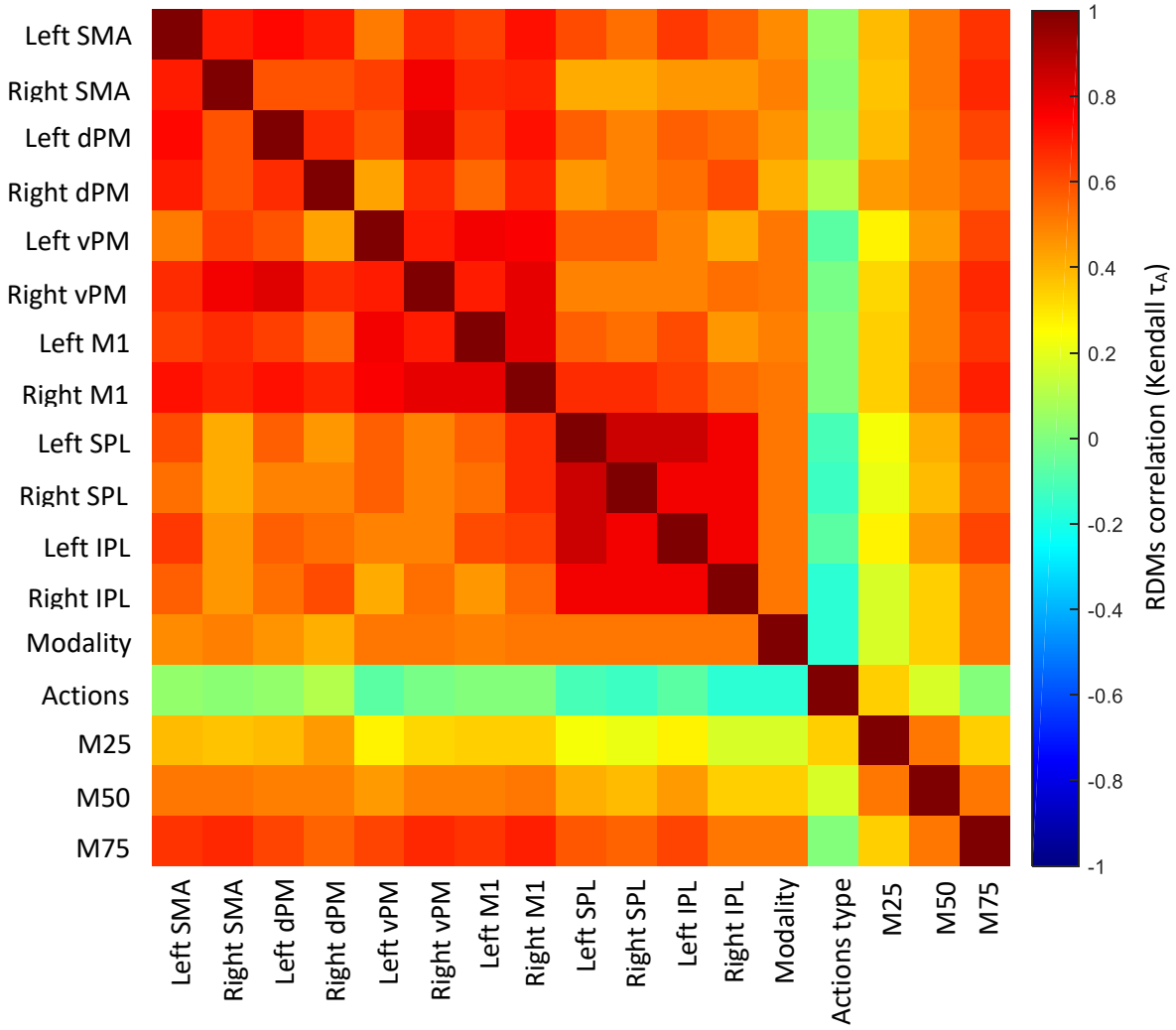

Figure 5.12. Correlation matrix across all brain and model RDMs. Each entry compares two RDMs by Kendall's τ_A. The matrix is symmetrical across a diagonal line of ones.

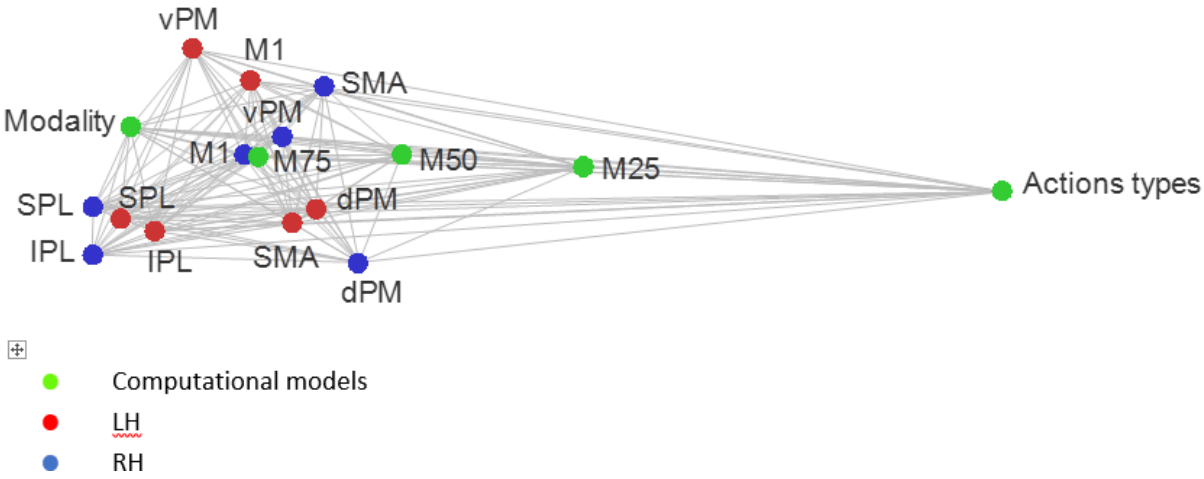

Figure 5.13. MDS plot of the relationship across ROI and model RDMs. Each point represents an RDM and the distances between the points represent the dissimilarity (1- τA correlation). The left hemisphere, right hemisphere and model RDMs are shown by the red, blue and green points respectively.

For the next step, we performed statistical inference to test the relatedness between brain and model RDMs, as listed in table 5.3. The correlation of fitted model predictions for the majority of the ROIs reached the noise ceiling, indicating that they explained the brain ROIs RDMs adequately, given the variability of the subject data. For instance, the mixed model M75 was able to significantly explain the data in the left M1 as well as the SMA, dPM, vPM and IPL of both hemispheres. The M50 and M25 model predictions reached the ceiling in the left SMA, left dPM (only for M50 model) and right dPM. In contrast, the modality model reached the ceiling in the right dPM, left vPM and right IPL. All the mixed models reached the ceiling in the left SMA and right dPM.

Table 5-3. RDM correlations using Kendall's τ_A between brain regions and all model predictions. Significant correlations are indicated by asterisks (*ns* = not significant: **P* < 0.05; ***P* < 0.01; ***P < 0.001). Lower and upper bounds of the noise ceiling are included in brackets. Bold numbers represent correlations within the ceiling.

ROI	***Left or Right***	***Ceiling***		***Correlation to model predictions***				
				Modality	Action	M25	M50	M75
SMA	LH	[0.176	0.318]	0.175^{*}	0.044^{ns}	$\mathbf{0.190}^{***}$	$\mathbf{0.219}^{**}$	$\mathbf{0.248}^{**}$
	RH	[0.237	0.341]	0.227^{**}	0.010^{ns}	0.187^{**}	0.236^{***}	$\mathbf{0.286}^{**}$
dPM	LH	[0.187	0.303]	0.179^{*}	0.019^{ns}	0.170^{**}	$\mathbf{0.198}^{**}$	$\mathbf{0.227}^{**}$
	RH	[0.075	0.251]	$\mathbf{0.135}^{*}$	0.059^{ns}	$\mathbf{0.190}^{**}$	$\mathbf{0.194}^{**}$	$\mathbf{0.198}^{**}$
vPM	LH	[0.229	0.381]	$\mathbf{0.230}^{**}$	-0.013^{ns}	0.160^{*}	0.217^{**}	$\mathbf{0.274}^{**}$
	RH	[0.346	0.448]	0.310^{***}	-0.036^{ns}	0.192^{**}	0.274^{***}	$\mathbf{0.356}^{***}$
M1	LH	[0.472	0.522]	0.324^{**}	0.004^{ns}	0.248^{**}	0.328^{***}	0.408^{***}
	RH	[0.394	0.472]	0.322^{***}	0^{ns}	0.236^{**}	0.322^{***}	$\mathbf{0.408}^{***}$
SPL	LH	[0.534	0.600]	0.459^{***}	-0.124^{ns}	0.187^{***}	0.335^{***}	0.484^{***}
	RH	[0.513	0.604]	0.472^{***}	-0.137^{ns}	0.177^{***}	0.335^{***}	0.493^{***}
IPL	LH	[0.387	0.470]	0.368^{**}	-0.084^{ns}	0.168^{**}	0.284^{**}	$\mathbf{0.400}^{**}$
	RH	[0.384	0.488]	$\mathbf{0.398}^{**}$	-0.114^{ns}	0.147^{*}	0.284^{**}	$\mathbf{0.421}^{**}$

5.5 Discussion

This study explored whether complex arm actions are accompanied by action-specific activation patterns within the premotor, primary motor and parietal cortices. Participants either imagined (MI) or concurrently observed and imagined (AO+MI) doing three different arm actions (Lifting, Knocking and Throwing). We used MVPA to investigate how the human brain represents different hand-related actions during AO+MI and MI conditions, based on the evoked fine-grained patterns. Additionally, we explored the functional organisation of AO+MI and MI in different brain regions.

Our first aim was to explore whether the multi-joint arm actions evoked distinguishable neural patterns within the frontal and parietal motor regions. Unlike univariate analyses that have shown broad overlapping of activations for imagining different hand actions in premotor and posterior parietal cortices (Lorey *et al.*, 2014), MVPA facilitates the identification of brain regions for which activation patterns differentiate between types of hand actions, even when

the overall amplitude of BOLD signal across voxels of these areas does not differ. Thus a given action information would be represented by differences in the fine-grained activation patterns that are blurred and indistinguishable in univariate analyses. The Searchlight analysis (Section 3.2), which was based on individual subjects' data, revealed a spatially distributed network, from which action types could be reliably decoded for all the participants, within the left vPM and bilateral M1 and SPL in the AO+MI condition and the left M1 and SPL in the MI condition. This network spans from the frontal to the parietal motor regions. Within the frontal regions, discrimination of action occurred through analysis of activation patterns in the vPM and M1. The vPM plays an important role in fine motor coordination and shapes hand actions in grasping tasks (Davare *et al.*, 2009). It has been assumed that the overlapping between the observation and execution of actions is due to mirror neurons, which were initially found in the macaque ventral premotor area F5 for observation and execution of hand or mouth goal-directed movements (Fabbri-Destro and Rizzolatti, 2008; Rizzolatti and Sinigaglia, 2010; Oztop *et al.*, 2013). Mirror neurons discharge both during the observation and execution of actions, and there is evidence of a similar system in the human brain (Rizzolatti & Sinigaglia 2010; Gazzola & Keysers 2009). It has been suggested that mirror neurons play an important role in many aspects of social cognition, including understanding observed actions and imitation (Rizzolatti *et al.*, 2001). The recruitment of M1 in action simulation suggests an intention to imitated the observed actions (Jeannerod, 2001; Caspers *et al.*, 2010), while Hetu et al., (2013) found no evidence of consistent involvement of M1 during MI. Similarly, the bilateral SPL plays a significant role in coding spatial aspects of movements (Vandenberghe *et al.*, 2001) and in enhancing short-term learning during observation (Ossmy and Mukamel, 2016). Based on the Searchlight map, different numbers of voxels per ROI were selected for subsequent analyses. Our MVPA results showed that for AO+MI, the type of actions could be decoded at a level of accuracy that was significantly above chance from every ROI. For MI,

these actions could be classified significantly accurately in the bilateral dPM, vPM, M1, IPL, SPL as well as left SMA. The highest classification accuracies for decoding action types and modality were found in the M1 and SPL of both hemispheres. These results replicate previous research showing that the pattern of activity within motor and motor related regions differentiates between different types of actions (Pilgramm *et al.*, 2016; Zabicki *et al.*, 2016) and between action modalities (Filimon *et al.*, 2015). This demonstrates that the frontal and parietal regions represent the content and modality of actions.

The second aim of this study was to functionally align the representational spaces of all participants into a common representational model, using hyperalignment to better localise the distributed motor network and enhance the classification accuracy. Importantly, our results illustrated that mapping from brain space into a common space affords a reliable region shared across participants that their classification performance exceeds the WSC. The Searchlight, based on the hyperaligned subject data, demonstrated that these actions could be decoded significantly accurately from all the motor and motor-related regions, giving a higher classification performance for M1, vPM and SPL. Our findings highlight the role of hyperalignment in building common representational spaces of the frontal-parietal motor regions, which then increases the power of MVPA to detect fine-grained information across participants. In the above validation, we estimated the hyperalignment parameters using the AO+MI data from the first session of AO+MI data, and applied them to the AO+MI and MI data from the second session.

Our third aim was to measure the neural pattern consistency between modalities. The results demonstrated that cross-modality classification using MI as a training set succeeded in the left IPL as well as the bilateral M1, dPM and SPL. Using AO+MI as a training set, the cross classification succeeded in the left vPM, right dPM and bilateral M1, IPL and SPL. This suggests that there is some similarity between AO+MI and MI induced neural patterns for

specific hand actions in broad areas of the human motor system. More specifically, our results showed a significantly higher cross-modal classification accuracy when the classifier was trained on MI data and tested on AO+MI data than in the reverse case. These findings are in line with previous results that suggest some degree of consistency between the neural codes of different action simulations, such as MI and ME (Oosterhof *et al.*, 2012b; Zabicki *et al.*, 2016). This can be explained by considering which information a classifier uses when it is trained on a series of neural patterns. If the pattern for AO+MI actions is relatively strong (due to visual input) compared to MI and cross-modal patterns, then training a classifier on AO+MI actions causes the decision boundary of the classifier to be based mainly on patterns evoked by these aspects of action that do not generalise to MI actions. Hence the classification accuracies of these MI actions will be relatively low. On the other hand, training a classifier on MI actions will cause the decision boundary to be based on a mixture of MI and cross-modal information, and generalisation to AO+MI actions will be relatively high (Oosterhof *et al.*, 2012b).

In contrast to MVPA classification, which detects the distinctions between neural responses associated with different experimental conditions, the fourth aim of this study was to examine the similarity structure of neural responses evoked by AO+MI and MI of different actions by comparing them to models predicting how the brain regions encode the modality, the action type or the mix dependency of both (Kriegeskorte *et al.*, 2008a; Rothlein and Rapp, 2014; Guntupalli *et al.*, 2016). We calculated RDMs in motor and motor related regions by using pairwise correlation distance between neural responses induced by simultaneously observing and imagining (AO+MI) or imagining (MI) 1 of 3 distinct multi-joint arm actions. With respect to the representational geometry of different actions during AO+MI and MI tasks, we found that the RDMs of premotor, primary and parietal cortices were correlated with each other, forming two distinct clusters in the frontal and parietal regions. The posterior parietal cortex (PPC), which includes IPL and SPL, showed greater similarity between the neural

responses evoked by a given action of AO+MI and MI, assuming a common code within these regions. A large number of studies have reported the role of PPC in understanding other's actions based on MNS, the processing of action related information, encoding of the goal of movement, storing the action representations, and movement intention (Culham and Valyear, 2006; Tunik *et al.*, 2007; Desmurget *et al.*, 2009; Oztop *et al.*, 2013; Aflalo *et al.*, 2015). In addition, we tested different model predictions and we found that the mixed model (M75) explained perfectly the neural organisation in most ROIs (except for left vPM and bilateral SPL), indicating that the action representations have both common and distinct components across modalities. Subsequently, based on the modality and mixed model predictions, most of the ROIs have a low to moderate similarity between the neural responses associated with AO+MI and MI tasks. However, M1 was showed to have a higher degree of functional equivalence between modalities, suggesting its sensitivity in encoding goal-related motor programmes for a given action rather than focussing on the modality of it (Cavallo et al., 2013).

In conclusion, the results suggest that imagined (MI) or observed and imagined (AO+MI) multi-joint arm actions (knocking, lifting and throwing) elicit distinct neural responses that can be decoded from the frontal and parietal motor regions. Thus these regions represent the content and the modality of actions using the same effector (Filimon et al., 2015; Pilgramm et al., 2016; Zabicki et al., 2016). The cross classifications reveal that AO+MI and MI evoke neural patterns that have some degree of consistency. Hyperalignment creates a common model for each motor region that captures the fine grained structure of brain responses during AO+MI and MI tasks with different actions. Additionally, AO+MI and MI share a similar representational geometry for different actions in motor and motor related areas, indicating that the representations of these modalities are neither equivalent nor distinct.

Chapter 6 : Single ROI-fMRI Neurofeedback Treatment of Phantom Limb Pain

6.1 Abstract

fMRI neurofeedback can be used to enable participants to modulate their brain activation via a feedback signal measured from a targeted region(s). This approach might provide control over the neurophysiological mechanisms that mediate behaviour and cognition and could potentially provide a different route for treating disease. Control over the endogenous pain modulatory system is a particularly important target because it could enable a unique mechanism for clinical control over pain. In this study, we demonstrated that using fMRI neurofeedback to guide training, patients with phantom limb pain (PLP) were able to learn to down-regulate activation in the rostral anterior cingulate cortex (rACC) and premotor cortex (PM), regions were involved in pain perception and regulation. Control experiments showed that this effect was not observed after similar training conducted using signal derived from a different brain region (auditory cortex). PLP patients who successfully trained to control activation in rACC and PM reported decreases in the ongoing level of pain after training, but it was not significant. These findings show that patients can gain voluntary control over activation in a specific brain region given appropriate training, that voluntary control over activation in rACC and PM lead to control over pain perception.

6.2 Introduction

Phantom limb pain (PLP) is a type of Central Neuropathic Pain (CNP) (Jensen et al. 2011), having prevalence of 80% in amputees (Floor 2002) and patients with arm paralysis due to Brachial Plexus Injury (BPI) (Finnerup et al. 2011). Similar to non-painful phantom limb sensation, PLP is generated in the brain rather than in the body. It is believed that the intensity of pain is proportional to the degree of cortical reorganization following amputation or BPI (Floor 2002, Weeks et al. 2010). Pharmacological treatments of this type of pain have limited efficiency and are often accompanied with side effects (Dworkin et al. 2007). There are numerous non-pharmacological treatments of PLP (Floor et al. 2002, Weeks et al. 2010) such as cognitive behavioural therapy, mindfulness, hypnosis, mirror therapy or repetitive Transcranial Magnetic Stimulation (rTMS). Mirror therapy is a well-documented type of therapy for phantom pain (Ramachandran and Altschuler 2009), though its neurological mechanism has not been sufficiently explored.

A relation between the motor cortex and more general CNP, has been demonstrated in other patient groups, such as patients with Spinal Cord Injury (Gustin et al. 2010). These patients have bilateral impairment of their limbs and cannot benefit from mirror therapy. Preliminary results showed that in spinal cord injured patients, EEG based neurofeedback from the motor cortex significantly reduces pain (Vuckovic et al. 2012). A recent study showed that neuro-stimulation therapies based on rTMS also target primary motor cortex (M1) to reduce CNP (Hosomi et al. 2013).

fMRI Neurofeedback, a technique that aims to enable voluntary control of brain activity, is used as an intervention in several conditions, including pain, ADHD, depression and phobias (DeCharms *et al.*, 2005, Moriyama *et al.*, 2012, Linden *et al.*, 2012, Zilverstand *et al.*, 2015, respectively). The approach involves measuring the brain activity and visually feeding it back to the participant in real-time (Ruiz *et al.*, 2013). The resulting readout is used

to enhance the ability of participants to either up- or downregulate activity levels in a specific brain region using cognitive strategies. Furthermore, it is hoped that the learned techniques can be used by participants outside of the scanner, inducing beneficial behavioural changes in these individuals (Paret *et al.*, 2014).

fMRI neurofeedback, for treatment of pain has been demonstrated on a mixed group of patients with chronic pain (deCharms et al. 2005) and on a healthy population with induced pain (Emmert et al., 2014). The Region of Interest (ROI) for neurofeedback modulation was rostral Anterior Cingulate Cortex (rACC), involved in the general chronic pain matrix (Garcia-Larrea and Peyron 2013). Given that most therapies for PLP and in general CNP are based on modulation of the M1, it is questionable if fMRI neurofeedback provided from that ROI would be as effective as fMRI neurofeedback provided from the rACC. In previous studies, subjects were able to regulate both the activity of the sensory-motor cortex (de Charms et al. 2004) and of the rACC (deCharms et al. 2005) but only the latter was related to chronic pain (deCharms et al. 2005). In contrast to EEG neurofeedback which requires multiple sessions in order to teach patients to regulate their brain waves, using fMRI neurofeedback it is possible to train patients to regulate their brain activity within a single daily session (deCharms 2005).

The aim of this study is to investigate whether phantom limb pain patients can, using fMRI neurofeedback, learn to modulate the brain activity and to compare between two neurofeedback protocols, one based on down-regulation of rACC and the other based on down-regulation of premotor region (PM).

6.3 Methods

6.3.1 Participants

Three male PLP patients with normal or correct to normal vision participated (mean age±SD=57±1). Two of them were right hand amputees and one was a left hand amputee as

shown in figure 6.1. This study was approved by the ethics committee of the NHS of Great Glasgow and Clyde. All participants provided their informed consent for the experiment.

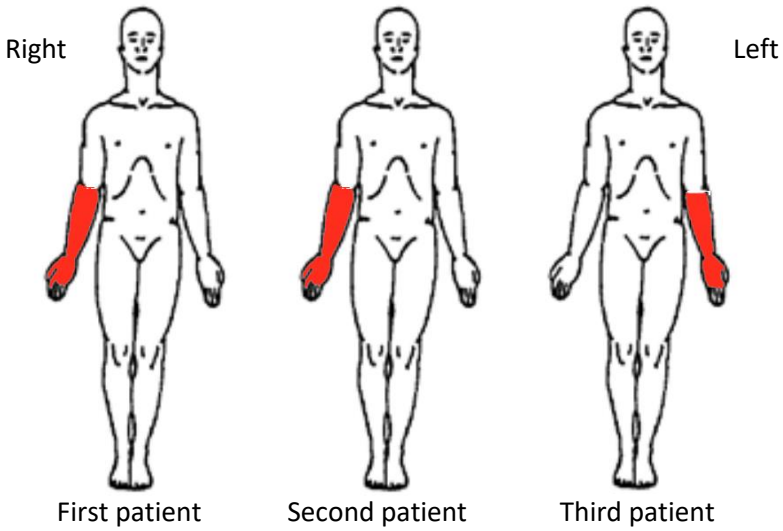

Figure 6.1. Body part of the three patients who participated in this study, red regions showing the painful phantom area.

6.3.2 Imaging parameters and fMRI Neurofeedback platform

The study was performed on a 3T Siemens Tim Trio MRI scanner at the University of Glasgow Centre for Cognitive Neuroimaging (CCNi) with a 32-channel head coil. T1 weighted structural scans were acquired at the beginning of the experiment (TR=2000ms, TE=2.52ms, 192 sagittal slices, 1 mm^3 isotropic voxels and image resolution 256×256). T2*-weighted functional scans were collected with an Echo-Planar Imaging (EPI) sequence (TR=2000ms, TE=30ms, whole brain coverage with 32 axial slices, with 0.3 mm gap, 3 mm^3 isotropic voxel).

The Neurofeedback system used Turbo-BrainVoyager (TBV) (Brain Innovation, Maastricht, The Netherlands) and a custom script running on presentation software called BrainStim to visualize the feedback signal as a thermometer with a fluctuating red bar indicating increasing and decreasing levels of activity in the target ROI. An LCD projector displayed the thermometer onto a rear projection screen that was viewable through a mirror mounted on the head coil.

6.3.3 Experimental procedure

Before testing, all participants were given an information sheet detailing the study and were asked to fill out three questionnaires: Brief Pain Inventory (Short Form) (Cleeland and Ryan, 1994), Neuropathic Pain Symptom Inventory (Bouhassira *et al.*, 2004) and 7 Point Guy/Farrar Patient Global Impression of Change (Hurst and Bolton, 2004). Participants were also required to fill out a consent form before starting the first scanning session.

All patients underwent two scanning sessions, each carried out on a separate day and lasting about 1 hour. Session One consisted of one anatomical scan, one functional localiser to identify PM as a target ROI, four neurofeedback runs during which patients received true feedback from their localised ROIs and four sham feedback runs during which they received sham feedback from the Superior Temporal Gyrus (Broadmann area 22). The second session comprised four neurofeedback runs during which they received feedback from rACC followed by four sham feedback runs. The third patient received eight neurofeedback runs in each session instead of the sham feedback. This was based on observation in the first two patients that 4 training sessions were not enough to learn the task.

6.3.3.1 Questionnaires

Brief Pain Inventory (short form) (BPI) assesses the extent to which pain interferes with daily activities on a scale from 0 to 10 (0 pain has not interfered, 10 pain completely interfered). Patients rated the degree that pain interfered with general activity such as general activity, mood, relations with other people, sleep and enjoyment of life.

Neuropathic Pain Symptom Inventory (NPSI) evaluates the different symptoms and dimensions of neuropathic pain. This questionnaire consists of the 10 common symptoms described by neuropathic patients (burning, pressure, squeezing, electric shocks, stabbing; pain evoked by brushing, pressure, or cold; tingling, pins and needles).

Patient Global Impression of Change (PGIC) addresses the change in the severity of a patient's illness over a particular time interval following treatment.

6.3.3.2 Regions of Interest localisations

The neurofeedback training of the first session started with a functional localiser run to delineate the PM-ROI, from which participants received the feedback signal. The functional localiser run lasted about 7 minutes and consisted of 9 blocks (30seconds) of imagining moving the amputee limb interleaved by 10 blocks (16 seconds) of rest. Instructions were displayed to the participants to either "Rest" or "Imagine". The functional data were pre-processed and analysed online using TBV, before an accumulative General Linear Model (GLM) was applied to the data. The PM-ROI was selected from the active voxels (threshold of $t > 5.0$) within a rectangle anterior to the precentral sulcus. The ROIs were defined in each participant's native space and subsequently used for the neurofeedback training runs to derive the neurofeedback signal. For further analysis, we normalized these ROIs into Talariach space, as illustrated in table 6.1 and identified based on the nearest Gray matter using a Talairach Daemon (Lancaster *et al.*, 2000). The targeted ROI of Session Two was based on rACC coordinates reported in DeCharms study (DeCharms *et al.*, 2005).

Table 6-1. Subject specific PM-ROI localised using a function run during a motor imagery task of the amputee limb. LH=Left Hemisphere, RH=Right Hemisphere, BA=Broadmann Area.

Subject No.	Anatomical area	Talairach coordinates: (x,y,z)	No. of voxels
1	LH, Precentral Gyrus, BA6	-30, -10, 61	1135
2	RH, Precentral Gyrus, BA4	33, -16, 52	908
3	LH, Precentral Gyrus, BA6	-28, -14, 55	1252

6.3.3.3 fMRI Neurofeedback training

The two fMRI neurofeedback sessions included 16 runs in total, each lasting for 430 seconds and consisting of nine downregulation blocks (each with a duration of 30 seconds) interleaved by 10 blocks (16 seconds) of rest as shown in figure 6.2. Participants were instructed to downregulate their targeted ROI by decreasing the height of the thermometer bar during the task block and relaxing during the rest blocks.

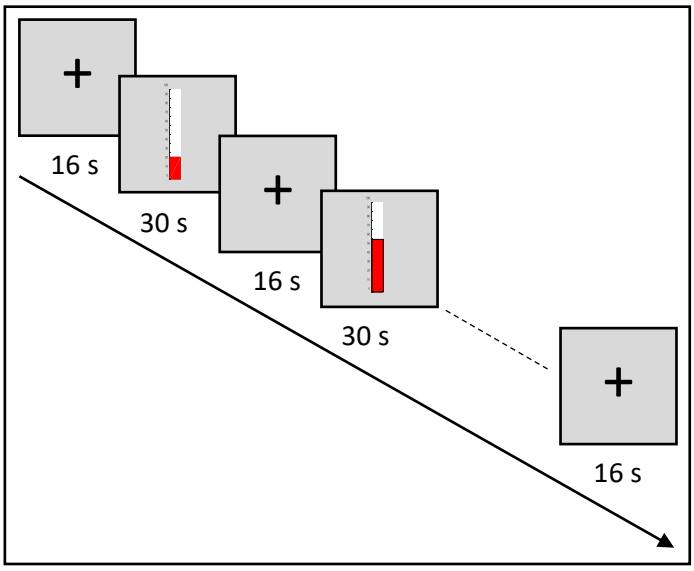

Figure 6.2. fMRI Neurofeedback training paradigm. Duration of 430s and consisting of nine neurofeedback blocks alternating with 10 fixation (rest) blocks.

6.3.4 Online data analysis

Real time fMRI data analysis and neurofeedback presentation was performed using TBV software and BrainStim. The scanner transmitted the acquired fMRI data volume by volume to the analysis computer that hosted TBV, through a fast network connection. Functional data were pre-processed in real time, which included linear de-trending, slice timing correction, 3D motion correction and spatial smoothing using a Gaussian kernel with full width at a half maximum (FWHM) of 8mm.

The feedback signal consisted of a thermometer with a continuously updated red column height at each TR (1 TR=2000ms), based on the following equation:

$$\boldsymbol{bar\ height}\ (\boldsymbol{t}) = \left(\frac{\boldsymbol{ROI}\ \ (\boldsymbol{t}) - \boldsymbol{ROI_{base}}}{\boldsymbol{ROI_{base}}}\right) \quad (6.1)$$

Where *ROI (t)* is the average ROI Blood Oxygen Level Dependent (BOLD) signals of the PM-ROI or ACC-ROI and during the neurofeedback block at time *t*. ROI_{base} is the average BOLD signals of the last three volumes in the fixation block.

6.3.5 Offline data analysis

The raw data were pre-processed offline using BrainVoyager QX 2.8.4 (Brain Innovation, Maastricht, The Netherlands). The first two volumes of each run were discarded to account for T1 equilibration effects. The pre-processing of the remaining functional data involved slice timing correction with cubic-spline interpolation, 3D motion correction with Trilinear/Sinc interpolation, linear trend removal, high-pass filtering with a cut-off set to 3 cycles and spatial smoothing with 4mm full-width at half-maximum (FWHM) isotropic Gaussian kernel. All functional images of each subject were aligned to the first functional volume after the anatomical scan and spatially normalized to Talairach space to enable group analysis across participants (Talairach & Tournoux, 1988).

First level analyses involved a general linear model (GLM) to analyse each participant individually, with one predictor 'feedback' for the neurofeedback runs convolved with a standard hemodynamic response function and covariates derived from six head motion parameters (Johnston *et al.*, 2010; Dijk *et al.*, 2012).

6.3.5.1 Region of Interest analysis

To examine the Neurofeedback training success, Beta values were estimated using a ROI-GLM analysis for each Neurofeedback run of each ROI (rACC and PM) and were used as an indicator for the neurofeedback success. A linear regression of the average beta weights over neurofeedback runs was used to examine the downregulation over runs as an index of self-learning.

6.3.5.2 Whole brain analysis

A whole brain second level Fixed Effect Analysis (FFX-GLM) was conducted for the neurofeedback runs of each ROI separately contrasting feedback vs. rest (for each ROI separately, $p<0.05$ with cluster-level thresholding of 702 mm^3 for rACC, 810 mm^3 for PM

6.4 Results

6.4.1 Questionnaires

All the questionnaires were understood and completed by the patients. They reported their pain intensity and nature as listed in table 6.2.

Table 6-2. Pain intensity and symptoms feeling using BPI questionnaire before and after the fMRI neurofeedback training of each patients rated in a scale from 0 (no pain) to 10 (pain as bad as you can imagine)

Patient			**1**	**2**	**3**
Pain during the last 24 hours before the experiment	At its worst		6	5	8
	At its least		4	4	5
Pain interference with	General activity		6	5	6
	Mood		4	4	7
	Relation with others		3	4	3
	Sleep		1	8	7
	Enjoyment of life		2	5	6
Pain symptoms during the last 24 before the experiment feel like:	Burning		5	5	8
	Squeezing		4	6	8
	Pressure		5	6	8
	Electrical shock		5	7	8
	Stabbing		5	3	8
	Needles		4	5	8
	Tingling		4	7	8
Pain before the fMRI neurofeedback experiment		PM	5	6	8
		ACC	5	5	8
Pain after the fMRI neurofeedback experiment		PM	4	4	9
		ACC	4	4	8

6.4.2 ROI analysis

All the patients underwent two neurofeedback session over two different days. Two patients completed 4 neurofeedback runs for rACC, four neurofeedback runs for PM and 8 sham feedback runs from the left auditory cortex (-51, 2, -4). The third patient completed eight neurofeedback runs for each ROI. During the neurofeedback training, they learnt to decrease the feedback signal acquired from either PM or rACC. The average beta weights in rACC and PM estimated during neurofeedback training is shown in figure 6.3.

The linear regression highlighted a gradual downregulation but not significant in the mean PM and rACC activities across neurofeedback runs to indicate a learning effect (y = -0.09x + 0.41, t = -3.46, p < 0.07; y = -0.05x + 0.11, t = -1.34, p < 0.3 for PM and rACC respectively).

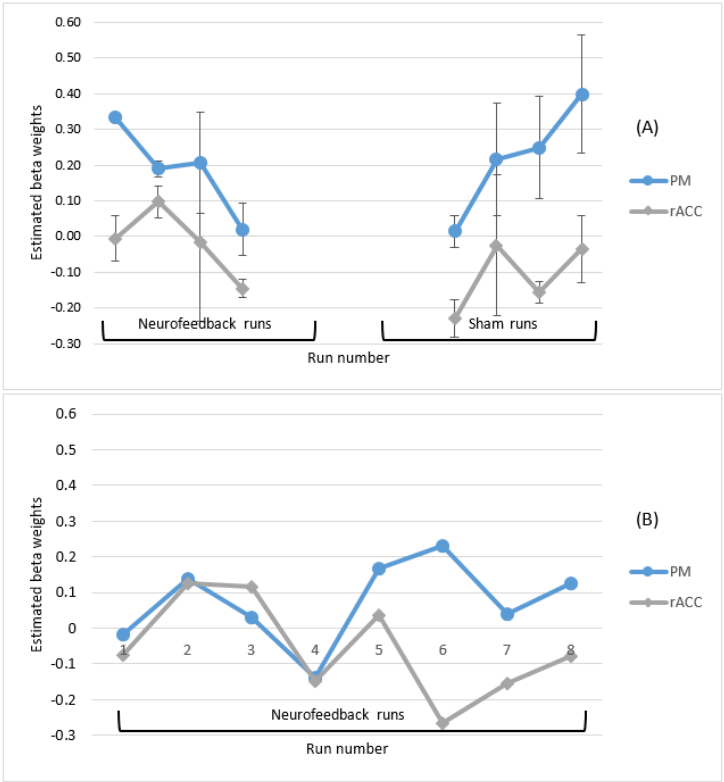

Figure 6.3. Estimated beta-weights for PM and rACC regions (mean±SEM). (A) Average beta-weights of two patients during the 4 neurofeedback runs and 4 sham feedback runs. (B) Beta-weights of the third patient for 8 neurofeedback runs.

6.4.3 Whole brain analysis

Whole brain FFX-GLM analysis was performed for both ROIs to investigate whether any brain regions, other than the identified PM or rACC, were activated during the neurofeedback training. The active regions of PM and rACC are listed in table 6.3 and illustrated in figure 6.4. The individual patient's regions are showing in Appendix A.

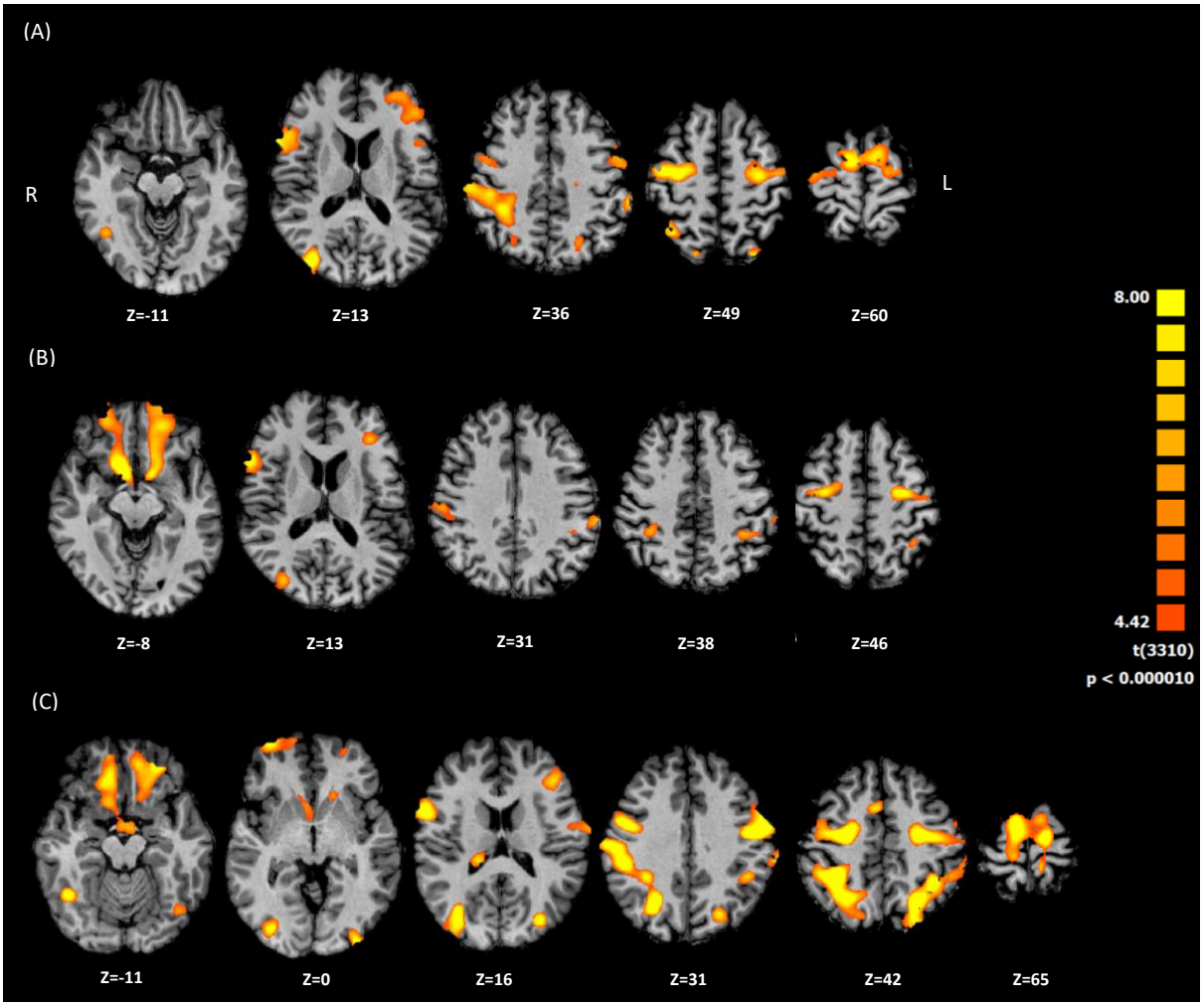

Figure 6.4. FFX-GLM analysis showed brain activations for (A) PM ROI; (B) rACC ROI (C) sham group. These activations are significant at p<0.00001 uncorrected.

Table 6-3. Brain clusters activated during the neurofeedback for both ROIs and sham. x,y,z are the Talairach coordinates, LH and RH= Left and right hemisphere. BA= Brodmann area.

ROI	Cortical Area	x	y	z	*t*	Size (mm^3)
PM	RH, Inferior Parietal Lobule, BA40	36	-40	43	11.13	9673
	RH, Precuneus, BA7	14	-70	52	7.86	392
	RH, Fusiform Gyrus, BA37	42	-55	-11	7.24	1026
	RH, Middle Occipital Gyrus, BA19	33	-76	13	9.81	2605
	LH, Superior Frontal Gyrus, BA6	-15	-5	64	14.84	23837
	LH, Precuneus, BA7	-21	-77	46	10.32	677
	LH, Precuneus, BA7	-24	-61	37	6.65	609
	LH, Inferior Frontal Gyrus, BA9	-51	5	32	7.30	7722
	LH, Inferior Parietal Lobule, BA40	-60	-35	40	8.88	652
rACC	RH, Postcentral Gyrus, BA2	54	-19	31	6.70	925
	RH, Inferior Frontal Gyrus, BA44	57	14	13	9.51	2468
	RH, Middle Frontal Gyrus, BA6	33	-7	46	8.63	1694
	RH, Inferior Parietal Lobule, BA40	33	-37	40	6.75	589
	RH, Cuneus, BA30	30	-76	10	7.90	1290
	RH, Sub-lobar	12	11	-8	11.27	15437
	LH, Middle Frontal Gyrus, BA6	-27	-7	46	9.20	2050
	LH, Inferior Frontal Gyrus, BA46	-33	32	13	7.03	938
	LH, Supramarginal Gyrus, BA40	-36	-40	37	6.91	1054
	LH, Inferior Parietal Lobule, BA40	-60	-28	31	6.89	579
Sham	RH, Inferior Temporal Gyrus, BA20	54	-10	-27	7.93	1324
	RH, Fusiform Gyrus, BA37	42	-55	-11	10.32	1286
	RH, Inferior Parietal Lobule, BA40	36	-40	40	16.17	49530
	RH, Thalamus, Pulvinar	18	-28	16	7.93	848
	RH, Medial Frontal Gyrus, BA32	6	11	43	9.73	730
	LH, Middle Frontal Gyrus, BA11	-24	41	-12	9.81	14778
	LH, Superior Parietal Lobule, BA7	-24	-61	43	13.29	11624
	LH, Precuneus, BA31	-27	-73	16	9.57	1180
	LH, Middle Occipital Gyrus, BA18	-33	-88	-2	8.95	1660
	LH, Fusiform Gyrus, BA19	-39	-64	-8	7	542
	LH, Precentral Gyrus, BA6	-51	-7	31	15.76	16272

6.5 Discussion

In the current study we investigated the effectiveness of fMRI neurofeedback in phantom pain regulation using two different target regions rACC and PM. The feedback signal represented the activity in either PM or rACC during the neurofeedback training and in the auditory cortex during the sham feedback. Current evidence suggests that there is a link between chronic pain and motor cortex reorganization but the causality remains unclear and hence PM was chosen as a targeted region (Mercier and Le´onard, 2001). The rACC was selected as a targeted region for this study because of its likely involvement in pain regulation and pain perception (Rainville, 2002; DeCharms *et al.*, 2005) despite its role in emotional processing, attention and executive functions (Allman et al. 2001; Davis et al. 2000). Brain imaging studies have found a complex network cerebral structures named the pain matrix associated with the different dimensions of pain, including the primary and secondary somatosensory, insular, anterior cingulate cortex, prefrontal cortices, and thalamus (Peyron *et al.*, 2000).

During the neurofeedback training, patients showed an increase in their ability to down-regulate the PM and rACC activity between the first and last neurofeedback run while they showed an increase activation during the sham feedback (for only two patients). The beta weights of neurofeedback runs did not consistently decrease, which may reflect the search for an effective strategy and the gradual skills learning for self-regulation. These findings are in line with previous neurofeedback studies, which show similar effects of down-regulation (DeCharms *et al.*, 2005; Emmert *et al.*, 2014).

At the behavioural level, the neurofeedback training of both ROIs indicates a slight decrease in pain intensity. However, the difference was not statistically significant (paired-sample *t*-test, $p<0.25$). Regardless of the absence in pain modulation, we found effects of changes in brain activity for both ROIs.

The whole brain analysis showed a widespread brain activation that is involved in neurofeedback training other than the targets ROIs. These activation included bilateral SMA, bilateral PM, bilateral Inferior Frontal Lobule (IPL), bilateral Precuneus, left inferior frontal gyrus, right fusiform gyrus and right middle occipital gyrus for PM-ROI and bilateral orbitofrontal cortex (OFC), bilateral PM, bilateral inferior frontal gyrus, bilateral IPL, right cuneus and right postcentral gyrus for rACC-ROI. The functionality of these regions are as listed below:

- SMA is involved in motor planning and control (Nachev et al. 2008; Grefkes et al. 2008). Indeed, the increase in the left SMA activation, supporting previous findings of practice-related activation increase regardless of the trained hand (for review see: (Halsband & Lange, 2006).
- The PM area plays an important role in planning, preparation and selection of movements (for review see: (Hétu et al. 2013; Bestmann et al. 2008; Hoshi et al. 2007).
- The IPL activation could be related to the integration of visuomotor information (Halsband & Lange 2006), or the internal recruitment of the stored motor representations (Cooke et al. 2003).
- The Precuneus is a prominent node within the default mode network (DMN) that associated with self-relevance and self-perception, in addition to attentional, cognitive, and affective processes (Xavier Castellanos *et al.*, 2008) with widespread connections to brainstem, limbic structures, thalamic and prefrontal regions that are all important to homeostasis and affective equilibrium (Raichle *et al.*, 2000; Cavanna and Trimble, 2006).
- The OFC is involved in decision making, controlling and adapting reward-related and punishment-related behaviour and in decoding and representing some primary

reinforcers such as pleasant touch, painful touch, taste, smell and more abstract reinforcers such as winning or losing money (Rolls, 2004).

In line with the previous findings (DeCharms *et al.*, 2005; Emmert *et al.*, 2014), we showed that patients gained control over the feedback signal derived from either PM (session one) or rACC (session two) by building an effective strategy, which led to decrease in the targeted ROIs activity. On the other hand, they lost their ability to modulate their brain activity during the sham feedback derived from the auditory cortex.

6.6 Limitations

This study investigates the feasibility of using two targeted regions for fMRI Neurofeedback in pain modulation. It clearly indicates that PM and rACC could serve as pain neurofeedback regions for future neurofeedback experiments. The current limitations should be considered when designing similar fMRI neurofeedback experiments:

- A low number of PLP patients due to difficulties in recruitment, including with issues in their mobility and its effect on entering the scanner and staying still.
- The study aimed to assess the effect of fMRI neurofeedback on pain rating, however due to a low number of patients, we could not find a significant behavioural effect thus further studies with a larger population are needed.
- The sham runs came immediately after the neurofeedback runs, which might bias the modulation due to the transfer effect of the neurofeedback. It's recommended to recruit a separate control group.

6.7 Rationale for the experimental chapters 6 and 7

In the experimental chapter 6, phantom limb pain patients were trained to use the fMRI neurofeedback system to modulate the level of neuronal activity in circumscribed brain regions.

Two neurofeedback paradigms were examined in two different session (over two days), one was based on down-regulation of rACC and the other was based on down-regulation of PM. Those patients received a true feedback and a sham feedback in each session. In the next experiment chapter (chapter 7), the lack of the experimental paradigm, the number of participants, the targeted region, the sham feedback and the behavioural effects were addressed. fMRI neurofeedback system was applied to train healthy participants to up-regulate their SMA activation while they were instructed to imagined doing complex body actions. A motor reaction time was measured before and after the neurofeedback training to assess the changes caused by a successful modulation.

Chapter 7 : Up-regulation of Supplementary Motor Area activation with fMRI Neurofeedback improves motor reaction time

7.1 Abstract

fMRI Neurofeedback (NF) is a potential tool to study the relationship between behaviour and brain activity. It enables people to self-regulate their brain signal and can alter the functional connectivity between brain regions. Here, we applied fMRI NF to train healthy participants to increase activity in their supplementary motor area (SMA) during a Motor Imagery (MI) task of complex body movements while they received a continuous feedback signal. This signal represented the activity of individually localized SMA in the NF group and a pre-recorded signal in the control group. In the NF group, but not in control group, results showed an increase in left SMA activation, as well as other regions including Cingulate Gyrus and Premotor area. Consistent with this a psychophysiological interaction (PPI) the analysis revealed changes for the NF group in functional connectivity between the SMA and other cortical and subcortical regions before and after the NF training. In addition, we found behavioural changes, i.e. shortening of motor reaction time in the NF group. These results suggest that NF can assist participants to develop greater control over motor and motor-related regions involved in motor skill learning. The results contribute to a better understanding of the underlying mechanisms of SMA NF based on MI with a direct implication for rehabilitation of motor dysfunctions.

7.2 Introduction

Motor Imagery (MI) is a form of motor simulation (Vogt *et al.*, 2013; Filimon *et al.*, 2015), visualised by the individual, without any overt movement (Blefari *et al.*, 2015) and both MI and motor execution (ME) are thought to share similar neural networks (Jeannerod, 2001). Further examination of this topic using an activation likelihood estimation (ALE) analysis highlights that MI activates a large number of primary and secondary motor areas in both hemispheres including supplementary motor area (SMA), inferior frontal gyri (IFG), precentral gyrus (PcG), middle frontal gyrus (MfG), anterior insula, inferior/superior parietal lobule (IPL/SPL), putamen, thalamus, and cerebellum (Hétu *et al.*, 2013). MI plays an important role in motor learning tasks (Schuster *et al.*, 2011), as well as improving motor performance of various tasks over different time periods (Gentili *et al.*, 2010). There is overlap in brain areas related to MI and motor learning as revealed by an ALE analysis of motor skills learning that suggest significant roles for dPM, SMA, somatosensory cortex, SPL, thalamus, putamen and the cerebellum (Hardwick *et al.*, 2013).

NF is a closed loop system that can measure a participant's brain activity and present it back to them as either a visual or an auditory feedback signal. The feedback signal facilitates the participant's ability to modulate their own brain activity with the aim of improving function. Previous results using Electroencephalography (EEG) based NF has shown that healthy participants and patients can be trained to alter their scalp electrical activity in a wide range of applications such as improving cognitive functions using MI (Scherer et al. 2015; for review see: Marzbani et al. 2016). However, limitations of EEG-NF include low spatial resolution and difficulty in providing feedback from subcortical brain areas. An alternative method of NF that addresses these limitations is provided by functional Magnetic Resonance Imaging (fMRI), which measures Blood Oxygen Level Dependent (BOLD) levels, and has enabled feedback signals from brain activity of deeper brain structures and with higher spatial resolution.

Several fMRI NF studies have demonstrated that participants can be trained to regulate the activity of different brain regions, such as regions responsible for emotions (anterior insula and amygdala (Caria *et al.*, 2010; Zotev *et al.*, 2011; Veit *et al.*, 2012)), the auditory cortex (Haller *et al.*, 2010), language areas (Rota *et al.*, 2009) and the visual cortex (Scharnowski *et al.*, 2012). These studies have reported behavioural changes following NF training, such as changes in emotional state and pain sensation (DeCharms *et al.*, 2005), reduction of tinnitus symptoms (Haller *et al.*, 2010), improvement of prosody identification and enhancement of visual sensitivity for target detection (Scharnowski *et al.*, 2012). Furthermore, several other NF studies have examined motor and motor-associated cortices, focussing on how exercises such as ME (Berman *et al.*, 2012; Neyedli *et al.*, 2017) and MI (Yoo et al., 2008; Scharnowski et al., 2015; Auer et al. 2015) can lead to an enhancement in motor performance. Clinically, sensorimotor-targeted regions can be used in motor rehabilitation related to stroke and neurological disorders (DeCharms *et al.*, 2005; Subramanian *et al.*, 2011b; Sitaram *et al.*, 2012; Linden and Turner, 2016).

The impact of NF on functional connectivity between brain regions provides a physiological measure for fMRI-NF training (Weiskopf *et al.*, 2007; Caria *et al.*, 2012) and a number of real-time fMRI studies have shown that NF based MI training can alter the functional connectivity between target regions and other brain regions compared with sham feedback or no feedback (Marins *et al.*, 2015; Xie *et al.*, 2015). However, the mechanisms by which fMRI-NF based MI affects functional connectivity and could result in improvements in motor performance, is unclear.

In the context of modulating motor cortex activity, fMRI-NF studies have reported the use of different motor regions to derive a feedback signal such as premotor area (PMA) (Sitaram *et al.*, 2012; Zhao *et al.*, 2013; Hui *et al.*, 2014; Marins *et al.*, 2015), primary motor cortex (M1) (Yoo *et al.*, 2008; Berman *et al.*, 2012; Chiew *et al.*, 2012; Blefari *et al.*, 2015;

Neyedli *et al.*, 2017) and SMA (Hampson *et al.*, 2011; Scharnowski *et al.*, 2015; Sepulveda *et al.*, 2016). However, fMRI-NF studies targeting SMA have revealed mixed findings, for instance Scharnowski et al (2015) and Sepulveda et al (2016) found that participants were able to increase their SMA activity during the NF training, but Hampson et al. (2011) did not find a significant increase in SMA activity. Lack of a significant effect might be due to the limited number of runs used. In addition, the two studies showing positive results used a small number of participants and did not include a control group and this makes their results difficult to interpret.

The present work aims to investigate: 1) Whether healthy participants are able to increase the activation levels in their SMA, which is involved in motor learning, planning and execution, during MI of complex actions, whilst receiving a visual feedback signal. 2) Does successful fMRI NF of SMA translate to changes in behavioural measures. 3) Whether any brain regions, other than the SMA, were activated during the MI guided by NF. 4) Whether successful up-regulation can result in connectivity changes beyond SMA. In contrast to previous fMRI-NF studies which showed no learning effect (Hampson et al. 2011) and small sample size without control group (Scharnowski *et al.*, 2015; Sepulveda *et al.*, 2016), participants were split into two groups: a NF group, which received real feedback, and a control group, which received sham feedback. All the participants underwent a Go/No-Go task to measure their motor reaction time before and after the NF training. If participants are able to successfully and selectively modulate SMA activity while performing an MI task, post-training tests should indicate faster reaction times for the NF group than the control group.

7.3 Methods and material

7.3.1 Participants

Twenty healthy participants with normal or corrected-to normal vision were recruited. Seventeen of them were right-handed and one was ambidextrous with a laterality index of 33.3 according to the Edinburgh Inventory (Oldfield, 1971). All participants were randomly split into two groups (single blind study): Ten participants in the NF group (five males, mean age: 26.1±5.1 years), who received true feedback, and ten in the control group (seven males, mean age: 23.2±2.6 years), who received sham feedback. The participants' abilities to perform motor imagery (MI) tasks were matched using the Vividness of Movement Imagery Questionnaires-2 (VMIQ-2) (Callow and Roberts, 2010) to reduce inhomogeneity between the experimental and control groups on their ability to perform motor imagery. Both groups where demographically matched in terms of age, education and handedness as shown in Table 7.1. The ethics committees of the College of Science and Engineering, University of Glasgow approved this study. All participants provided their informed consent for the experiment.

Table 7-1. Demographic features for participants in the NF and control groups

		NF Group (Mean±SD)	**Control Group (Mean±SD)**	***p-value* (two tailed *t*-test)**
Age (years)		26.1±5.1	23.2±2.6	0.175
Education (years)		17.2±2.3	16.6±2	0.621
Handedness		81.4±15.7	74.3±23.7	0.490
MI vividness	Third person perspective	21.6±10.1	18.6±4.8	0.462
	First person perspective	18.5±4.2	18.1±4.3	0.839

7.3.2 Imaging parameters and fMRI neurofeedback platform

The study was performed on a 3T Siemens Tim Trio MRI scanner at the University of Glasgow Centre for Cognitive Neuroimaging (CCNi) with a 32-channel head coil. T1 weighted structural scans were acquired at the beginning of the experiment (TR=2000ms, TE=2.52ms,

192 sagittal slices, 1 mm^3 isotropic voxels and image resolution 256×256). T2*-weighted functional scans were collected with an Echo-Planar Imaging (EPI) sequence (TR=2000ms, TE=30ms, whole brain coverage with 32 axial slices, 0.3 mm gap and 3 mm^3 isotropic voxel).

The NF system used Turbo-BrainVoyager (Brain Innovation, Maastricht, The Netherlands) and a custom script running on MATLAB (Mathworks Inc., Natick, MA, USA) to visualize the feedback signal as a thermometer. An LCD projector displayed the thermometer onto a rear projection screen that could be viewed through a mirror mounted on the head coil.

7.3.3 Experimental procedure

All participants underwent the same procedure, which consisted of: a questionnaire interview outside the scanner, a pre-scan behavioural test, a localizer run, fMRI NF training (true feedback for the NF group and sham feedback for the control group) and a post-scan behavioural test.

7.3.3.1 Behavioural test

The Go/No-go task measures Reaction Time (RT) and reflects interaction between the underlying inhibitory and activational components of motor control. Participants completed 250 trials of this task before and after the NF training session, once for each hand. They were instructed to press the space bar on the keyboard using their index finger as quickly and accurately as possible when a go-trial was displayed, but inhibit their response when a no-go trial was presented. The task was run under Inquisit 5 software (a software to create a wide range of psychological and experimental paradigms). Each trial consisted of a fixation point (+) presented for 800ms, followed by a blank white screen for 500ms, followed by a rectangular cue (horizontal 2.5×7.5cm, or vertical 7.5×2.5cm) displayed for one of the five intervals (100, 200, 300, 400, 500ms) to avoid the expectation confound. Finally, go and no-go targets were

coloured green and blue respectively and were presented for 1000ms, unless a response occurred (Fillmore *et al.*, 2006). Figure 1 shows the different in reaction time before (pre) and after (post) the fMRI NF traning for both group and hands. A 2×2×2 (hand×group×pre/post) mixed effect analysis of variance (ANOVA) was performed to analyse between and within group effects. A paired-sample t-test was used as a post-hoc test to compare between the pre-post experiment reaction time of each group and hand separately.

7.3.3.2 Functional localizer

The NF training session started with a functional localiser run, to identify the Supplementary Motor Area (SMA), from which the participant received the feedback signal. The localiser lasted for about 5 minutes and consisted of 7 fixation blocks (16s) interleaved by 6 blocks of bimanual index finger-tapping (30s). Written instructions were given to the participants to either "Rest" or "Tap". The functional data were pre-processed and analysed online with an accumulative General Linear Model (GLM) embedded in Turbo-BrainVoyager. The SMA-ROI was delineated from the active voxels (threshold of $t > 5.0$) within a rectangle, anterior to the precentral sulcus and superior to the cingulate sulcus, as shown in figure 7.1. The ROIs were defined in each participant's native space and subsequently used for the NF training runs to derive the NF signal. For further analysis, we normalized these ROIs into Talairach space, as illustrated in table 7.2 and identified them based on the nearest Gray matter using a Talairach Daemon (Lancaster *et al.*, 2000).

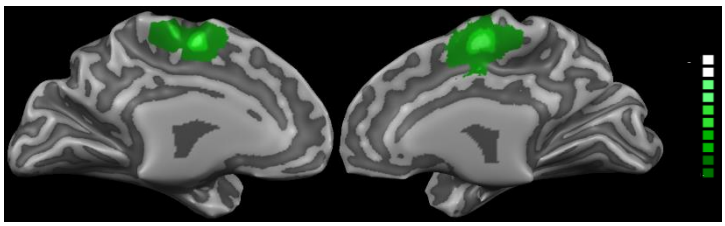

Figure 7.1. Overlap of individual SMA-ROI for the 20 participants of both groups. The subject specific SMA-ROIs were identified prior to the NF training using a functional localiser run during an index finger tapping task.

Table 7-2. Subject specific SMA-ROI in Talairach space

	Subject no.	Anatomical area	Talairach coordinates			No. of voxels
			x	y	z	
NF group	1	LH, Medial Frontal Gyrus	-6	-7	52	1163
	2	LH, Medial Frontal Gyrus	-6	-19	58	702
	3	LH, Medial Frontal Gyrus	-3	-10	52	1754
	4	RH, Medial Frontal Gyrus	6	-10	58	1333
	5	LH, Medial Frontal Gyrus	-4	-14	48	1463
	6	LH, Medial Frontal Gyrus	0	-7	49	1520
	7	LH, Paracentral Lobule	-9	-25	52	2984
	8	RH, Medial Frontal Gyrus	9	-10	47	1730
	9	RH, Medial Frontal Gyrus	3	-10	52	2569
	10	RH. Medial Frontal Gyrus	9	-13	52	1186
Control group	11	RH, Medial Frontal Gyrus	2	-11	51	1683
	12	LH, Medial Frontal Gyrus	-10	-8	48	1520
	13	LH, Medial Frontal Gyrus	-7	-17	51	1539
	14	LH, Medial Frontal Gyrus	-4	-5	57	1344
	15	LH, Cingulate Gyrus	-10	-11	45	1408
	16	LH, Medial Frontal Gyrus	-7	-5	57	2086
	17	LH, Medial Frontal Gyrus	-4	-8	57	1792
	18	RH, Cingulate Gyrus	8	-2	48	2072
	19	RH, Medial Frontal Gyrus	8	-8	54	1848
	20	LH, Medial Frontal Gyrus	-4	-10	49	1268

7.3.3.3 fMRI neurofeedback

All the participants took part in seven 430s NF training runs, where they were instructed to upregulate their targeted ROI by doing an MI task of complex body actions. Each NF training run consisted of nine 30s blocks of NF interleaved with ten 16s fixation blocks as shown in figure 7.2. During the NF blocks, participants saw a thermometer, and were instructed to increase its level by imagining doing complex actions. During the fixation blocks, participants looked at a fixation cross, and were instructed to relax and count numbers "1,2,3…" to keep their baseline signal low. Counting down, and other more complex mathematical operations have been shown to activate motor related networks (Hanakawa, 2011; Berman *et al.*, 2012).

The control group was presented with sham feedback that presented a randomly chosen pre-recorded brain signal from a participants in the experimental group (Chiew *et al.*, 2012; Hui *et al.*, 2014).

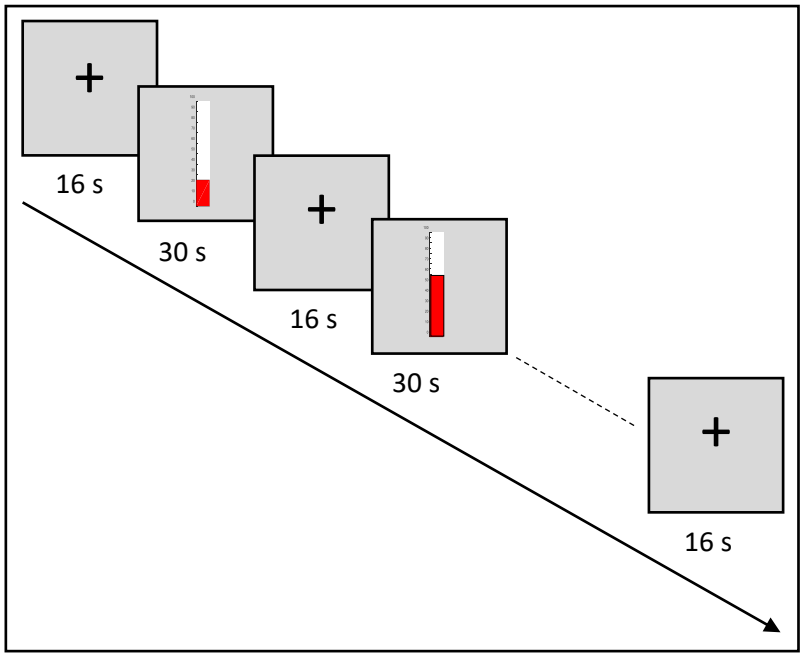

Figure 7.2. fMRI NF training paradigm of one run. A run lasted for 430s and consisted of nine 30s NF blocks alternating with ten 16s fixation (rest) blocks.

7.3.4 Online data analysis

Real time fMRI data analysis and NF presentation was performed using Turbo-BrainVoyager software and MATLAB. The scanner transmitted the acquired fMRI data volume by volume to the analysis computer that hosted Turbo-BrainVoyager through a network connection. Functional data were pre-processed in real time, which included linear de-trending, slice timing correction, 3D motion correction and spatial smoothing using a Gaussian kernel with full width at half maximum (FWHM) of 8mm, then added to a cumulative general linear model (GLM).

The feedback signal consisted of a thermometer with a continuously updated red column height at each TR (1 TR=2000ms), based on the following equation 7.1:

$$\boldsymbol{bar\ height}\ (\boldsymbol{t}) = \left(\frac{\boldsymbol{ROI_{SMA}(t) - ROI_{SMA_{base}}}}{\boldsymbol{ROI_{SMA_{base}}}}\right) - \left(\frac{\boldsymbol{ROI_{reference}(t) - ROI_{r_{base}}}}{\boldsymbol{ROI_{r_{base}}}}\right) \quad (7.1)$$

Where $ROI_{SMA}(t)$ and $ROI_{reference}(t)$ are the average BOLD signals of the SMA-ROI and a reference ROI during the NF block at time *t*. ROI_{SMA_base} and ROI_{r_base} are the average BOLD

signals of the last three volumes in the fixation block of SMA-ROI and reference ROI, respectively. The reference ROI, used to correct for global scanning effects, encompassed a rectangular region covering all the voxels within an axial slice (z=10) distant from the motor network, and showed no activation when the localizer run was analysed.

7.3.5 Offline data analyses

The raw data were pre-processed offline using BrainVoyager QX 2.8.4 (Brain Innovation, Maastricht, The Netherlands). The first two volumes of each run were discarded to allow for T1 equilibration effects. The pre-processing of the remaining functional data involved slice scan-time correction with cubic-spline interpolation, 3D motion correction with Trilinear/Sinc interpolation, linear trend removal, high-pass filtering with a cut-off set to 3 cycles and spatial smoothing with 4mm full-width at half-maximum (FWHM) isotropic Gaussian kernel. All functional images of each subject were aligned to the first functional volume after the anatomical scan and spatially normalized to Talairach space to enable group analysis across participants (Talairach & Tournoux, 1988).

In the first level analysis, all the pre-processed functional data of each subject were analysed using a General Linear Model (GLM) with two predictors (tapping and rest for the localiser, feedback and rest for NF), convolved with a hemodynamic response function and covariates derived from six head motion parameters (Johnston *et al.*, 2010; Dijk *et al.*, 2012), an estimate of the white matter signal (Jo *et al.*, 2010; Zilverstand *et al.*, 2015) and the ventricular signal (Birn *et al.*, 2009; Zilverstand *et al.*, 2015) for modelling physiological artefacts (e.g. respiration and cardiac effects) and scanner instability. Group data were evaluated based on a second level random effect analysis general linear model (RFX-GLM). The obtained statistical maps were corrected for multiple comparisons using cluster-level thresholding (Goebel *et al.*, 2006). In this method, the uncorrected voxel-level threshold was set at $p<0.01$, and then the thresholded maps were submitted to a whole-brain correction

criterion based on the estimate of the map's spatial smoothness and on an iterative procedure (Monte Carlo simulation) for estimating cluster-level false-positive rates. After 1000 iterations, the minimum cluster-size that produced a cluster-level false positive rate (alpha) of 5% was applied to threshold the statistical maps.

7.3.5.1 Region of Interest analysis

To examine the NF training success, beta weights were estimated using a ROI-GLM analysis for each NF run of each subject's ROI, (identified by the functional localiser presented in table 7.2) and were used as an indicator for the NF success. A 2×2 mixed effect analysis of variance (ANOVA) was performed to analyse between and within group effects. A paired *t*-test was used as a post-hoc test to compare the beta weights of the first and the last runs in each group. Furthermore, a linear regression of the average beta weights over NF runs was used to examine the upregulation over runs as an index of self-learning. In addition, an event-related average time course was computed for the last and first NF runs.

7.3.5.2 Whole-brain analysis

To verify the SMA selection during the online NF experiment, a whole brain RFX-GLM analysis was performed for the localizer runs. The contrast tapping vs. rest was computed and a threshold was set at $p<0.01$ uncorrected, with cluster-level thresholding of 899 mm^3.

A whole brain second level RFX-GLM analysis was conducted for the NF runs contrasting feedback vs. rest (for each group separately, $p<0.01$ uncorrected, with cluster-level thresholding of 981 mm3 for the NF group and 1139 mm3 for the Control group). A two sample *t*-test was performed to contrast NF vs control for a group comparison, thresholding at $p<0.01$ uncorrected with cluster-level thresholding of 432 mm3.

7.3.5.3 Psychophysiological interaction (PPI) analysis

To examine the degree of interaction between the SMA and other brain regions during self-regulation, a PPI analysis was applied. PPI is a functional connectivity analysis that explores the functional coupling between the seed region (SMA) to other brain areas (physical variable) modulated by the experimental context, such as MI (psychological variable) (Friston *et al.*, 1997). The results of PPI can be interpreted as estimates of task-specific functional connectivity between the seed and target regions. For the PPI analysis, a GLM was set up with the psychological regressor (experimental condition convolved with the canonical hemodynamic response), physiological regressor (SMA time-course) and a regressor for their interactions. Head motion correction parameters were included in the GLM model as nuisance predictors. These analyses were performed for each NF run of both groups. The group connectivity was assessed with a two-sample *t*-test (NF feedback group vs control group) at a cluster threshold of $p<0.03$ (945 mm^3).

7.4 Results

7.4.1 Behavioural results

Figure 7.3 shows the difference in reaction time of the two groups before and after the NF training for both hands. The repeated measures ANOVA test of the reaction time showed a significant effect of hand×pre/post interaction ($F(1,9)=8.85$, $p=0.016$), but neither main effects of hand ($F(1,9)=0.06$, $p=0.81$), group $F(1,9)=0.89$, $p=0.36$), pre/post experiment $F(1,9)=1.07$, $p=0.326$) nor interaction effects hand×group interaction ($F(1,9)=2.65$, $p=0.13$), group×pre/post interaction ($F(1,9)=0.1$, $p=0.75$), hand×group×pre/post interaction ($F(1,9)=4.04$, $p=0.07$). Paired-sample t-tests between pre-post experiment reaction time of both group for one hand revealed a significant effect of NF training in the right hand of the NF group ($t(9)=3.106$, $p=0.013$) compared to the control

group ($t(9)=0.535$, $p=0.606$). There was no significant effect for the left hand for both groups ($t(9)= 0.471$, $p=0.648$ and $t(9)=0.353$, $p=0.732$ for NF and control group respectively).

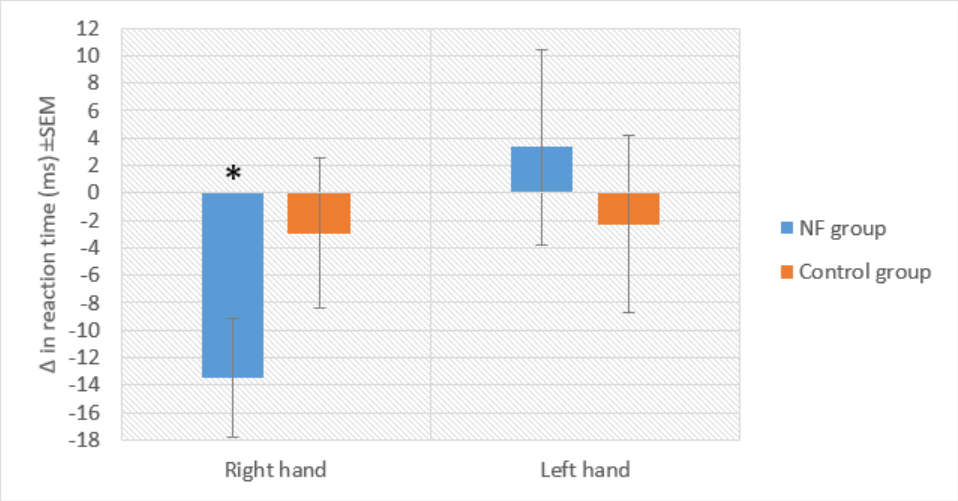

Figure 7.3. Reaction time (ms) difference before and after the self-regulation of both hands for the two groups. Errors bar represent the standard mean error (SEM). * $p<0.05$.

7.4.2 ROI analysis

Each participant completed 7 NF runs in one session, during which, most of them learnt to increase the brain activity acquired from their functionally localised SMA regions. They reported imagining punching or boxing. The average beta weights in the SMA estimated during each run of the NF and control group is showed in figure 7.4. The repeated measures ANOVA test of the beta weights showed a significant effect of group ($F(1,9)=40.7$, $p<0.0001$), however neither run ($F(6,54)=0.158$, $p=0.98$) or the interaction of group with run ($F(6,54)=1.33$, $p=0.256$) showed significant effects. Paired t-test revealed a significant increase in SMA activity from the first to the last run ($t(9)=-1.83$, $p<0.04$) in the NF group but the control group showed no significant change ($t(9)= 0.88$, $p<0.2$).

Moreover, a linear regression highlighted a gradual increase in the mean SMA activity across runs in the NF group indicating a learning effect ($y = 0.062x + 0.252$, $t = 3.95$, $p < 0.01$). The control group did not show such learning progress ($y = -0.074x - 0.035$, $t = -1.56$, $p = 0.17$).

Additionally, figure 7.5 shows the averaged time course of BOLD signal during the NF blocks of both groups. This figure plots the first and the last runs for both groups and shows an increase in SMA activity for the NF group.

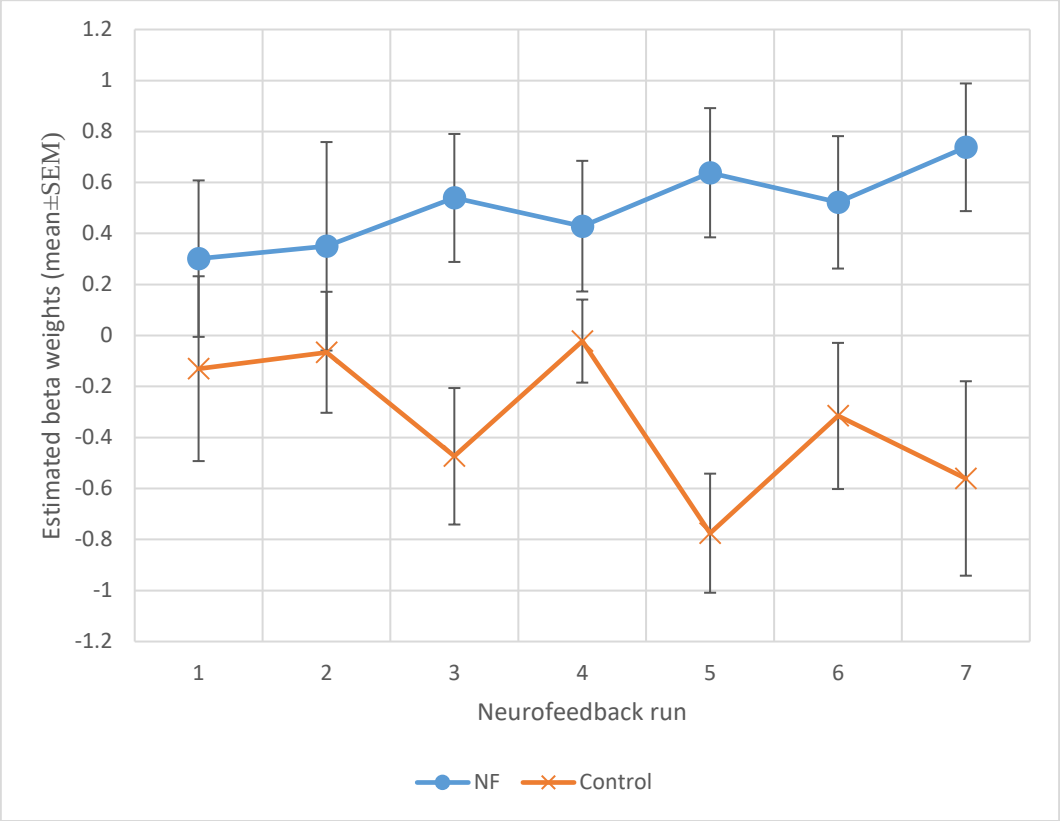

Figure 7.4. The mean beta weights of NF and control groups across NF runs. The beta weights were used as an indicator the success of the self-regulation.

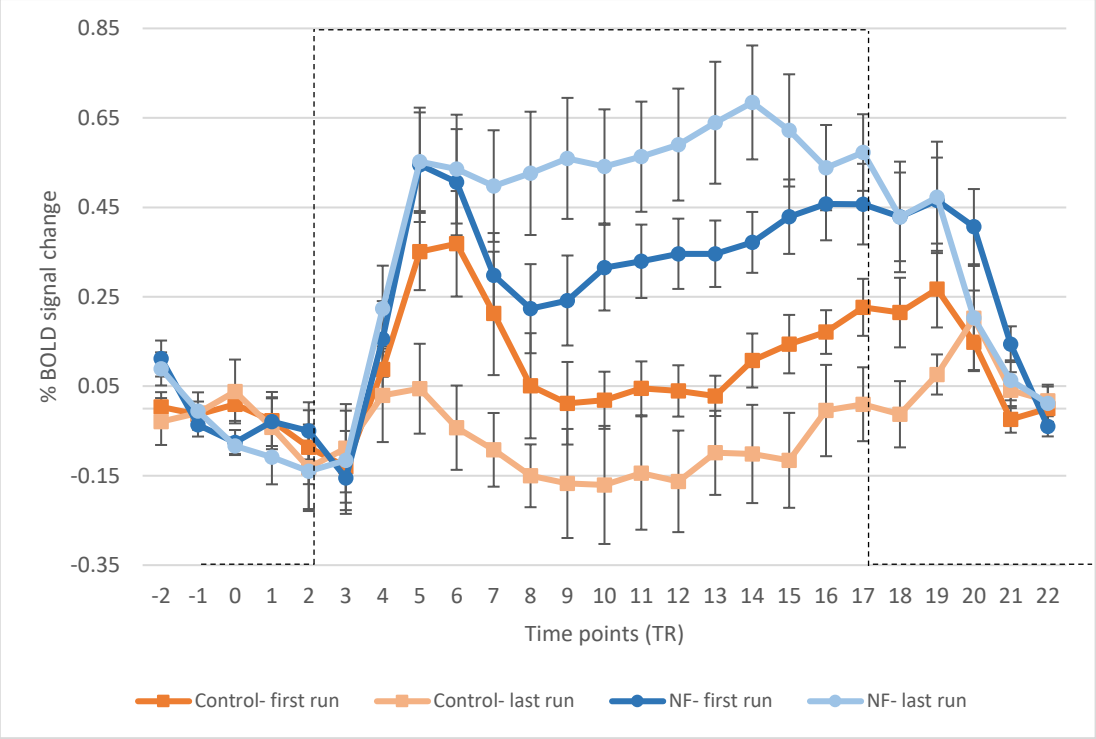

Figure 7.5. Average BOLD signal change of target SMA regions of NF and control groups comparing the first and last runs. NF training helped to increase the SMA activity of the NF group (blue lines) compared to the control group where it decreased it (orange lines). Error bars are standard error of the mean. Dashed lines represent the task block.

7.4.3 Whole brain analysis

7.4.3.1 Functional localiser

A whole brain random effects GLM analysis of the functional localiser runs showed widespread activation spanning over bilateral M1 and S1, left Superior Frontal Gyrus, right Lentiform Nucleus, bilateral thalamus, left Lingual Gyrus and Culmen (cerebellum) as shown in figure 7.6. However, results did not show a significant activation in SMA. The axial overlay map of figure 7.6 illustrates that the activation was mostly associated with motor and motor related areas. Moreover, left Lingual Gyrus was activated possibly due to its role for identification and recognition of words.

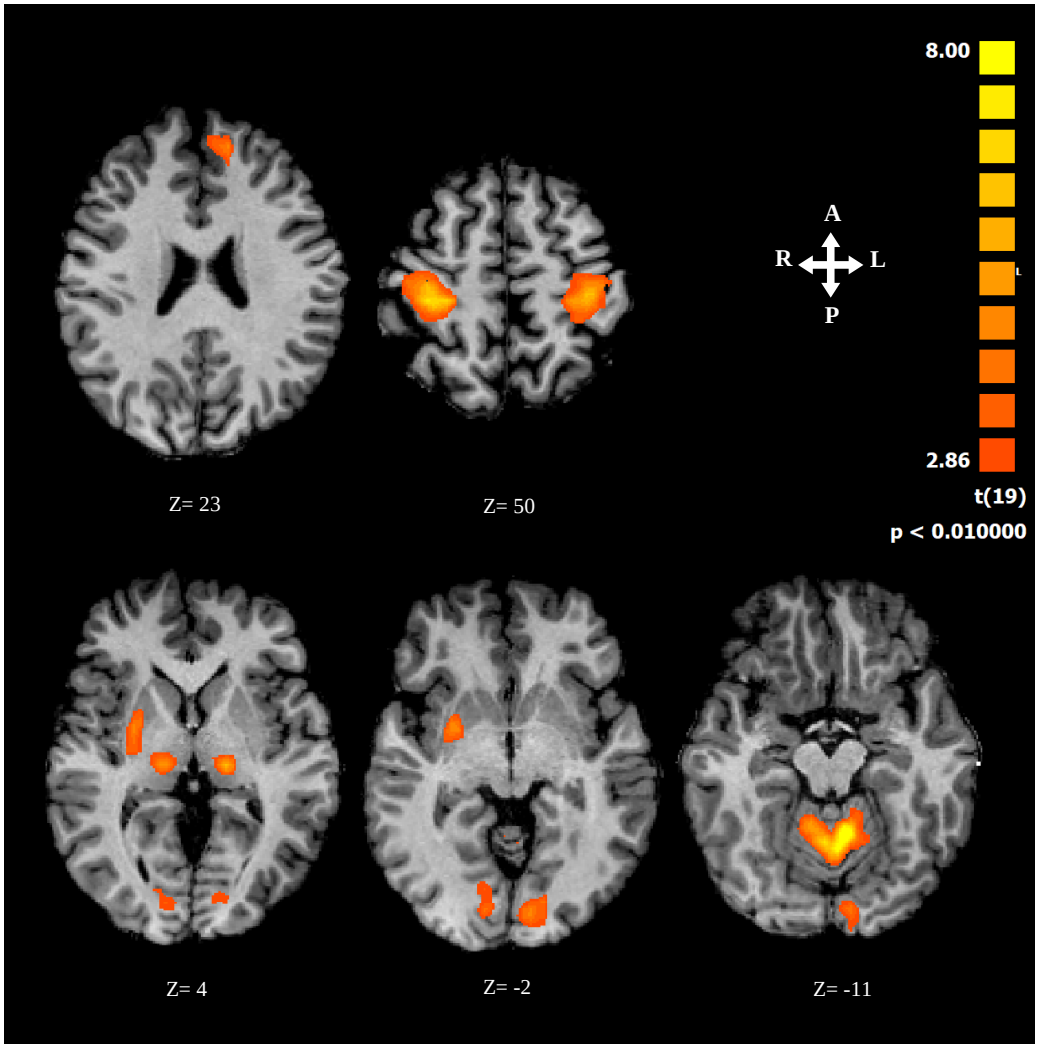

Figure 7.6. Results of the analysis of all the functional localizer runs of both groups overlaid on axial slices. The map was theresholded at P<0.01 (cluster size>899mm^3)

7.4.3.2 NF runs

A whole brain random effects GLM analysis was performed for both NF and control groups to investigate whether any brain regions, other than the individually identified SMA, were activated during the MI guided by the NF. The active regions of NF and control groups are listed in table 7.3 and illustrated in figure 7.7. NF training resulted in a significant increase in the targeted SMA activation in the NF group compared to the control group. Furthermore, additional activations were found in the bilateral Lentiform Nucleus, left Motor Cortex and left Supramarginal Gyrus for the NF group and in the bilateral Basal Ganglia, bilateral Middle Frontal Gyrus and Inferior Parietal Lobule for the control group.

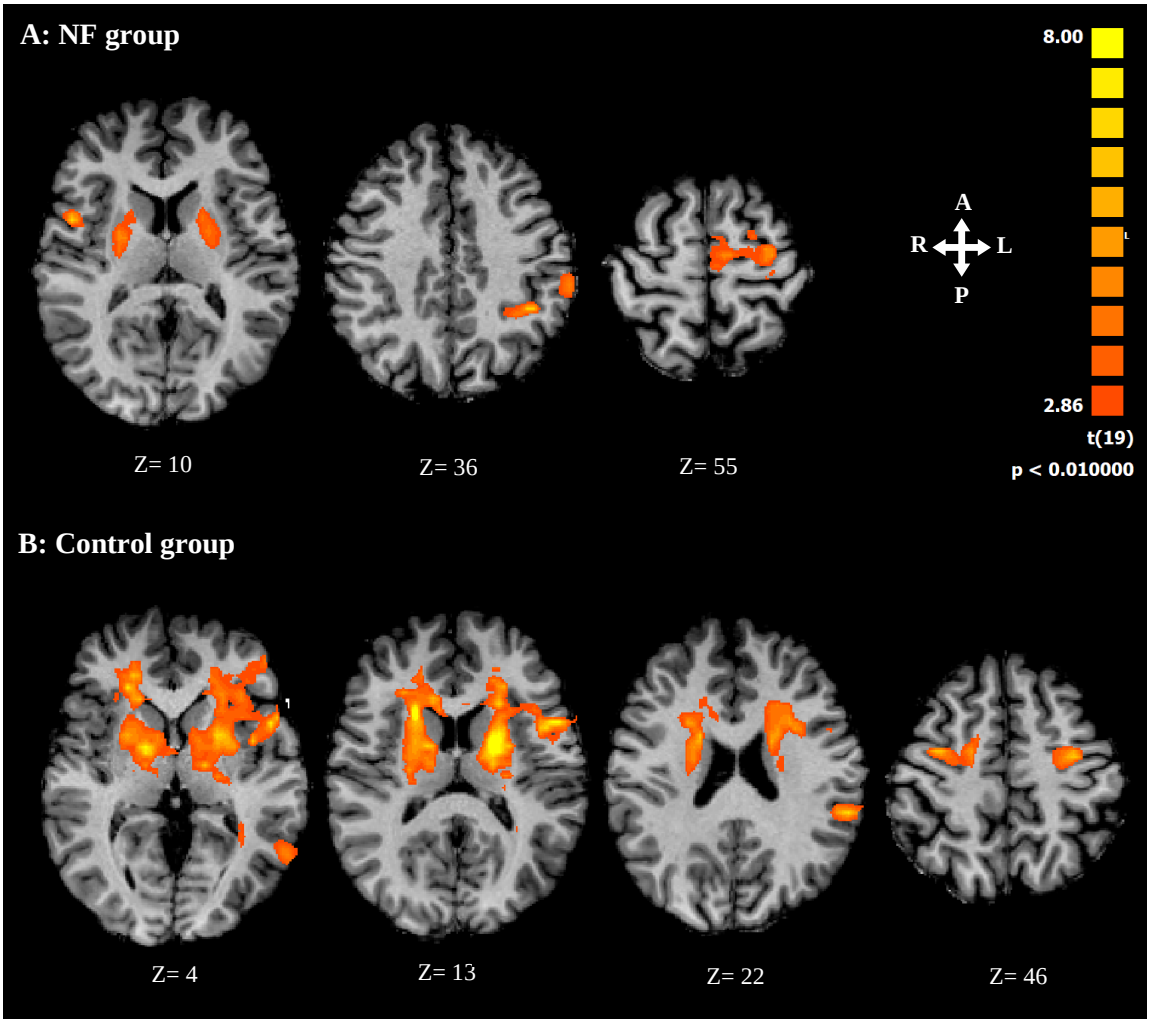

Figure 7.7. Results of the analysis of NF runs shown for the (A) NF group and (B) control group. These activations are significant at p<0.01 (cluster size> 981mm^3 and >1139 mm^3 respectively).

Table 7-3. Clusters of brain activation during the NF for NF and control groups. (Note: x,y,z are the Talairach coordinated, LH= Left hemisphere. RH= right hemisphere.)

Group	Cortical Area	x	y	z	*t*	*p*-value	Size
NF	LH, Lateral Globus Pallidus	-21	-7	4	5.2415	0.00053	1924
	LH, Inferior Parietal Lobule, BA 40	-60	-28	34	7.9406	0.00002	1258
	LH, Supramarginal Gyrus, BA 40	-42	-40	37	7.7510	0.00002	1263
	LH, Precentral Gyrus, BA 6	-30	-13	52	7.2034	0.00005	4863
	RH, Putamen	24	-1	7	5.8323	0.00024	1995
	RH, Precentral Gyrus, BA 44	48	5	10	7.1174	0.00005	1405
Control	LH, Middle Temporal Gyrus, BA 21	-57	-55	4	7.2142	0.00005	1504
	LH, Putamen	-18	-1	13	12.8867	0	24743
	LH, Inferior Parietal Lobule, BA 40	-57	-34	22	7.5089	0.00003	1756
	RH, Caudate Body	21	17	13	11.4746	0	15864
	RH, Middle Frontal Gyrus, BA 6	36	-4	46	6.7628	0.00008	1605

To assess whether SMA activation in the NF group was significantly different from activation in the control group. A two sample *t*-test was performed to contrast the RFX-GLM maps of both groups. The NF group showed higher activations in clusters located in the left motor and cingulate regions (BA6 and BA24 respectively) compared to the control group that showed higher activations in the left Claustrum, bilateral Middle/Superior Frontal Gyrus (BA8) and right Angular Gyrus as illustrated in Figure 7.8 and listed in Table 7.4.

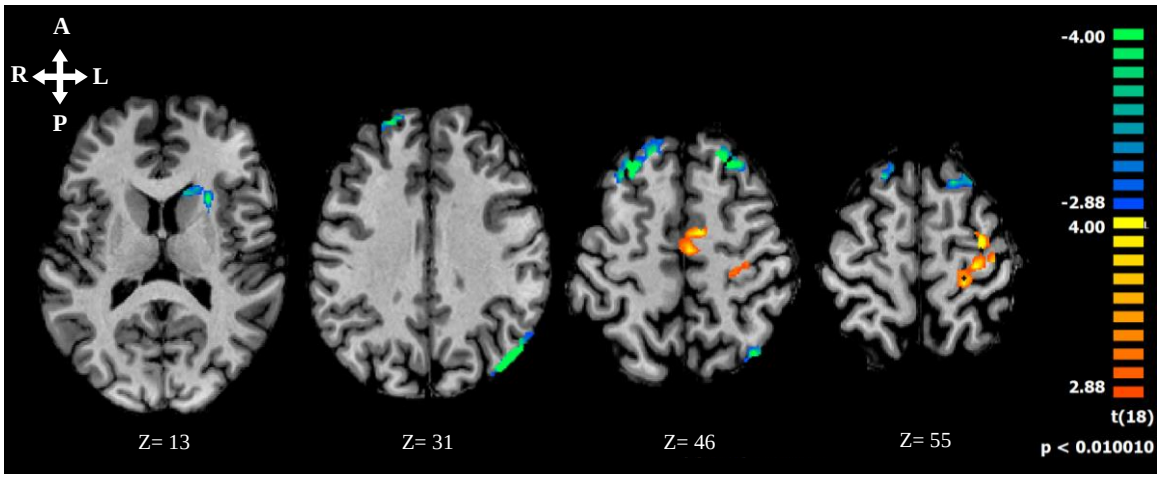

Figure 7.8. A contrast map between the RFX-GLM of NF and control groups. Red/yellow colour represents significant actions in the NF group while the blue/green colour indicates higher activation in the control group. The map was thresholded at $P<0.01$ (cluster size>432mm^3).

Table 7-4. Comparison of brain activations between NF and control groups. (Note: x,y,z are the Talairach coordinated, LH= Left hemisphere. RH= right hemisphere. BA= Brodmann area.)

Cortical Area	x	y	z	*t*	*p*-value	size
LH, Claustrum	-24	14	13	-4.9600	0.00010	1120
LH, Angular Gyrus, BA 39	-42	-70	31	-12.2802	0	1823
LH, Cingulate Gyrus, BA 24	-9	-4	46	4.2579	0.00047	875
LH, Superior Frontal Gyrus, BA 8	-24	32	47	-5.3152	0.00004	796
LH, Precentral Gyrus, BA 6	-33	-7	58	5.9098	0.00001	1994
RH, Middle Frontal Gyrus, BA 8	36	26	43	-6.1933	0.00000	2628

7.4.3.3 PPI analysis

To further explore how NF learning might be modulating activity throughout the brain a PPI analysis was conducted using the individually identified SMA regions as seed ROIs. PPI analysis showed a significant connectivity (p<0.03) between SMA and Cingulate cortex (BA24) and Caudate Head for the NF group. For the control group, the interaction was between SMA and bilateral Lingual Gyrus (BA18), left Declive and left Fusiform Gyrus (BA37). Group PPI comparison revealed a strong correlation between the SMA and left Thalamus and Putamen in the NF groups (yellow-red clusters), as well as between the SMA and bilateral Inferior/Middle Temporal Gyrus and left Precuneus (BA7) in the Control group (blue-green clusters) as shown in figure 7.9 and table 7.5.

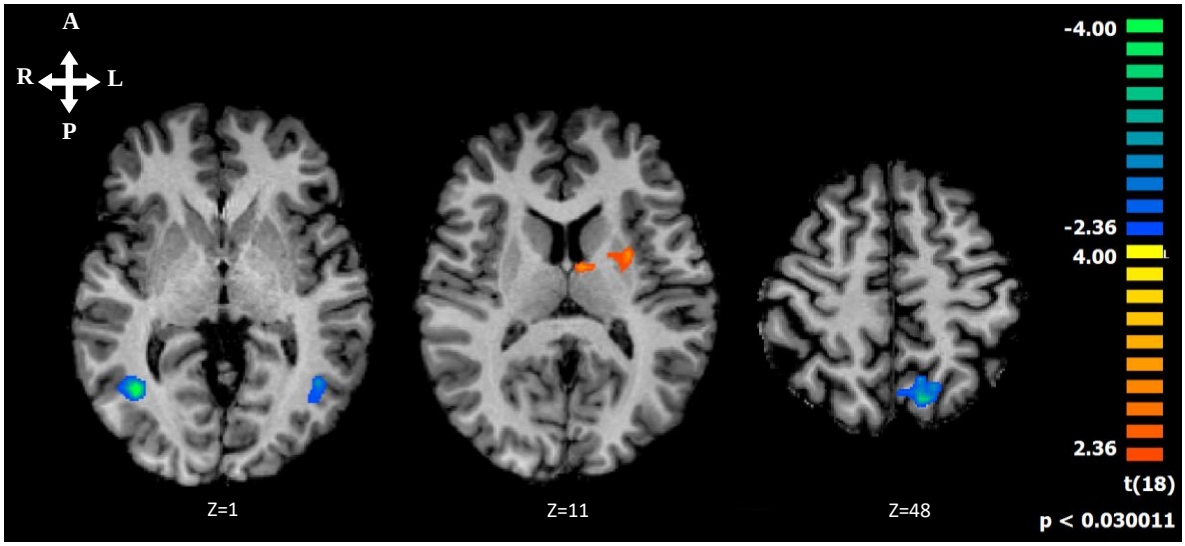

Figure 7.9. Significant differences using PPI contrast between NF and control groups at P<0.03 (cluster size>945mm^3).

Table 7-5. Comparison of PPI activations between NF and control groups. x,y,z are the Talairach coordinated, LH= Left hemisphere. RH= right hemisphere. BA= Brodmann area.

Cortical Area	x	y	z	*t*	*p*-value	size
LH, Middle Temporal Gyrus, BA 37	-42	-55	1	-4.8685	0.00012	1718
LH, Thalamus, Anterior Nucleus	-6	-4	10	3.7737	0.00139	1067
LH, Precuneus, BA 7	-15	-64	46	-3.9976	0.00084	1019
RH, Inferior Temporal Gyrus, BA 37	39	-61	-2	-5.3667	0.00004	3650

7.5 Discussion

In this study we demonstrated that healthy volunteers could learn, in a single session, to increase the activity in their functionally localised SMA regions, during a MI task of complex body actions whilst receiving a continuous feedback signal (displayed as a thermometer bar height). This feedback signal represented the activity of individually localized SMA regions in the NF group and a pre-recorded signal in the control group. The estimated beta weights, as well as the average BOLD signal (Figures 4 and 5, respectively), of the SMA increased with the number of runs, indicating a learning effect. These findings are similar to previous studies (Banca et al. 2015; Scharnowski et al. 2015; Blefari et al. 2015) which indicated that one single session of NF training is enough to accomplish training. The results also showed that successful modulation of SMA activity of the NF group led to improved motor performance in the motor reaction task (figure 7.3).

Participants in both groups had an equal capability to perform MI as measured by the VMIQ-2 questionnaire. Those in the NF group who received feedback information from their SMA regions could use the feedback signal to increase their ROI activation as shown in Figure 4. In contrast to the NF group, the control group received a pre-recorded feedback signal that did not match the changes in their brain activity, therefore preventing them from finding an effective strategy to control their brain activity and a subsequent decrease in SMA activity. The beta weights of the NF group did not consistently increase, which may reflect the search for an effective strategy and the gradual skills learning for self-regulation. Participants reported the use of different MI strategies during the NF training, including first-person perspective MI of punching or boxing. The debriefing of the participants after the NF experiment showed that most of them initially struggled to identify the best imagery strategy. Common documented strategies in NF studies of MI include clenching and pitching (Blefari et al. 2015; Chiew et al. 2012; Yoo et al. 2008). Relating this to ME studies of sequential finger movements (Neyedli

et al. 2017; Berman et al. 2012) indicate that both these types of motor activity have been shown to activate common cortical regions such as SMA, bilateral PMA, M1, posterior parietal lobe (PPL) and the cerebellum (Hanakawa *et al.*, 2008; Hétu *et al.*, 2013; Sharma and Baron, 2013). The shared neural substrate between MI and ME support the feasibility of NF training using MI to enhance motor performance.

The Go/No-go task showed a decrease in reaction time of both groups (figure 7.3). Importantly the reaction time of the NF group was significantly lower after the NF training. This finding further supports that the MI training guided by true NF is more effective in improving motor performance than any effect of sham feedback. This task involved planning and initiation of movements during the Go task and inhibition of inappropriate actions during No-go. All of these mechanisms are mediated by the SMA (Nachev et al. 2008). The SMA has direct connections to the corticospinal tract, precentral gyrus (M1), and ventrolateral thalamus (Arai et al. 2012; Nachev et al. 2008; Johansen-Berg et al. 2004) and it has been shown that modulating SMA activity can increase the cortical excitability of M1 (Arai et al. 2012; Shirota et al. 2012) thus increasing the SMA activity will lead to reduced motor reaction times.

The whole-brain analysis revealed widespread brain activation in the NF group other than the targeted area (SMA). These activations included for the NF group the left SMA, left PMA, left IPL and bilateral basal ganglia and for the control group, the bilateral PMA, left IPL and bilateral basal ganglia. The SMA is involved in motor planning and control (Grefkes *et al.*, 2008; Nachev *et al.*, 2008). Indeed, the NF group showed an increase in the left SMA activation, consistent with previous findings of left hemisphere dominance in practice-related activation increase regardless of the trained hand (Halsband & Lange, 2006). The PMA plays an important role in planning and preparation of movements (Hoshi *et al.*, 2007; Hétu *et al.*, 2013). Our results of activation in the left PM highlight the dominant role of this area in movement selection (Bestmann *et al.*, 2008) while the right PM activation are consistent with

spatial processing during the early stage of motor learning (Halsband and Lange, 2006). The IPL activation could be related to the integration of visuomotor information (Halsband and Lange, 2006), or the internal recruitment of stored motor representations (Cooke *et al.*, 2003). Particularly, the left IPL is suggested to be involved in the storing/retrieval of motor plans (Van Elk, 2014) and visually guided motor tasks (Torres *et al.*, 2010). Further, the basal ganglia is involved in motor processes and cognitive functions, such as learning based on the assessment of outcomes (Arsalidou *et al.*, 2013). Interestingly, the putamen is thought to be essential in the learning of novel complex motor actions and less important in well trained movements (Ceballos-Baumann, 2003), hence the pattern of basal ganglia activation observed in the NF group supports the neural efficiency hypothesis (Dayan and Cohen, 2011), which suggests that a task can be carried out using fewer neural substrates, as fast learning proceeds (Poldrack, 2000). Importantly, in contrast to the NF group, the control group showed widespread activation in the basal ganglia due presumably to subjects attempting to discover the best MI task using trial-and-error strategies. This pattern of activation highlighted the engagement of basal ganglia with executive functions (e.g. planning), that activate the head and body the of right caudate along with working-memory processes (e.g. maintain and manipulate information) that activate the bilateral putamen, and reward processes that activate anterior parts of bilateral caudate head (Arsalidou *et al.*, 2013). Comparison of brain activation between the NF and the control groups revealed significantly higher activations in the left SMA, left PMA and left cingulate gyrus of the NF group, further supporting our hypothesis that the NF group would be able to increase the activation of SMA during NF training.

The PPI comparison showed an increase in functional coupling during the NF training between the SMA and other brain regions. Our results demonstrated an enhancement in functional connectivity between the SMA and the thalamus and putamen in the NF group. These two regions play an important role in relaying and selecting motor output (Arsalidou *et*

al. 2013; Sommer, 2003) which supports motor skill learning (Dayan and Cohen, 2011). On the contrary, the control group showed a positive correlation between the SMA and left Precuneus during the NF training, which might be explained by a high demand on spatial information input from the Precuneus to the motor region. Finally, the positive coupling between the SMA and bilateral fusiform gyrus in the control group might be associated with forming a visual memory of the motor procedure, particularly with the upper limbs of the body (Olsson *et al.*, 2008).

In-line with the previous studies of fMRI NF (Bray *et al.*, 2007b; Chiew *et al.*, 2012; Sitaram *et al.*, 2012; Zhao *et al.*, 2013; Scharnowski *et al.*, 2015), we demonstrated that the use of a MI task during real-time fMRI NF is effective in up-regulating activity in the motor related regions and can improve motor performance. Our study presents the first controlled study that highlights the feasibility of increasing SMA activation during one session. Clinically, learning control over the SMA could be used to treat Tourette's syndrome where SMA activity is linked to motor tics (Hampson *et al*. 2011; Bohlhalter *et al*. 2006) and Parkinson's Disease where the SMA activity is reduced by perfoming motor tasks (Munzert *et al.*, 2009; Subramanian *et al.*, 2016)

Chapter 8 : General Discussion

8.1 General summary

The experimental studies in this thesis have examined the decoding of the motor representations of different multi-joint arm actions during either pure motor imagery or motor imagery guided by active observation of the same action. The thesis also presents a functional algorithm that aligns neural representation spaces across participants. Further to this, it investigated the development of a neurofeedback system, implemented with fMRI, targeting brain activations in different brain regions for the purposes of altering perception.

In this general discussion, I will review the key findings and the implications of the experimental chapters, and relate them to the aims of this thesis. The experimental studies can be considered in the context of the decoding and aligning of motor representational spaces (Chapters 4 and 5) and the use of fMRI neurofeedback training to modulate pain perception (Chapter 6) and enhance motor reaction time (Chapter 7).

8.1.1 Common model of motor representation

I started with the aim of finding a functional alignment that can align local representational spaces in the motor domain across participants into common model representational space. Hyperalignment, a novel method of functional alignment, has been shown to successfully align the representational spaces across participants in the ventral temporal cortex (Haxby *et al.*, 2011). Extending hyperalignment to other cortical regions requires predefined ROIs that are functionally equivalent across participants, and the extent of

the spatial distribution of each dimension in the common representational space is only limited by the size of the ROI. Successful hyperalignment that aligns the cortical systems requires a rich sampling of neural responses across the entire cortex. It involves activating as many sensory, perceptual, cognitive, and social systems as possible. In chapter 4, I collected cortical responses to a set of blended movements that densely sampled a particular movement space while participants performed a visuomotor task (AO+MI). From these responses, I derived transformation parameters for the hyperalignment. I validated the hyperalignment derived from the blended actions to map an independent motor imagery study by aligning the representational spaces of the motor cortex into a common model representational space. I explored whether the order in which participants were entered into the hyperalignment procedure mattered in generating a common model space that produces the most discriminative subject-independent classifier. Our results showed that the hyperalignment algorithm is potentially sensitive to subject order, due to the inter-subject response variability and different weights of subjects' contributions toward computing the intermediate common model (figure 4.3). I also performed between-subject classification (BSC) based on hyperalignment and anatomical alignment, as well as within-subject classification analyses to decode action types (lift vs knock vs throw). Between-subject classification after hyperalignment performed better than between-subject classification based on anatomical alignment (figure 4.6). These results demonstrated the general validity of the hyperalignment transformations derived from the blended actions data. Furthermore, the results suggest that a classifier trained on a set of subjects can predict categorical information in a new subject, at least as well as a classifier that was trained on that test subject's own data. I then derived the hyperalignment parameters from the motor imagery study. Our results revealed that both hyperalignment models afford comparable levels of classification performance. These findings demonstrate the feasibility of deriving hyperalignment parameters using different data resources. Finally, I explored the cost

in classification accuracy when a to-be-classified participant's data were excluded from the dataset used for deriving hyperalignment parameters. The BSC performance based on hyperalignment decreased, but it was still better than BSC based on anatomical alignment (figure 4.8). This would be relevant if hyperalignment based on one set of participants was used to perform classification on data from a new subject, and could be used in applications like real-time decoded neurofeedback.

8.1.2 Multivariate pattern analysis of MI vs AO+MI

The main aims of Chapter 5 were to extend hyperalignment to map the representational spaces in the motor and motor related regions across participants, and also to demonstrate the similarity of neural code between MI and AO+MI of different hand actions. I re-analysed the data of the first experiment to examine whether multi-joint arm actions during different modalities (MI and AO+MI) elicited unique fine-grained activation patterns, and if they could be decoded from the fronto-parietal motor regions. Our results showed that the type of actions could be decoded significantly accurately during MI and AO+MI tasks, with a highest classification performance in M1 and SPL of both hemispheres. These results replicate previous research showing that patterns of activity within motor and motor related regions can differentiate between different types of actions (Pilgramm *et al.*, 2016; Zabicki *et al.*, 2016) and between action modalities (Filimon *et al.*, 2015). This also demonstrates that the frontal and parietal regions represent the content and modality of actions. I then applied hyperalignment to better localise the distributed motor network and enhance the classification accuracy. I validated the hyperalignment derived from the AO+MI task of blended actions to map the independent MI and AO+MI data of multi-joint arm actions. Hyperalignment was successful in building common representational spaces of the frontal-parietal motor regions that increased the power of MVPA to detect fine-grained information across participants (figures 5.6 and 5.9). I also examined the consistency of the neural code between AO+MI and

MI by attempting cross-modality classification. Our findings suggested a common neural code, with AO+MI and MI induced neural patterns for specific hand actions in broad areas of the human motor system (figure AOMI_MI 10). Furthermore, I explored the similarity in structure of neural responses elicited by AO+MI and MI of different arm actions. A representational similarity analysis (RSA) was used to estimate the correlation distance between the neural responses of AO+MI and MI of lifting, knocking and throwing actions to form a representational dissimilarity matrix (RDM). I compared the RDMs of the fronto-parietal motor regions to models predicting how the brain regions encode the modality, the actions type or the mix dependency of both. I found that motor regions were correlated with each other and formed two distinct clusters in the frontal and parietal cortex (figure 5.12), emphasising the role of premotor and motor regions in simulating and selecting the action parameters, and the posterior parietal cortex in processing action related information. In addition, I tested different model predictions and found that mixed models explained the neural geometry in most fronto-parietal regions, indicating that the action representations had both common and distinct components across modalities (figure 5. 13).

8.1.3 Neurofeedback

During neurofeedback, the BOLD signal is processed and displayed in real-time to the participant in order to enable self-regulation of brain activity. Research using fMRI neurofeedback has shown that it is possible to self-regulate the activity in brain regions or networks, and that this regulation can impact behavioural variables. Most of the early research has focused on healthy subjects, in order to understand the neural substrates and possibilities of neurofeedback. The aim of these studies was to demonstrate the general feasibility and to show a significant regulation effect. In recent years, the focus has shifted towards clinical applications.

In the second part of this thesis, an fMRI neurofeedback system was established to examine the modulation of brain activity in healthy and clinical populations, and also to test if fMRI neurofeedback training altered the functions of the targeted brain regions as a consequence.

In chapter 6, I examined the feasibility of training phantom limb pain patients to modulate their brain activity by the means of fMRI neurofeedback. I compared two neurofeedback paradigms, one based on down-regulation of the rACC and the other based on down-regulation of the premotor region (PM). The behavioural changes revealed a slight decrease in the phantom pain intensity due to the neurofeedback self-regulation. However, comparing the last to the first fMRI neurofeedback run, patients down-regulated their PM and rACC activity in one session whilst they showed an increase in these targeted regions' activities during the sham feedback (signal derived from the auditory cortex) (figure 6.3). During the neurofeedback training, patients gained control over the feedback signal derived from either PM or rACC by building an effective strategy, which led to decrease in the targeted ROIs activity. On the other hand, they lost their ability to modulate their brain activity during the sham feedback derived from the auditory cortex. These findings are in line with previous neurofeedback studies, which show similar effects of down-regulation (DeCharms et al. 2005; Emmert et al. 2014).

Chapter 7 demonstrated that healthy participants can use fMRI neurofeedback to module the activity of the SMA, which is involved in motor learning, planning and execution, during MI tasks involving complex body actions. Participants in the neurofeedback group received a continuous feedback signal as a fluctuating thermometer bar representing the percentage change of SMA activity, while the sham group received a pre-recorded feedback signal. The estimated beta weights showed a progressive increase of SMA activity in the neurofeedback group compared to the control group (figure 7.4 and 7.5). These findings are in

line with previous studies indicating that participants can learn to self-regulate their brain activity (Banca et al. 2015; Scharnowski et al. 2015; Blefari et al. 2015). The successful modulation of SMA activity in the neurofeedback group improved the motor performance by significantly reducing motor reaction time. This finding supports the idea that the MI training guided by true feedback is more effective in improving motor performance than any effect of sham feedback. The whole brain GLM analysis of the neurofeedback group revealed widespread cortical activation in the motor and motor related regions (including the SMA, PM, IPL and basal ganglia) that play an important role in planning, selecting, learning and preparation of movements. In contrast, the control group showed consistent activation in the basal ganglia, likely due to participants attempting to discover the best MI task using operant conditioning. With regards to understanding the mechanism underlying neurofeedback training, I ran a functional connectivity analysis focusing on the targeted region (SMA), which provided an opportunity to investigate the direction of information flow. The results indicated an enhancement in functional connectivity between the SMA and the thalamus and putamen (regions responsible for motor skill learning) in the neurofeedback group, while the control group showed a positive coupling between the SMA and precuneus and fusiform gyrus, which might be associated with a high demand on spatial and visual memory processing.

8.2 Implications

8.2.1 Shared neural representation

Previous fMRI studies have shown that action types and modalities can be decoded from the evoked neural responses (Filimon *et al.*, 2015; Pilgramm *et al.*, 2016; Zabicki *et al.*, 2016) by tailoring a new classifier for each subject. Using hyperalignment, I showed that the fine-scale neural representations of motor regions were also shared across subjects. After hyperalignment, I could successfully perform between-subject classification more accurately than anatomical alignment from the fronto-parietal motor regions. This suggests not only that

the neural representations of motor components are shared across subjects, but also that hyperalignment aligns by rotating these representations across subjects.

8.2.2 Representational Similarity Analysis

RSA addresses the problem of comparing neural representations of stimuli in different subjects (or systems) without aligning the underlying features. It achieves this by comparing the geometry of the representational spaces across subjects (Kriegeskorte *et al.*, 2008b). A key difference between RSA and our approach is that one can only compare neural representations of stimulus sets that were presented to all the subjects using RSA. Using hyperalignment, once the subjects are hyperaligned using a common stimuli set (the blended actions), I can compare neural representations of different stimuli presented to different sets of subjects across different studies in the common model space. There is a time cost to running the common stimuli set to derive the hyperalignment parameters, but that opens up the possibility of comparing the neural representations of any new stimulus set we can think of in the future, in a new set of subjects. If movie presentation is not feasible due to time constraints, one can still perform hyperalignment within the experiment.

8.2.3 Localisation of information

Our earlier version of the hyperalignment algorithm (chapter 4) constrained information localisation within the shared ROI (left hemisphere motor cortex). Despite the individual variability in neural responses, information at a cortical location (a voxel) in the template subject's ROI is a weighted sum of all voxels within that ROI of another subject. I used a cortex based alignment (chapter 5) to parcellate the ROIs, thereby implicitly constraining the information at a cortical location in the template brain, taking into the account the anatomical variability across subjects. I then applied Searchlight to localise and to select the informative voxels within the predefined ROIs to eliminate the contribution of noisy voxels.

8.2.4 Procrustean transformation

Previous functional alignment methods have used function-based activation along with the anatomical features to align brains across subjects (Sabuncu *et al.*, 2010; Conroy *et al.*, 2013). Most of these methods estimate an optimal warping in either 3 or 2 dimensional space that aligns functional topographies across subjects with minimal anatomical distortion. However, they were also shown to be inappropriate in terms of the accuracy of between-subject classification of face & object categories in VT (Conroy *et al.*, 2013). Hyperalignment uses Procrustean transformation (Schönemann, 1966) to align voxels across subjects in a high-dimensional space defined by these voxels in a ROI. It does not take into account topological information or the location of these voxels within a ROI. Each dimension in the common model space is a weighted sum of voxels within a cortical volume. Procrustean alignment is a linear regression with an orthogonality constraint on the transformation matrix. Information measured in an fMRI voxel is an aggregate of neural signals measured through BOLD across space and time (Kriegeskorte *et al.*, 2009). In addition, there is no evidence that 3 mm^3 voxels are the basic units of neural computation. Therefore, by aligning a weighted sum of voxels in a neighbourhood across subjects, I attempt to align the underlying distributed functional neural signatures that are shared across subjects. The orthogonality constraint for the transformation matrix separates the Procrustean alignment from a general linear regression. The orthogonality of the transformations restricts the transformation to a rigid rotation in space, so that preserves the similarity structure (representation geometry) of the data, which has been shown to be shared across subjects and species, and has been argued to be an important aspect of cognition and cortical representation (Kriegeskorte *et al.*, 2008b).

8.2.5 Functional brain atlas

Correspondence across subjects is critical for generalising any neuroimaging finding from study sample to population. Historically, anatomical features have provided such

correspondence and served well for univariate analyses. A standard group analysis pipeline using GLM is dependent on such correspondence (Beckmann *et al.*, 2003). Brain atlases created using Talairach and MNI templates have been of great help in comparing and aggregating results from various studies, and in providing valuable insights through the meta-analyses which is made possible by such atlases (Yarkoni *et al.*, 2011). Multivariate pattern analyses, which treat each voxel's signal as an independent measure, have been successful in extracting information that univariate analyses failed to do (Haxby *et al.*, 2001; Cox and Savoy, 2003; Haynes and Rees, 2005; Kay *et al.*, 2008; Miyawaki *et al.*, 2008), but they lose correspondence of information patterns across subjects. Therefore, I cannot easily compare two studies using MVPA beyond the coarse spatial scale of ROIs. The hyperalignment algorithm addresses this issue by providing a method to functionally align subjects into a common model that preserves fine-grained information in local representational spaces. Information patterns from two different studies can be aggregated and compared in this common space, opening the possibility of building a functional atlas of brain activation patterns from a multitude of neuroimaging studies. Each activation pattern becomes a vector in this high dimensional space of features. Since these features are common across subjects and experiments, I can perform group analyses and metal-analyses comparing activation patterns from different studies. By inverting the mapping from a subject's voxel space to a common model space, I can map any vector in this functional atlas back onto that subject's brain as voxel activations.

8.2.6 Individual differences

I have evaluated the common model spaces derived using hyperalignment in the context of decoding of information representation across subjects. But there is meaningful variability of anatomy and function across individuals and groups (Mueller *et al.*, 2013). In our experimental design, the motor cortex provides more subject neural response variability for the representation of actions than the representation of objects in the VT cortex (Haxby *et al.*,

2011). Therefore, the representation of different movements amongst a space of actions might be more sensitive to perturbation than the representation of different visual objects.

8.2.7 What is different in patients compared to healthy volunteers?

It is important to take into account the different characteristics of patient groups in comparison to young, healthy participants. It is known that many cognitive abilities including working and long-term memory, as well as processing speed, decline starting from the 20s (Park *et al.*, 2002; Park and Reuter-Lorenz, 2009). Therefore, it might be useful to test the neurofeedback paradigm in older healthy adults as a first step toward clinical applications. Furthermore, the disease may impose certain specific restrictions on patients. For example, chronic pain patients or tinnitus patients with hyperacusis may not tolerate the MRI environment as well as healthy participants. Similarly, phantom limb pain patients might require special experimental arrangements due to having mobility problems. Moreover, it should be taken into consideration that while patient groups are a very specific population subgroup, they may be a better representation of the general public in terms of ethnical and educational diversity than typically healthy participants who are often recruited in a research/academic environment and therefore show a bias towards participants with higher education. In this sense, patient studies may give a more realistic estimate of the effect of neurofeedback within the general population.

8.2.8 With or without strategy?

It is still unclear whether it is better to provide subjects with an initial strategy or not. However, if subjects are to be informed about an initial strategy and about the purpose of the experiment, it would most likely be advantageous to inform them as comprehensively as possible, including a clear definition of the aims and objectives of the neurofeedback training (Lotte *et al.*, 2013). In addition, a pre-training session that allows the subject to gain some experience with either the feedback system or train in possible mental strategies outside the

scanner may be beneficial, along with a practical demonstration of the setup (Lotte *et al.*, 2013). However, if a strategy is provided to the subjects, it is also unclear which strategy is best. It will certainly depend on the regulated region, but even with the same regulation tasks the best strategy may vary between subjects (Nan *et al.*, 2012).

8.2.9 Is it possible to modulate target regions that are included in the neurofeedback network?

Many fMRI neurofeedback studies used target regions that include the networks involved in self-regulation. Emmert *et al.*, (2016) reported that the anterior insula and the anterior cingulate cortex are consistently activated during self-regulation in fMRI neurofeedback, independently of the targeted regions. This raises the question of whether these areas are really up-regulated by neurofeedback training, or merely activated by the cognitive effort of trying to regulate. However, just because similar regions are active, this does not mean that the underlying neural processing is exactly the same. Recent studies that have looked at activation patterns that are shared, and those that distinguish between physical and emotional pain, have found some response patterns that were unique for physical pain within the right anterior insula (Corradi-Dell 'Acqua *et al.*, 2016). Similarly, successful self-regulation of the insula or anterior cingulate may show a different activation pattern than attempted self-regulation (e.g. with sham feedback). Future studies should therefore look at the specific effect of self-regulation, controlling for cognitive processes during neurofeedback training. In this context, it is important to look at studies that also attempt down-regulation of targeted regions as they might need to counteract the activation of the neurofeedback network. Down-regulation of the anterior cingulate has previously been attempted in a pain study with healthy subjects and chronic pain patients (DeCharms *et al.*, 2005). It seems that they did succeed in down-regulation, however the data only show the difference between up-regulation and down-regulation conditions, which might have increased due to better up-regulation. Other pain

regulation studies later confirmed that down-regulation of the rostral anterior cingulate cortex is possible (Emmert *et al.*, 2014; Rance *et al.*, 2014).

8.2.10 Shaping neural representations using neurofeedback

An emerging implication of my work (chapter 7) as well as of others is that fMRI neurofeedback training, using mental imagery related to the specific functional processing of brain regions, may enable the shaping of neural representations without the conscious awareness of participants (Bray *et al.*, 2007a). This neurofeedback-driven instrumental conditioning could be applied in the sensorimotor cortex, or in perceptual regions. Neurofeedback training employs mental imagery as a surrogate for engaging neural processes that enable a broader repertoire of responses within the targeted regions, which may have multiple or similar overlapping neural representations (Winawer *et al.*, 2010). Chapter 7 has demonstrated the use of motor imagery to enhance motor execution, as they both share the same motor cortical regions.

An exploratory opportunity afforded by neurofeedback-guided shaping of neural representations would be to prepare specific regions of cortex prior to fitting a neural prosthesis, which could be physical, cognitive or psychological. On the basis of this, if motor cortex activity could be manipulated so specifically, it may then be possible to train activity in a precise region of the motor cortex prior to fitting a prosthesis. For example, fMRI neurofeedback training of the activation in the hand area motor region (knob region along the precentral sulcus (Yousry *et al.*, 1997)) (Berman *et al.*, 2012; Neyedli *et al.*, 2017) could be performed prior to fitting a prosthetic hand. This would preferentially and pre-emptively engage necessary neural processes, which could then be further selectively trained and pruned through prosthetic hand use, and neurofeedback. An analogous sensory prosthesis can also be imagined, such as training activation in auditory brain regions prior to fitting a hearing aid.

8.3 Limitations

Successful functional alignment requires rich sampling of neural responses across the entire cortex. It involves activating as many sensory, perceptual, cognitive, and social systems as possible. Engaging these systems in isolation is a daunting task that involves an indefinite amount of stimulation and scanning. However, our everyday experience engages most of these systems simultaneously. Haxby et al. (2011) used movie viewing to mimic this experience and it has been shown to engage most of these systems reliably and across most of the cortex. Therefore, the common model space derived from the movie data generalised over the category perception experiments, and they found that the classification performance of the BSC obtained via hyperalignment of VT cortex was equivalent to that of WSC and higher than BSC based on anatomical alignment, thus confirming the validity of the common model space across a range of stimuli and experiments. In our study, I used blends of three natural actions (lift, knock and throw) to sample the neural responses of the motor cortex during AO+MI tasks. The AO+MI condition has been proven to evoke a stronger neural activation in the motor regions than MI or AO in isolation. The common model space derived from the blended action data might be limited only to the upper limbs (as the blended actions movie only showed multi-joint arm actions) and cannot be generalised to different motor studies due to the limited number of actions.

The fMRI neurofeedback experiment of phantom limb pain (PLP) provides the first study on PLP patients. However, this study is hampered by a low number of phantom limb pain patients, due to difficulties in recruitment, including their mobility limitation and its effect on entering the fMRI scanner and staying still during data collection. This problem affects the significance of the results. It is also not recommended to recruit a separate control group which received sham feedback; it is better to use the same experimental group as a control, but this might then bias the modulation due to the transfer effect.

8.4 Suggestion for Future works

- Repeating the experiment in chapter 4 using a large number of daily actions to obtain a rich sample of neural responses using the AO+MI condition. These neural responses can be used to derive a common model space of the motor regions, and can facilitate between-subject classifications. This common model space could be generalised over different studies and stimuli.
- Combining hyperalignment and neurofeedback in a novel type of decoded neurofeedback that enables individuals to modify the spatial neural pattern in a specific brain region to mimic the desired brain states of others. In this scenario, the feedback signal provided to the participants would show how much the currently evoked activity pattern is similar to the desired pattern, by using a subject independent classifier. This classifier enables individuals to match their neural activation pattern to a predefined pattern collected based on the activity of other participants and aligned to a common model space using hyperalignment.
- Adding a second control group to the experiment in chapter 7. The task of this control group will be to imagine doing complex actions without receiving any feedback (neither true nor sham). This experimental condition will help to investigate the effect of motor imagery without feedback on enhancing motor functions. Furthermore it will shed the light on effectiveness of fMRI neurofeedback on speeding up the motor learning processes.

Appendix A

A.1 Individual beta weights

The estimated beta values of each patient during real feedback from the motor area in session one (blue graph), real feedback from the ACC in session two (orange graph) and sham feedback (light blue and light orange).

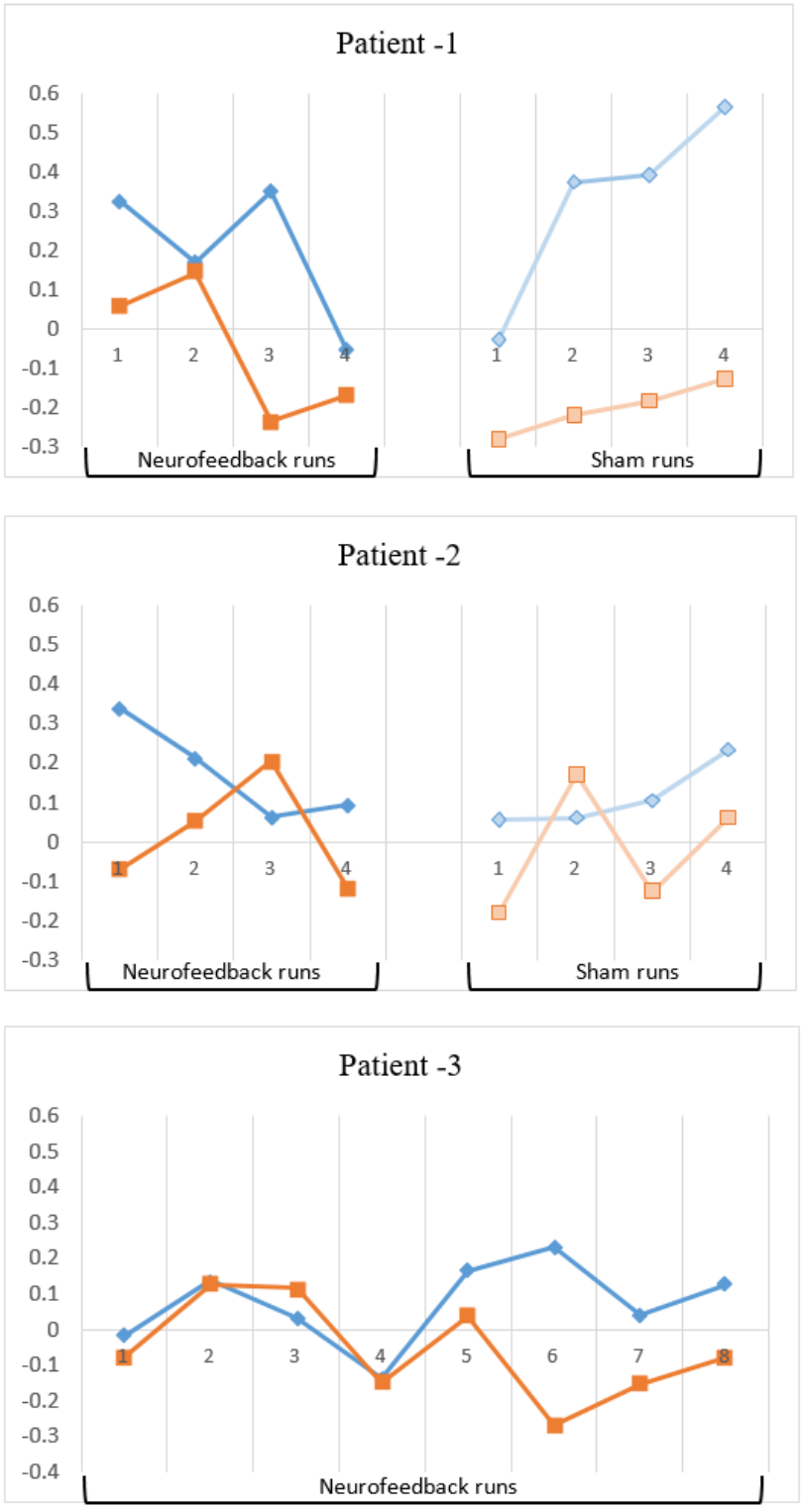

Figure A.1. Patients estimated beta weights of PM and ACC regions during the real and sham feedback. The blue line represents session one targeted PM-ROI and orange line represent session two targeted ACC-ROI. The light colour lines indicate the sham feedback during the corresponding session.

A.2 GLM analysis of each patient during the fMRI neurofeedback.

1- Patient-1:

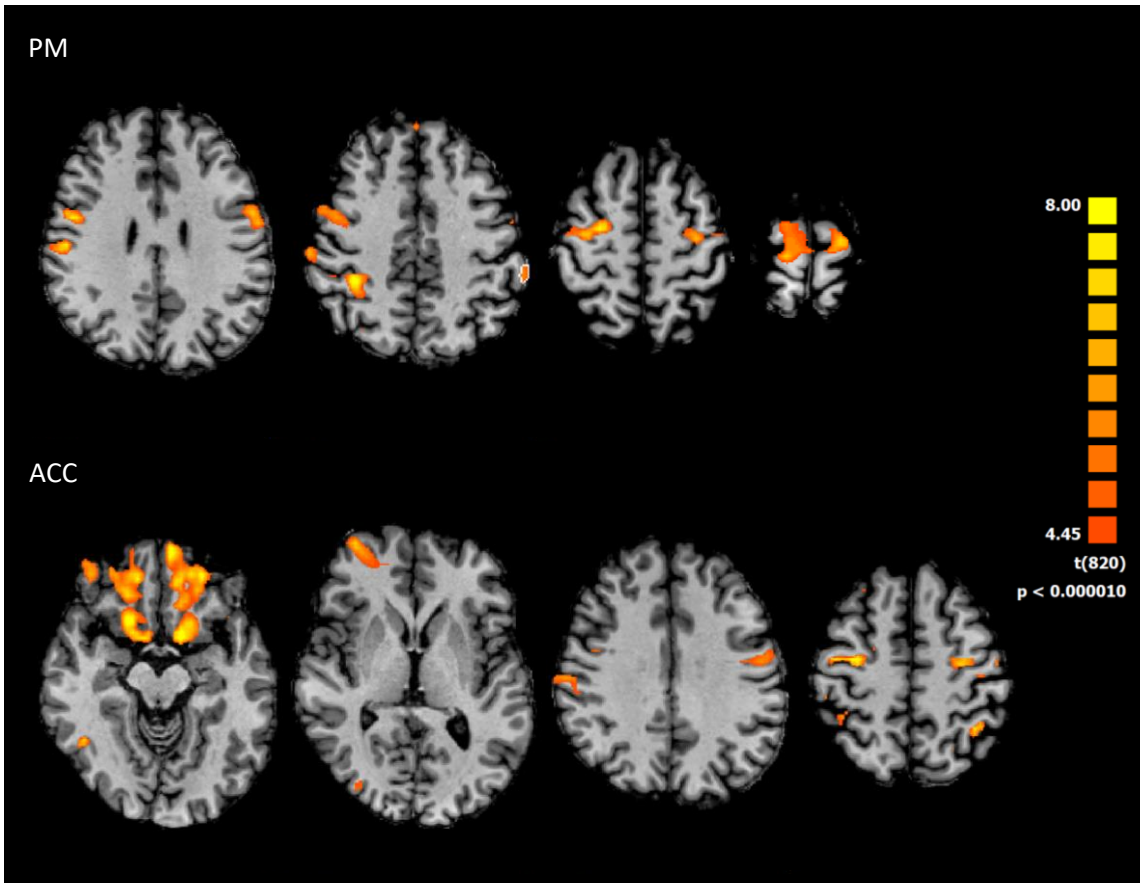

Figure A.2. The FFX-GLM map of the first patient of PM and ACC sessions.

2- Patient-2:

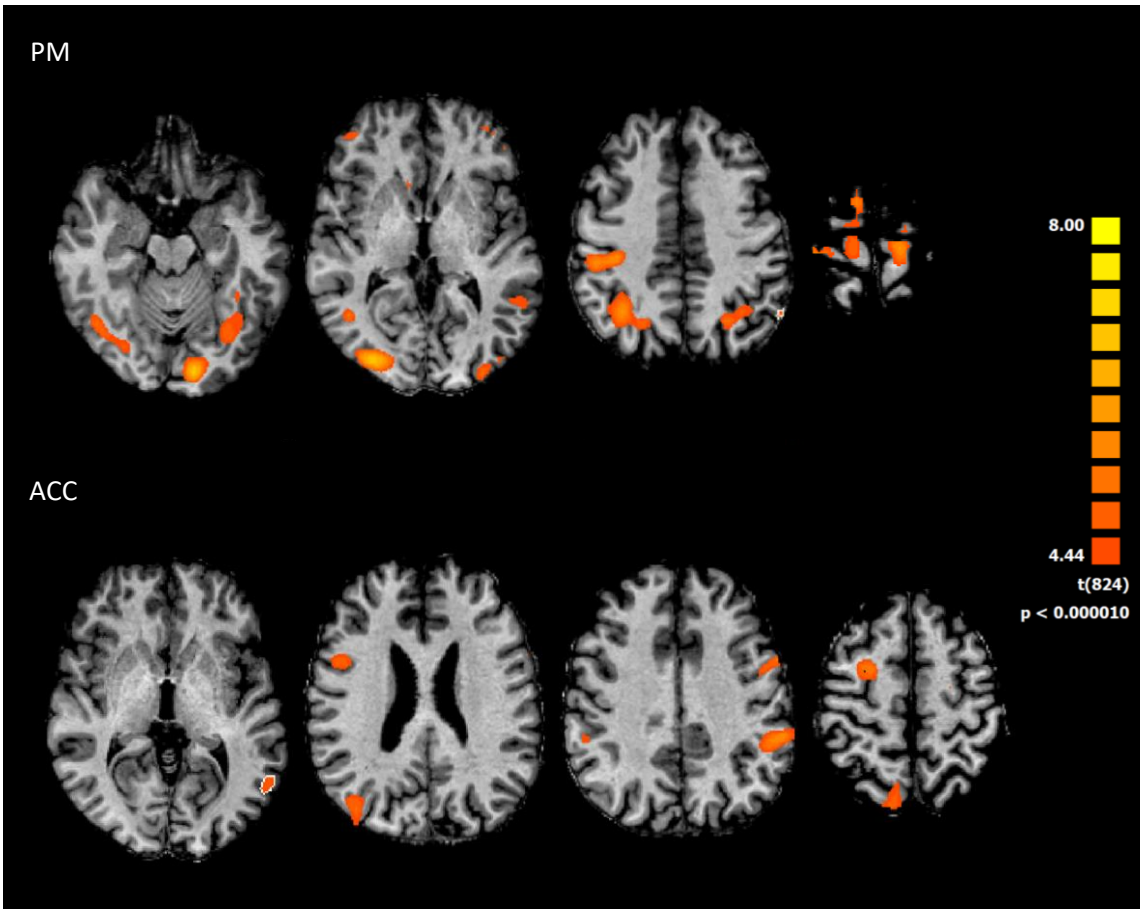

Figure A.3. The FFX-GLM map of the second patient of PM and ACC sessions

3- Patient-3:

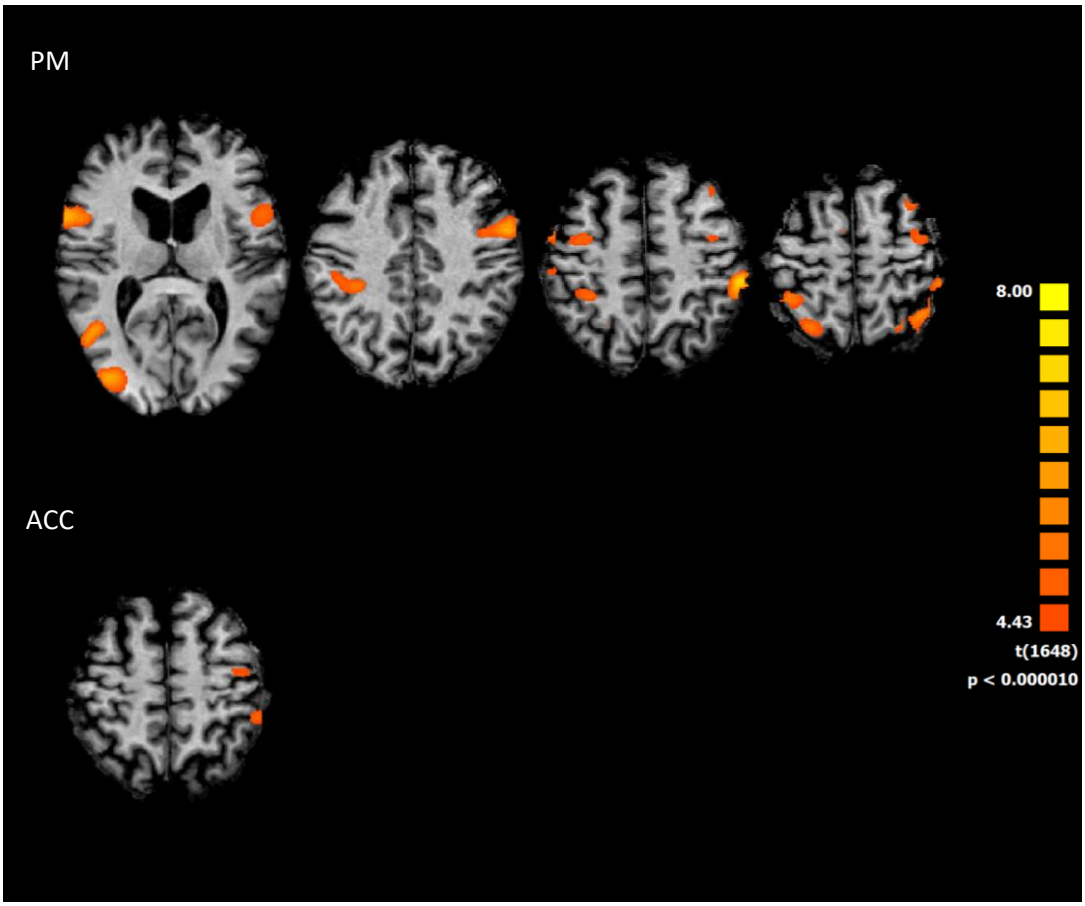

Figure A.4. The FFX-GLM map of the third patient of PM and ACC sessions

References

Aflalo, T., Kellis, S., Klaes, C., Lee, B., Shi, Y., Pejsa, K., Shanfield, K., Hayes-Jackson, S., Aisen, M., Heck, C., Liu, C. and Andersen, R. A. (2015) 'Decoding motor imagery from the posterior parietal cortex of a tetraplegic human', *Science*, 348, pp. 906–910.

Allman, J. M., Hakeem, A., Erwin, J. M., Nimchinsky, E. and Hof, P. (2001) 'The anterior cingulate cortex. The evolution of an interface between emotion and cognition', *Annals of the New York Academy of Sciences*, 935, pp. 107–117.

Aron, A. R., Robbins, T. W. and Poldrack, R. A. (2014) 'Inhibition and the right inferior frontal cortex: one decade on', *Trends in Cognitive Sciences*, 18, pp. 177–185.

Arsalidou, M., Duerden, E. G. and Taylor, M. J. (2013) 'The centre of the brain: Topographical model of motor, cognitive, affective, and somatosensory functions of the basal ganglia', *Human Brain Mapping*, 34(11), pp. 3031–3054.

Arzy, S., Thut, G., Mohr, C., Michel, C. M. and Blanke, O. (2006) 'Neural Basis of Embodiment: Distinct Contributions of Temporoparietal Junction and Extrastriate Body Area', *The Journal of Neuroscience*, 26, pp. 8074–8081.

Ashby, F. G. (2011) *Statistical Analysis of FMRI Data*. Cambridge, Mass, MIT Press.

Auer, T., Dewiputri, I., Frahm, J. and Schweizer, R. (2016) 'Higher-order brain areas associated with real-time functional MRI neurofeedback training of the somato-motor cortex', *Neuroscience*, pp. 1–12.

Auer, T., Schweizer, R. and Frahm, J. (2015a) 'Training efficiency and transfer success in an extended real-time functional Mri neurofeedback training of the somatomotor cortex of healthy subjects', *Frontiers in Human Neuroscience*, 9, pp. 1–14.

Auer, T., Schweizer, R. and Frahm, J. (2015b) 'Training efficiency and transfer success in an extended real-time functional MRI neurofeedback training of the somatomotor cortex of healthy subjects', *Frontiers in Human Neuroscience*, 9, pp. 1–14.

Balleine, B. W. and O 'doherty, J. P. (2010) 'Human and Rodent Homologies in Action Control: Corticostriatal Determinants of Goal-Directed and Habitual Action', *Neuropsychopharmacology*, 35, pp. 48–69.

Banca, P., Sousa, T., Duarte, I. C. and Castelo-Branco, M. (2015) 'Visual motion imagery neurofeedback based on the hMT+/V5 complex: evidence for a feedback-specific neural circuit involving neocortical and cerebellar regions', *Journal of Neural Engineering*, 12, pp. 1–12.

Bear, M. F., Paradiso, M. A. and Paradiso, M. A. (2007) *Neuroscience. Exploring the Brain*. Third Edit. New York, N.Y.: Lippincott Williams & Wilkins.

Beckmann, C. F., Jenkinson, M. and Smith, S. M. (2003) 'General multilevel linear modeling for group analysis in fMRI', *neuroImage*, 20, pp. 1052–1063.

Berman, B. D., Horovitz, S. G., Venkataraman, G. and Hallett, M. (2012) 'Self-modulation of primary motor cortex activity with motor and motor imagery tasks using real-time fMRI-based neurofeedback', *NeuroImage*, 59, pp. 917–925.

Bestmann, S., Swayne, O., Blankenburg, F., Ruff, C. C., Haggard, P., Weiskopf, N., Josephs, O., Driver, J., Rothwell, J. C. and Ward, N. S. (2008) 'Dorsal Premotor Cortex Exerts State Dependent Causal Influences on Activity in Contralateral Primary Motor and Dorsal Premotor Cortex', *Cerebral Cortex*, 18, pp. 1281–1291.

Birbaumer, N. (2006) 'Breaking the silence: Brain-computer interfaces (BCI) for communication and motor control', *Psychophysiology*, 43(6), pp. 517–532.

Birbaumer, N., Ruiz, S. and Sitaram, R. (2013) 'Learned regulation of brain metabolism', *Trends in Cognitive Sciences*, 17, pp. 295–302.

Birn, R. M., Murphy, K., Handwerker, D. A. and Bandettini, P. A. (2009) 'fMRI in the presence of task-correlated breathing variations', *NeuroImage*, 47, pp. 1092–1104.

Blakemore, S. J. and Decety, J. (2001) 'From the perception of action to the understanding of intention', *Nature Review*, 2, pp. 561–567.

Blefari, M. L., Sulzer, J., Hepp-Reymond, M.-C., Kollias, S. and Gassert, R. (2015) 'Improvement in precision grip force control with self-modulation of primary motor cortex during motor imagery', *Frontiers in behavioral neuroscience*, 9, pp. 1–18.

Block, H., Bastian, A. and Celnik, P. (2013) 'Virtual Lesion of Angular Gyrus Disrupts the Relationship between Visuoproprioceptive Weighting and Realignment', *Journal of Cognitive Neuroscience*, 25, pp. 636–648.

Bohlhalter, S., Goldfine, A., Matteson, S., Garraux, G., Hanakawa, T., Kansaku, K., Wurzman, R., Hallett, M. and Hallett, M. (2006) 'Neural correlates of tic generation in Tourette syndrome: an event-related functional MRI study', *Brain*, 129, pp. 2029–2037.

Bouhassira, D., Attal, N., Fermanian, J., Alchaar, H., Gautron, M., Masquelier, E., Rostaing, S., Lanteri-Minet, M., Collin, E., Grisart, J. and Boureau, F. (2004) 'Development and validation of the Neuropathic Pain Symptom Inventory', *Pain*, 108, pp. 248–257.

Bray, S., Shimojo, S. and O'Doherty, J. P. (2007a) 'Direct Instrumental Conditioning of Neural Activity Using Functional Magnetic Resonance Imaging-Derived Reward Feedback', *The Journal of NeuroscienceJournal of Neuroscience*, 27(28), pp. 7498–7507.

Bray, S., Shimojo, S. and O 'doherty, J. P. (2007b) 'Behavioral/Systems/Cognitive Direct Instrumental Conditioning of Neural Activity Using Functional Magnetic Resonance

Imaging-Derived Reward Feedback', *The Journal of Neuroscience*, 27, pp. 7498 –7507.

Brodal, P. (2010) *The central nervous system: structure and function*. New York: Oxford University Press.

Brodmann, K. (2006) *Brodmann's Localisation in the Cerebral Cortex*. Third Edition. Springer.

Buccino, G. (2014) 'Action observation treatment: a novel tool in neurorehabilitation', *Philosophical Transactions of the Royal Society B: Biological Sciences*, 369(1644), pp. 1–8.

Buccino, G., Vogt, S., Ritzl, A., Fink, G. R., Zilles, K., Freund, H. J. and Rizzolatti, G. (2004) 'Neural circuits underlying imitation learning of hand actions: An event-related fMRI study', *Neuron*, 42(2), pp. 323–334.

Büchel, C., Coull, J. T. and Friston, K. J. (1999) 'The Predictive Value of Changes in Effective Connectivity for Human Learning', *Science*, 283, pp. 1538–1541.

Buxton, R. B. (2009) *Introduction to functional magnetic resonance imaging: principles and techniques*. Second Edi. Cambridge: Cambridge University Press.

Callow, N. and Roberts, R. (2010) 'Imagery research: An investigation of three issues', *Psychology of Sport & Exercise*, 11, pp. 325–329.

Cano-De-La-Cuerda, R., Molero-Sánchez, A., Carratalá-Tejada, M., Alguacil-Diego, I. M., Molina-Rueda, F., Miangolarra-Page, J. C. and Torricelli, D. (2015) 'Theories and control models and motor learning: Clinical applications in neurorehabilitation', *Neurología*, 30, pp. 32–41.

Caria, A., Sitaram, R. and Birbaumer, N. (2012) 'Real-Time fMRI: A Tool for Local Brain Regulation', *The Neuroscientist*, 18(5), pp. 487–501.

Caria, A., Sitaram, R., Veit, R., Begliomini, C. and Birbaumer, N. (2010) 'Volitional control of anterior insula activity modulates the response to aversive stimuli. A real-time functional magnetic resonance imaging study', *Biological Psychiatry*, 68(5), pp. 425–432.

Caria, A., Veit, R., Sitaram, R., Lotze, M., Weiskopf, N., Grodd, W. and Birbaumer, N. (2007) 'Regulation of anterior insular cortex activity using real-time fMRI', *NeuroImage*, 35(3), pp. 1238–1246.

Carter, R., Aldridge, S., Page, M., Parker, S., Frith, C. D., Frith, U. and Shulman, M. B. (2009) *The human brain book*. New York, N.Y.: DK Pub.

Caspers, S., Geyer, S., Schleicher, A., Mohlberg, H., Amunts, K. and Zilles, K. (2006) 'The human inferior parietal cortex: Cytoarchitectonic parcellation and interindividual variability', *NeuroImage*, 33(2), pp. 430–448.

Caspers, S., Zilles, K., Laird, A. R. and Eickhoff, S. B. (2010) 'ALE meta-analysis of action observation and imitation in the human brain', *NeuroImage*, 50, pp. 1148–1167.

Cavallo, A., Bucchioni, G., Castiello, U. and Becchio, C. (2013) 'Goal or movement? Action representation within the primary motor cortex', *European Journal of Neuroscience*, 38(10), pp. 3507–3512.

Cavanna, A. E. and Trimble, M. R. (2006) 'The precuneus: a review of its functional anatomy and behavioural correlates', *Brain*, 129, pp. 564–583.

Ceballos-Baumann, A. O. (2003) 'Functional imaging in Parkinson's disease: activation studies with PET, fMRI and SPECT', *Journal of Neurology*, 250, pp. 15–23.

Chiew, M., Laconte, S. M. and Graham, S. J. (2012) 'Investigation of fMRI neurofeedback of differential primary motor cortex activity using kinesthetic motor imagery', *NeuroImage*,

61, pp. 21–31.

Cleeland, C. S. and Ryan, K. M. (1994) ‘Pain assessment: global use of the Brief Pain Inventory’, *Annals Academy Medicine*, 23, pp. 129–138.

Connolly, A. C., Guntupalli, J. S., Gors, J., Hanke, M., Halchenko, Y. O., Wu, Y.-C., Abdi, H. and Haxby, J. V. (2012) ‘The representation of biological classes in the human brain’, *The Journal of neuroscience*, 32(8), pp. 2608–18.

Conroy, B. R., Singer, B. D., Guntupalli, J. S., Ramadge, P. J. and Haxby, J. V (2013) ‘Inter-subject alignment of human cortical anatomy using functional connectivity’, *NeuroImage*, 81, pp. 400–411.

Conroy, B. R., Singer, B. D., Haxby, J. V and Ramadge, P. J. (2009) ‘fMRI-Based Inter-Subject Cortical Alignment Using Functional Connectivity’, *Advances in Neural Information Processing System*, 22, pp. 378–386.

Cooke, D. F., Taylor, C. S. R., Moore, T. and Graziano, M. S. A. (2003) ‘Complex movements evoked by microstimulation of the ventral intraparietal area’, *PNAS*, 100, pp. 6163–6168.

Corradi-Dell ’Acqua, C., Tusche, A., Vuilleumier, P. and Singer, T. (2016) ‘Cross-modal representations of first-hand and vicarious pain, disgust and fairness in insular and cingulate cortex’, *Nature Communications*, 7, pp. 1–12.

Cox, D. D. and Savoy, R. L. (2003) ‘Functional magnetic resonance imaging (fMRI) “brain reading”: Detecting and classifying distributed patterns of fMRI activity in human visual cortex’, *NeuroImage*, 19(2), pp. 261–270.

Critchley, H. D., Wiens, S., Rotshtein, P., Öhman, A. and Dolan, R. J. (2004) ‘Neural systems supporting interoceptive awareness’, *Nature Neuroscience*, 7(2), pp. 189–195.

Culham, J. C. and Valyear, K. F. (2006) ‘Human parietal cortex in action’, *Current Opinion in*

Neurobiology, 16, pp. 205–212.

Daniel, R. and Pollmann, S. (2014) 'A universal role of the ventral striatum in reward-based learning: Evidence from human studies', *Neurobiology of Learning and Memory*, 114, pp. 90–100.

Davare, M., Montague, K., Olivier, E., Rothwell, J. C., Lemon, R. N. and Davare, M. (2009) 'Ventral premotor to primary motor cortical interactions during object-driven grasp in humans', *Cortex*, 45, pp. 1050–1057.

Davis, K. D., Taub, E., Duffner, F., Lozano, A. M., Tasker, R. R., Houle, S. and Dostrovsky, J. O. (2000) 'Activation of the anterior cingulate cortex by thalamic stimulation in patients with chronic pain: a positron emission tomography study', *Journal of Neurosurgery*, 92, pp. 64–69.

Dayan, E. and Cohen, L. G. (2011) 'Neuroplasticity Subserving Motor Skill Learning', *Neuron Review*, 72, pp. 443–454.

DeCharms, R., Maeda, F., Glover, G. H., Ludlow, D., Pauly, J. M., Soneji, D., Gabrieli, J. D. E. and Mackey, S. C. (2005) 'Control over brain activation and pain learned by using real-time functional MRI', *PNAS*, 102, pp. 18626–18631.

Desmurget, M., Reilly, K. T., Richard, N., Szathmari, A., Mottolese, C. and Sirigu, A. (2009) 'Movement Intention After Parietal Cortex Stimulation in Humans', *Science*, 324, pp. 811–813.

Dijk, K. R. A. Van, Sabuncu, M. R. and Buckner, R. L. (2012) 'The influence of head motion on intrinsic functional connectivity MRI', *NeuroImage*, 59, pp. 431–438.

Draganski, B., Gaser, C., Busch, V., Schuierer, G., Bogdahn, U. and May, A. (2004) 'Neuroplasticity: changes in grey matter induced by training', *Nature*, 427, pp. 311–312.

Dum, R. P. and Strick, P. L. (1991) 'The Origin of Corticospinal Projections from the Premotor Areas in the Frontal Lobe', *The Journal of Neuroscience*, 7, pp. 667–669.

Dum, R. P. and Strick, P. L. (2005) 'Frontal Lobe Inputs to the Digit Representations of the Motor Areas on the Lateral Surface of the Hemisphere', *The Journal of Neuroscience*, 25, pp. 1375–1386.

Eaves, D. L., Riach, M., Holmes, P. S. and Wright, D. J. (2016) 'Motor Imagery during Action Observation: A Brief Review of Evidence, Theory and Future Research Opportunities', *Frontier in Neuroscience*, 10, pp. 1–10.

Edelman, R. R. (2006) *Clinical magnetic resonance imaging*. Third Edit. Philadelphia: PA: Saunders Elsevier.

Van Elk, M. (2014) 'The left inferior parietal lobe represents stored hand-postures for object use and action prediction', *Frontiers in Psychology*, 5, pp. 1–12.

Emmert, K., Breimhorst, M., Bauermann, T., Birklein, F., Van De Ville, D. and Haller, S. (2014) 'Comparison of anterior cingulate vs. insular cortex as targets for real-time fMRI regulation during pain stimulation.', *Frontiers in behavioral neuroscience*, 8(October), pp. 1–13.

Emmert, K., Kopel, R., Sulzer, J., Brühl, A. B., Berman, B. D., Linden, D. E. J., Horovitz, S. G., Breimhorst, M., Caria, A., Frank, S., Johnston, S., Long, Z., Paret, C., Robineau, F., Veit, R., Bartsch, A., Beckmann, C. F., Van De Ville, D. and Haller, S. (2016) 'Meta-analysis of real-time fMRI neurofeedback studies using individual participant data: How is brain regulation mediated?', *NeuroImage*, 124, pp. 806–812.

Ertelt, D., Small, S., Solodkin, A., Dettmers, C., McNamara, A., Binkofski, F. and Buccino, G. (2007) 'Action observation has a positive impact on rehabilitation of motor deficits after

stroke', *NeuroImage*, 36, pp. 164–173.

Evans, A. C., Collins, D. L., Mills, S. R., Brown, E. D., Kelly, R. L. and Peters, T. M. (1993) '3D statistical neuroanatomical models from 305 MRI volumes', *Nuclear Science Symposium and Medical Imaging Conference*. IEEE Conference Record Nuclear Science Symposium and Medical Imaging Conference, pp. 1813–1817.

Fabbri-Destro, M. and Rizzolatti, G. (2008) 'Mirror Neurons and Mirror Systems in Monkeys and Humans', *Physiology*, 23, pp. 171–179.

Fahle, M. (2002) 'Perceptual learning: gain without pain', *Nature Neuroscience*, 5, pp. 923–924.

Filimon, F., Rieth, C. A., Sereno, M. I. and Cottrell, G. W. (2015) 'Observed, executed, and imagined action representations can be decoded from ventral and dorsal areas', *Cerebral Cortex*, 25(9), pp. 3144–3158.

Fillmore, M. T., Rush, C. R. and Hays, L. (2006) 'Acute effects of cocaine in two models of inhibitory control: Implications of non-linear dose effects', *Addiction*, 101(9), pp. 1323–1332.

Fischl, B., Sereno, M. I., Tootell, R. B. H. and Dale, a M. (1999) 'High-resolution inter-subject averaging and a surface-based coordinate system', *Human Brain Mapping*, 8, pp. 272–284.

Folstein, J. R., Palmeri, T. J. and Gauthier, I. (2013) 'Category Learning Increases Discriminability of Relevant Object Dimensions in Visual Cortex', *Cerebral Cortex*, 23, pp. 814–823.

Formisano, E., De Martino, F., Bonte, M. and Goebel, R. (2008) '"Who" Is Saying "What"? Brain-Based Decoding of Human Voice and Speech', *Science*, 322, pp. 970–973.

Friston, K. J., Ashburner, J., Frith, C. D., Poline, J.-B., Heather, J. D. and Frackowiak, R. S. J. (1995) 'Statistical Analysis of fMRI Data', *Human Brain Mapping,* 2, pp. 165–189.

Friston, K. J., Buechel, C., Fink, G. R., Morris, J., Rolls, E. and Dolan, R. J. (1997) 'Psychophysiological and Modulatory Interactions in Neuroimaging', *NeuroImage,* 6, pp. 218–229.

Frost, M. A. and Goebel, R. (2012) 'Measuring structural–functional correspondence: Spatial variability of specialised brain regions after macro-anatomical alignment', *NeuroImage,* 59, pp. 1369–1381.

Gallese, V., Fadiga, L., Fogassi, L. and Rizzolatti, G. (1996) 'Action recognition in the premotor cortex', *Brain*, 119, pp. 593–609.

Gazzola, V. and Keysers, C. (2009) 'The Observation and Execution of Actions Share Motor and Somatosensory Voxels in all Tested Subjects: Single-Subject Analyses of Unsmoothed fMRI Data', *Cerebral Cortex,* 19, pp. 1239–1255.

Gentili, R., Han, C. E., Schweighofer, N. and Papaxanthis, C. (2010) 'Motor Learning Without Doing: Trial-by-Trial Improvement in Motor Performance During Mental Training', *J Neurophysiol,* 104, pp. 774–783.

Goebel, R., Esposito, F. and Formisano, E. (2006) 'Analysis of Functional Image Analysis Contest (FIAC) data with BrainVoyager QX: From single-subject to cortically aligned group General Linear Model analysis and self-organizing group Independent Component Analysis', *Human Brain Mapping,* 27(5), pp. 392–401.

Graziano, M. (2006) 'The Organization of Behavioral Repertoire in Motor Cortex', *Annual Review Neuroscience ,* 29, pp. 105–134.

Grefkes, C., Eickhoff, S. B., Nowak, D. A., Dafotakis, M. and Fink, G. R. (2008) 'Dynamic

intra-and interhemispheric interactions during unilateral and bilateral hand movements assessed with fMRI and DCM', *neuroImage*, 41, pp. 1382–1394.

Grill-Spector, K., Henson, R. and Martin, A. (2006) 'Repetition and the brain: neural models of stimulus-specific effects', *Trends in Cognitive Sciences*, 10, pp. 14–23.

Guillot, A. and Collet, C. (2017) 'Duration of Mentally Simulated Movement: A Review', *Journal of Motor Behavior*, 37, pp. 10–20.

Guillot, A., Collet, C., Nguyen, V. A., Malouin, F., Richards, C. and Doyon, J. (2009) 'Brain activity during visual versus kinesthetic imagery: An fMRI study', *Human Brain Mapping*, 30(7), pp. 2157–2172.

Guntupalli, J. S., Hanke, M., Halchenko, Y. O., Connolly, A. C., Ramadge, P. J. and Haxby, J. V. (2016) 'A Model of Representational Spaces in Human Cortex', *Cerebral Cortex*, 26(6), pp. 2919–2934.

Haines, D. E. and Ard, M. D. (2013) *Fundamental Neuroscience for Basic and Clinical Applications*. Philadelphia: Elsevier Health Sciences.

Haller, S., Birbaumer, N. and Veit, R. (2010) 'Real-time fMRI feedback training may improve chronic tinnitus', *European Radiology*, 20(3), pp. 696–703.

Halsband, U. and Lange, R. K. (2006) 'Motor learning in man: A review of functional and clinical studies', *Journal of Physiology*, 99, pp. 414–424.

Hamilton, J. P., Glover, G. H., Hsu, J.-J., Johnson, R. F. and Gotlib, I. H. (2011) 'Modulation of Subgenual Anterior Cingulate Cortex Activity With Real-Time Neurofeedback', *Human Brain Mapping*, 32, pp. 22–31.

Hampson, M., Scheinost, D., Qiu, M., Bhawnani, J., Lacadie, C. M., Leckman, J. F., Constable, R. T. and Papademetris, X. (2011) 'Biofeedback of Real-Time Functional Magnetic

Resonance Imaging Data from the Supplementary Motor Area Reduces Functional Connectivity to Subcortical Regions', *Brain Connectivity*, 1, pp. 91–98.

Hanakawa, T. (2011) 'Rostral premotor cortex as a gateway between motor and cognitive networks', *Neuroscience Research*, 70, pp. 144–154.

Hanakawa, T., Dimyan, M. A. and Hallett, M. (2008) 'Motor Planning, Imagery, and Execution in the Distributed Motor Network: A Time- Course Study with Functional MRI', *Cerebral Cortex December*, 18, pp. 2775–2788.

Hardwick, R. M., Caspers, S., Eickhoff, S. B. and Swinnen, S. P. (2017) 'Neural Correlates of Motor Imagery, Action Observation, and Movement Execution: A Comparison Across Quantitative Meta-Analyses', *Not publish yet*.

Hardwick, R. M., Rottschy, C., Miall, R. C. and Eickhoff, S. B. (2013) 'A quantitative meta-analysis and review of motor learning in the human brain', *NeuroImage*, 67, pp. 283–297.

Hausfeld, L., Valente, G. and Formisano, E. (2014) 'Multiclass fMRI data decoding and visualization using supervised self-organizing maps', *NeuroImage*, 96, pp. 54–66.

Haxby, J. V, Connolly, A. C. and Guntupalli, J. S. (2014) 'Decoding Neural Representational Spaces Using Multivariate Pattern Analysis', *Annual Review of Neuroscience*, 37, pp. 435–456.

Haxby, J. V, Gobbini, M. I., Furey, M. L., Ishai, A., Schouten, J. L. and Pietrini, P. (2001) 'Distributed and Overlapping Representations of Faces and Objects in Ventral Temporal Cortex', *Science*, 293, pp. 2425–2430.

Haxby, J. V, Guntupalli, J. S., Connolly, A. C., Halchenko, Y. O., Conroy, B. R., Gobbini, M. I., Hanke, M. and Ramadge, P. J. (2011) 'A common, high-dimensional model of the

representational space in human ventral temporal cortex', *Neuron*, 72(2), pp. 404–416.

Haynes, J.-D. and Rees, G. (2005) 'Predicting the orientation of invisible stimuli from activity in human primary visual cortex', *Nature Neuroscience*, 8, pp. 686–691.

Haynes, J.-D. and Rees, G. (2006) 'Decoding mental states from brain activity in humans', *Nature Review*, 7, pp. 523–534.

Henson, R. (2006) 'Efficient Experimental Design for fMRI', in Friston, K. et al. (eds) *Statistical Parametric Mapping . The Analysis of Functional Brain Images*. Elsevier, pp. 193–210. Friston, K. et al. (eds).

Herculano-Houzel, S. (2009) 'The human brain in numbers: a linearly scaled-up primate brain', *Frontier in Human Neuroscience*, 3, pp. 1–11.

Hétu, S., Grégoire, M., Saimpont, A., Coll, M.-P., Eugène, F., Michon, P.-E. and Jackson, P. L. (2013) 'The neural network of motor imagery: An ALE meta-analysis', *Neuroscience and Biobehavioral Reviews*, 37, pp. 930–949.

Hoffstaedter, F., Grefkes, C., Zilles, K. and Eickhoff, S. B. (2013) 'The "'What'" and "'When'" of Self-Initiated Movements', *Cerebral Cortex*, 23, pp. 520–530.

Holm, S. (1979) 'A Simple Sequentially Rejective Multiple Test Procedure', *Scandinavian Journal of Statistics*, 6(6), pp. 65–70.

Holmes, P. and Calmels, C. (2008) 'A Neuroscientific Review of Imagery and Observation Use in Sport', *Journal of motor behaviour*, 40, pp. 433–445.

Hommel, B. (2009) 'Action control according to TEC (theory of event coding)', *Psychological Research*, 73, pp. 512–526.

Hoshi, E., Tanji, J., Tanaka, K. and Watanabe, T. (2007) 'Distinctions between dorsal and

ventral premotor areas: anatomical connectivity and functional properties', *Current Opinion in Neurobiology*, 17, pp. 234–242.

Huettel, S. A., Song, A. W. and McCarthy, G. (2008) *Functional Magnetic Resonance Imaging*. Second Edi. Sinauer Associates.

Hui, M., Zhang, H., Ge, R., Yao, L. and Long, Z. (2014) 'Modulation of functional network with real-time fMRI feedback training of right premotor cortex activity', *Neuropsychologia*, 62, pp. 111–123.

Hurst, H. and Bolton, J. (2004) 'Assessing the Clinical Significance of Change Scores Recorded on Subjective Outcome Measures', *Journal of Manipulative and Physiological Therapeutics*, 27, pp. 26–35.

Iannetti, G. D., Salomons, T. V, Moayedi, M., Mouraux, A. and Davis, K. D. (2013) 'Beyond metaphor: contrasting mechanisms of social and physical pain', *Trends in Cognitive Sciences*, 17, pp. 371–378.

Ietswaart, M., Johnston, M., Dijkerman, H. C., Joice, S., Scott, C. L., Macwalter, R. S. and Hamilton, S. J. C. (2011) 'Mental practice with motor imagery in stroke recovery: randomized controlled trial of efficacy', *Brain*, 134, pp. 1373–1386.

Jeannerod, M. (1995) 'Mental Imagery in the Motor Context', *Neuropsycholog*, 33, pp. 1419–1432.

Jeannerod, M. (2001) 'Neural Simulation of Action: A Unifying Mechanism for Motor Cognition', *NeuroImage*, 14, pp. 103–109.

Jezzard, P., Matthews, P. M. and Smith, S. M. (2003a) 'Functional MRI: An introduction to methods', *Journal of Magnetic Resonance Imaging*, 17(3), pp. 383–383.

Jezzard, P., Matthews, P. and Smith, S. (2003b) *Functional Magnetic Resonance Imagning*.

Edited by P. Jezzard. Oxford University Press.

Jo, H. J., Saad, Z. S., Simmons, W. K., Milbury, L. A. and Cox, R. W. (2010) 'Mapping sources of correlation in resting state FMRI, with artifact detection and removal', *NeuroImage*, 52, pp. 571–582.

Johnson, K. A., Hartwell, K., LeMatty, T., Borckardt, J., Morgan, P. S., Govindarajan, K., Brady, K. and George, M. S. (2012) 'Intermittent "Real-time" fMRI Feedback Is Superior to Continuous Presentation for a Motor Imagery Task: A Pilot Study', *Journal of Neuroimaging*. Blackwell Publishing Inc, 22(1), pp. 58–66.

Johnston, S. J., Boehm, S. G., Healy, D., Goebel, R. and Linden, D. E. J. (2010) 'Neurofeedback: A promising tool for the self-regulation of emotion networks', *NeuroImage*, 49(1), pp. 1066–1072.

Kamitani, Y. and Tong, F. (2005) 'Decoding the visual and subjective contents of the human brain', *Nature Neuroscience* , 8, pp. 679–685.

Kay, K. N., Naselaris, T., Prenger, R. J. and Gallant, J. L. (2008) 'Identifying natural images from human brain activity', *Nature*, 452, pp. 352–356.

Keysers, C. and Gazzola, V. (2009) 'Expanding the mirror: vicarious activity for actions, emotions, and sensations', *Current Opinion in Neurobiology*, 19, pp. 666–671.

Khaligh-Razavi, S. M. and Kriegeskorte, N. (2014) 'Deep Supervised, but Not Unsupervised, Models May Explain IT Cortical Representation', *PLOS Computational Biology*, 10(11), pp. 1–29.

Klann, J., Binkofski, F. C. and Caspers, S. (2015) 'On the neuroanatomical parcellation and multiple functions of the inferior parietal lobule', in Laihinen, A. and Emmans, D. (eds) *Comparative Neuropsychology and Brain Imaging*. LIT-Verlag, pp. 75–84. Laihinen, A.

and Emmans, D. (eds).

Kober, S. E., Witte, M., Ninaus, M., Neuper, C., Wood, G., Scherer, R. and Yordanova, J. (2013) 'Learning to modulate one's own brain activity: the effect of spontaneous mental strategies', *Frontiers in Human Neuroscience*, 7, pp. 1–12.

Koechlin, E. and Summerfield, C. (2007) 'An information theoretical approach to prefrontal executive function', *Trends in Cognitive Sciences*, 11, pp. 229–235.

Kolb, B. and Whishaw, I. Q. (2003) *Fundamentals of Human Neuropsychology*. Fifth. Worth Publishers.

Koush, Y., Rosa, M. J., Robineau, F., Heinen, K., Rieger, S. W., Weiskopf, N., Vuilleumier, P., De Ville, D. Van and Scharnowski, F. (2013) 'Connectivity-based neurofeedback: Dynamic causal modeling for real-time fMRI', *NeuroImage*, 81, pp. 422–430.

Kriegeskorte, N. (2011) 'Pattern-information analysis: From stimulus decoding to computational-model testing', *NeuroImage*, 56, pp. 411–421.

Kriegeskorte, N., Cusack, R. and Bandettini, P. (2009) 'How does an fMRI voxel sample the neuronal activity pattern: Compact-kernel or complex spatiotemporal filter?', *NeuroImage*, 49, pp. 1965–1976.

Kriegeskorte, N., Goebel, R. and Bandettini, P. (2006) 'Information-based functional brain mapping', *PNAS*, 103(10), pp. 3863–3868.

Kriegeskorte, N., Mur, M. and Bandettini, P. (2008a) 'Representational similarity analysis - connecting the branches of systems neuroscience.', *Frontiers in systems neuroscience*, 2(November), p. 4.

Kriegeskorte, N., Mur, M. and Bandettini, P. (2008b) 'Representational similarity analysis – connecting the branches of systems neuroscience', *Frontiers in Systems Neuroscience*,

2, pp. 1–28.

Kriegeskorte, N., Mur, M., Ruff, D. A., Kiani, R., Bodurka, J., Esteky, H., Tanaka, K. and Bandettini, P. A. (2008c) 'Matching Categorical Object Representations in Inferior Temporal Cortex of Man and Monkey', *Neuron*, 60, pp. 1126–1141.

Kwasnicka, D., Dombrowski, S. U., White, M. and Sniehotta, F. (2016) 'Theoretical explanations for maintenance of behaviour change: a systematic review of behaviour theories', *Health Psychology Review*, 10, pp. 277–296.

Kwongt, K. K., Belliveaut, J. W., Cheslert, D. A., Goldbergt, I. E., Weisskofft, R. M., Poncelett, B. P., Kennedyt, D. N., Hoppelt, B. E., Cohent, M. S., Turnert, R., Cheng, H.-M., Bradyt, T. J. and Rosent, B. R. (1992) 'Dynamic magnetic resonance imaging of human brain activity during primary sensory stimulation', *Proceedings of the National Academy of Sciences of the United States of America*, 89, pp. 5675–5679.

Lacroix, J. M. (1986) 'Mechanisms of biofeedback control', in Davidson, R. J., Schwartz, G. E., and Shapiro, D. (eds) *Consciousness and Self-Regulation*. Boston, MA: Springer. Davidson, R. J., Schwartz, G. E., and Shapiro, D. (eds).

Lancaster, J. L., Woldorff, M. G., Parsons, L. M., Liotti, M., Freitas, C. S., Rainey, L., Kochunov, P. V, Nickerson, D., Mikiten, S. A. and Fox, P. T. (2000) 'Automated Talairach Atlas Labels For Functional Brain Mapping', *Human Brain Mapping*, 10, pp. 120–131.

Laurienti, P. J., Burdette, J. H., Wallace, M. T., Yen, Y.-F., Field, A. S. and Stein, B. E. (2002) 'Deactivation of Sensory-Specific Cortex by Cross-Modal Stimuli', *Journal of Cognitive Neuroscience*, 14, pp. 420–429.

Lerner, A., Bagic, A., Hanakawa, T., Boudreau, E. A., Pagan, F., Mari, Z., Bara-Jimenez, W.,

Aksu, M., Sato, S., Murphy, D. L. and Hallett, M. (2009) 'Involvement of Insula and Cingulate Cortices in Control and Suppression of Natural Urges', *Cerebral Cortex*, 19, pp. 218–223.

Lewis-Peacock, J. A. and Postle, B. R. (2008) 'Temporary Activation of Long-Term Memory Supports Working Memory', *The Journal of Neuroscience*, 28, pp. 8765–8771.

Liew, S.-L., Rana, M., Cornelsen, S., Barros, M. F. de, Birbaumer, N., Sitaram, R., Cohen, L. G. and Soekadar, S. R. (2016) 'Improving Motor Corticothalamic Communication After Stroke Using Real-Time fMRI Connectivity-Based Neurofeedback', *Neurorehabilitation and Neural Repair*, 30(7), pp. 671–675.

Linden, D. E. J. and Turner, D. L. (2016) 'Real-time functional magnetic resonance imaging neurofeedback in motor neurorehabilitation', *NeuroImage*, 29, pp. 412–418.

Logothetis, N. K., Pauls, J., Augath, M., Trinath, T. and Oeltermann, A. (2001) 'Neurophysiological investigation of the basis of the fMRI signal', *Nature*, 412, pp. 150–157.

Lorey, B., Naumann, T., Pilgramm, S., Petermann, C., Bischoff, M., Zentgraf, K., Stark, R., Vaitl, D. and Munzert, J. (2013) 'How equivalent are the action execution, imagery, and observation of intransitive movements? Revisiting the concept of somatotopy during action simulation', *Brain and Cognition*, 81, pp. 139–150.

Lorey, B., Naumann, T., Pilgramm, S., Petermann, C., Bischoff, M., Zentgraf, K., Stark, R., Vaitl, D. and Munzert, J. (2014) 'Neural simulation of actions: Effector- versus action-specific motor maps within the human premotor and posterior parietal area?', *Human Brain Mapping*, 35(4), pp. 1212–1225.

Lotte, F., Larrue, F., Mühl, C., Scherer, R., Blankertz, B. and Kaufmann, T. (2013) 'Flaws in

current human training protocols for spontaneous Brain-Computer Interfaces: lessons learned from instructional design', *Frontier in Human Neuroscience*, 7, pp. 1–11.

Lotze, M. and Halsband, U. (2006) 'Motor imagery', *Journal of Physiology*, 99, pp. 386–395.

Macuga, K. L. and Frey, S. H. (2012) 'Neural representations involved in observed, imagined, and imitated actions are dissociable and hierarchically organized', *NeuroImage*. Elsevier Inc., 59(3), pp. 2798–2807.

Magno, E., Foxe, J. J., Molholm, S., Robertson, I. H. and Garavan, H. (2006) 'The Anterior Cingulate and Error Avoidance', *The Journal of Neuroscience*, 26, pp. 4769–4773.

Mahmoudi, A., Takerkart, S., Regragui, F., Boussaoud, D. and Brovelli, A. (2012) 'Multivoxel pattern analysis for fMRI data: A review', *Computational and Mathematical Methods in Medicine*, 2012.

Malouin, F. and Richards, C. L. (2013) 'Clinical Applications of Motor Imagery in Rehabilitation', in Lacey, S. and Lawson, R. (eds) *Multisensory Imagery*. New York: Springer Science+Business Media, pp. 397–419. Lacey, S. and Lawson, R. (eds).

Mandelkow, H., de Zwart, J. A. and Duyn, J. H. (2016) 'Linear Discriminant Analysis Achieves High Classification Accuracy for the BOLD fMRI Response to Naturalistic Movie Stimuli', *Frontiers in Human Neuroscience*, 10, pp. 1–12.

Marins, T. F., Rodrigues, E. C., Engel, A., Hoefle, S., Basílio, R., Lent, R., Moll, J. and Tovar-Moll, F. (2015) 'Enhancing Motor Network Activity Using Real-Time Functional MRI Neurofeedback of Left Premotor Cortex', *Frontiers in behavioral neuroscience*, 9, pp. 1–12.

Marxen, M., Jacob, M. J., Müller, D. K., Posse, S., Ackley, E., Hellrung, L., Riedel, P., Bender, S., Epple, R. and Smolka, M. N. (2016) 'Amygdala Regulation Following fMRI-

Neurofeedback without Instructed Strategies', *Frontiers in Human Neuroscience*, 10, pp. 1–14.

Marzbani, H., Marateb, H. R. and Mansourian, M. (2016) 'Methodological note: Neurofeedback: A comprehensive review on system design, methodology and clinical applications', *Basic and Clinical Neuroscience*, 7(2), pp. 143–158.

Mayka, M. A., Corcos, D. M., Leurgans, S. E. and Vaillancourt, D. E. (2006) 'Three-dimensional locations and boundaries of motor and premotor cortices as defined by functional brain imaging: A meta-analysis', *NeuroImage*, 31, pp. 1453–1474.

McKeown, M. J., Hansen, L. K. and Sejnowsk, T. J. (2003) 'Independent component analysis of functional MRI: What is signal and what is noise?', *Current Opinion in Neurobiology*, 13(5), pp. 620–629.

Megumi, F., Yamashita, A., Kawato, M. and Imamizu, H. (2015) 'Functional MRI neurofeedback training on connectivity between two regions induces long-lasting changes in intrinsic functional network.', *Frontiers in human neuroscience*, 9, p. 160.

Menon, V. (2015) 'Salience Network Introduction and Overview', in Toga, A. W. (ed.) *Brain Mapping: An Encyclopedic Reference*. Elsevier, pp. 597–611. Toga, A. W. (ed.).

Menon, V. and Uddin, L. Q. (2010) 'Saliency, switching, attention and control: a network model of insula function Introduction and overview', *Brain Structure Function*, 214, pp. 655–667.

Mercier, C. and Le´onard, G. (2001) 'Interactions between Pain and the Motor Cortex: Insights from Research on Phantom Limb Pain and Complex Regional Pain Syndrome', *Physiotherapy Canada*, 63, pp. 305–314.

Miller, K. J., Schalk, G., Fetz, E. E., Nijs, M. den, Ojemann, J. G. and Rao, R. P. N. (2010)

‘Cortical activity during motor execution, motor imagery, and imagery-based online feedback’, *PNAS*, 107, pp. 4430–4435.

Misaki, M., Kim, Y., Bandettini, P. A. and Kriegeskorte, N. (2010) ‘Comparison of multivariate classifiers and response normalizations for pattern-information fMRI’, *NeuroImage*, 53, pp. 103–118.

Miyawaki, Y., Uchida, H., Yamashita, O., Sato, M.-A., Morito, Y., Tanabe, H. C., Sadato, N. and Kamitani, Y. (2008) ‘Visual Image Reconstruction from Human Brain Activity using a Combination of Multiscale Local Image Decoders’, *Neuron*, 60, pp. 915–929.

Muckli, L. and Petro, L. S. (2017) ‘The Significance of Memory in Sensory Cortex’, *Trends in Neurosciences*, 40, pp. 255–256.

Mueller, S., Wang, D., Fox, M. D., Yeo, B. T. T., Sepulcre, J., Sabuncu, M. R., Shafee, R., Lu, J. and Liu, H. (2013) ‘Individual Variability in Functional Connectivity Architecture of the Human Brain’, *Neuron*, 77, pp. 586–595.

Munzert, J., Lorey, B. and Zentgraf, K. (2009) ‘Cognitive motor processes: The role of motor imagery in the study of motor representations’, *Brain Research Reviews*, 60, pp. 306–326.

Mur, M., Bandettini, P. A. and Kriegeskorte, N. (2009) ‘Revealing representational content with pattern-information fMRI - An introductory guide’, *Social Cognitive and Affective Neuroscience*, 4(1), pp. 101–109.

Nachev, P., Kennard, C. and Husain, M. (2008) ‘Functional role of the supplementary and pre-supplementary motor areas’, *Nature*, 9, pp. 856–869.

Nachev, P., Wydell, H., Neill, K. O. ’, Husain, M. and Kennard, C. (2007) ‘The role of the pre-supplementary motor area in the control of action’, *Human Brain Mapping Journal*, 36,

pp. 155–163.

Nan, W., Rodrigues, J. P., Ma, J., Qu, X., Wan, F., Mak, P.-I., Mak, P. U., Vai, M. I. and Rosa, A. (2012) 'Individual alpha neurofeedback training effect on short term memory', *International Journal of Psychophysiology*, 86, pp. 83–87.

Naselaris, T., Kay, K. N., Nishimoto, S. and Gallant, J. L. (2011) 'Encoding and decoding in fMRI', *NeuroImage*, 56, pp. 400–410.

Naselaris, T., Prenger, R. J., Kay, K. N., Oliver, M. and Gallant, J. L. (2009) 'Bayesian Reconstruction of Natural Images from Human Brain Activity', *Neuron*, 63, pp. 902–915.

Nedelko, V., Hassa, T., Hamzei, F., Schoenfeld, M. A. and Dettmers, C. (2012) 'Action Imagery Combined With Action Observation Activates More Corticomotor Regions Than Action Observation Alone', *Journal of Neurologic Physical Therapy*, 36(4), pp. 182–188.

Neyedli, H. F., Sampaio-Baptista, C., Kirkman, M. A., Havard, D., Lührs, M., Ramsden, K., Flitney, D. D., Clare, S., Goebel, R. and Johansen-Berg, H. (2017) 'Increasing Lateralized Motor Activity in Younger and Older Adults Using Real-time fMRI during Executed Movements', *Neuroscience*, pp. 1–10.

Nicholson, A. A., Rabellino, D., Densmore, M., Frewen, P. A., Paret, C., Kluetsch, R., Schmahl, C., Théberge, J., Neufeld, R. W. J., McKinnon, M. C., Reiss, J., Jetly, R. and Lanius, R. A. (2017) 'The neurobiology of emotion regulation in posttraumatic stress disorder: Amygdala downregulation via real-time fMRI neurofeedback', *Human Brain Mapping*, 38(1), pp. 541–560.

Nili, H., Wingfield, C., Walther, A., Su, L., Marslen-Wilson, W. and Kriegeskorte, N. (2014)

‘A Toolbox for Representational Similarity Analysis’, *PLOS Computational Biology*, 10(4), pp. 1–11.

Nishimoto, S. and Nishida, S. (2016) ‘Lining Up Brains via a Common Representational Space’, *Trends in Cognitive Sciences*, 20, pp. 565–567.

Nishimoto, S., Vu, A. T., Naselaris, T., Benjamini, Y., Yu, B. and Gallant, J. L. (2011) ‘Report Reconstructing Visual Experiences from Brain Activity Evoked by Natural Movies’, *Current Biology*, 21, pp. 1641–1646.

Norman, K., Polyn, S., Detre, G. and Haxby, J. (2006) ‘Beyond mind-reading: multi-voxel pattern analysis of fMRI data’, *Trends in cognitive sciences*, 10(9), pp. 424–430.

O’Doherty, J. P., Dayan, P., Friston, K., Critchley, H. and Dolan, R. J. (2003) ‘Temporal difference models and reward-related learning in the human brain’, *Neuron*, 38, pp. 329–337.

O ’shea, J., Johansen-Berg, H., Trief, D., Gö, S. and Rushworth, M. F. S. (2007) ‘Functionally Specific Reorganization in Human Premotor Cortex’, *Neuron*, 54, pp. 479–490.

Ogawa, S., Lee, T. M., Kay, A. R. and Tank, D. W. (1990) ‘Brain magnetic resonance imaging with contrast dependent on blood oxygenation’, *Biophysics*, 87, pp. 9868–9872.

Oldfield, R. C. (1971) ‘The Assessments and Analysis of Handedness: The Edinburgh Inventory’, *Neuropsychologyia*, 9, pp. 97–113.

Olsson, C.-J., Jonsson, B., Nyberg, L., Hugdahl, K. and Risberg, J. (2008) ‘Learning by doing and learning by thinking: an fMRI study of combining motor and mental training’, *Frontiers in Human Neuroscience*, 2, pp. 1–7.

Oosterhof, N. N., Tipper, S. P. and Downing, P. E. (2012a) ‘Viewpoint (in)dependence of action representations: an MVPA study.’, *Journal of cognitive neuroscience*, 24(4), pp.

975–989.

Oosterhof, N. N., Tipper, S. P. and Downing, P. E. (2012b) 'Visuo-motor imagery of specific manual actions: A multi-variate pattern analysis fMRI study', *NeuroImage*, 63(1), pp. 262–271.

Oosterhof, N. N., Tipper, S. P. and Downing, P. E. (2013) 'Crossmodal and action-specific: Neuroimaging the human mirror neuron system', *Trends in Cognitive Sciences*, 17(7), pp. 311–318.

Ossmy, O. and Mukamel, R. (2016) 'Activity in superior parietal cortex during training by observation predicts asymmetric learning levels across hands', *Nature*, 6, pp. 1–9.

Oztop, E., Kawato, M. and Arbib, M. A. (2013) 'Mirror neurons: Functions, mechanisms and models', *Neuroscience Letters*, 540, pp. 43–55.

Paret, C., Ruf, M., Gerchen, M. F., Kluetsch, R., Demirakca, T., Jungkunz, M., Bertsch, K., Schmahl, C. and Ende, G. (2016) 'fMRI neurofeedback of amygdala response to aversive stimuli enhances prefrontal-limbic brain connectivity', *NeuroImage*, 125, pp. 182–188.

Park, D. C., Lautenschlager, G., Hedden, T., Davidson, N. S., Smith, A. D. and Smith, P. K. (2002) 'Models of Visuospatial and Verbal Memory Across the Adult Life Span', *Psychology and Aging*, 17, pp. 299–320.

Park, D. C. and Reuter-Lorenz, P. (2009) 'The Adaptive Brain: Aging and Neurocognitive Scaffolding', *Annual Review Psychology*, 60, pp. 173–196.

Pereira, F., Mitchell, T. and Botvinick, M. (2008) 'Machine learning classifiers and fMRI: A tutorial overview', *NeuroImage*, 45, pp. 199–209.

Petersen, S. E. and Dubis, J. W. (2012) 'The mixed block/event-related design', *Neuroimage.*, 62, pp. 1177–1184.

Peyron, R., Laurent, B. and García-Larrea, L. (2000) 'Functional imaging of brain responses to pain. A review and meta-analysis (2000)', *Neurophysiol Clinical*, 30, pp. 263–288.

Pilgramm, S., de Haas, B., Helm, F., Zentgraf, K., Stark, R., Munzert, J. and Krüger, B. (2016) 'Motor imagery of hand actions: Decoding the content of motor imagery from brain activity in frontal and parietal motor areas', *Human Brain Mapping*, 37(1), pp. 81–93.

Poldrack, R. A. (2000) 'Imaging Brain Plasticity: Conceptual and Methodological Issues— A Theoretical Review', *NeuroImage*, 12, pp. 1–13.

Poldrack, R. A., Clark, J., Paré-Blagoev, E. J., Shohamy, D., Creso Moyano, J., Myers, C. and Gluck, M. . (2001) 'Interactive memory systems in the human brain', *Nature*, 414, pp. 546–550.

Polyn. Sean M., Natu, V. S., Cohen, J. D. C. and Norman, K. A. N. (2005) 'Category-Specific Cortical Activity Precedes Retrieval During Memory Search', *Science*, 310, pp. 1963–1966.

Pooley, R. A. (2005) 'AAPM/RSNA Physics Tutorial for Residents Fundamental Physics of MR Imaging', *RadioGraphics*, 25, pp. 1087–1099.

Posner, M. I., Rothbart, M. K., Sheese, B. E. and Tang, Y. (2007) 'The anterior cingulate gyrus and the mechanism of self-regulation', *Cognitive, Affective, & Behavioral Neuroscience*, 7(4), pp. 391–395.

Posse, S., Fitzgerald, D., Gao, K., Habel, U., Rosenberg, D., Moore, G. J. and Schneider, F. (2003) 'Real-time fMRI of temporolimbic regions detects amygdala activation during single-trial self-induced sadness', *NeuroImage*, 18, pp. 760–768.

Power, J. D. and Petersen, S. E. (2013) 'Control-related systems in the human brain', *Current Opinion in Neurobiology*, 23, pp. 223–228.

Prinz, W. (1997) ‘Perception and Action Planning’, *European Journal of Cognitive Psychology*, 9, pp. 129–154.

Rademacher, J., Caviness, J. V. S., Steinmetz, H. and Galaburda, A. M. (1993) ‘Topographical Variation of the Human Primary Cortices’, *Cerebral Cortex*, 3, pp. 313–329.

Raichle, M. E. (2015) ‘The Brain’s Default Mode Network’, *Annual Review of Neuroscience*, 38, pp. 433–447.

Raichle, M. E., Macleod, A. M., Snyder, A. Z., Powers, W. J., Gusnard, D. A. and Shulman, G. L. (2000) ‘A default mode of brain function’, *PNAS*, 98, pp. 676–682.

Raichle, M. E. and Snyder, A. Z. (2007) ‘A default mode of brain function: A brief history of an evolving idea’, *NeuroImage*, 37, pp. 1083–1090.

Rainville, P. (2002) ‘Distributed representation of nociception underlying the experience of pain’, *Current Opinion in Neurobiology*, 12, pp. 195–204.

Raizada, R. D. S., Tsao, F.-M., Liu, H.-M. and Kuhl, P. K. (2010) ‘Quantifying the Adequacy of Neural Representations for a Cross-Language Phonetic Discrimination Task: Prediction of Individual Differences’, *Cerebral Cortex*, 20, pp. 1–12.

Rana, M., Gupta, N., Dalboni Da Rocha, J. L., Lee, S. and Sitaram, R. (2013) ‘A toolbox for real-time subject-independent and subject-dependent classification of brain states from fMRI signals’, *Frontiers in Neuroscience*, 7, pp. 1–11.

Rance, M., Ruttorf, M., Nees, F., Schad, L. R. and Flor, H. (2014) ‘Real time fMRI feedback of the anterior cingulate and posterior insular cortex in the processing of pain’, *Human Brain Mapping*, 35, pp. 5784–5798.

Reddy, L., Tsuchiya, N. and Serre, T. (2010) ‘Reading the mind’s eye: Decoding category information during mental imagery’, *NeuroImage*, 50, pp. 818–825.

Rizzolatti, G., Fadiga, L., Gallese, V. and Fogassi, L. (1996) 'Premotor cortex and the recognition of motor actions', *Cognitive Brain Research*, 3, pp. 131–141.

Rizzolatti, G., Fogassi, L. and Gallese, V. (2001) 'Neurophysiological mechanisms underlying the understanding and imitation of action', *Nature*, 2, pp. 661–670.

Rizzolatti, G. and Sinigaglia, C. (2010) 'The functional role of the parieto-frontal mirror circuit: interpretations and misinterpretations', *Nature*, 11, pp. 264–274.

Rolls, E. T. (2004) 'The functions of the orbitofrontal cortex', *Brain and Cognition*, 55, pp. 11–29.

Rota, G., Sitaram, R., Veit, R., Erb, M., Weiskopf, N., Dogil, G. and Birbaumer, N. (2009) 'Self-regulation of regional cortical activity using real-time fmri: the right inferior frontal gyrus and linguistic processing', *Human Brain Mapping*. Wiley Subscription Services, Inc., A Wiley Company, 30(5), pp. 1605–1614.

Rothlein, D. and Rapp, B. (2014) 'The similarity structure of distributed neural responses reveals the multiple representations of letters', *NeuroImage*, 89, pp. 331–344.

Rowe, D. B. and Hoffmann, R. G. (2006) 'Multivariate statistical analysis in fMRI: A survey of the basic theory', *IEEE Engineering in Medicine and Biology Magazine*, 25(2), pp. 60–64.

Rowe, J. B. and Siebner, H. R. (2012) 'The motor system and its disorders', *NeuroImage*, 61, pp. 464–477.

Rozzi, S., Ferrari, P. F., Bonini, L., Rizzolatti, G. and Fogassi, L. (2008) 'Functional organization of inferior parietal lobule convexity in the macaque monkey: Electrophysiological characterization of motor, sensory and mirror responses and their correlation with cytoarchitectonic areas', *European Journal of Neuroscience*, 28(8), pp.

1569–1588.

Ruiz, S., Buyukturkoglu, K., Rana, M., Birbaumer, N. and Sitaram, R. (2014) ‘Real-time fMRI brain computer interfaces: Self-regulation of single brain regions to networks’, *Biological Psychology*, 95, pp. 4–20.

Ruiz, S., Lee, S., Soekadar, S. R., Caria, A., Veit, R., Kircher, T., Birbaumer, N. and Sitaram, R. (2013) ‘Acquired self-control of insula cortex modulates emotion recognition and brain network connectivity in schizophrenia’, *Human Brain Mapping*, 34, pp. 200–212.

Rushworth, M. F. S., Nixon, P. D., Wade, D. T., Renowden~, S. and Passingham, R. E. (1998) ‘The left hemisphere and the selection of learned actions’, *Neuropsychotogia*, 36, pp. 11–24.

Sabuncu, M. R., Singer, B. D., Conroy, B., Bryan, R. E., Ramadge, P. J. and Haxby, J. V. (2010) ‘Function-based intersubject alignment of human cortical anatomy’, *Cerebral Cortex*, 20(1), pp. 130–140.

Samejima, K., Ueda, Y., Doya, K. and Kimura, M. (2005) ‘Representation of Action-Specific Reward Values in the Striatum’, *Science*, 310, pp. 1337–1340.

Schad, L. R. (2004) ‘Problems in texture analysis with magnetic resonance imaging’, *Dialogues in Clinical Neuroscience*, 6, pp. 235–242.

Scharnowski, F., Hutton, C., Josephs, O., Weiskopf, N. and Rees, G. (2012) ‘Improving Visual Perception through Neurofeedback’, *The Journal of NeuroscienceJournal of Neuroscience*, 32(49), pp. 17830–17841.

Scharnowski, F., Veit, R., Zopf, R., Studer, P., Bock, S., Diedrichsen, J., Goebel, R., Mathiak, K., Birbaumer, N. and Weiskopf, N. (2015) ‘Manipulating motor performance and memory through real-time fMRI neurofeedback’, *Biological Psychology*, 108, pp. 85–

97.

Scharnowski, F. and Weiskopf, N. (2015) ‘Cognitive enhancement through real-time fMRI neurofeedback’, *Current Opinion in Behavioral Sciences*, 4, pp. 122–127.

Scherer, R., Faller, J., Friedrich, E. V. C., Opisso, E., Costa, U., Kübler, A., Müller-Putz, G. R. and Bianchi, L. (2015) ‘Individually Adapted Imagery Improves Brain-Computer Interface Performance in End-Users with Disability’, *PLOS ONE*, 10, pp. 1–12.

Schlerf, J. E., Verstynen, T. D., Ivry, R. B. and Spencer, R. M. C. (2010) ‘Evidence of a Novel Somatopic Map in the Human Neocerebellum During Complex Actions’, *J Neurophysiol*, 103, pp. 3330–3336.

Schneider, F., Bermpohl, F., Heinzel, A., Rotte, M., Walter, M., Tempelmann, C., Wiebking, C., Dobrowolny, H., Heinze, H. J. and Northoff, A. G. (2008) ‘The Resting Brain and our Self: Self-Relatedness Modulates Resting State Neural Activity in Cortical Midline Structures’, *Neuroscience*, 157, pp. 120–131.

Schönemann, P. H. (1966) ‘A generalized solution of the orthogonal Procrustes problem’, *Psychometrika*, 31, pp. 1–10.

Schünke, M., Schulte, E. and Schumacher, U. (2010) *Thieme atlas of anatomy*. Stuttgart; New York: Thieme.

Schuster, C., Hilfiker, R., Amft, O., Scheidhauer, A., Andrews, B., Butler, J., Kischka, U. and Ettlin, T. (2011) ‘Best practice for motor imagery: a systematic literature review on motor imagery training elements in five different disciplines’, *BMC Medicine*, 9:75, pp. 1–35.

Schwartz, S., Maquet, P. and Frith, C. (2002) ‘Neural correlates of perceptual learning: A functional MRI study of visual texture discrimination’, *PNAS* , 99, pp. 17137–17142.

Sepulveda, P., Sitaram, R., Rana, M., Montalba, C., Tejos, C. and Ruiz, S. (2016) ‘How

feedback, motor imagery, and reward influence brain self-regulation using real-time fMRI', *Human Brain Mapping*, 37(9), pp. 3153–3171.

Sharma, N. and Baron, J. (2013) 'Does motor imagery share neural networks with executed movement : a multivariate fMRI analysis', *Frontiers in Human Neuroscience*, 7, pp. 1–8.

Shibata, K., Watanabe, T., Sasaki, Y. and Kawato, M. (2011) 'Perceptual Learning Incepted by Decoded fMRI Neurofeedback Without Stimulus Presentation', *Science*, 334, pp. 1413–1415.

Sitaram, R., Ros, T., Stoeckel, L., Haller, S., Scharnowski, F., Lewis-Peacock, J., Weiskopf, N., Blefari, M. L., Rana, M., Oblak, E., Birbaumer, N. and Sulzer, J. (2017) 'Closed-loop brain training: the science of neurofeedback', *Nature Reviews Neuroscience*, 18(2), pp. 86–100.

Sitaram, R., Veit, R., Stevens, B., Caria, A., Gerloff, C., Birbaumer, N. and Hummel, F. (2012) 'Acquired Control of Ventral Premotor Cortex Activity by Feedback Training: An Exploratory Real-Time fMRI and TMS Study', *Neurorehabilitation and Neural Repair*, 26(3), pp. 256–265.

Smith, D. and Holmes, P. (2004) 'The Effect of Imagery Modality on Golf Putting Performance', *Journal of Sport & Exercise Psychology*, 26, pp. 385–395.

Snell, R. S. (2010) *Clinical neuroanatomy*. Philadelphia: Wolters Kluwer Health/Lippincott Williams & Wilkins.

Sommer, M. A. (2003) 'The role of the thalamus in motor control', *Current Opinion in Neurobiology*, 13, pp. 663–670.

Song, S., Zhan, Z., Long, Z., Zhang, J. and Yao, L. (2011) 'Comparative Study of SVM

Methods Combined with Voxel Selection for Object Category Classification on fMRI Data', *PLOS ONE*, 6, pp. 1–11.

Squire, L. (2013) *Fundamental neuroscience*. Amsterdam: Elsevier/Academic Press.

Sridharan, D., Levitin, D. J. and Menon, V. (2008) 'A critical role for the right fronto-insular cortex in switching between central-executive and default-mode networks', *PNAS*, 105, pp. 12569–12574.

Strehl, U., Ros, T., Gruzelier, J. H. and Drechsler, R. (2014) 'What learning theories can teach us in designing neurofeedback treatments', *Frontiers in Human Neuroscience*, 8, pp. 1–8.

Strominger, N. L., Demarest, R. J. and Laemle, L. B. (2012) *Noback's Human Nervous System*. Seventh Edition. New York : Humana Press.

Subramanian, L., Busse Morris, M., Brosnan, M., Turner, D. L., Morris, H. R., J Linden, D. E., Koenig, T., Gruzelier, J. H. and Ros, T. (2016) 'Functional Magnetic Resonance Imaging Neurofeedback-guided Motor Imagery Training and Motor Training for Parkinson's Disease: Randomized Trial', *frontiers in Behavioral Neuroscience*, 10, pp. 1–13.

Subramanian, L., Hindle, J. V, Johnston, S., Roberts, M. V, Husain, M., Goebel, R. and Linden, D. (2011a) 'Neurobiology of Disease Real-Time Functional Magnetic Resonance Imaging Neurofeedback for Treatment of Parkinson's Disease', *Neurobiology of Disease*, 31, pp. 16309–16317.

Subramanian, L., Hindle, J. V, Johnston, S., Roberts, M. V, Husain, M., Goebel, R. and Linden, D. (2011b) 'Real-Time Functional Magnetic Resonance Imaging Neurofeedback for Treatment of Parkinson's Disease', *Neurobiology of Disease*, 9, pp. 16309 –16317.

Sulzer, J., Haller, S., Scharnowski, F., Weiskopf, N., Birbaumer, N., Blefari, M. L., Bruehl, A.

B., Cohen, L. G., Decharms, R. C., Gassert, R., Goebel, R., Herwig, U., Laconte, S., Linden, D., Luft, A., Seifritz, E. and Sitaram, R. (2013) 'Real-time fMRI neurofeedback: Progress and challenges', *NeuroImage*, 76, pp. 386–399.

Sun, Y., Wei, W., Luo, Z., Gan, H. and Hu, X. (2016) 'Improving motor imagery practice with synchronous action observation in stroke patients', *Topics in Stroke Rehabilitation*, 23, pp. 245–253.

Talairach, J. and Tournoux, P. (1988) *Co-planar stereotaxic atlas of the human brain. 3-Dimensional proportional system: an approach to cerebral imaging*. New York: Thieme Medical.

Taube, W., Mouthon, M., Leukel, C., Hoogewoud, H.-M., Annoni, J.-M. and Keller, M. (2015) 'Brain activity during observation and motor imagery of different balance tasks: An fMRI study', *Cortex*, 64, pp. 102–114.

Torres, E. B., Raymer, A., Gonzalez Rothi, L. J., Heilman, K. M. and Poizner, H. (2010) 'Sensory-spatial transformations in the left posterior parietal cortex may contribute to reach timing.', *Journal of neurophysiology*, 104(5), pp. 2375–88.

Tunik, E., Rice, N. J., Hamilton, A. and Grafton, S. T. (2007) 'Beyond grasping: Representation of action in human anterior intraparietal sulcus', *NeuroImage*, 36, pp. 77–86.

Vandenberghe, R., Gitelman, D. R., Parrish, T. B. and Mesulam, M. M. (2001) 'Functional Specificity of Superior Parietal Mediation of Spatial Shifting', *NeuroImage*, 14, pp. 661–673.

Vangeneugden, J., Pollick, F. and Vogels, R. (2009) 'Functional differentiation of macaque visual temporal cortical neurons using a parametric action space', *Cerebral Cortex*,

19(3), pp. 593–611.

Veit, R., Singh, V., Sitaram, R., Caria, A., Rauss, K. and Birbaumer, N. (2012) 'Using real-time fmri to learn voluntary regulation of the anterior insula in the presence of threat-related stimuli', *Social Cognitive and Affective Neuroscience*, 7(6), pp. 623–634.

Villiger, M., Esté Vez, N., Hepp-Reymond, M.-C., Kiper, D., Kollias, S. S., Eng, K., Hotz-Boendermaker, S. and Avenanti, A. (2013) 'Enhanced Activation of Motor Execution Networks Using Action Observation Combined with Imagination of Lower Limb Movements', *PLOS ONE*, 8, pp. 1–11.

Vogt, S., Di Rienzo, F., Collet, C., Collins, A. and Guillot, A. (2013) 'Multiple roles of motor imagery during action observation', *Frontiers in human neuroscience*, 7, p. 807.

Vovk, U., Pernuš, F. and Likar, B. (2007) 'A review of methods for correction of intensity inhomogeneity in MRI', *IEEE Transactions on Medical Imaging*, 26(3), pp. 405–421.

Ward, N. S. (2004) 'Mechanisms underlying recovery of motor function after stroke', *Archives of Neurology*, 61, pp. 1844–1848.

Weiskopf, N., Sitaram, R., Josephs, O., Veit, R., Scharnowski, F., Goebel, R., Birbaumer, N., Deichmann, R. and Mathiak, K. (2007) 'Real-time functional magnetic resonance imaging: methods and applications', *Magnetic Resonance Imaging*, 25, pp. 989 – 1003.

Weiskopf, N., Veit, R., Erb, M., Mathiak, K., Grodd, W., Goebel, R. and Birbaumer, N. (2003) 'Physiological self-regulation of regional brain activity using real-time functional magnetic resonance imaging (fMRI): methodology and exemplary data', *NeuroImage*, 19, pp. 577–586.

van der Wel, R. P. R. D., Sebanz, N. and Knoblich, G. (2013) 'Action Perception from a Common Coding Perspective', in Johnson, K. and Schiffrar, M. (eds) *People Watching:*

Social, Perceptual, and Neurophysiological Studies of Body Perception. New York: Oxford University Press. Johnson, K. and Schiffrar, M. (eds).

Williams, S. E., Guillot, A., Rienzo, F. Di and Cumming, J. (2015) 'Comparing self-report and mental chronometry measures of motor imagery ability', *European Journal of Sport Science*, 15, pp. 703–711.

Winawer, J., Huk, A. C. and Boroditsky, L. (2010) 'A motion aftereffect from visual imagery of motion', *Cognition*, 114, pp. 276–284.

Wise, S. P., Boussaoud, D., Johnson, P. B. and Caminiti, R. (1997) 'Premotor and parietal cortex: corticocortical connectivity and combinatorial computations', *Annual Review of Neuroscience*, 20, pp. 25–42.

Wong, L., Manson, G. A., Tremblay, L. and Welsh, T. N. (2013) 'On the relationship between the execution, perception, and imagination of action', *Behavioural Brain Research*, 257, pp. 242–252.

Wright, C. J. and Smith, D. (2017) 'The effect of PETTLEP imagery on strength performance', *International Journal of Sport and Exercise Psychology*, 7, pp. 18–31.

Wurm, X. M. F. and Lingnau, A. (2015) 'Decoding Actions at Different Levels of Abstraction', *The Journal of neuroscience : the official journal of the Society for Neuroscience*, 35(20), pp. 7727–7735.

Xavier Castellanos, F., Margulies, D. S., Kelly, C., Uddin, L. Q., Ghaffari, M., Kirsch, A., Shaw, D., Shehzad, Z., Di Martino, A., Biswal, B., S Sonuga-Barke, E. J., Rotrosen, J., Adler, L. A. and Milham, M. P. (2008) 'Cingulate-Precuneus Interactions: A New Locus of Dysfunction in Adult Attention-Deficit/ Hyperactivity Disorder', *Biological Psychiatry*, 63, pp. 332–337.

Xie, F., Xu, L., Long, Z., Yao, L. and Wu, X. (2015) 'Functional connectivity alteration after real-time fMRI motor imagery training through self-regulation of activities of the right premotor cortex', *BMC Neuroscience*, 16(1), pp. 16–29.

Yarkoni, T., Poldrack, R. A., Nichols, T. E., Essen, D. C. Van and Wager, T. D. (2011) 'Large-scale automated synthesis of human functional neuroimaging data', *Nature Methods*, 8, pp. 665–670.

Yonelinas, A. P. (2002) 'The Nature of Recollection and Familiarity: A Review of 30 Years of Research', *Journal of Memory and Language*, 46, pp. 441–517.

Yoo, S.-S., O'Leary, H. M., Fairneny, T., Chen, N.-K., Panych, L. P., Park, H. and Jolesz, F. a (2006) 'Increasing cortical activity in auditory areas through neurofeedback functional magnetic resonance imaging', *Neuroreport*, 17(12), pp. 1273–1278.

Yoo, S. S., Lee, J. H., O'Leary, H., Panych, L. P. and Jolesz, F. A. (2008) 'Neurofeedback fMRI-mediated learning and consolidation of regional brain activation during motor imagery', *International Journal of Imaging Systems and Technology*, 18(1), pp. 69–78.

Yousry, T. A., Schmid, U. D., Alkadhi, H., Schmidt, D., Peraud, A., Buettner, A. and Winkler, P. (1997) 'Localization of the motor hand area to a knob on the precentral gyrus A new landmark', *Brain*, 120, pp. 141–157.

Yoxon, E., Tremblay, L. and Welsh, T. N. (2015) 'Effect of task-specific execution on accuracy of imagined aiming movements', *Neuroscience Letters*, 585, pp. 72–76.

Zabicki, A., De Haas, B., Zentgraf, K., Stark, R., Munzert, J. and Krüger, B. (2016) 'Imagined and Executed Actions in the Human Motor System: Testing Neural Similarity Between Execution and Imagery of Actions with a Multivariate Approach', *Cerebral Cortex*, pp. 1–14.

Zamorano, F. J., Bruehl, A. B., Mathiak, K. A., Ka, M., Em, A., Koush, Y., Dyck, M., Js, C., Tj, G., Fd, Z., Alawi, E. M., Koush, Y., Dyck, M., Cordes, J. S., Gaber, T. J., Zepf, F. D., Palomero-Gallagher, N., Sarkheil, P., Bergert, S., Zvyagintsev, M. and Mathiak, K. (2015) 'Social reward improves the voluntary control over localized brain activity in fMRI-based neurofeedback training', *Frontiers in Behavioural Neuroscience*, 9, pp. 1–14.

Zatorre, R. J., Douglas Fields, R. and Johansen-Berg, H. (2012) 'Plasticity in gray and white: neuroimaging changes in brain structure during learning', *Nature Neuroscience*, 15, pp. 528–536.

Zhang, X., De Beukelaar, T. T., Possel, J., Olaerts, M., Swinnen, S. P., Woolley, D. G. and Wenderoth, N. (2011) 'Movement Observation Improves Early Consolidation of Motor Memory', *The Journal of Neuroscience*, 31, pp. 11515–11520.

Zhao, X., Zhang, H., Song, S., Ye, Q., Guo, J., Yao, L., Rokem, A. and Olsson, C. J. (2013) 'Causal interaction following the alteration of target region activation during motor imagery training using real-time fMRI', *Frontiers in Human Neuroscience*, 7, pp. 1–8.

Zilverstand, A., Sorger, B., Sarkheil, P. and Goebel, R. (2015) 'fMRI neurofeedback facilitates anxiety regulation in females with spider phobia', *Frontiers in Behavioral Neuroscience*, 9, pp. 1–12.

Zimmer, H. D. (2008) 'Visual and spatial working memory: From boxes to networks', *Neuroscience and Biobehavioral Reviews*, 32, pp. 1373–1395.

Zotev, V., Krueger, F., Phillips, R., Alvarez, R. P., Simmons, W. K., Bellgowan, P., Drevets, W. C., Bodurka, J. and Domschke, K. (2011) 'Self-Regulation of Amygdala Activation Using Real-Time fMRI Neurofeedback', *PLOS ONE*, 6(9), pp. 1–17.

Zotev, V., Phillips, R., Yuan, H., Misaki, M. and Bodurka, J. (2014) ‘Self-regulation of human brain activity using simultaneous real-time fMRI and EEG neurofeedback’, *NeuroImage*, 85, pp. 985–995.